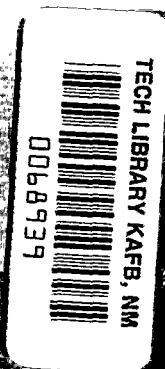


NASA TECHNICAL
TRANSLATION



NASA TT F-585

C. 1

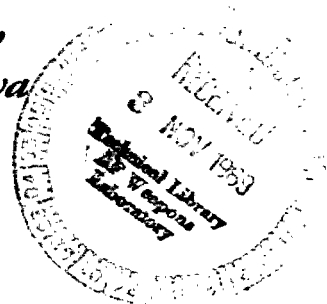


LOAN COPY
NEW
RENO

SHOCK WAVES IN REAL GASES

by T. V. Bazhenova, L. G. Gvozdeva, Yu. S. Lobastov,
I. M. Naboko, R. G. Nemkov, and O. A. Predvoditeleva

"Nauka" Press, Moscow, 1968



NATIONAL AERONAUTICS AND SPACE ADMINISTRATION • WASHINGTON, D. C. • OCTOBER 1969



SHOCK WAVES IN REAL GASES

By T. V. Bazhenova, L. G. Gvozdeva, Yu. S. Lobastov, I. M. Naboko,
R. G. Nemkov, and O. A. Predvoditeleva

Translation of "Udarnyye volny v real'nykh gazakh."
Institute of High Temperatures, Academy of Sciences USSR and the
Power Institute imeni G. M. Krzhizhanovskiy.
"Nauka" Press, Moscow, 1968

NATIONAL AERONAUTICS AND SPACE ADMINISTRATION

For sale by the Clearinghouse for Federal Scientific and Technical Information
Springfield, Virginia 22151 - CFSTI price \$3.00

SHOCK WAVES IN REAL GASES

T. V. Bazhenova, et al.

ANNOTATION

In this book are presented experimental studies embracing an integrated group of problems pertaining to the propagation of shock waves in reacting media. It describes experimental techniques, presents an analysis of the features of a real gas flowing in a shock tube. Results are presented of experiments in the study of propagation of small disturbances in a reacting gas, of normal and Mach reflection of shock and detonation waves and of the ionization structure of shock waves.

The book should be of interest to scientists and engineers working in fields related to supersonic flow of high-temperature gases.

A. S. Predvoditelev, Corresponding Member of the Academy of Sciences of the USSR, Editor-in-Chief.

A. S. Predvoditelev, Editor-in-Chief

TABLE OF CONTENTS

Annotation	ii
From the Editor	vi
Introduction	x
Chapter 1 - Methods of Measuring Shock-Wave Parameters	1
1. Visualizing the Structure of the Flow Behind a Shock Wave by the Topley Method	1
2. Recording the Process in a Shock Tube by Continuous Photographic Scanning	2
3. High-Speed Photography of Processes in Shock Tubes by the Spark Method	4
4. High-Speed Photography Using the SFR Camera	6
5. Measuring the Flow Velocity in a Shock Tube by the Spark Method	9
6. Pressure Pickups	15
7. Measuring the Surface Temperature of the Shock-Tube Walls	17
8. Microwave Measurement of Electrophysical Variables in the Gas Behind a Shock Wave	21
Chapter 2 - Deviation of the Flow in a Shock Tube From the Ideal Without Consideration of the Physiochemical Transformations in the Gas	32
1. Effect of the Boundary Layer on the Gas-Flow Variables Behind a Shock Wave	32
2. Experimental Data on the Effect of Multi-Dimensionality of the Gas Flow in a Shock Tube on the Flow Variables	35
3. Features Peculiar to the Propagation of a Reflected Shock Wave in a Shock Tube	38
Chapter 3 - Gasdynamic Flow Variables Behind a Shock Wave in a Gas Undergoing Relaxation	44
1. Mach Number of the Flow and the Thermodynamic Variables of the Gas Behind Shock Waves Propagating in CO ₂ , N ₂ and O ₂ at Velocities of 1500-3000 m/sec	44
2. Velocity of the Flow and the Rate of Propagation of a Small Disturbance in the Flow Behind a Shock Wave	46
3. Structure of the Mach Line of a Gas Undergoing Relaxation in the Approximation of Geometrical Acoustics	52

Chapter 4 - Reflection of Normally Incident Shock Waves in Reacting Gases	58
1. Unsteady Propagation of a Reflected Shock Wave in a Reacting Gas	58
2. Study of the Nonsteady Propagation of a Reflected Wave in CO_2 Undergoing Relaxation	63
3. Determining the Dissociation Relaxation Time of Mixtures of CO_2 with N_2 at $T = 1000\text{--}3000^\circ\text{K}$ on the Basis of Nonsteady Propagation of a Reflected Shock Wave	69
4. Effect of Nonequilibrium Ionization on the Propagation of a Reflected Shock Wave in Argon	70
Chapter 5 - Reflection of Oblique Incident Shock Waves in a Reacting Gas (Mach Reflection)	73
1. Irregular Reflection of Shock Waves in an Ideal Gas	73
2. Experimental Study of Irregular Reflection of Strong Shock Waves	82
3. Features Peculiar to Mach Configuration in a Real Gas	86
4. Variation in the Pressure and Temperature of the Wedge Surface	92
Chapter 6 - Reflection and Refraction of Detonation Waves	95
1. Effect of Boundary Conditions on the Onset of Detonation	95
2. Detonation Wave Structure	99
3. Effect of Variation of Tube Cross Section on the Detonation-Wave Structure	109
4. Triple Configurations Arising on Refraction of Detonation Waves	113
5. Regular and Irregular Reflection of Detonation Waves	121
Chapter 7 - Ionization Structure of Shock Waves in Air and Nitrogen	124
1. Analysis of the Effect of Easily-Ionized Admixtures on Electron-Concentration Measurements	125
2. Determining of the Time Needed for Reaching Equilibrium Ionization Behind Incident Shock Waves in Air	127
3. The Ionization Structure of Shock Waves in Nitrogen	129
4. Measuring the Electron Temperature on the Basis of Self Radio-Frequency Radiation of a Gas Behind a Shock Wave	132
5. Cross Section of Elastic Collisions Between Electrons and Neutral Particles in a Gas Ionized by a Shock Wave	135
Appendix 1 - Physical Variables in Air Behind a Normal Shock and Behind a Reflected Shock Wave for Equilibrium and Frozen Dissociation [109]	138
Appendix 2 - Physical Variables of Carbon Dioxide and Nitrogen Behind Shock Waves for Different Degrees of Physical and Chemical Transformations	144
Appendix 3 - Equilibrium Thermodynamic Functions of Carbon Dioxide in the Temperature Range of $1100\text{--}4500^\circ\text{K}$ at Pressures of 0.1-1-13 ATM	148

Appendix 4 - Calculating the State of the Gas Behind an Attached Wave and the Angle of Inclination of a Shock Attached to a Wedge	157
Appendix 5 - Calculation of Triple Configurations by the Method of Shock Polars	160
References	164

FROM THE EDITOR

In his timeless book: Rules for the direction of the mind, Descartes has made a statement which bears repeating. It can be paraphrased to state: if one wants to understand a problem well, the latter should be freed of all the redundant concepts, reduced to simple elements and be broken up into some number of possible parts by means of enumeration.

However, when performing this logical operation one should remember that we must encounter in the process the following logical stages. Firstly, the problem should contain some unknown, since otherwise it is useless; secondly, this unknown should be noted by something, otherwise it will never be subjected to study; thirdly, the problem should be noted also by some known feature. In addition, it should be complete, i. e., should not contain indeterminacies which may steer the investigator to the study of matters which cannot be determined from the given concept.

On the other hand, the component parts of any study consist either in establishing some matter on the basis of logical prerequisites, or in establishing a cause on the basis of its results. Further, all these operations are performed by means of the language. It becomes clear from this that the use of language is of great importance in formulating truths which are discovered.

This last aspect of this train of thought was noted in particular by the known Italian geometrician F. Enriques in his work "Problems of Science." His approach is along the following lines: it should be noted that the language, which serves for expressing our thoughts, is a system of symbolic designation of a given item. The use of this powerful tool involves serious dangers. In a system of logical constructions which sometime contain a large group of facts and items it is easy to forget the significance of words which include a large volume of concepts. Thus, in order not to get lost in senseless word constructions, one should always be guided by the condition that the cognitive opinion always contains a comparison of juxtaposition of claims and counterclaims.

All this above discussion was presented to draw attention to the fact that the term "plasma" which is used in modern scientific literature does not contain precisely defined concepts. Hence the problem should be raised on the concepts which should properly be thought as contained in this word.

First of all, the use of the term "plasma" in our cognizance suggest something which has the properties of a continuum. In conjunction with this one may raise the question of whether a gas may have states such in which concepts of discontinuum and continuum exist side by side.

As is known, each gas molecule occupies a very small space in which positive and negative charges are arranged in a given pattern. Consequently, this is a defined electrodynamic formation. When these formations are brought sufficiently close [as is the case] in a highly compressed gas, there is produced an internal electromagnetic field, more precisely, electrothermal since the gas molecules are subjected to thermal motion. The field of ponderomotive

forces of internal electromagnetic energy of the gas is approximated by modern science by a finite, and sometimes also by an infinite sum of central forces. These forces are conventionally called van-der-Waals forces. As to a concrete idea about the character of the thermal motion of molecules in such gaseous systems, it is described by starting assumptions on which various authors base the distribution functions by their statistical attributes and ascribe a kinematic state and a position in space to molecules which determine them. As is easy to see, this description of a gaseous system contains the concept of collective existence of molecules. This raises the question whether it is possible to regard this state of a gas of a "plasma state." From the point of view of its etymology, the answer is yes.

Let us now pass to such a rarefied gas when the internal electromagnetic energy in the system as a whole is close to zero and manifests itself only on approach of molecules in the form of interaction potentials. As an example of such a gaseous system we can use a system of material points moving according to laws of mechanics without initial conditions. As is known, the statistical attributes of such a system are governed by the normal Laplace-Gauss distribution. These systems have no elements of collective interaction and, consequently, there will exist a field of ponderomotive forces which can be approximated by summations of central forces. However, this field cannot seriously disturb the character of the thermal motion of molecules, i.e., the statistical attributes of the system will, as before, obey the Laplace-Gauss normal distribution.

Can such a gas be called plasma within the rigorous etymological context of the word? Of course, not.

It is well known that by increasing the temperature of a gas it is possible to attain such a state in which its internal electromagnetic field will be so appreciable, that the motion of individual electrodynamic patterns of the system will be nonholonomic and, consequently, the assumptions on which the normal distribution functions are based will no longer be satisfied. And this means that the behavior of the thermal motion in such system will not be similar to that of thermal motion in ordinary or weakly-ionized gases. As a specimen of sorts of such motions we can use the thermal motion in an electron gas, whose theory was given by A. A. Vlasov.

It is precisely these states of a gas which were labeled as plasma states by J. J. Thomson and Rayleigh. The above deliberation, in our opinion, shows that it is not permissible to combine all the states of an ionized gas under the common label of "plasma." It is known from as early as Aristotle's time that an inappropriate extension of a concept makes the latter indeterminate and serves as a source for accumulation of indefinite opinions which detour the study from the proper track.

If we conform to the interpretation of the term "plasma" as defined by Thomson and Rayleigh, then we naturally arrive at ideas which determine the ways of theoretical and experimental studies of plasma properties. The theory of the problem reduces to finding methods for describing the thermal state of such a medium. Here none of the available statistical methods are suitable,

since by its very nature the system is nonholonomic. An a priori creation of methods for describing thermal motion in plasmas is a quite difficult task and it is doubtful whether it will be resolved in the near future. The construction of thermodynamics and of the theory of visible plasma flows depends on its solution.

From our point of view it is easier to solve this problem a posteriori by study of the properties of ionized gas and then transforming the latter into the plasma state. The most promising approach with this respect is study of variations in the dispersion constants of the longwave part of the optical spectrum of monatomic gases as they approach the plasma state. In fact, if we construct a theory of the dispersion of light in an ionized gas on the basis of macroscopic Maxwell's equations, then the transition from the simple statistical state of the gas to its plasma state should have a pronounced effect on the calculation of the integral complex value of the refractive index. Due to the collective interactions prevailing in the plasma state, the thermal motion in a gas should exhibit wave properties. Hence the interaction between an external optical wave with the internal waves can result in modulation effects which are similar to the Mandel'shtamm-Brillouin effect which is observed in liquids.

The wave behavior of the thermal motion in the plasma state of a gas is due primarily to the circumstance that only this type of motion together with cyclical motions permits disregard of the initial state of the system. And the latter is necessary in order that the internal motions in the gas agree with the principles of thermodynamics.

Plasma as defined by Thomson and Rayleigh should, in addition, have still another specific property, i. e., electromagnetic emission, similar to those which are received by radio-telescopes from outer space or from the sun. It is at present difficult to say in which frequency region will the maximum of this radiation lie. It is quite probable that the local excess density of the charge will vary according to the laws of nonlinear vibrations. And this will suggest a discrete spectrum, with a still unknown amplitude distribution. It would appear that the resolution of this question is contingent only on a properly set up experiment.

Passing on from monatomic to multiatomic gases, one can claim with a high degree of justification that plasma state of a gas will most probably be established after dissociation will take place. But the latter process cannot take place indeterminately, i. e., without the effect of factors which lead the system to its final plasma-state. Hence the study of thermal dissociation of gases appears, in view of the above considerations, to be a quite important problem.

Study of plasma state on mixing of different gases is an even more difficult problem primarily since new formations of matter may occur in gases in the process of reaching the plasma state. These formations as such also have a tremendous scientific and practical significance. Here we should make a distinction between two trends, depending on the energy sources used for maintaining the process of the conversion of the substance. It is possible, for example to use thermal and electrical sources of energy, the latter source

being more economical. This served as the cause for setting up a new branch of physical chemistry, i. e., electrochemistry of gases.

Scientific development does not always proceed along a logical path of concept development. Science is one of the links in a chain which characterize national culture, for which reason it cannot exist unless related with social and economic problems.

The development of nuclear power generation and missile technology has faced science with the problem of study of ionized gas and gas in the plasma state. The present book concerns itself precisely with this major problem. It presents studies which were performed starting with 1953 by workers of the Power Engineering Institute of the USSR Academy of Sciences under the leadership of this writer. The work which was done solves only a small aspect of the problem, i. e., we have studied the behavior of gas only under conditions of gas dynamic flows, where shock discontinuities increase the temperature of the gas only to low thermal ionization. In this case resort can be had to classical methods of statistical physics.

As was stated above, the character of thermal motion in plasma should become different than in nonplasma gas and this requires a radical supplementation of the basic assumptions of gas dynamics.

The formation and behavior of shock discontinuities in plasma should be governed by different laws. It is difficult to predict a priori the character of these changes. Consequently, this again shows the need for setting up properly thought out experiments.

The authors hope that the present book will make a contribution toward the solution of the problem at hand.

INTRODUCTION

Shock waves are one of the most interesting natural phenomena. From the time that their existence was predicted theoretically more than hundred years ago by Riemann, Rankine and Hugoniot, the theory of shock waves was based primarily on the gasdynamics of an ideal gas, in which no chemical transformations take place. The only exception was the theory of detonation, which takes into account the instantaneous generation of heat across a shock wave front as a result of a chemical reaction.

In considering the properties of strong shock waves consideration should always be given to the real properties of the gas, since the temperature increase taking place behind a shock wave produces physicochemical transformations, i.e., excitation of internal degrees of freedom and ionization, in the flow behind the wave.

The relationship between the composition of a gas and its variables (temperature and pressure) on equilibrium is determined by known thermodynamic laws. Equilibrium in a reacting medium ensues when the rates of disintegration processes (dissociation and ionization) are equal to the rate of recombination processes which take place simultaneously. Detailed tables of the composition and parameters of air, carbon dioxide and nitrogen behind shock waves have been calculated for these conditions in a wide range of pressures at temperatures of up to 20,000°K [1-4]. The state of equilibrium is established behind a shock wave at a finite distance from the front, for which reason a certain time, known as the relaxation time, is needed for the equilibrium to come into effect. The flow behind a shock wave in the nonequilibrium region has different properties, i.e., the degree of dissociation and ionization increases in this region from zero across the front to the equilibrium value, and this is accompanied by a several-thousand degree drop in the gas temperature, since the kinetic energy of the gas molecules is used up for exciting internal degrees of freedom. The fact that the gas behind a shock wave is not in equilibrium affects the shape of the shock wave which is produced at bodies in supersonic flow, the distance between the front and the body, the interaction between shock waves and the structure of the supersonic flow.

The rate at which equilibrium values of variables behind a shock wave are established can be calculated if the rate constants of all the elementary processes taking place in the gas are known. However, these constants can at present be calculated only for individual reactions [5], at the time when heating of each gas is accompanied by tens of different reactions. Consequently, experimental studies must be made of the formation of shock waves and the properties of flow in the nonequilibrium region behind shock wave must be determined in order to obtain information on the rates of physicochemical transformations.

During the last few years a large volume of work was performed in the USSR and Western countries in the theoretical and experimental studies and in publication of correlating monographs on nonequilibrium processes behind shock waves [5-7, 11, 31, 32, 44]. Primary attention in these studies was given to consideration of the kinetics of elementary processes taking place behind shock waves and to determination of the structures of shock waves with consideration of physicochemical transformations.

Extreme difficulties are encountered in giving a rigorous description of various kinds of flows of a relaxing gas, for which reason extensive effort is exerted in the USSR and abroad in solving this problem. Problems were solved for flow of air about a blunt body [8, 9], the structure of normal shock wave in air [10], a blunt body in an equilibrium hypersonic flow [12], a cone and a wedge in a flow with relaxation [13, 14], Prandtl-Meyer flow with rotational relaxation [15], structure of centered rarefaction wave [16, 17] and nonsteady-state propagation of a shock wave in a gas undergoing relaxation [18], flow of gas undergoing relaxation in nozzles [19, 20], and the structure of a one-dimensional detonation wave [33, 34].

Experimental studies on physical gasdynamics proceed primarily by way of measuring a given variable behind a normal shock in a gas undergoing relaxation [21-23] and by studying the flow of a gas undergoing relaxation in a nozzle [26, 27]. The variables measured include the time of relaxation for the dissociation of oxygen and air [24, 25], and of vibration of nitrogen, oxygen and carbon dioxide molecules, of certain kinds of vibrations of carbon dioxide molecules, the ionization time of argon and air [29, 5], as well as the relaxation time for oxidation of hydrogen [30, 31] and acetylene [32] behind a detonation wave.

Some experimental data is available on the mechanism of propagation of weak disturbances in a relaxing gas with a high-frequency (frozen) speed of sound [28].

Modern technology encounters a number of phenomena in which flow of gas undergoing relaxation and formation of strong shock waves take place. Among these we may count, for example, the high-temperature gas jet in MHD generators [35, 36], the jet of products of combustion ejected by jet engines into the atmosphere or the air-less space [37], the layer of high-temperature gas which is produced behind the shock wave originating on reentry of space vehicles into the denser atmospheric layers of the earth and other planets [38, 39] interaction between shock waves and obstacles on explosions, propagation of detonation in shafts, etc.

The effect exerted by the nonequilibrium of physicochemical processes on the flow variables turns out to be quite appreciable in a number of cases. When plasma flows in the duct of a MHD generator, the conductivity of the thermally ionized gas depends on the rate of recombination of electrons with ions, which takes place as the gas continues to expand in the nozzle [40]. When a certain relationship is reached between the rate of expansion and the rate of recombination, the latter process may either partially or completely cease and the electron concentration in the flow will be appreciably higher than that on equilibrium [41]. The nonequilibrium excitation of vibrations in a gas results in changing the ratio of specific heats $\gamma = \frac{C_p}{C_v}$, which affects the relationship governing the expansion of the gas [37].

The final rate of dissociation and excitation of vibrations of the molecules of the gas flowing at supersonic speed past a body can result in increasing the gas temperature at the surface of the body situated behind a detached shock wave as compared with the equilibrium values calculated upon consideration of

energy losses for dissociation and excitation of vibrations [43]. Plasma formations which arise when bodies move in the atmosphere at hypersonic speeds affect the radio communications with these bodies [38, 42]. The concentration of free electrons in plasma formations depends on the relaxation of the process of thermal ionization of gases at high temperatures, which takes place behind the shock wave.

On interaction of strong shock waves with obstacles there arise complex flows whose structure depends on the rate of the physicochemical processes [at hand].

The study of formation and propagation of shock waves in a real gas provides a goodly amount of information for constructing a theory of wave processes in a chemically reacting medium. Consideration of these processes by the method of discontinuities makes it possible to provide a uniform description of front phenomena of different character. These ideas, which were developed by A.S. Predvoditelev, served as the basis for setting up experimental studies of the propagation of detonation and shock waves and flows behind shock waves in real gases, which are capable of exothermic and endothermic reactions. These studies were performed in shock and detonation tubes.

An item of particular importance in the formation and propagation of shock waves in a shock tube is the fact these processes result from the superposition of acoustic waves with infinitesimal amplitudes. From this point of view the motion of a gas which is produced behind a shock wave is, by its nature, nonsteady even when the shock wave moves at constant velocity, since, as the shock wave moves the motion embraces increasingly new layers of the gas. The gas flow behind a shock wave has a peculiar structure in which regions situated at different distances from the shock fronts participate in the motion during different time periods. This feature introduces a variation of a kind into the flow of a real gas behind a shock wave in a shock tube.

In shock waves propagating ahead of a flame front in tubes or ahead of the contact surface after breaking the shock-tube diaphragm the determination of flow variables behind a shock wave depends appreciably on the conditions at the contact surface and across the shock front. In this sense the shock wave and the flame front, as well as the shock wave and the contact surface, make up a single entity. A change of state at one of the boundaries results in reconstruction of the entire flow and affects the state at the other boundary. A change in boundary conditions may be brought about by variations in the geometry of the duct in which the shock wave propagates, changes in the variables of the medium when the wave passes the boundary between two media, changes in the state of the gas due to dissociation or exothermal reactions. In real gases these phenomena are complicated by the presence of various kinds of losses which arise on interaction between the flow and the shock tube walls. All these phenomena cannot be completely predicted theoretically and require an experimental study.

In the study of molecular processes in gases and of their effect on the flow variables we have used a methodical approach which consisted in calculating the relationship between the gas variables on various assumptions regarding

the molecular state. In the region of variables where the effect of physical processes on this relationship is quite appreciable, the relationship between the flow variables were determined experimentally. Experimental data were compared with theoretical results and this produced a picture of the state of the gas molecules under the given conditions.

When proceeding in the above manner, we have first checked the accuracy with which the relationship between the gas variables behind a normal shock, derived on the basis of the laws of conservation on the assumption of a one-dimensional and steady-state flow, is applicable to a real flow of gas behind a shock wave in a shock tube. For this purpose we have measured variables behind a shock wave in gases the molecular state of which is known and we have established the scale and character of deviations from ideal for a flow in a shock tube. Results of these experiments were considered when analyzing the results of experiments in a reacting gas.

Studies were made of certain gasdynamic processes under conditions when equilibrium state of the gas is reached during a finite time period. For this we have studied characteristic and at the same time relatively simple gasdynamic processes, i.e., nonsteady propagation of a reflected shock wave in a gas undergoing relaxation and the propagation of small disturbances in a supersonic flow. Analysis of these processes has enabled us to obtain data on the relaxation times for dissociation and vibrations of carbon dioxide and its mixtures with nitrogen at temperatures of 2500–6000°K and on the structure of a small disturbance in a gas undergoing relaxation.

The data obtained on the effect of physicochemical transformation on the normal reflection of a shock wave made it possible to analyze a more complex gasdynamic phenomenon, i.e., nonregular reflection of a shock wave on oblique incidence (the so-called Mach reflection) in a real gas at high temperatures. An experimental study of this phenomenon has shown that the real properties of the gas result in a principally new system of shock waves, i.e., a system with a double configuration attendant to Mach reflection.

The relationship between gasdynamic phenomena and physicochemical transformations is particularly pronounced in detonation waves. For this reason experimental studies were made of the formation, refraction, diffraction and reflection of detonation waves from normal and oblique surfaces.

The ionization processes which arise on propagation of shock waves in real gases were studied in air and nitrogen with relatively low-speed shock waves, when the ionization process does not appreciably affect the gas flow. Under these conditions we measured the time needed for establishing the equilibrium degree of ionization and electron temperature behind shock waves.

CUT ALONG THIS LINE

FOLD LINE

NATIONAL AERONAUTICS AND SPACE ADMINISTRATION
WASHINGTON, D.C. 20546
OFFICIAL BUSINESS

POSTAGE AND FEES PAID
NATIONAL AERONAUTICS & SPACE ADMINISTRATION

NATIONAL AERONAUTICS AND SPACE ADMINISTRATION
CODE USS-T
WASHINGTON, D.C. 20546

NASA TTF No.
585

FOLD LINE

CUT ALONG THIS LINE

changes, the sign of the gradient of the refractive index changes also. Thus, a shock wave moving horizontally from left to right with the knife edge vertical and placed to the left will appear dark, while a wave moving in the opposite direction will appear light on the gray background.

The propagation of shock waves and the flow structures behind them, when using the Töpler [schlieren] method, were recorded by means of various light sources and image receiving devices, whose selection was conditioned by the features of the process under study.

2. Recording the Process in a Shock Tube by Continuous Photographic Scanning

A method which is simplest to implement and at the same time yields a wealth of information on the processes in the inspected part of a shock tube is that of continuous photographic scanning. The window of the chamber under observation is closed by a screen with a narrow slot situated parallel to the longitudinal axis of the chamber along which the wave propagates. The light source in this case is a flashing lamp with a total duration of sufficiently intensive lighting at least not lower than the duration of the process phase of interest. The pattern of the motion of the inhomogeneity along the slot is recorded on a film which is held at the surface of the photo-recorder drum and which forms a closed cylindrical surface. The maximum film speed on the drum was 185 m/sec in our experiments. The objective lens of the photorecorder remains open during the entire experiment, for which reason the phase of the process which corresponds to the instant of flashing of the lamp is positively recorded on the film. It is only necessary to sufficiently precisely synchronize the instant at which the lamp flashes with the stage of the process under study in the shock tube.

/18

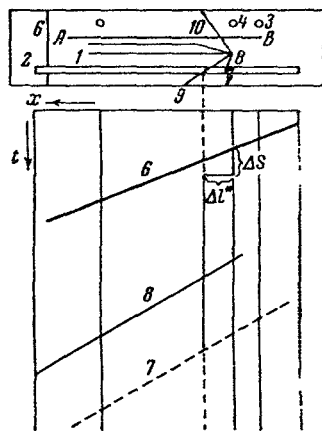


Figure 1. Arrangement for Obtaining Continuous Scanning of a Process Taking Place in a Shock Tube.

The photographing was initiated by a signal which arose on a piezometric pressure pickup at the instant when the shock front passes past it. Any delay in starting up the recording apparatus and the illuminating system relative to the instant of receiving the signal from the pressure sensor were determined on the basis of parameters of the synchronizing unit's circuit. The signal from the pressure pickup was amplified, delayed and then opened a thyatron relay. The anode capacitor of the relay is discharged through this relay and through the primary winding of the transformer. The high-voltage impulse which was thus produced in the stepup winding of the transformer was fed through a separating capacitor to the initiating electrode of the light source. To select the necessary delay time in the synchronization unit's circuit, a provision was made for adjusting the time constant of the capacitance-charging circuit in the thyatron-relay circuit.

/17



Figure 2. A Continuous Photographic Scan of the Propagation and Reflection of a Shock Wave from the End of the Tube.

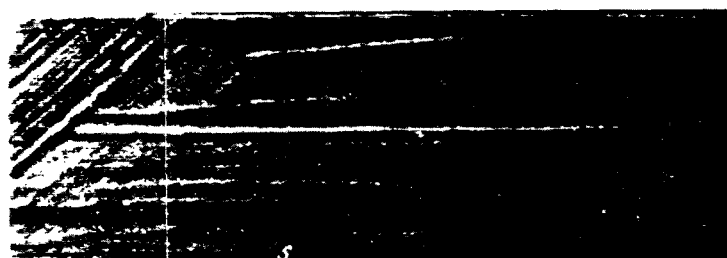


Figure 3. A Photographic Scan of the Mach Line and the Motion of a Stria in the Flow Behind a Shock Wave.

Figure 1 shows a schematic which clarifies the mutual location of traces of inhomogeneities, shown on photographs of continuous scanning of processes in a shock tube (Figs. 2 and 3). The upper part of Fig. 1 shows schematically the window of the viewing part of the tube. An obstacle - wedge half 1 - is placed in the chamber. The image of the flow pattern and of the motion of the incident shock wave 6 and contact surface 7, as well as of the "stria" 8 is constructed by means of a slot on screen 2. The screen is provided with apertures 3 and 4, which produce line-type images on the moving film. These lines serve as references of a kind in processing the films, in measuring the distances and times on the motion pattern of the traces of all inhomogeneities which are recorded on the film.

It is not too difficult to note that the traces of the motion of the wave, forward boundary of the interference and of the "stria" will be depicted on the film in the form of slanting lines 6, 7 and 8, respectively. The tangent of the angle between these lines and the "time axis", i. e., the direction of film motion, is proportional to the velocity at which these inhomogeneities move.

The Mach line, i. e., the line 9 of the small disturbance which is produced at the leading edge of the wedge half from the side of the generatrix parallel to

the axis of the flow, will be depicted by a line stationary in time. For the given position of the slot, shock 10 will not be recorded on the film. In order to obtain its image it is necessary to move slot AB to the forward part of the chamber's window or to cut a new slot there. The use of two slots will make technically more difficult the deciphering of the photographs, but it does not introduce any principal difficulties.

By clearly recording the position of the obstacle in the chamber relative to the "reference" points 3 and 4 (Fig. 1) and the position of slot 2, knowing the speed of the photorecorder drum which is synonymous with the velocity of the film and having first measured the image reduction, it is possible to use the schlieren photographs shown in Figs. 2 and 3 to determine the speed of the wave, the velocity of the interface, the velocity at which the gas moves behind the shock wave (on the basis of the velocity of the "stria"), to measure the slope of the line of the small disturbance relative to the flow axis (thus obtaining the flow's Mach number), the inclination of the oblique shock, to measure the rate of propagation of the small disturbance and to decipher the pattern on oblique incidence of a shock wave on a solid wall. These measurements are discussed in detail below.

/19

3. High-Speed Photography of Processes in Shock Tubes By the Spark Method

Considerable scope for visualizing the flow structure in a shock tube is offered by the use of the schlieren method in conjunction with high-speed photography of the process. High-speed photography can be performed by using the IAB-451 instrument in combination with a flashing lamp, i. e., "discharger", in which a high-frequency spark discharge takes place, as the light source. The requirements put to the light source and the image receiver in this case should provide for sufficient intensity of individual flashes with the smallest possible frame exposure time and for not too small frame size with a frame frequency which yields acceptable resolution in time of the process being observed. A quality of great importance of high-speed spark-discharge photography in the study of flows in shock tubes is the fact that it is possible to synchronize the time of the picture taking with any stage of the process under study by starting up a series of illuminating discharges by a signal from the process under study proper.

The exposure time of a frame, the duration of individual flash in a series is determined by the capacitance, resistance and inductance of the discharge circuit. Reducing the inductance and a proper selection of the resistance make it possible to obtain a flash duration of up to 5-3 microseconds. In order to obtain short flashes of the given intensity one should use high voltages with a lower capacity. Designs of spark setups for high-frequency photography are described in [47-50].

Our arrangement used a capacitor bank with a total capacitance of 1 mf. It was charged from the AKI-2-50 instrument used for testing conductor breakdown with voltages up to 22 kV. The voltage was supplied to the discharge circuit through a 7 kohm resistor, with the discharge capacitance of the capacitor being 0.02 mf. The signal initiating the picture taking was supplied through the synchronizing unit to a thyatron [sic], connected between the capacitor bank and the discharge circuit proper.

The high-frequency spark discharge was obtained in the spark gap of the discharge lamp. The design of this lamp is described in detail in [47-50]. This is a "linear" light source with an adjustable spark gap. The shape of the lighting body of the "lamp" is determined by conditions which are most convenient for illuminating the collimating slot of the IAB-451. The lamp is evacuated and filled with hydrogen to a pressure of 1 atm. /20

The process was recorded on a film placed on the photorecorder drum. The film length was 1 m, linear film velocity 185 m/sec. The size of the frame on the film being 3.5 x 15 mm, the filming frequency was about 60,000 frames/second

The specifics of photorecording of processes in a shock tube is such that sharp synchronization is possible only in the case when the photographing process is started up by a signal arriving from a shock wave which has already formed, since the time of breaking the diaphragm and of wave formation can be precalculated only with a high degree of scatter. It happens that the time which passes from the time the diaphragm breaks to the start of stages which are of interest is smaller than the scatter in the diaphragm-breaking time. In conjunction with this it is difficult to record processes in shock tubes by photographic cameras in which the phenomenon is synchronized with the picture taking by initiating the phenomenon by an electrical impulse supplied by the photographic camera. The breaking of the diaphragm, which takes during a time which cannot be practically monitored turns out to be a component part of the total time of development of the phenomenon under study. Under these circumstances the recording of the needed process stage on the film is purely random. If, however, the filming sequence is started by a shock wave already propagating, then the indeterminacy introduced by the initial stage of the process is eliminated.

The delay time was varied in the range of 150-600 microseconds (this is the total delay time from the instant that the wave passes past the pressure pickup to the appearance of the first frame on the film).

High-speed photography of the process makes it possible to study the structure of the supersonic flow in the shock tube. The most complete information on the flow past obstacles in a shock tube can be obtained also by high-speed photography. Many details of schlieren diagrams obtained by continuous scanning can be properly interpreted only after comparison with the pattern of the same process obtained by high-frequency photography. /21

Figure 4 shows a picture of the propagation of a shock wave and of the flow behind it in a tube. The photographs show the shape of the front of the incident and reflected waves.

The use of these photographs makes also possible obtaining quantitative data describing the process in the shock tube, i.e., the velocity of the incident and reflected shock waves, the angles of inclination of oblique shocks and the lines of weak disturbances which arise at the half wedge which is situated in the flow of gas behind the shock wave.

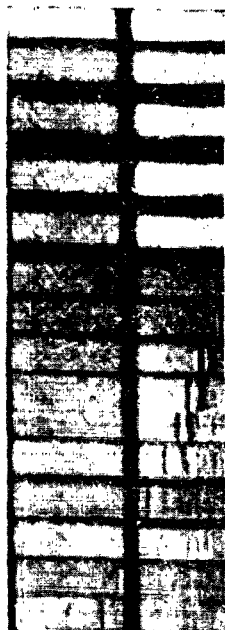


Figure 4. A Sequence of Photo Frames of the Propagation of a Shock Wave in a Tube.

4. High-Speed Photography Using the SFR Camera

The methods described above for recording the schlieren picture of the flow by means of spark light sources and continuous recording on a film placed on a rotating drum have a limited time resolution. This is due to the fact that there is a limit on increasing the drum speed which is determined by the strength of the drum material and of the film. They cannot move faster than 185-300 m/sec.

Processes which have a duration of not more than several microseconds must be recorded by a method using a rotating mirror. Then the image can move along a stationary film at a high speed. A number of cameras using this method are available, with the best time resolution provided by the SFR camera.

In this device [51] the speed at which the mirror rotates can be adjusted from 3 to 75 thousand revolutions/sec. The SFR in the time-magnifier version gives a series of successive photographs of the process with a frequency from 25,000 to 2,500,000 frames per second. The frame diameter is 10 mm for a two-row insert and 5 mm for a four-row insert. Unlike the ZhFR and ZhLV cameras, the SFR does not have a waiting regime. Here the instant at which the process under study starts is determined by the SFR proper. A high-voltage transformer in the control panel produces a high-voltage pulse at the instant when the mirror occupies some predetermined position. This pulse starts up the process under study in order to photograph a given stage of it. The ignition pulse is supplied with the mirror in a position such that the process stage under study ensues during the time which the mirror needs for rotating into the position corresponding to the start of the recording time. This time can be arbitrary, but should not be changed from one experiment to another. For this purpose the SFR camera is convenient for the study of detonation processes, for example. The gaseous mixture in the detonation tube can be ignited by a spark from a high-voltage pulse. In a shock tube the diaphragm-breaking time cannot be controlled and varies from experiment to experiment.

/22

The shock tube can be synchronized with the SFR either by stabilizing the diaphragm-breaking process by, for example, breaking the diaphragm by an electrical discharge, or, forgoing synchronization, to record the needed part of the process once per several experiments. Using a one-sided mirror approximately one out of eight experiments is successful, while when a two-sided mirror is used success is achieved in one out of four experiments.

If it is necessary to synchronize the start of recording not only with the instant at which a given stage of the process under study ensues, but also with some other instant (for example, the start of shutter opening or the start of

flashing of the illuminating lamp), then a 300 V pulse is taken off from the primary winding of the high-voltage transformer at the time of firing. It is supplied through an electronic network which provides the necessary delay to the thyatron key, which controls the ignition of the lamp or the opening shutter. Sometimes a synchronization scheme is used under which the illuminating lamp does not flash if the instant at which the recording starts does not coincide with the needed stage of the process [53].

The SFR camera can be used for photographing self-luminosity, for photographing shadow and interferometer patterns. The duration of film exposure when photographing self luminosity is limited by explosion-type cutoff shutters [52].

In taking shadow or interferometer pictures the film exposure time is specified by the duration of the illuminating flash. Illumination can be obtained by using the IPS-200, IPS-500 and IPS-1000 flashing lamps, with the flashing duration selected on the basis of above considerations. If it is necessary to obtain equal illumination of all the frames in a series, use should be made of the arrangement described in [53]. During a specified time the flashing lamp is shunted by a thyatron, and this prevents the lamp from flashing.

The SFR camera can be used together with shadow instruments, for example, with the IAB-451.

Figure 5 depicts an arrangement of combined use of the SFR-L and IAB-451 instruments. S is the light source, O_1 and O_2 are lenses of the Töpler instrument, K is the inhomogeneity under study and H is the Foucault knife edge. The SFR-L is depicted in the time-magnifier version.

The image of the photographed object K is constructed by the objective lenses O_5 and O_6 in the plane intersecting the middle of the reflecting facet of mirror P. At some distance from the mirror a series of rectangular lenses, assembled into lens insert L is arranged along an arc of circle. When the mirror rotates, the image of the object is projected in sequence by the lenses onto the plane of the film. /23

Before the first lens there is a diaphragm with square apertures, which are projected onto diaphragm D_2 in front of the lens insert in such a manner that at each time instant light passes only through one lens in any given row. For a four-row insert the diaphragm D_2 has four apertures, displaced horizontally and vertically, while for a two-row insert it has two apertures. When the image of one of the apertures coincides with an operating aperture of any lens in the lens insert, the image of the remaining apertures is situated between the operating apertures of neighboring lenses. This system thus acts as an optical shutter.

The operation of the lens system of the SFR and IAB-451 instruments is achieved by using reduced lens systems A, which project the image of the object under study on the film with the required size reduction and the plane of the

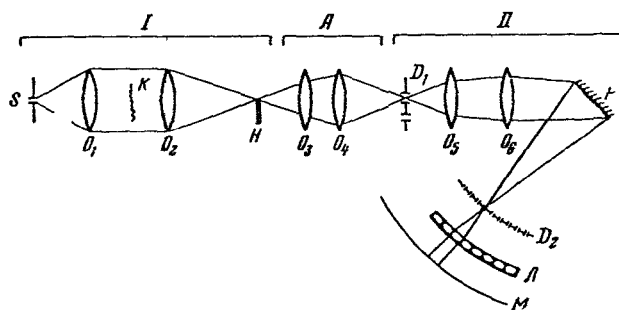


Figure 5. Arrangement for Recording a Schlieren Pattern of a Process by the SFR Camera.

output pupil [aperture] of the IAB-451 (plane of the Foucault knife edge) onto the plane of the input apertures of the SFR camera (diaphragm D_1 with light apertures).

In order that the shadow picture obtained by means of the IAB-451 not be distorted when transferred to the film, the linear dimensions of the image of the input aperture of the SFR in the plane of the Foucault knife edge are made larger than the linear dimensions of the output aperture of the IAB-451 (the size of the output aperture of the IAB-451 is determined by the magnitude of the greatest deviation of an elementary image of the light source from the axis which is produced by pressure gradients in the field under study). In fact, when the recording system projects onto the plane of the knife edge the light aperture of diaphragm D_1 , this also introduces into the Foucault plane an additional "double knife edge."

In order that it do not effect the picture being taken, the edge of the Foucault knife edge and all the images of the light source, both deflected and nondeflected, should be contained inside the "double knife edge" opening.

/24

The general principles of the design of the optical system for connecting the SFR with shadow and interferometer instruments are presented in [54-56]. We shall describe an arrangement of a transfer system of SFR and IAB-451 instruments consisting of objective lenses I-13 ($F = 300$ mm) and RO-2 ($F = 75$ mm) [57, 58].

Objective lens I-13 is placed at a distance of 4-5 cm from the knife-edge plane, and objective lens RO-2 is placed at a distance from lens I-13 at such a distance that the image of the object under study be projected onto infinity. The SFR in the time-magnifier version with a two-row insert is placed so that the image of the illuminated slot be projected onto the middle of one of the apertures of diaphragm D_1 . The SFR is aimed at infinity. An image of a part of the field of view of the IAB-451 80 mm in diameter is recorded on a frame 10 mm in diameter. The output aperture of the IAB-451 is projected on diaphragm D_1 with a 4-fold reduction. If a double knife edge with a 3.6 mm opening between its edges is placed in the plane of the Foucault knife edge, then its image in the plane

of D_1 will be 0.9 mm wide. If then the width of the light aperture D_2 of each lens in the two-row insert is reduced to 1 mm, then with the frame dimension remaining 10 mm, the exposure of each frame will be reduced 4-fold. In each experiment one obtains 30 successive frames of the process; the frame diameter being 10 mm, an 8-fold reduction and an exposure time of 0.5 microseconds [sic].

By varying the focal distances of the objective lenses in the transfer system, it is possible to obtain the required reduction factor, since it is usually necessary to obtain on the film not the image of the entire field of view of the IAB-451, but only of a part of it.

When the MTO-500 and RO-2-12M objective lenses are used in the image-reduction arrangement, the reduction factor is ten. When the focal distance of lens O_3 is increased to 400 mm and lens O_4 has a focal distance of 50 mm, the image is reduced 4-fold.

The SFR camera was used primarily for recording schlieren pictures of the propagation of detonation waves. In some cases it was also used for study of processes in shock tubes (study of irregular reflection of shock waves).

5. Measuring the Flow Velocity in a Shock Tube by the Spark Method

One of the major variables which determine the state of the flow behind a shock wave in a shock tube is its velocity. It is precisely the flow velocity which is most sensitive to the increase of the boundary layer thickness in the shock wave's "plug."

We have used an electrical spark method for measuring the flow velocity, with the "marker" whose motion can be visualized and compared with the flow velocity being some volume of the gas heated by the electrical discharge (see, for example, [59-66]).

/25

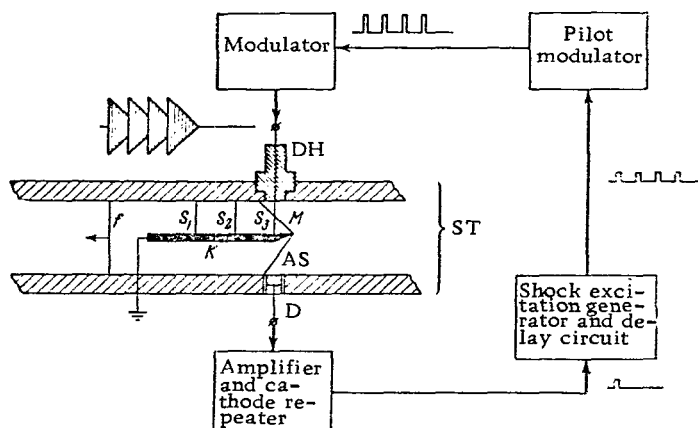


Figure 6. Schematic Diagram of a Setup for Measuring the Flow Velocity.

Measurement of the flow velocity with relatively high Mach numbers of the flow ($M_0 > 3$) is the subject matter of only several studies [60, 63, 65]. All these studies were performed in hypersonic wind tunnels. In this section we describe a technique for measuring the flow velocity by the spark method using a shock tube.

The schematic diagram of the setup is shown in Fig. 6. Here UT is the shock tube, f is the shock front, K is the half wedge, M is the Mach line, AS is the attached shock, D is the pressure pickup, DH is the discharge head through which is led out a high voltage (pulse-type) electrode, inserted flush with the chamber wall; the other electrode is either the half wedge placed in the flow, or an electrode placed in the chamber wall. The shock tube used had a square flow passage with dimensions of 40 by 40 mm. The half wedge was placed in the center of the flow passage so that the length of the discharge gap was 20 mm. Letters S_1 , S_2 and S_3 denote the positions of successive "striae", i.e., optical inhomogeneities. The striae are formed by the discharge in the moving plug behind the shock wave. The discharge frequency is selected so that at the time of a sequential discharge the preceding stria has moved through a sufficient distance from the discharge gap and each discharge would form a new stria.

At the instant when the shock wave passes, the pressure pickup puts out a signal which, after a preset delay, is supplied to the starter of the shock excitation generator. The delay of the pulse from the pickup is needed so that the shock front would move away at such a distance from the discharge gap for which the discharge would not be able to pass through the low-pressure quiescent gas ahead of the shock wave. On the other hand, it is undesirable that a stria would form before the shock wave arrives, since this increases the error of this method (see further on).

/26

The series of pulses from the shock excitation generator's output (the frequency and number of pulses can vary) is supplied to a pilot modulator. A series of rectangular pulses with an amplitude of about 1 kV is taken off the pilot output.

The modulator converts each pilot pulse into a "train" of high-voltage damped oscillations. The rate of attenuation of these oscillations depends on the magnitude of the input resistance, as well as on the existence or lack of existence of breakdown of the discharge gap.

To estimate the possible error of the electrical spark method in measuring the flow velocity, i.e., to estimate the difference between the velocity of the flow and of the thermal inhomogeneity, it is necessary to clarify the manner in which the instability of the flow affects the motion of the thermal inhomogeneity. Here we will give a solution for this, sufficiently characteristic case when the flow velocity varies linearly along the plug. The result of this analysis is somewhat different from that given in [67].

For sufficient completeness of presentation we are presenting here a brief discussion of the limits of applicability of starting equation (1.4) and show the

derivation from it of the known results (1.9) and (1.11) which are also of importance for the subsequent discussion (see also [61, 67]).

Let $u_s(t)$ be the velocity of the stria at the time t and $u(t)$ is the flow velocity in the section containing the stria. We shall assume that the thermal inhomogeneity is formed at $t = 0$. It will also be assumed that for sufficiently small t the following relationships apply:

$$M_s = (|v|/a) \ll 1, \quad (1.1)$$

$$\begin{aligned} Re_s = (|v|r/\nu) &\ll Re_{cr}, \\ Re_{cr} &\sim 10^3, \end{aligned} \quad (1.2)$$

where $v = u - u_s$, r is the characteristic dimension of the thermal inhomogeneity, a is the speed of sound in the flow and ν is the kinematic viscosity of the flow.

Assuming that $r \sim 10^{-1}$ cm and $\chi \sim \nu \sim 10^{-1}$ cm²/sec (χ is the thermal diffusivity), we arrive at the assertion that

$$\tau_q \sim (r^2/\chi) \gg \tau_0 \sim 10^{-2} \text{ secs}, \quad (1.3)$$

where τ_0 is the characteristic time of following the temperature inhomogeneity (stria) and τ_q is the characteristic time of thermal "spreading" (see [68], Section 51). /27

By virtue of Eqs. (1.1), (1.2) and (1.3) it is sensible to model the motion of a thermal inhomogeneity by the flow past a solid body of the same shape, regarding the liquid as incompressible, the flow as potential, disregarding the thermal conductivity and taking into account only the viscous resistance force. This modeling of the motion of an inhomogeneity is an asymptotic description of a kind which is the more valid, the smaller M_s and Re_s .

On these assumptions the motion of a thermal inhomogeneity is defined by Eq. (1.4), i.e., the equation of "associated" masses

$$M_s \frac{du_s}{dt} = F[u - u_s] + \rho V_s \frac{du}{dt}, \quad (1.4)$$

where M_s is the mass of the stria, V_s is its volume, ρ is the density of the flow and F is the resisting force.

Force F consists of the inertia part F_m and viscous force F_v . Force F_m is defined as

$$F_m = m \frac{d(u - u_s)}{dt}, \quad (1.5)$$

where m is an associated mass (in general a tensor). For the particular case when the thermal inhomogeneity is ball-shaped, F_v is given by the following expression (see [68], Section 24), where R is the radius of the ball

$$F_v = \frac{9m}{R} \left[\frac{vv}{R^2} + \sqrt{\frac{v}{\pi}} \int_{-\infty}^t \frac{dv}{d\tau} \frac{d\tau}{\sqrt{t-\tau}} \right], \quad (1.6)$$

$$m = (M_s / 2).$$

We now consider two manners in which the stria forms: 1) ahead of the shock front, in the quiescent low-pressure gas; 2) in the shock-wave plug. It will be assumed in both cases that the plug is ideal, i.e., that the flow variables along it are constant. Comparing (1.5) and (1.6) and having resort to initial conditions [see further Eqs. (1.8) and (1.10)], we can conclude that for sufficiently small t it is also possible to disregard the viscous resistance

$$|F_v| \ll |F_m|. \quad (1.7)$$

This conclusion obviously also applies for a cylindrical stria.

1. The initial condition is

$$\begin{aligned} u(t) &= u_0 \varepsilon(t), \\ \varepsilon(t) &= \begin{cases} 1, & t > 0 \\ 0, & t < 0, \end{cases} \\ u_s(t) &= 0, \quad t < 0 \end{aligned} \quad (1.8)$$

and the solution corresponding to it

/28

$$\begin{aligned} u_s(t) &= \lambda u_0 \varepsilon(t), \\ \lambda &= [(\rho V_s + m) / (M_s + m)]. \end{aligned} \quad (1.9)$$

2. The initial condition is

$$\begin{aligned} u(t) &= u_0 = \text{const}, \quad (t \geq 0), \\ u_s(0) &= v, \end{aligned} \quad (1.10)$$

and the solution corresponding to it

$$u_s(t) = u_0 = \text{const}. \quad (1.11)$$

Thus, in case 1 there exists a well-defined difference between the velocities of the inhomogeneity and the flow (proportional to the difference in densities). In case 2 the inhomogeneity accurately follows the flow (on the assumption of a plug with constant dimensions). Results (1.9) and (1.11) are known (see, for example, [61, 67]).

Solution (1.9), i.e., case of thermal inhomogeneity created ahead of the wave, is valid only for a sufficiently small difference in the densities of the inhomogeneity and the flow. Even in this case the solution is valid only for sufficiently small t . In fact, it is sufficient to point out that when $\text{Re}_s > \text{Re}_{cr}$, the potential flow past a thermal inhomogeneity as modeled by a solid body becomes hydrodynamically unstable and should be completed by turbulization of this inhomogeneity (see also [61]). Here a part of the energy of the relative motion dissipates and finally v , the relative velocity decreases. We note that [70] gives exact (numerical) solutions for the interaction of a shock wave with an inhomogeneity in an inviscid and nonconducting gas. These calculations are interesting by the fact that they make it possible to estimate the manner in which the inhomogeneity moves (for sufficiently small t) in the case when $v(0)$, the relative velocity is high and the simple approximation of "associated masses" is incorrect.

Let the inhomogeneity, as before, remain in the plug. But now we no longer assume that the flow velocity along the plug is constant, but that it varies linearly along the plug

$$\begin{aligned} u(x) &= ax + u_0, \\ x_s^+(0) &= 0, \\ a &= \text{const}, \end{aligned} \quad (1.12)$$

where x is the coordinate along the shock-wave plug.

This approximation is sufficiently satisfactory for the initial stage of motion of the thermal inhomogeneity. In addition, this approximation gives an overall qualitative idea about the manner in which the non-constancy of the flow velocity affects the motion of the inhomogeneity.

It is obviously true that

/29

$$\frac{du [x_s(t)]}{dt} = au_s. \quad (1.13)$$

Using the above expression it is easy to find the following solution for u_s

$$u_s = u_0 \exp [(\lambda a) t], \quad (1.14)$$

where λ is the same as in Eq. (1.9).

It can be seen from Eq. (1.14) that if, for example, the flow is accelerated (u_0 and a of the same sign) and if the density of the inhomogeneity is lower than that of the gas surrounding it, then the inhomogeneity leads the flow (see [67]). On the other hand, if for some t Re_s becomes greater than Re_{cr} , then starting with this t solution (1.14) becomes invalid (see a similar remark concerning solution (1.9)) and the relative velocity finally decreases.

It can be shown that from Eq. (1.14) there follows an expression for the relative error δ_s

$$\delta_s(t) = \frac{u_s - u}{u} = \left[\frac{1}{1 - \exp(-\lambda a t)} - 1 \right] \quad (1.15)$$

Thus, $\delta_s(t)$ increases monotonically from zero to $(\lambda - 1)$ with an increase in t . This result is different from that of [67], where the relative error increases to ∞ . The corresponding "relaxation" time can be defined as $(1/\lambda a)$

The actual value of λa is not known apriori. Hence Eq. (1.15) can be used only for estimating the lower boundary of that time t_Δ , during which the error is smaller than some Δ . For this we can take an overestimated a and λ (for example, $\lambda = \lambda_{max}$). Using this estimate for t_Δ it is possible to determine the error directly by means of an experiment (see below).

We now return to the question of the possible error in determining the flow velocity, i.e., what is the accuracy with which it is possible to measure the flow velocity in the point where a stria is found? This problem is equivalent to the following: with what precision is it possible to measure the position of a tangent to the stria at the point of its formation, where its velocity is identical with that of the flow? Under our conditions the trace of the stria, as a rule is rectilinear over the entire section over which it is observed. This assertion is obviously valid only within experimental error. It follows from this that either the velocity of the stria coincides with the flow velocity (within the experimental error), or "breakaway" of the stria velocity from the velocity of the flow takes place during a time $(1/\lambda a)$, which is small in comparison with the time scale of the scan (and hence this change is not noticeable on the scan). However, the

second possibility is eliminated by the actual estimate of the minimum value of $(1/\lambda a)$.

Thus, under conditions described above, the main contribution to the error is made by errors in measurement and not by actual leading of the flow by the spark [-induced] inhomogeneity.

The measurement errors, including the imprecision in determining the rate of rotation of the drum, etc., are about (2-4)%. On the other hand, the error of the method, i.e., the error due to the actual difference between the velocity of the flow and of the stria is smaller than 2%. In [65] the error in measuring the flow velocity by the spark method was estimated at 2% (see also the discussion of errors of the electric spark method in [67, 69]).

/30

By measuring the slopes of lines S^+ and S^- , corresponding to the motion of a weak shock wave which arrives on breakdown, down and up the flow, it is possible to determine the rate of propagation u^\pm of these disturbances. It is obvious that for sufficiently small disturbances $u^\pm = u + a$, where a is the velocity at which the front of the acoustic wave propagates. For sufficiently small M , when it is possible to disregard the acoustic dispersion, a is the speed of sound. Thus, under certain conditions the slope of lines S^+ and S^- can be used for determining the speed of sound (see [64]).

A scan of a stria formed in stationary air at atmospheric pressure is shown in Fig. 7. One can see the trace of the stationary stria and the traces of the disturbances due to the breakdown. Similar control experiments, which were performed with an output pulse at maximum, showed that the speed of sound, measured on the basis of the slope of lines corresponding to the motion of discharge disturbances coincides with the theoretical velocity, within the experimental error. This points to the fact that these disturbances have a relatively small amplitude and in its turn is related to the relatively small magnitude of the discharge capacitor (500 mmf). In the main series of experiments we have attempted to reduce the amplitude of disturbances to a minimum. For this the amplitude of the pulse supplied to the discharge head was reduced to that absolutely necessary for getting breakdown. Obviously, acoustic disturbances are always present, but in this case they are so small that they are not noticeable on photographic scans. These pictures sometimes also display lines which are called "polygons", i.e., traces of optical inhomogeneities which are apparently produced by fluctuations in the gas density (see [71]).

Under certain conditions the flow velocity can also be measured by these polygons. However, these polygons are much less clear than lines of artificial inhomogeneities, and this increases the error of measurements. In addition, sufficiently clear polygons are produced not with any shock-wave variables.

/31

6. Pressure Pickups

Pressure changes in the tube in which the shock waves propagated were recorded by means of piezoelectric pressure pickups. The sensitive element used in measuring the pressure was either barium titanate and TsTS ceramics.



Figure 7. Scanning Photograph of the Motion of a Thermal Inhomogeneity in Still Air; $p = 1$ atm.

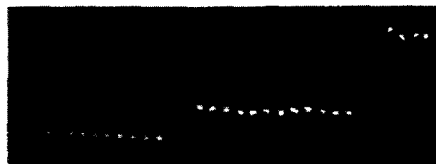


Figure 8. Oscillogram of the Pressure Behind a Shock Wave.

The pickups were produced as follows. The barium titanate ceramic was cemented to a zinc rod. The zinc and the ceramic have identical acoustic impedances due to which the wave, which is excited in the piezoelement by the pressure pulse attendant to the propagation along the axis of the piezoelement passes into the zinc rod without being reflected at the interface. This presents the possibility of inducing natural oscillations of the piezoelements. Use was made of barium titanate crystals from 10 to 1 mm in diameter and 2-10 mm high. For a wave propagating with the velocity of 2000 m/sec such pickup geometry ensures a time resolution of 5-1 microseconds, respectively. The zinc rod was about 15-20 cm long. In a rod of this size a deformation wave which is reflected from its end is returned to the piezoelement after 100-120 microseconds. The pickups using TsTS ceramics were provided with brass wave path [instead of the zinc rod].

The surface of the piezoelement and of the rod were carefully polished to match one another and were cemented together by the BF-2 cement. The rod together with the crystal was placed into a metal housing. The space between the housing and the rod was filled with a substance with a good capability for absorbing deformation waves, i.e., rubber, wax, cork, polyfluoroethylene resin or foam plastic.

The piezoelement maintained electrical contact with the housing by means of a wire soldered to the metallized base of the element. The positive charge was taken off the zinc rod. An example of an oscillogram of the pressure behind a shock wave is depicted in Fig. 8.

The pressure pickups were calibrated by weak shock waves ($M = 1.5-3$) with initial pressures of about 0.5-1 atm.

/32

The pickup readings were used primarily to study the manner in which the pressure behind the shock wave changes and for determining the time at which the shock wave arrives at a given point in the tube. One can familiarize oneself with different designs of pressure pickups, the technology of producing them and techniques of calibrating and operating them by reference to [72-77].

7. Measuring the Surface Temperature of the Shock-Tube Walls

The shock wave interacts with the shock tube walls during a very short time interval (about several microseconds), for which reason the instrument for measuring the heat flux should be highly sensitive and have a low inertia, such that it would succeed in "following" the changes in the surface temperature which takes place during 1 microsecond. For this we used a thin conducting film as a resistance thermometer. In order to measure the varying surface of the body the film should be so thin that its temperature be identical with the surface temperature with a satisfactory accuracy. It is known from the theory of thin films that, starting with some known thickness of film, specified physical parameters of the film and the backing layer, it is possible to regard the film temperature as the sought temperature of the surface, disregarding the temperature gradient across the thickness of the film.

The theory of thin-film resistance thermometers reduces to solving and analyzing the problem of finding the temperature field of a plate and a semiinfinite body which are in contact.

To solve the problem, [78] introduces the following assumptions: 1) the problem is one-dimensional; 2) the thermal coefficients of both bodies are specified and do not depend on the temperature. Let us assume that, starting with some time, the system is heated on the free surface of the plate by a thermal flux q_0 . It is required to solve the boundary-value problem

$$\frac{\partial T_m}{\partial t} = a_m \frac{\partial^2 T_m}{\partial x^2} \quad (t > 0, \quad 0 > x > -l), \quad (1.16)$$

$$\frac{\partial T_i}{\partial t} = a_i \frac{\partial^2 T_i}{\partial x^2} \quad (t > 0, \quad x > 0), \quad (1.17)$$

$$T_m(x, 0) = T_i(x, 0) = 0, \quad (1.18)$$

$$T_i(\infty, t) = 0 \quad (t \geq 0), \quad (1.19)$$

$$T_m(0, t) = T_i(0, t), \quad (1.20)$$

$$\frac{\lambda_m}{\lambda_i} \frac{\partial T_m(0, t)}{\partial x} = \frac{\partial T_i(0, t)}{\partial x}, \quad (1.21) \quad \underline{/33}$$

$$\lambda_m \frac{\partial T_m(-lt)}{\partial x} + q = 0, \quad (1.22)$$

where a is the thermal diffusivity, λ is the thermal conductivity, T is the temperature, t is the time, x is the direction of heat propagation and l is the thickness of the metal plate. Subscript m refers to the metal plate and subscript i refers to the backing.

The solution is obtained by the operator method. The resulting expressions are:

1) for the temperature field of the semiinfinite body

$$T_i(x, t) = \frac{4q_0 \sqrt{a_i t} z}{\lambda_i (1+z)} \sum_{n=0}^{\infty} \left(\frac{1-z}{1+z} \right)^n i \operatorname{erfc} \frac{1}{2} \times \\ \times \left[\frac{(2n+1) l / \sqrt{a_m} + \frac{x}{\sqrt{a_i}}}{\sqrt{t}} \right] \quad (1.23)$$

2) for the temperature of the plate

$$T_m(x, t) = \frac{2q_0 \sqrt{a_i t} z (1-z)}{\lambda_i (1+z)} \sum_{n=0}^{\infty} \left(\frac{1-z}{1+z} \right)^n i \operatorname{erfc} \frac{1}{2} \left[\frac{2nl - (x-l)}{\sqrt{a_m t}} \right] + \\ + \frac{2q_0 \sqrt{a_i t} z}{\lambda_i} \sum_{n=0}^{\infty} \left(\frac{1-z}{1+z} \right)^n i \operatorname{erfc} \frac{1}{2} \left[\frac{2nl + l + x}{\sqrt{a_m t}} \right] \quad (1.24)$$

Here $z = \sqrt{\frac{\lambda_i c_i \rho_i}{\lambda_m c_m \rho_m}} = \frac{\varepsilon_i}{\varepsilon_m}$ is the plate's thermal activity coefficient, c is the specific heat and ρ is the density of the medium.

The problem was solved for $z < 1$. The contact temperature is determined at $x = 0$. It has the form

$$T_b = T_i(0, t) = T_m(0, t) = \frac{4q_0 \sqrt{a_i t}}{\lambda_i (1+z)} \sum_{n=0}^{\infty} \left(\frac{1-z}{1+z} \right)^n i \operatorname{erfc} \frac{2n+1}{2F_0}, \quad (1.25)$$

where $F_0 = \frac{a_m t}{l^2}$.

The temperature of the free surface of the plate is determined from

$$T_0 = T_m(-l, t) = \frac{2q_0 \sqrt{at} z (1-z)}{\lambda_i (1+z)} \sum_{n=0}^{\infty} \left(\frac{1-z}{1+z} \right)^n i \operatorname{erfc} \frac{n+1}{\sqrt{F_0}} + \\ + \frac{2q_0 \sqrt{at} z}{\lambda_i} \sum_{n=0}^{\infty} \left(\frac{1-z}{1+z} \right)^n i \operatorname{erfc} n \sqrt{F_0} \quad (1.26)$$

The temperatures of both sides of the film are practically identical at any given time when the value of F_0 is such that it is possible to disregard the temperature gradient across the film's thickness and to assume that the contact temperature is the same as the temperature of any point of the film with sufficient accuracy. When $F_0 > 200$ the temperature over the thickness of the film is equalized almost instantaneously and consequently, the film temperature represents the surface temperature of its backing. Thus, for platinum films about 0.1 microns and less thick the temperatures of both sides become equalized within 0.01 microseconds.

Various methods are available for producing film-type resistance thermometers [79]. Use is made for this purpose of Ni, Au, Pt, Ag and Cu. We have used platinum resistance thermometers. The pickup body was made from BD-1 glass. The platinum-glass pair was selected due to identical coefficients of linear expansion of these materials, since otherwise the film could be destroyed while applied and while heated due to thermal stresses.

Platinum leadouts were soldered into the glass body of the pickup, and a thin film was applied by chemical deposition at elevated temperature between the leadouts onto a well-ground surface. The starting material was a platinum-coating paste consisting of chloroplatinic acid, lavender and rosemary oils in the following proportions: 1 mm³ of crystalline chloroplatinic acid, 3 drops of lavender and 4 drops of rosemary oils. The technology for applying thin films was developed by E. A. Mit'kina and Yu. G. Polyakov of the LFG ENIN [Leningrad Branch of the G. M. Krzhizhanovskiy State Power Engineering Institute] [79].

A thin layer of the paste is applied to the degreased and dried backing surface. The density of the paste should be such that the strip should spread. The vaporation of solvents and deposition of the platinum starts with raising the gas burner. The heating is ceased when a shiny deposit appears. The film acquires conductivity. Then the air supply is increased and the flame temperature is raised. A narrow tongue of flame is directed onto the film and the annealing process is started. The platinum becomes sintered into the softened glass thus forming a strong film.

The pickups were calibrated by the stationary method by heating them in a furnace. Their resistance at different temperature was determined by a White-stone bridge to within 0.010 ohms.

The measuring circuit of the pickup is shown in Fig. 9. The resistance thermometer is connected into the circuit in series with an additional resistance R_h which is selected so as to ensure linearity between the amplitude of the electrical pulse and the variation in the film temperature.

The voltage from the load resistance is fed to an OK-17M or IO-4 oscillograph through an amplifier with amplification of $K = 40$.

/35

The change in voltage ΔU on heating the film resistance thermometer is expressed as

$$\Delta U = I_1 R_p - I_2 (R_p + \Delta R),$$

where R_p is the pickup resistance before heating; $I_1 = E / (R_p + R_h)$ is the pickup current before heating, while $I_2 = E / (R_p + R_h + \Delta R)$ is the current through the pickup after heating. Substituting the expressions for I_1 and I_2 into the expression for ΔU , we get

$$\begin{aligned} \Delta U &= -\frac{E}{R_p + R_h} R_h + \frac{E}{R_p + R_h + \Delta R} (R_p + \Delta R) = \\ &= \frac{E \Delta R R_h}{(R_p + R_h)^2 \left(1 + \frac{\Delta R}{R_p + R_h}\right)}. \end{aligned} \quad (1.27)$$

Since $R / (R_h + R_p) \ll 1$, this quantity can be disregarded. $\Delta R = R_0 \alpha \Delta t$, hence $\Delta U = f(\Delta t)$ is a linear function of the temperature variations, since for a given pickup E , R , R_h and R_p are constant. Knowing them it is possible to determine variations in the film temperature by changes in the voltage. In our experiments the circuit parameters were: $R_p \simeq R_0 = 40-100$ ohms, $R_h = 100$ ohms and $E = 1.25$ V.

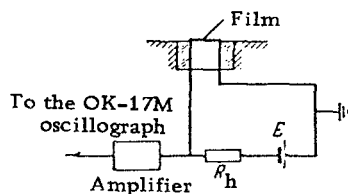


Figure 9. Measuring Circuit of the Resistance Thermometer.

If a body's temperature is known, then in principle it is possible to determine the heat flux into the body. Due to the short experimental time, the pickup body of the shock tube wall may be regarded as equivalent to a semiinfinite body, when the heat flux is determined from

$$q(\tau) = \frac{\lambda_i}{\sqrt{\pi a_i}} \int_0^\infty \frac{d\varphi(\kappa)}{d\kappa} \frac{d\kappa}{(\tau - \kappa)^{3/2}}, \quad (1.28)$$

where $\varphi(\kappa)$ is the time dependence of the surface temperature, λ_i , and a_i are the

the thermal coefficients of the wall [conductivity and diffusivity], τ is the time and x is the variable of integration.

When using resistance thermometers one must analyze the effect of the specific heat of the film on the heat transfer, since the quantity of heat accumulated by the film during the transfer process will have an appreciable effect on the error in calculating the heat flux. A heat flux calculated from a formula for a semiinfinite rod varies depending on the time instant from the start of heat transfer at which the resistance thermometer's readings are recorded.

/36

During the first 3 microseconds from the time the pickup's heating is started almost all the heat received by the latter is accumulated in the film. About 2-5 microseconds later only 7-8% of the total amount of heat remains in the film, all the remaining heat being distributed along the glass backing. Consequently, the problem of heating up the pickup can be replaced with sufficient accuracy by the problem of heating up a semiinfinite rod (the glass backing) with constant thermophysical properties, if the time dependence of the temperature at its boundary is known only for times greater than 3 microseconds from the start of heating. The equivalence of these two problems is considered in detail in [78].

Formula (1.28) is inconvenient for practical use, since it requires numerical solution of the integral.

Sometimes the temperature curve is approximated by an n th degree polynomial or by a summation of exponents. We have calculated the heat flux by expanding the integral in a series in terms of time intervals during which the surface temperature is regarded as constant and equal to the average temperature at the given section.

Thus, resistance thermometers make it possible to measure the heat flux into the shock-tube wall and to judge about the magnitude of heat losses which take place on propagation of the wave along the tube and on its reflection from the end of the tube.

8. Microwave Measurement of Electrophysical Variables in the Gas Behind a Shock Wave

The conductivity and dielectric constant or the concentration of free electrons and the frequency of their collision with the gas particles are among the more important electrophysical characteristics of a gas heated by a shock wave. Measuring of these variables by probe, magnetic induction, resonator or waveguide methods involves a number of difficulties, which are characteristic of work with shock tubes [80, 81].

Methods most suitable for this purpose, i.e., such which ensure good resolution in space and time, do not introduce gasdynamic disturbances into the flow and do not effect on the velocity distribution of electrons, is probing by centimeter and millimeter radiowaves of low intensity (about 10^{-6} watts/cm²) in free space. The range of variation of electron concentrations is 10^9 - 10^{14} electrons per cm³.

/37

By measuring the absorption coefficient for radiowaves at two frequencies in ionized gas it is possible to determine simultaneously and independently such characteristics as the electron concentration and effective frequency of elastic collisions between electrons and gas particles [82]. These two variables in their turn determine the d-c conductivity of the gas. This circumstance serves as the basis of the method used.

The absorption coefficient of radiowaves was measured simultaneously using the wavelength pairs of 3.4 and 1.8 cm or 1.6 and 0.8 cm (Fig. 10). Each radio channel consisted of a low-power klystron generator, first isolating attenuator, dielectric narrow-beam transmitting antenna, two dielectric focusing lenses, precision calibrating and second isolating attenuators, detecting unit and recording apparatus (Fig. 11).

Wavelengths of 3.4 and 1.8 cm were generated by the 51-I and GS-627 generators, while the GS-702 and GS-701 were used for generating the 1.6 and 0.8 cm waves. The calibrating generator in the channel for the 0.8 cm wave was the D5-8, the isolating attenuator was the AVR0812/20, while the signal was detected by the DS-0812 unit. The superhigh frequency signal when using the 3.4 [sic] cm wavelength was rectified using DK-I2 crystals, with the D403 used for the 1.8 cm, the D601B for the 1.6 cm and the D601A for the 0.8 cm wave.

Each crystal had a load resistance of 630 ohms, which is equal to the input resistance of the calibrating instrument which was used in reading the crystal's characteristics.

In adjusting the radio channels particular attention was paid to obtaining the best [possible] resolution in space and time and of a beam which would be as parallel as possible. This was obtained using specially designed (according to [83]) dielectric (polystyrene) transmitting antennas and focusing lenses from the same material. For operation in the three-centimeter range the transmitting antenna had the following dimensions: $L = 200$ mm, $d_{\max} = 17$ mm, d_{\min} [sic] $= 10$ mm, which made it possible to obtain a narrow directionarily diagram with an opening angle of 24.5° with side lobes at minimum power. In addition, the ratio beam leaving such an antenna not only diverged very little, but also had a small cross section. A narrow parallel beam was obtained by focusing the beam by a lens. The beam's dimensions were determined using a sheet from a special material which absorbs well radio radiation. A check was made in the measuring section of the completely assembled radio channel [84].

The absorbing sheet was placed inside the organic glass section first along the forward (relative to the generator) wall of the section. As the radio beam was increasingly more covered by the absorbing sheet, which can be regarded as an imitation of a fully absorbing gas, the readings of the indicator connected to the detector unit changed. Knowing the characteristics of the crystal it was possible to determine the variation in intensity as a function of the amount by which the beam was covered. Having determined the intensity distribution in the beam by moving the sheet over different cross sections of the beam, it is possible to determine its cross sectional dimensions and the degree of parallelism.

/38

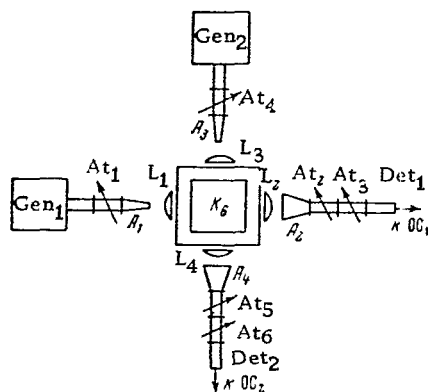


Figure 10. Microwave Measuring Unit.

Using the 3.4 cm wave (with the previously described transmitting antenna) it was possible to obtain a radio beam with an effective size of 30 mm. The term effective size denotes that cross sectional dimension of the beam the covering of which absorbs 90% of the intensity, thus preventing it from arriving at the pickup.

When measuring the absorption of radiowaves simultaneously on the 1.6 and 0.8 cm frequencies behind reflected shock waves, the dimensions of both beams were made identical along the axis of the tube and equal to 20 mm. The divergence of beam due to lack of parallelism, obtained by comparing the effective dimensions at the forward and back walls of the chamber was 1 mm.

The radio beams had elliptical cross sections, which was taken into account when adjusting the channels. The viewing test section was made from an integral piece of organic glass; it was 250 mm long and the inside duct dimensions were 7 x 7 cm. To reduce the reflection of radio waves the wall thickness was made a multiple of an integral number of wave halves in the given material. In run-in experiments we have also used metal viewing test sections with large polyfluoroethylene and glass windows.

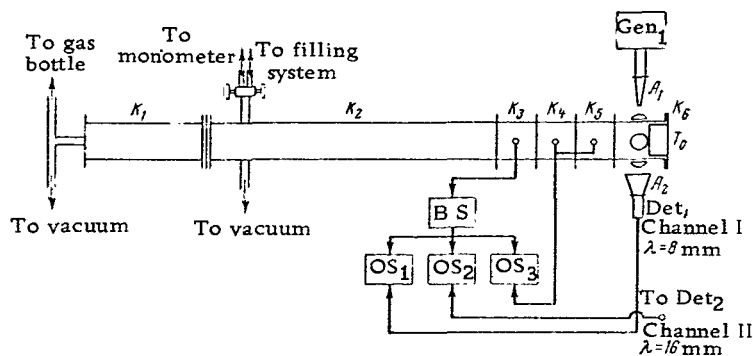


Figure 11. Schematic of Setup For Measuring the Absorption of Radio Waves.

Adjustment of the microwave channel consisted in obtaining the smallest possible standing-wave ratio (SWR) of the voltage in the transmitting line, obtaining a narrowly-focused radio beam, focusing it onto the receiving antenna, reducing SWR of the receiving line to a minimum and tuning the detector unit.

The transmission line (generator, waveguide, antenna) was tuned by placing an output meter line between the generator (with the attenuation in At_1 at about

5 db) and the final waveguide with the antenna (see Fig. 11). This instrument measured the SWR with the antenna submerged to different depths into the waveguide. A position was sought in which the SWR was at minimum, which corresponded to the best radiation conditions. The radio beam was focused by moving the transmission line together with the generator along the beam. The receiving channel was tuned similarly on the basis of maximum readings of a pointer-type indicator, connected to the detecting unit. The receiving antennas were horn units with a wider directionality diagram than the transmitting antennas. An output meter line was placed between At_2 and At_3 for tuning the receiving channel. The minimum possible SWR was obtained by varying, by means of isolating attenuator At_3 the damping in the system. The SWR in the receiving system should not exceed 1.25, since multiple reflections may highly distort the received signal. A sufficiently low SWR, equal to 1.07 was found when the attenuation in the isolating attenuator was about 10 db.

In studies of processes behind incident shock wave the microwave generators operated continuously. To mark the total absorption level, a rectangular pulse 10 microseconds in duration and with an amplitude of 40 V was supplied to the generator's modulator 50 microseconds before starting up the scanning of the recording oscillograph. This pulse interrupted the generating regime of the klystron for 10 microseconds and mark of the total absorption level. This mark is needed due to the moderate drifting of the level of the signal put out by the generator. When performing measurements behind reflected shock waves, the microwave generators operated in the regime of modulation by rectangular pulses produced by the GIP-2 generator. The duration of its signals was about 20 microseconds with an amplitude of 40 V. In this case the curve of absorption of the radiowaves is included between two lines, the upper being the total absorption line and the lower being the total transmission line. /40

The crystal detectors, which used 630 ohm load resistances, operated at currents of 50 microamps. This provided for a sufficiently high level of the signal being measured above the noise, although this removed the crystals from the square mode [of operation]. The receiver was calibrated by measuring the characteristics of detectors by means of the measuring attenuators and setting up a relationship between the current through the crystals (in milliamps) and the attenuation which is introduced (in db).

When the relationship between the deflection of the beam on the oscillograph and the current through the detector is linear, the calibrating curve can be used for comparing the amplitude measured on the photographic film with the radio signal attenuation. The crystal characteristics were checked with currents of 50 microamps after each series of experiments, since they changes somewhat with time. The strength of the signal fed to the receiver was maintained constant for which reason also the current through the crystal was constant all the time (with the exception of the time of the experiment). The detector also operated within the limits of its characteristic, i.e., the maximum current did not exceed 50 microamps. The signal from the detector was fed to a cathode repeater, was amplified in a video amplifier and supplied to the input of an IO-4 oscillograph.

The absorption oscillograms were processed using a tool-maker's microscope. The accuracy of reading amplitudes was limited by the line thickness and was not less than 2% (with the exception of the very small amplitudes). The measurement of attenuation on the measuring attenuator's scale was within 2.9-3%. Thus, the overall accuracy of measuring the absorption amplitude was about 5%.

Study of Conditions for Interaction Between Radio Waves and the Ionized Gas

The purpose of these studies consisted in clarifying the role of the material of test-chamber walls in the interaction between the radio waves and the ionized gas and in clarifying the manner in which the radio waves propagate (consideration of front distortion). It is also necessary to clarify the effect of radio-wave reflection on the absorption coefficient which is measured.

The effect of wall material was determined behind incident shock waves in air and argon in three series-connected chambers: 1) in chambers with windows from K-8 optical glass; 2) with polyfluoroethylene windows and 3) in a chamber made entirely from organic glass. The measurements were made with a 3 cm wavelength, using two identical microwave channels situated in sequence along the direction of the shock wave propagation. First we used chambers with polyfluoroethylene and glass windows (first series of experiments), and then the chamber with glass windows and the one made from organic glass (second series). The distance between the axes of radio beams in both cases was 250 mm. The results of measuring the absorption of radio waves at the same frequency show that the absorption curves in each pair are well reproducible with a divergence of less than 5%. This divergence is less than the difference in absorption in a single channel using the same initial pressure and shock wave velocity between one experiment and another.

/41

The absorption of radio waves was thus found to be independent (within the precision limits of our apparatus) of the material of windows of the test sections, and is determined [solely] by the parameters of the ionized gas.

During the experiments we have studied the effect of radio-beam defocusing on the coefficient of its absorption by ionized gas. These experiments were made behind incident shock waves using a 3 cm wave and three versions of receiving and transmitting antennas. To compare the absorption magnitudes we have created identical conditions: pressure p_0 ahead of the shock waves in air was 1 mm of Hg and $M_0 = 10$. In the first version standard horn antennas were used for receiving and transmitting, in version 2 use was made of two conical antennas from polystyrene, while the 3rd version used two conical polystyrene antennas with two focusing lenses. The beam was best focused and most parallel in the 3rd version. In this case it is possible to regard the radio wave as plane inside the test section and being normally incident onto the layers of the ionized gas. In the second version the beam was divergent, but sufficiently narrow, while in the 1st version the beam was both divergent and wide.

These experiments have shown that the absorption coefficient for radio waves was lowest in the 3rd version. In the 2nd version it systematically

exceeded the value of the 3rd version by 20%, while in the 1st version it exceeded that of the 3rd version two-fold. If the probing beam differed highly from a plane electromagnetic wave, then there existed a fictional and sometimes appreciable absorption which was apparently due to scatter. The system consisting of dielectric antennas and focusing lenses upon proper tuning has made it possible to obtain a sufficiently plane electromagnetic wave.

To study the effect of reflection of radiowaves by the ionized gas on the absorption coefficient which was measured, we have reflection coefficients R and simultaneously with this the absorptions of radiowaves with the frequency of 18,750 Megacycles. The experiments were performed behind reflected shock waves in air with initial pressures p_0 of 2 and 5 mm of Hg, $M_0 = 6.6-8.15$, in argon with p_0 of 2.5 and 10 mm of Hg and $M_0 = 4.4-7.8$.

The $R = 1$ level in our experiments was the signal reflected from the surface of a copper piston placed into the viewing-section passage, which approximated a medium with a perfectly reflecting boundary. Since the ionized gas is homogeneous in the direction of propagation, it was assumed in our calculations that the reflection takes place only from the forward boundary of the ionized gas relative to the radiator.

Oscillograms of absorption and reflection in air behind a reflected wave show that, although these waves are absorbed entirely, the level of the reflected intensity is quite small ($|R|^2 = 0.027$).

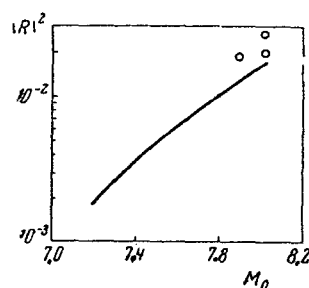


Figure 12. Comparison of Experimental Data For the Reflection Coefficient for 16 mm Radio Waves by Air Behind a Reflected Shock Wave For an Initial Pressure $p_0 = 2$ mm of Hg.

[85] are compared in Fig. 12.

An oscillogram of the reflection of radiowaves by argon heated by a reflected shock wave to approximately $10\,000^\circ\text{K}$, is presented in Fig. 13. In this case the waves are reflected completely.

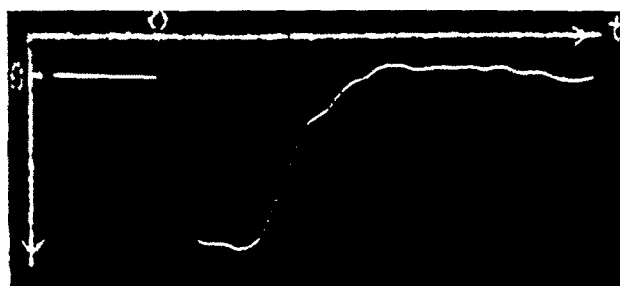


Figure 13. Oscillogram of the Reflection of 16 mm Radio Waves from Argon Behind a Reflected Shock Wave With $p_0 = 2$ mm of Hg, $M_0 = 7$.

In the case of $M_0 < 7.9$ the reflection was always weak, i.e., $|R|^2 < 0.027$. The experimental values (points) and the theoretical curve

Measurements show that up to 4000°K and a pressure of 1.7 atm the reflection coefficient did not exceed 0.027 and the absorption coefficient was equal to unity. On the other hand, in argon the reflection coefficient is appreciable even when the absorption coefficient is less than unity.

In addition to measuring the absorption and reflection coefficient for radio waves, we have also measured the self-radiation of gases heated by a shock wave using an 0.8 cm wave. For this we have used a superheterodyne laboratory radiometer with a passband of 30 Megacycles with a noise level corresponding a temperature of 1500°K in the pulsating regime. The GSh-6 gas-discharge noise generator was used as a calibrating standard. When calibrating, a dielectric plate, analogous to the material of the viewing-section window, was placed between the emitting horn of the generator and the receiving horn of the radiometer. The noise generator operated in the pulse regime with a pulse frequency of 1 kcps.

Calculating the Electrophysical Variables of a Gas on the Basis of Experimentally Measured Coefficients of absorption of Radio Waves of Two Frequencies

The refractive and absorption indexes of a plane harmonic radiowave which is normally incident onto a layer of a homogeneous weakly-ionized gas are related to the conductivity σ and dielectric permeability ϵ of this gas [82]. The concentration n_e of free electrons and their collision frequency ν with neutral particles depends on σ and ϵ .

One of the methods of independent determination of n_e and ν is measuring the absorption of radio waves at two different frequencies ω_1 and ω_2 . The conductivity is determined by the well-known expression [82]

$$\sigma = \frac{n_e e^2 \nu}{m_e (\omega^2 - \nu^2)} = 0.25 \cdot 10^9 \frac{n_e \nu}{\omega^2 - \nu^2}. \quad (1.29)$$

For a relatively low density n_e behind a shock wave ($4\pi\sigma \ll \epsilon\omega$) the attenuation coefficient δ for radio waves is [82]

$$\delta = \frac{4\pi\sigma}{c \sqrt{\epsilon}} \quad (1.30)$$

where c is the speed of sound;

$$\epsilon = 1 - \frac{4\pi n_e}{m_e (\omega^2 - \nu^2)} = 1 - 0.3 \cdot 10^{10} \frac{n_e}{\omega^2 - \nu^2}. \quad (1.31)$$

From Eqs. (1.29) through (1.31) one can obtain the following relationship between the absorption indexes δ_1 and δ_2 of radio waves with frequencies ω_1 and ω_2 and the plasma variables n_e and v :

/44

$$\begin{aligned}\delta_1 &= 0.1 \frac{vn_e}{\omega_1^2 + v^2} \cdot \frac{1}{\sqrt{1 - 0.3 \cdot 10^{10} \frac{n_e}{\omega_1^2 + v^2}}}, \\ \delta_2 &= 0.1 \frac{vn_e}{\omega_2^2 + v^2} \cdot \frac{1}{\sqrt{1 - 0.3 \cdot 10^{10} \frac{n_e}{\omega_2^2 + v^2}}}.\end{aligned}\quad (1.32)$$

System of equations (1.32) uniquely defines the values of n_e and v , if δ_1 , δ_2 , ω_1 and ω_2 are known. However, it is in general quite difficult to solve this system. We shall now consider a simplification of this system for a case when the second term in the expression for ε is small as compared with unity. This simplification can be made even before knowing the values of the quantities entering Eq. (1.31), since the second term is smaller than unity as long as ε is positive. If, however, this term becomes greater than unity, then ε cannot be measured since then the radio waves are reflected totally and Eqs. (1.32) are no longer valid.

In the case when $0.3 \cdot 10^{10} n_e (\omega^2 + v^2) \ll 1$, the radicand in Eq. (1.32) can be expanded in a power series and, by approximately determining the root, the expressions for δ take on the form

$$\delta_1 \cong 0.1 \frac{vn_e}{\omega_1^2 + v^2} \left(1 + \frac{3}{2} \cdot 10^9 \frac{n_e}{\omega_1^2 + v^2} + \dots \right), \quad (1.33)$$

$$\delta_2 \cong 0.1 \frac{vn_e}{\omega_2^2 + v^2} \left(1 + \frac{3}{2} \cdot 10^9 \frac{n_e}{\omega_2^2 + v^2} + \dots \right). \quad (1.34)$$

Using the above two expressions one can easily determine n_e as an explicit function of v , ω_1 , ω_2 , δ_1 and δ_2

$$n_e = \frac{[\delta_2 (\omega_2^2 + v^2) - \delta_1 (\omega_1^2 + v^2)] (\omega_1^2 + v^2) (\omega_2^2 + v^2)}{0.15 \cdot 10^{10} [\delta_1 (\omega_1^2 + v^2)^2 - \delta_2 (\omega_2^2 + v^2)^2]}. \quad (1.35)$$

Substitution of n_e from Eq. (1.35) into Eq. (1.34) determines the relationship between the sought quantity v and the experimentally determined δ_1 and δ_2 . For processing a large number of experiments it is possible to construct a nomogram of v as a function of δ_1 and δ_2 . To determine v for one pair of values of δ_1 and δ_2 we have solved the system of equations (1.33)–(1.35) using successive approximations.

Specifying some value of v from the zero approximation ($\epsilon = 1$), we find the value of n_e from Eq. (1.35). Then we substitute this value into Eq. (1.34) and check whether it satisfies this equation. This is repeated until v and n_e are found which satisfy Eqs. (1.34) and (1.35) with the desired accuracy.

/45

In the general case the error in determining v and n_e on the basis of δ_1 and δ_2 measured to within $\Delta\delta_1$ and $\Delta\delta_2$ is

$$\Delta v = \frac{(\omega_1^2 + v^2)(\omega_2^2 + v^2)[(\omega_1^2 + v^2)\Delta\delta_1 - (\omega_2^2 + v^2)\Delta\delta_2]}{0.01 \cdot n_e \cdot 2v^2(\omega_1^2 + \omega_2^2)}, \quad (1.36)$$

$$\Delta n_e = \frac{\Delta\delta_2(\omega_1^2 + v^2)(\omega_2^2 + v^2) - \Delta\delta_1(\omega_2^2 + v^2)(\omega_1^2 + v^2)}{0.01 \cdot 2v^3(\omega_1^2 + \omega_2^2)}. \quad (1.37)$$

The values of δ_1 and δ_2 could be measured in our experiments within 3–5%. This accuracy is lower than that with which δ is calculated from Eq. (1.33) even when first-order infinitesimals are taken into account; for which reason for processing results in this given range of variables and for error analysis one may use the formulas of the zero approximation

$$v^2 = \frac{\delta_2\omega_2^2 - \delta_1\omega_1^2}{\delta_1 - \delta_2}, \quad (1.38)$$

$$n_e = 9.4 \frac{\delta_1(\omega_1^2 + v^2)}{v}. \quad (1.39)$$

The greatest relative error in determining v and n_e behind a reflected shock wave is, for example, for $M_0 = 6.6$, $E_0 = 0.2$ and $E_{n_e} = 0.3$.

Since the equilibrium degree of ionization of air when the temperature is varied from 3000 to 5000° varies by several orders of magnitude and the possible variation in the electron concentration in the nonequilibrium zone is also of several orders of magnitude, the accuracy of experimental measurement of v and n_e is satisfactory.

When the radio-wave attenuation magnitude in our experiments became quite high (up to 25 db) it became necessary to calculate n_e , v and σ_0 from complete equations, without any simplifications

$$\delta = \frac{2\omega}{c} \kappa, \quad (1.40)$$

where

$$\kappa = \sqrt{-\frac{\varepsilon}{2}} + \sqrt{\left(\frac{\varepsilon}{2}\right)^2 + \left(\frac{2.15}{\omega}\right)^2}, \quad (1.41)$$

$$\sigma_0 = 2.5 \cdot 10^8 \frac{n_e}{v} = \sigma \frac{\omega^2 + v^2}{v^2}. \quad (1.42)$$

In our case Eqs. (1.40)-(1.42) for two values of δ_1 and δ_2 measured with 8 and 16 mm waves were successfully reduced to the two equations

/46

$$\begin{aligned} 4.1\delta_1(1+x^2)(\sqrt{0.004\delta_1^2+x^2}-0.06\delta_1) = \\ = \delta_2(1+4x^2)(\sqrt{0.016\delta_2^2+x^2}-0.06\delta_2), \end{aligned} \quad (1.43)$$

where

$$\begin{aligned} x = \frac{v}{2.36 \cdot 10^{11}}, \quad \omega_1 = 2.36 \cdot 10^{11}, \quad \omega_2 = 1.18 \cdot 10^{11}, \\ \sigma_0 = 0.24 \cdot 10^{10} \delta_1 \frac{1+x^2}{x^3} (\sqrt{0.004\delta_1^2+x^2}-0.06\delta_1). \end{aligned} \quad (1.44)$$

The electron concentration is determined from Eq. (1.42).

It is expedient to estimate the maximum values of n_e and σ_0 , which can be measured using this method in the wavelength range of 1.6 and 0.8 cm.

The maximum electron concentration is determined from

$$\varepsilon = 1 - 3.19 \cdot 10^9 \frac{(n_e)_{\max}}{\omega^2 + v^2} = 0. \quad (1.45)$$

Whence

$$\begin{aligned} (n_e)_{\max} &= 3.14 \cdot 10^{-10} (\omega^2 + v^2), \\ (\sigma_0)_{\max} &= 2.54 \cdot 10^8 \frac{(n_e)_{\max}}{v}. \end{aligned}$$

The values of $(n_e)_{\max}$ and $(\sigma_0)_{\max}$ for the range of effective collision frequencies encountered in practice, with a minimum frequency of 18,750 Megacps are presented below

$\nu, 1/\text{sec} \dots$	$0.5 \cdot 10^{11}$	10^{11}	$5 \cdot 10^{11}$
$(n_e)_{\max} \text{ cm}^{-3} \dots$	$5.2 \cdot 10^{12}$	$7.5 \cdot 10^{12}$	$8.3 \cdot 10^{13}$
$(\sigma_0)_{\max}, \text{ mho/m} \dots$	2.9	2.1	4.7

Thus, for a gas conductivity of less than 1 mho/m the measurements are performed in a region far from the limit.

CHAPTER 2

DEVIATION OF THE FLOW IN A SHOCK TUBE FROM THE IDEAL WITHOUT CONSIDERATION OF THE PHYSICOCHEMICAL TRANSFORMATIONS IN THE GAS

The limited volume in which the shock wave is forced to propagate in a shock tube results in the fact that the flow behind a plane shock wave is not one-dimensional. The interaction between the flow of gas carried away by the shock wave and the shock-tube wall results in the appearance of a boundary layer at the tube walls. Methods of calculating the boundary layer are presented in a large number of publications. Usually in calculating the boundary layer it is assumed that the pressure in the direction perpendicular to the wall is constant and that the velocity and gas-temperature fields in the wall-adjointing region are [self] similar. In calculating a boundary layer which arises in a flow about an infinite plate it is usually assumed that the appearance of the boundary layer does not affect the variables of the main body of the flow, which can be situated at any great distance from the disturbed region.

/47

The formation of a boundary layer in a gas flowing behind a shock wave in a shock tube has its peculiar features. As the shock wave propagates the motion embraces increasingly new masses of the gas, with different sections of the flow behind the shock wave participating in the motion for different amounts of time. In addition, the formation of the boundary layer in the shock wave affects the gas variables in the core of the flow, since the shock-tube walls cannot be regarded as infinitely distant from one another. The stagnation of flow near the wall changes the flow rate of the gas through the tube. The flow behind the shock wave undergoes energy losses which affect the propagation of incident as well as reflected shock waves. In order to determine the effect of losses due to viscosity and thermal conductivity of the gas on the flow variables of shock waves in a shock tube, we have performed experimental and theoretical investigations.

1. Effect of the Boundary Layer on the Gas-Flow Variables Behind a Shock Wave

/48

Due to viscosity and thermal conductivity the flow of gas behind a shock wave differs appreciably from that predicted theoretically. A boundary layer forms on the shock tube walls as the gas moves through the tube. On the wall, between the shock wave and the contact-surface, it acts as an "aerodynamic" sink, through which the gas leaks out from the region of the "plug." This accelerates the contact surface (which also means increasing the gas velocity near this surface) and reduces the distance between the contact surface and the shock wave as compared with the flow of inviscid gas. This distance tends to the limiting value of l_{\max} , which is determined by the equality between the velocities of the contact surface and of the shock wave. Here the flow rate of the gas flowing into the shock wave is equal to the flow rate of the gas which moves behind the contact surface through the boundary layer.

The effect of a laminar boundary layer on the flow variables of the gas in the plug and on the distance between the contact surface and the shock wave were studied experimentally and theoretically in [86-89], while the effect of a

turbulent layer is discussed in [90, 91]. Knowing the manner in which the shock-wave velocity varies along the tube, it is possible to find the variations in the flow variables behind a shock wave [92, 95, 96].

The character of the flow behind a shock wave in a shock tube varies along the tube [5]. In the beginning, i.e., near the diaphragm, the wave passes through the so-called acceleration section, at which the plug behind the shock wave is formed and where it is accelerated. This is followed by a section of uniform motion, where the wave velocity remains practically constant. And finally, in a tube of sufficient length this is followed by a deceleration section where the wave velocity drops gradually. Due to the fact that the shock wave velocity is not uniform, the manner in which the boundary layer affects the flow variables is also nonuniform at different parts of the tube.

The plug length at the acceleration section is relatively small and accordingly, the boundary layer near the contact surface is relatively thin. Under these conditions the effect of the boundary layer on the "external" flow (i.e., on the flow outside the boundary layer) is relatively small and can be calculated by the method of small disturbances. The effect of the boundary layer on the external flow when the region of heated gas behind an incident shock wave is sufficiently small can be calculated by a method developed in [95] (method of linearization).

In [92, 93] the attenuation of the traveling shock wave is attributed to the appearance of weak rarefaction waves, which are produced by the formation of the wall-adjointing layer; these waves overtake the shock wave and attenuate it. In these references were also obtained analytical expression for the variation in flow variables behind a shock wave and for its damping in cases when the boundary layer is either entirely laminar or turbulent. Calculations on the assumption of a turbulent boundary layer are in good agreement with the experimental results of [98].

/49

In choosing a given boundary-layer theory, proper consideration must be given to the expected character of the boundary layer. Usually this is done on the basis of the Reynolds number

$$Re = \frac{x}{\mu} \left(\frac{U_0 - v_1}{v_1} \right)^2,$$

where μ is the kinematic viscosity of the undisturbed flow, x is the distance from the shock front and v_1 is the velocity of the flow relative to the walls.

The critical Reynolds number at which a laminar boundary layer becomes turbulent was determined experimentally by many authors [99, 100]. For moderate shock-wave velocities Re^{cr} is found to be of the order of $2-4 \cdot 10^5$ for rough tubes and of $1-3 \cdot 10^6$ for smooth tubes, as was shown in [99]. The transition Re for strong shock waves is as high as $5 \cdot 10^7$.

In the more general cases, when sufficiently long tubes are used, or when operating under conditions when the volume of the shock-heated gas is sufficiently

large, the boundary layer thickness at the contact surface becomes appreciable. Hence it is no longer possible here to calculate the effect of the boundary layer on the external flow by the method of small disturbances.

References [89, 91] have developed a nonlinear theory of the interaction between the external flow and the boundary layer which take into account the effect of the changes of flow in the plug on the boundary-layer variables. In particular, this theory can be used to estimate the inhomogeneity of the flow in the plug at the uniform-flow segment. This theory also makes it possible to determine the length of the plug as a function of the distance from the diaphragm.

It is assumed in the above studies that the main effect of the boundary layer on the behavior of the flow in the plug consists in leaking out of the mass into the enlarging boundary layer. It is assumed that for the uniform stage of shock-wave motion, the flow in the plug in a coordinate system moving with the front can be regarded as steady and isentropic.

Let there be known a function $V(x)$, where $V(x) = (\rho(x)u(x)/\rho(0)u(0))$ and $(u(0), \rho(0))$ are the flow velocity and density immediately behind the shock, while $u(x)$ and $\rho(x)$ are the same quantities in a plug section with coordinate x . Then the variables inside the plug can be calculated using ordinary formulas for steady flow in a nozzle with an area ratio equal to $A(x)/A_0 = 1/V(x)$.

/50

It turns out [89, 91] that on some additional assumptions (the main of which is that the variation in ρ as compared with u along the plug is small, which is approximately valid for large M) it is possible to find an integral equation for V [91]

$$x = \frac{1}{n-1} \int_V^1 \frac{[1-V]^{n/1-n}}{[He(V)]^{1/1-n}} dV, \quad (2.1)$$

$n = 1/2$ for a laminar layer and $1/5$ for a turbulent layer.

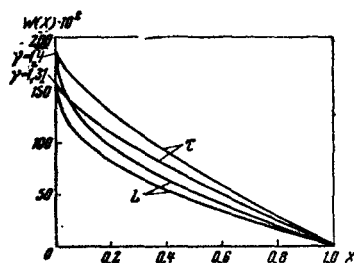
In Eq. (2.1) $He(V)$ is a known function of V and M_0 . As the first approximation we can take

$$He[V(x)] \cong \text{const} = (He)_c, \quad (2.2)$$

where the slowly-varying function of x is replaced by a constant. It can be shown that in this approximation we will have

$$\begin{aligned} V(x) &= 1 - X^{1-n}, \\ X &= x/l_m, \\ l_m &= 1/(He)_c^{1/1-n}. \end{aligned} \quad (2.3)$$

Figure 14. Variation in the Flow Velocity Behind a Shock Wave as a Function of the Distance; $u_0 = 2100$ m/sec.



Here l_m is equal to the "maximum" length of the plug, i.e., $V(l_m) = 0$. Thus,

calculation of $V(X) = 1 - X^{1-n}$ follows from the general equation (2.1) on assumption (2.2). It can be shown that approximation (2.2) is the better, the larger M_0 .

Unlike [89, 91], l_m was determined experimentally and then satisfying the expression

$$u(x/l_m)|_{x=l_{fk}} = (u)_k, \quad (2.4)$$

i. e., requiring that the theoretical velocity of the contact surface (for l_{fk} , the plug length, determined experimentally) be equal to its experimental value $(u)_k$.

As an example of calculations using the method of [89, 91], Fig. 14 depicts a theoretically calculated graph of the reduced velocity $W(X) \cdot (W(X) = u(X) / \sqrt{2c_p T^0})$ (T^0 being the stagnation temperature) in a coordinate system moving with the shock front. The calculations were made for an ideal gas with $\gamma = 1.31$ (one pair of curves) and $\gamma = 1.4$ (second pair of curves). Curves denoted by L have been calculated for a laminar boundary layer, while those marked with τ are for turbulent boundary layer.

Calculations similar to those depicted in Fig. 14 show that at the shock tube segment where the contact-surface velocity is close to that of the shock wave, the flow variables in the plug are quite inhomogeneous. In particular, under ordinary experimental conditions ($M = 4-8$) the flow velocity in a stationary coordinate system increases from the shock toward the contact surface by (10-20)%.

2. Experimental Data on the Effect of Multi-Dimensionality of the Gas Flow in a Shock Tube On the Flow Variables

The formation of a shock wave in a shock tube is not one-dimensional because the diaphragm separating the high-pressure chamber and the duct does not open instantaneously, but during some finite time amounting to hundreds of microseconds [101]. The diaphragm is destroyed gradually and this results in a train of waves which overtake the first shock wave and interact with it and thus increase the time of final formation of the wave. As a rule, the diaphragm is distorted before it breaks and hence distorted waves are produced in the tube passage at the initial propagation stage, these waves are reflected from the tube walls and give rise to a system of transverse waves. Gradual opening of the diaphragm results in turbulizing the gas flow behind the contact surface. Turbulization of the contact region aids in amplifying the heat transfer between the hot gas of the plug and the cold driver gas. This heat transfer at the boundary of the test and driver gases is usually not taken into account in the shock tube theory.

The initial stage of wave propagation in a tube is shown in Fig. 15 [117]. One can see the distorted forward front which is gradually straightened out, one can also see the interaction between several disturbances which arise when the

breaks. The wave front is formed precisely in the process of this interaction. The structure of the flow of the driver gas on photographs of the initial stage of wave propagation usually differs sharply from the flow of the test gas, which arises behind the shock wave. It is possible to observe the manner in which the distance between the wave and the contact surface increases rapidly at the early stage of plug formation.

The shock wave velocity is at maximum at distances of about 60 diameters from the diaphragm. At this tube segment the flow structure behind the wave also contains disturbances. Schlieren photographs of the plug have a characteristic pattern, i.e., the intersecting disturbances form a grid of a kind (see Fig. 4). The slope of lines forming the grid is the same as the slope of small disturbances, i.e., of Mach lines produced artificially in the flow.

/52

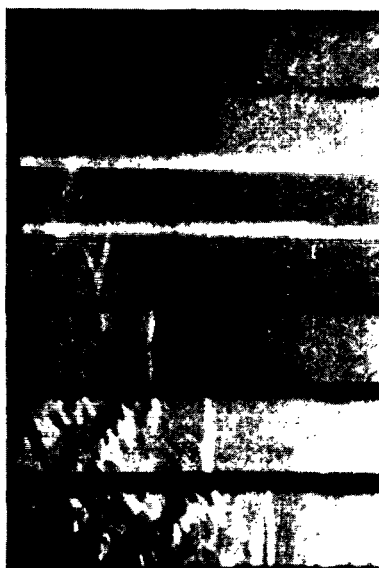


Figure 15. Shock Wave Near the Diaphragm.

The shape of the velocity curve and the absolute velocities are satisfactorily described by theory [91], but experimental data do not suffice for making specific conclusions on the nature of the boundary layer.

In experiments with low wave Mach number and with temperatures at which there are practically no physicochemical molecular transformations, the M_1 , Mach numbers of the flow are found to be above or equal to the theoretical value.

By measuring the velocity of the gas behind the shock wave on the basis of the velocity of a stria (see Section 5 of Chapter 1) we were able to obtain some data on the velocity variation along the plug's length from the front to the contact surface and to estimate the inhomogeneity of flow variables behind the shock waves. The experimentally obtained points and the calculated curves of the possible flow-velocity variation along the plug, which was made on the assumption of a laminar (L) or turbulent (τ) boundary layers and different γ (Fig. 14) in the flow is shown in Fig. 16. It can be seen that the flow velocity increases from the shock toward the contact surface by 18%.

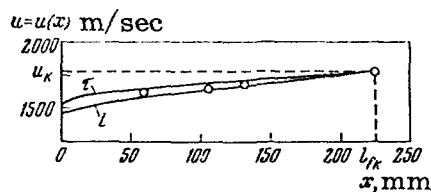


Figure 16. Comparison of the Theoretical and Experimental Flow Velocities Behind a Shock Wave Front in N_2 . The Initial Pressure is 20 mm of Hg, $M_0 = 5.18$.

For a number of values of M_0 of the flow the theoretical and experimental values have been presented in Fig. 17. The experimental conditions are presented in Table 2.1.

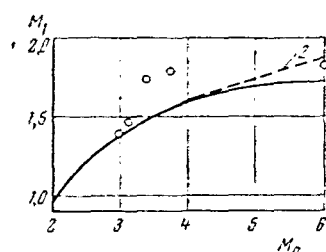


Figure 17. The Mach Number of the Flow as a Function of M_0 , the Mach

Number of a Shock Wave in Air. Initial Pressure 7.3-11 mm of Hg.

- 1—Calculations With Consideration of Internal Degrees of Freedom;
2—Calculations for an Ideal Gas.

these conditions the effect of multi-dimensionality of the flow on the flow parameters is most pronounced.

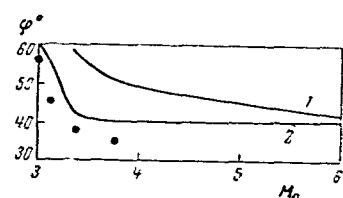


Figure 18. The Slope of an Oblique Shock, Produced on a Half Wedge Placed in a Flow Behind a Shock Wave as a Function of the Mach Number of the Wave.

- 1—Calculated With $\gamma = 1.4$;
2—Calculated on the Basis of the Measured M_1 .

TABLE 2.1

M_0	p_0 , mm Hg	M_{1ex}	M_{1theo}	p_1/p_0	μ , atm theo
2.98	11	1.39	1.39	10	0.15
3.14	7.4	1.47	1.44	11.6	0.1
3.34	7.3	1.74	1.50	13	0.12
3.74	8.7	1.79	1.56	16.8	0.19
6.03	9	1.83	1.75	42.4	0.5

The table presents theoretical values of M_1 obtained by consideration of the excitation of internal degrees of freedom. The experimental values were obtained by measuring the M_1 of the flow in the middle part of the plug, where they are at maximum. The experiments were performed with low-pressure flows. Under

Higher-than-expected Mach numbers in the flow were discovered when measuring the directions of Mach lines which arise at the thin edge of the half wedge with an angle of $7^\circ 30'$. The angle of inclination φ of the oblique shock which is produced in a flow of gas behind a shock wave about this half wedge yields additional information on the state of the gas in the shock tube. The relationship between the angle of inclination of an oblique shock at the wedge and the angle and velocity of the incident shock wave is determined by M_1 , the mach number of the flow behind the shock wave and the ratio of specific heats γ .

The curves on Fig. 18 denotes calculations on the basis of flow variables behind the shock, corresponding to conservation laws and calculations on the basis of the experimentally

measured M_1 of the flow. The divergence between the curves reflects the previously discovered mismatch between the calculated and measured M_1 of the flow. The experimentally obtained values of the angle of the oblique shock, which are shown as dots in Fig. 18 [sic] lie closer to the curve calculated on the basis of the experimentally measured values of M_1 . This further substantiates the claim that the Mach number in the flow behind a shock wave is higher than expected on the basis of theoretical calculations. /54

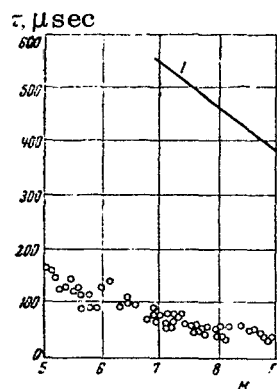


Figure 19. Comparison of Measured and Calculated Distances From the Shock Wave to the Contact Surface in Argon.

The observed higher values of the Mach number of the flow are a result of the increasing flow velocity which accompanies the enlarging of the boundary layer, since the flow velocity increases faster than the speed of sound, as this follows from calculations on the basis of theory of [91, 96].

Acceleration of the flow behind a shock wave reduces the distance between the shock and the contact surface. The length of the plug in argon at $p_0 = 1$ mm of Hg is shown in Fig. 19. The theoretically calculated (curve 1) plug lengths were obtained on the assumption that the entire mass of gas contained in the duct between the diaphragm and the section coinciding with the beginning of the segment being considered is contained in the plug between the wave and the contact surface at the instant when the wave arrives in the observed segment. The experimental lengths of the plug are on the average 1.5 to 2.5 fold smaller than the theoretical.

3. Features Peculiar to the Propagation of a Reflected Shock Wave in a Shock Tube

The boundary layer behind an incident shock waves is responsible for a number of peculiarities in the propagation of the reflected wave. As a result of the interaction between the reflected shock and the stagnated layer of gas near its wall, the wave front undergoes complex deformations. It breaks up into three shocks in the form of the Greek letter λ . This phenomenon is called bifurcation.

A bifurcation develops as follows (Fig. 20). After being reflected the shock wave is not distorted by the boundary layer. While moving it starts changing shape and finally forms a triple configuration near the side wall. Shock R which is inclined to the side wall is regarded as propagating through the boundary layer.

In our experiments the velocity of shock R was usually 50% higher than the velocity of the reflected wave proper. Behind the shock wave one can see clearly intense disturbances moving in the same direction as the shock wave, and their front, which was first quite sharp, starts to wash out. These disturbances are apparently produced by gas flowing from a higher-pressure to a lower-pressure region. /55

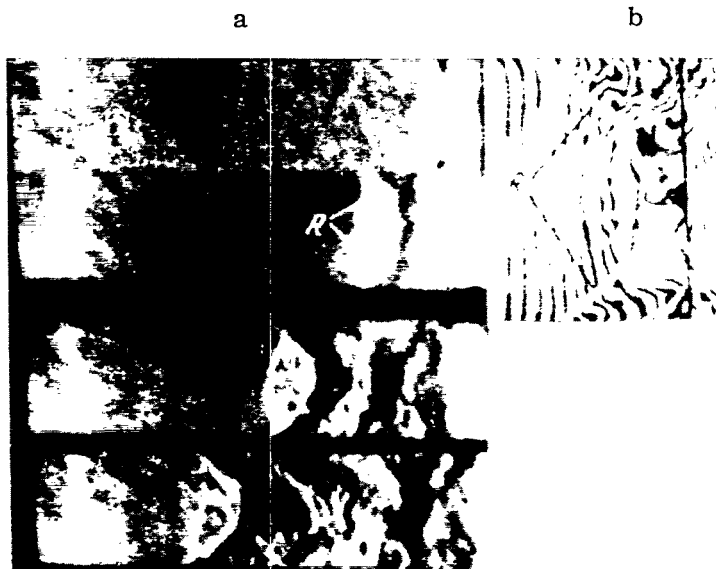


Figure 20. Formation of a Lambda Configuration in a Re-lected Shock Wave in Argon (a) and Carbon Dioxide (b).

After passing some distance, which depends on the γ of the gas and the M of the incident wave, as well as on conditions under which the gas flow takes place (tube diameter, surface roughness), the foot of the branched shocks ceases to increase in size and the boundary of the high-pressure region is slowly decelerated.

The complex density distribution in the gas behind a reflected shock due to bifurcation is seen on the instantaneous interferogram (Fig. 20b) obtained in [131].

This process in the x, t plane give a typical pattern of the reflection of a shock wave (Fig. 21). The middle, clearest line 1 corresponds to the motion of the reflected shock wave proper in the core of the flow. Line 2, the first from the incident wave, corresponds to the propagation of the shock along the boundary layer, while line 3, which is then scattered, corresponds to the motion of the boundary of the gas compressed by the shock wave in the boundary layer.

The formation of the lambda configuration is given in [103], which has calculated the pressure in the boundary layer and in the core behind a reflected shock. Figure 22 depicts the relationship $p/p_1 = f(M)$, obtained in [103], where p in one case is the pressure in the core behind the reflected shock p_2 , while in the other case it is $p_{b,1}$, the pressure in the boundary layer behind the reflected shock. In regions 1 and 3 the pressure in the boundary layer behind the reflected wave is higher than that in the flow core under the same conditions, and it can be assumed that the boundary layer passes continuously underneath the "foot" of the shock wave into the region behind the reflected wave. In this case there is no bifurcation.

/56



Figure 21. Scan of a Schlieren Photograph of the Reflection of a Shock Wave From the End of a Shock Tube.

In region 2 the pressure behind the reflected wave in the flow core is higher than that for the boundary layer under the same conditions. It may be assumed that the gas flows into a region adjoining the shock wave's "foot." The reflected wave in split, forming a bifurcation region. The size of region 2 is a function of the ratio of specific pressures γ and becomes smaller as γ increases. The relationships between the size of region 2 for different γ and M of the incident wave are presented in [104].

A detailed theoretical treatment of the λ -configuration on interaction between a reflected shock wave and the boundary layer in a shock wave is given in [102]. It is based on the fact that the usually considered unstable regions (resulting from viscosity and thermal conductivity) are replaced by a mixing region and the interaction of the latter with inviscid flows is considered. It is specified that the frictional tensions at the boundaries of this newly-introduced region are zero, and that the velocity and temperature component are equal to their corresponding velocity and temperature components of inviscid flows.

Let us examine a scheme of an λ -configuration (Fig. 23). Separation of the boundary layer results in accumulation of gas in region 3 and formation of shock wave AR. Intersection of AR with the reflected wave AL results in formation of shock wave AB. It is shown in [130] that the density in region 3 is practically constant and may be lower than the density behind a reflected shock (region 2). /57

It is assumed in examining this scheme that near horizontal wall ox there exists a viscous flow which is described by equations of nonsteady free turbulence [102], above which flows an inviscid gas. Thus, the thicknesses of the boundary layers at side wall ox are disregarded in analyzing the flow. In this case the two-dimensional unsteady flow of the gas and the unsteady mixing will be self-similar processes, while the inviscid flow in region 5 behind shock AR (in the coordinate system of point R, which moves at constant speed), will be steady up to disturbance AB which propagates toward this flow.

Let us consider further the flow about point A. The intersection of shock waves forms a tangential discontinuity AM, on which it is necessary to satisfy the condition that $p_2 = p_4$ and the requirement that the separating flows be parallel, i. e., $v_2 \parallel v_4$. As a result of turbulent mixing there is produced the mixing region KAN. Detailed analysis given in [102] shows that the effect of mixing about A is not too great.

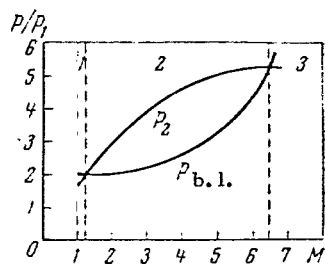


Figure 22. The Pressure $p_{b.l.}$ in the Boundary Layer and p_2 in the Flow Core Behind a Reflected Shock Wave, Referred to p_1 , the Pressure Behind an Incident Shock Wave, as a Function of the Mach Number of the Incident Wave (Calculated for a Gas With $\gamma = 1.4$).

reflection of shock waves in tubes and their part in the total energy of the flowing gas, we have performed special experiments.

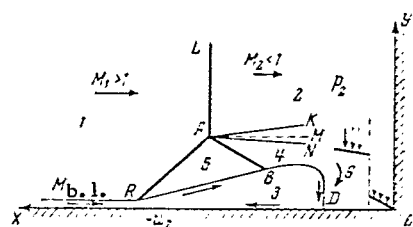


Figure 23. Splitting of a Reflected Wave into Three Shocks and Formation of the λ -Configuration.

Measurements of heat fluxes to the tube walls on reflection of shock waves showed that the energy loss for heating the wall is 1-2% of the total energy of the incoming flow.

The effect of the total energy losses on the velocity of the shock wave was estimated in a series of experiments with reflected shock waves in nitrogen with thermally conducting and nonconducting butts [of shock tubes]. The velocity of incident waves was in the range of 1400-3500 m/sec with initial pressures of 3 and 12 mm of Hg.

The dimensions of region 3 are determined from the following considerations. The small gas jet which adjoins the horizontal wall in the boundary layer behind an incident shock wave and which has separated from the wall in region 3 again returns to the horizontal wall in point D. The coordinate of point D is determined by equating the pressure in the gas jet under consideration to pressure p_2 behind the reflected wave. Per-

forming the same considerations for the gas flow in the regions bounded by waves of the splitting, the authors of [102] show that the velocity of the reflected wave and the pressure behind it should decrease in direct proportion to the distance passed by the wave.

The presence of the appreciable heat flux produced by the heated gas moving toward the walls should result in changing the flow variables and the velocity at which the shock wave propagates. The energy loss as a result of this heat flow should have its most pronounced effect on the propagation of the reflected wave. In order to estimate the effect of heat losses attendant to

/58

The heat flux magnitudes were obtained by recalculating the dependence of the surface temperature of the shock tube channel as a function of time, which was measured by means of resistance thermometers. In the first series of experiments the thermometer was installed in the side wall of the viewing section at different distances from the end. In this case we obtained a heat flux in the boundary layer behind the incident and reflected waves. In the second series the resistance thermometer was installed in the center of the tube's butt, flush with its surface.

In nitrogen at 1000—4000° no physicochemical molecular transformations take place with the exception of excitation of vibrations. The relaxation time of molecular vibrations at the temperature behind a reflected shock wave for an incident wave velocity of 1400 m/sec is about 200–600 microseconds [5], i.e., it is greater than the time during which the gas is in the heated state, which is limited by the instant of collision between the reflected wave and the contact surface. At incident wave velocities in excess of 2100 m/sec this time becomes less than 4 microseconds if the initial pressure is $p_0 = 12$ mm of Hg, and less than 12 microseconds in the case of $p_0 = 3$ mm of Hg, i.e., it is smaller than the ultimate time resolution of the setup.

Thus, in experiments with nitrogen for incident waves with $M > 6$, the propagation of the shock wave should be steady-state and should take place at a velocity corresponding to complete thermodynamic equilibrium of the gas. Under these conditions it is possible to use the experimental values of the velocity of the reflected shock wave for estimating the total velocity losses.

The experimental results are depicted in Fig. 24. The dependence of the velocity of the reflected wave on the velocity of the incident wave under conditions of complete thermodynamic equilibrium is given by curve 1, while for the case when the gas is assumed to be ideal, it is given by curve 2.

The velocity of the reflected wave in the immediate vicinity of the tube butt (thermally insulated and made from metal) is in satisfactory agreement with the calculated values only for $M < 4$. For larger M the scatter of experimental points increases and their average value is by 10–12% lower than that obtained theoretically. This leads to the conclusion that the reflection of a shock wave under experimental conditions involves losses which reduce the speed of the reflected wave by 10%. This is taken into account in analyzing the results which are based on determining the reflected-wave velocity.

/59

The reduced reflected-wave velocities are apparently attributable to the reconstruction of the flow behind the reflected wave as a result of its interaction with the boundary layer [102].

The reflected shock wave propagates through a gas which was set into motion by the incident wave. In the case when the flow of this gas is inhomogeneous, the velocity of the reflected wave should be variable. As was pointed out above (Section 2) the velocity of the gas and the Mach number increase along the plug. The velocity of the gas behind the reflected wave relative to the wall is zero. The gas which moves at a high velocity can be stopped by a stronger shock wave, i.e., by one moving at a higher speed. This follows from the law of conservation of energy. Consequently, increasing the gas flow velocity behind a traveling wave should result in accelerating the shock wave reflected from a straight butt.

In fact, when measuring the velocity of the reflected shock wave we have noted an increase in the velocity of this wave near the contact surface which in some cases was as much as 30%.

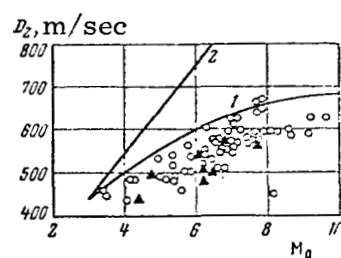


Figure 24. The Velocity of a Re-
flected Shock Wave Near the Butt
of a Shock Tube in N_2 as a Function
of the Mach Number of the Incident
Wave.

CHAPTER 3

GASDYNAMIC FLOW VARIABLES BEHIND A SHOCK WAVE IN A GAS UNDERGOING RELAXATION

1. Mach Number of the Flow and the Thermodynamic Variables of
the Gas Behind Shock Waves Propagating in CO_2 , N_2 and
 O_2 at Velocities of 1500-3000 m/sec

At the high temperatures which are produced behind shock waves, the gas molecules undergo physicochemical transformations. The internal degrees of freedom of the molecules are excited, dissociation ensues, new compounds form and the gas is ionized. All these processes affect the gasdynamic variables of the flow behind the shock wave. The extent of the effect of the physicochemical transformations on the flow variables of the gas is determined by the degree of molecular transformation. In the flow behind strong shock waves the degree of molecular excitation is high and the equilibrium excited state is reached rapidly, since the relaxation time of excitation processes at high temperatures is small. The gas variables reach their equilibrium values in fractions of microseconds.

/60

However, each gas has a temperature range (and correspondingly, a range of values of M_0 , the Mach number of the wave), for which molecular excitation has an appreciable effect on the flow variables, and at the same time the excitation process duration is of sufficient length, comprising tens and hundreds of microseconds. Under conditions which have corresponding to them large relaxation times the gas flow is determined by nonequilibrium variables. The flow structure under these conditions is highly variegated. This consists, in particular in the fact that at small distances from the source the small disturbances propagate at a speed equal to the high-frequency speed of sound [13, 14, 18, 115, 127]. The thermodynamic variables of the gas under these conditions can be determined by measuring the gasdynamic flow variables.

In the given chapter we consider N_2 , O_2 and CO_2 as characteristic examples of gases where the relaxation process has an appreciable effect on the flow variables.

One of the variables which depends appreciably on the thermodynamic state of the flow is M_1 , the Mach number of the flow. The angle of inclination of a small disturbance in the flow, which is determined by the ratio of the flow velocity to the speed of sound, has different values depending on the extent of molecular excitation.

/61

The velocity of the flow behind the shock wave (in the laboratory [stationary] coordinate system) is greatest for a completely equilibrium state behind the wave. It differs from the values corresponding to the "frozen" state by up to 10% of the equilibrium value (for $M_0 = 11$). We define a completely equilibrium state of the flow as such for which the extent of excitation of internal degrees of molecular freedom and the molecular dissociation corresponds to the translational

temperature of the molecules. The frozen state is defined as such in which molecular rotations are excited in equilibrium with the translational temperature and there is no excitation of vibrations and dissociation on passing through the shock. For the diatomic N_2 and O_2 molecules and for the triatomic CO_2 molecule transition through the shock to the frozen state corresponds to a process with a specific heat $c_p = 7/2 R$ (and $\gamma = c_p/c_v = 1.4$).

Between the above extreme cases we consider partially frozen cases which correspond to: a) absence of dissociation and complete excitation of vibrations for molecules of N_2 , O_2 and CO_2 ; for the CO_2 molecule in addition to b) absence of dissociation and excitation of two kinds of vibrations, i. e., deformation and symmetrically valent with vibrational numbers $\omega_2 = 672.2$ and $\omega_1 = 1351.2$ respectively and c) absence of dissociation and excitation of only one kind of vibrations with $\omega_2 = 672.2$.

The state of the flow behind shock wave with CO_2 was considered in [120-122, 106-112].

The dissociation and excitation of internal degrees of freedom of CO_2 molecules is appreciable as early as at 2000-3000°K. Data are available about highly different relaxation times for the excitation of vibrations of CO_2 molecules. Deformation ($\omega_2 = 672 \text{ cm}^{-1}$) vibrations in the temperature range of 1500-3000°K are excited during a time $\tau_1 = 1-3$ microseconds (see, for example, [29]).

Different excitation times for symmetrical valent vibrations in the above temperature range were obtained by different authors. Some [112, 120] assume that at least to 2500°K the valent vibrations are excited during a time by an order of 1.5-2 greater than τ_1 , while others [121, 122] report that excitation of deformation and valent vibrations should take place almost simultaneously in the above temperature range.

The flow variables behind a shock wave in CO_2 for states with different degrees of molecular excitation were calculated using the laws of conservation of momentum and energy and the equation of continuity together with the equation of state. Using the known value of the enthalpy as a function of the temperature, it is possible to calculate all the flow variables behind the wave, if the initial state of the gas is known. The enthalpy is calculated on the assumption that the CO_2 molecule, being linear, can be regarded, on consideration of excitation of rotation and vibration, as a rigid rotator and harmonic oscillator [118].

/62

The slope of the Mach line in the flow is determined by the ratio u/a . The speed of sound a depends on the composition, temperature and state of excitation of the internal degrees of molecular freedom and on the extent to which these variables differ from the initial variables during the propagation of the sonic signal. The speed of sound drops as equilibrium is approached. The equilibrium speed of sound a_0 , which corresponds to a fully equilibrium flow, differs from the frozen speed of sound by up to 35% of its value in the flow behind the wave with

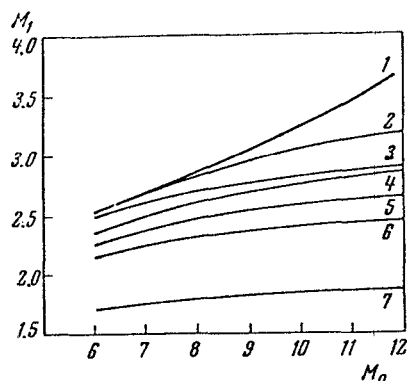


Figure 25. Theoretical Curves of M_1 , the Mach Number of the Flow, as a Function of M_0 , the Shock-Wave Mach Number, on Different Assumptions on the Degree of Excitation of the Gas Molecules Behind a Shock Wave in CO_2 :

1—Equilibrium Speed of Sound in an Equilibrium Flow; 2—All Kinds of Molecular Vibrations in the Flow Subjected to Equilibrium Excitation, the Speed of Sound is Calculated Taking into Account the Excitation of All Kinds of Vibrations in the Acoustic Wave; 3—Deformation and Valent Symmetrical Vibrations in the Flow Subjected to Equilibrium Excitation in the Flow and in the Acoustic Wave; 4—All Kinds of Molecular Vibrations in the Flow Subjected to Equilibrium Excitation, Use is Made of the Frozen Speed of Sound, $\gamma = 1.4$; 5—Vibrations Corresponding to ω_1 and ω_2 are Subjected to Equilibrium Excitation, Use is Made of the Frozen Speed of Sound, $\gamma = 1.4$; 6—Only Vibrations Corresponding to ω_2 are Subjected to Equilibrium Excitation, the Frozen Speed of Sound is Used, $\gamma = 1.4$; 7—Calculated on the Assumption of Complete Absence of Vibrational Excitation in the Flow and the Acoustic Wave.

$M_0 = 11$. Consequently, the Mach numbers of the flow of CO_2 calculated for the proposed states with maximally different degrees of molecular excitation, will differ by up to 40–45% for $M_0 = 11$. This difference, naturally, becomes smaller for smaller M_0 .

Figure 25 shows theoretically calculated curves of M_1 , the Mach number of the flow as a function of M_0 , the Mach number of the incident wave, in CO_2 .

Only two states of the flow were considered for O_2 and N_2 . The case of complete equilibrium was treated on the basis of data calculated in [119]. The state of complete equilibrium for Mach numbers of the flow up to 8 practically corresponds to the state with completely excited vibrations, since the degree of dissociation under these conditions is low and it does not appreciably affect the flow variables. The second state of the flow considered was the fully frozen state. It is calculated on the basis of relationships across the shock with $\gamma = 1.4$, without consideration of any molecular transformations.

/63

The agreement between the experimentally obtained Mach numbers of the flow with one of the theoretical curves can be apparently regarded as proof of existence of this state of the flow, on the assumption of which the given curve has been calculated.

2. Velocity of the Flow and the Rate of Propagation of a Small Disturbance in the Flow Behind a Shock Wave

It is obvious that any hypothesis about the state of the gas based on measuring variables such as the Mach number of the flow [28, 106, 107, 113], the angle of the oblique shock [28, 114] which arise at an obstacle placed in the shock tube, or

velocity of a wave reflected from the end of the tube [108-112] can be sufficiently reliable only in the case when the problem of the velocity with which a small acoustic disturbance propagates in a flow of a gas under relaxation is uniquely solved.

It is known that the speed of sound in a medium under relaxation depends on the frequency. An acoustic signal with a complex frequency composition is dispersed. At frequencies close to relaxation frequencies of the medium's molecules one observes anomalously high (from the point of view of classical acoustics) absorption [115, 116]. Low-frequency acoustic signals propagate with the equilibrium speed of sound, while high-frequency signals, which move at a frequency exceeding that of relaxation processes in the gas, have a "frozen" speed of sound. If sufficient time is not available for molecular excitation during the passage of the acoustic signal, then the speed of the high-frequency signal is determined from the ratio of specific heats $\gamma = 1.4$

The rate of propagation of small disturbances was determined in experiments in a shock tube with CO_2 , N_2 and O_2 with Mach numbers of the wave of 3-11.

An obstacle - half wedge - with an opening angle $\theta = 10 - 15^\circ$ was placed in a shock tube $40 \times 40 \text{ mm}^2$ in cross section at a distance of 270 cm from the diaphragm. One generatrix of the half wedge was placed parallel to the axis of the flow on the edge of the half wedge. A disturbance, whose angle of inclination (Mach angle) was determined by the ratio u/a of the velocity of the flow to the local speed of sound, appeared on the side of this generatrix. The Mach angle could be measured directly from schlieren photographs obtained with high-frequency spark photography (Fig. 26), as well as by single-frame photography (Fig. 27). This value can also be determined by recording the pattern of the flow about the obstacle by continuous scanning (Fig. 28). On the arrangement for recording this process (see Fig. 1, Chapter 1) are denoted distances which can be measured to determine the Mach angle. In accordance with notation on Fig. 1, the Mach angle is given by

/64

$$\alpha = \arctan \frac{\Delta x}{\Delta L}, \quad (3.1)$$

where

$$\Delta L = \Delta l' \frac{1}{k},$$

and k is the reduction factor on photo-recording of the process.

When the process is recorded by photographic scanning the measurement accuracy is somewhat lower than when using high-speed photography, but when the screen with the slot and the apertures are carefully positioned relative to the obstacle placed in the tube, the experimental data are sufficiently reliable even in this case. The Mach numbers of the flow determined on the basis of the experimentally obtained angle α from the expression $M_1 = 1/\sin \alpha$ are shown in



Figure 26. High-Frequency Frame Photography of the Flow About an Obstacle Behind a Shock Wave in CO_2 .

sound, while curve 5 corresponds to the frozen speed of sound (see also Fig. 25 in Section 1 of present chapter).

The experimental values displayed in Fig. 29, obtained by high-speed (black dots) or continuous photography are in satisfactory agreement. Continuous recording of the process, which is somewhat inconvenient with respect to deciphering of results, makes it possible to follow the position of the Mach line over the entire length of the plug. This kind of observation is particularly interesting in CO_2 , since high-speed schlieren photographs show inhomogeneities in the flow density. When the frame is exposed to the flow during a short time period (about 3 microseconds) and the number of "working" frames is relatively small (3-4) the measured Mach angle may turn out to be different from the average value which is determined by the thermodynamic state of the flow. Photographic scans show that the trace of the Mach line in CO_2 is wider and subjected to greater fluctuations than the traces in N_2 and O_2 . The increased trace width in CO_2 corresponds to flow inhomogeneities. The average distance Δl between the reference line and the trace of the Mach line remains practically constant over a length of 2/3 of the total size of the plug in CO_2 , as well as in N_2 and O_2 .

Fig. 29. The theoretical curves of M_1 vs M_0 for N_2 and O_2 were taken from [119]. Figure 29a depicts two theoretical curves of $M_1 = t(M_0)$ behind shock waves in nitrogen: curve 1 corresponds to complete equilibrium, while curve 2 is for the case of frozen molecular vibrations. It is assumed for both curves that the ratio of specific heats C_p/C_v in the acoustic wave (let us call it γ_s) is 1.4.

In Fig. 29b the theoretical curve 1 and 2 correspond to complete equilibrium, but γ_s used for curve 1 is that at equilibrium, while for curve 2 it is equal to 1.4

Figure 29c shows four theoretical curves. They correspond to Mach numbers calculated on the assumption that all kinds of molecular vibrations are undergoing equilibrium excitation in the CO_2 gas, there is no dissociation, while the speed of sound is low-frequency for curve 2 and high-frequency for curve 4. Curves 3 and 5 show the theoretical relationship between M_1 and M_0 on the assumption that time is not available for excitation for asymmetric valent molecular vibrations in the flow, curve 3 corresponds to equilibrium speed of sound, while curve 5 corresponds to the frozen speed of sound (see also Fig. 25 in Section 1 of present chapter).

/66

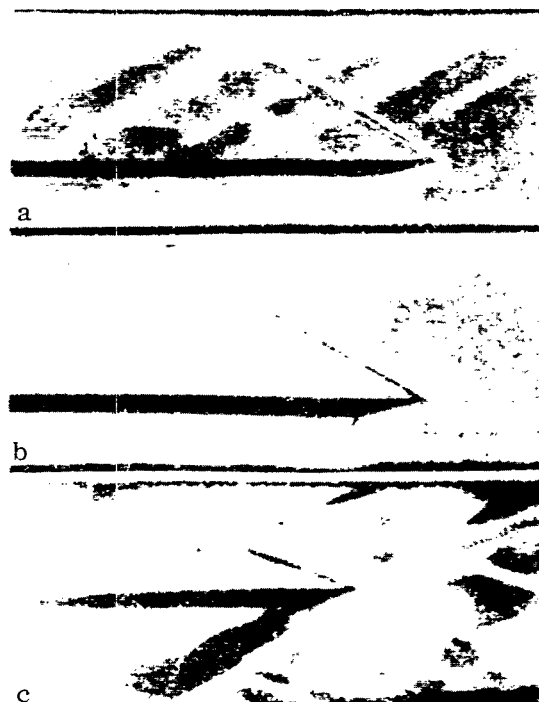


Figure 27. Single Photograph of the Flow About an Obstacle Using a Flashing Light Source in N_2 (a); in O_2 (b); in CO_2 (c).

The pattern obtained during the first 15-30 microseconds should not be considered, since it corresponds to unsteady flow and to the region near the contact surface, where apparently, the effect of the driver gas is felt.

In the Mach number range of $M_0 = 3-7.5$ the flow velocity behind the shock wave was determined by following a stria which was produced in the flow by a spark discharge (Section 5, Chapter 1). Figure 28 shows these schlieren striae in the flow behind the wave. Using this method the velocity was determined to within 2%. The theoretical and experimental flow velocities in N_2 , O_2 and CO_2 are shown in Fig. 30. The curves of Fig. 30a and b are for the following: curve 1 (a) corresponds to the assumption of frozen vibrations in N_2 , curve 1 (b) corresponds to the state of complete equilibrium in O_2 .

Curves 2 in Fig. 30a and b and curve 1 in Fig. 30c give the theoretical values of the contact surface velocity in the regime of "maximum" plug length, i. e., maximum value for the flow velocity under this regime.

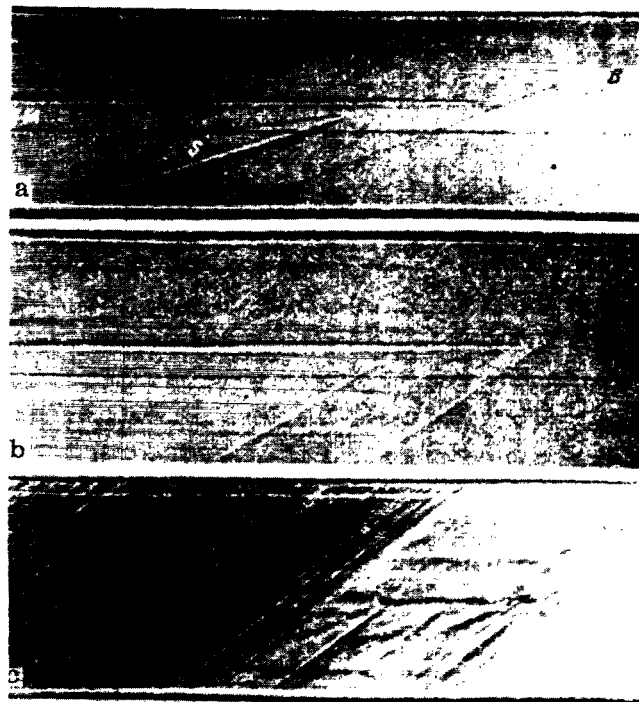


Figure 28. Continuous Photographic Scan of Flow About an Obstacle in a Shock Wave in N_2 (a); O_2 (b); CO_2 (c):

W—Denotes the Shock Wave; M—is the Trace of the Mach Line and S_1 is the Trace of the Stria.

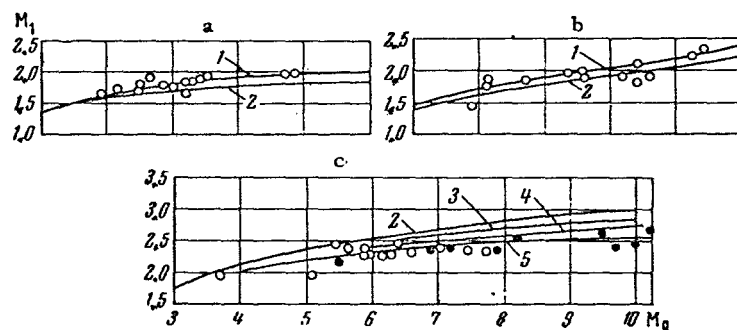


Figure 29. Curve of M_1 , Mach Number of the Flow as a Function of M_0 , Mach Number of the Shock Wave in N_2 (a); O_2 (b) and CO_2 (c). The Points Denote Experimental Values.

The velocity in CO_2 (Fig. 30c) was calculated for the state with fully excited vibrations - curve 2; and with asymmetric valent vibrations not excited - curve 3. The measured M and u can be used to calculate the speed of sound since $c = u/M$.

The speed of sound was also measured by another method. By continuous recording of the flow about the obstacle (Fig. 28) it is possible, in addition to determining the Mach number of the flow, to measure the rate of propagation of the acoustic signal in the flow of gas behind the shock wave. It is also possible to determine the average rate of propagation of an elementary disturbance at a distance from the forward edge of the half edge to the point where the screen's slot is situated (we shall denote this velocity by a). This path is traversed by the signal during a time which can be determined from a photograph of the process. It corresponds to a time interval Δt from the start of flow about the wedge to the appearance of a disturbance in the screen's slot. As a result we get (see Fig. 1 of Chapter 1), that

$$a = \frac{\Delta x}{\Delta t} = \frac{\Delta x}{\Delta \sigma \sigma}, \quad (3.2)$$

where σ is a coefficient related to the velocity of the film and making it possible to determine the duration of the process by the length of its trace on the film.

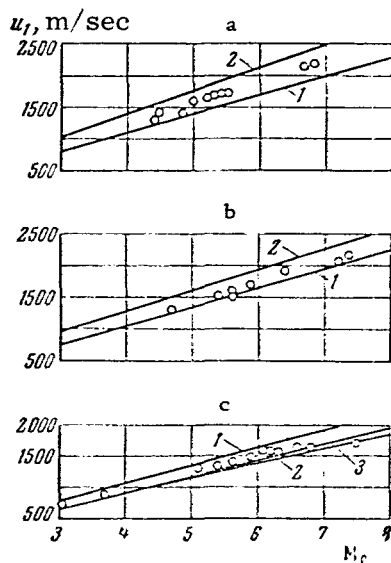


Figure 30. Flow Velocity u_1 as a Function of M_0 of the Shock Wave in N_2 (a); in O_2 (b) and in CO_2 (c). The Dots Denote Experimental Values.

Figure 31 shows variations in the speed of sound in the flow behind a shock wave as a function of the wave's Mach number. The theoretical curves are numbered in the same sequence as in Fig. 29. Curve 3 on Fig. 31 b corresponds to the state of the flow of O_2 with completely excited vibrations and frozen dissociation.

The accuracy of experimental determination of M , u and c is

$$\Delta M/M \simeq \pm 2.5\%; \quad \Delta u/u \simeq \pm 2\%; \quad \Delta c/c \simeq \pm 5\%.$$

Comparison of experimental data and theoretical curves makes it possible to arrive at some conclusions about the state of the flow and the magnitude of γ_s in the sonic disturbance behind shock waves in N_2 , O_2 and CO_2 for $3 \leq M_0 \leq 7$.

1. The state of the flow is described as follows: molecular vibrations in N_2 are frozen

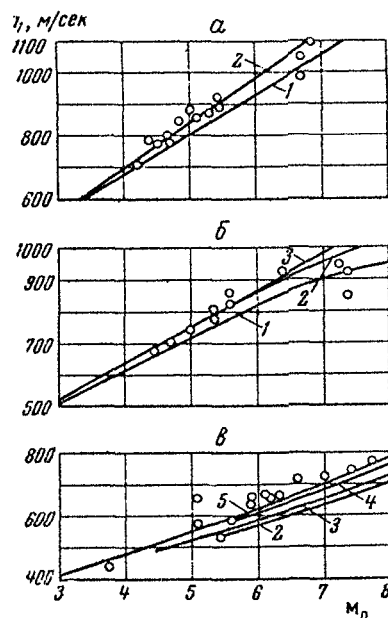


Figure 31. The Speed of Sound in the Flow Behind a Shock Wave as a Function of the Mach Number of the Wave in N_2 (a); O_2 (b) and CO_2 (c).

in the range $3 \leq M_0 \leq 6$ transition to vibrational equilibrium ensues when $M = 7$; in O_2 a fully equilibrium state is achieved, while asymmetric valent vibrations are frozen in CO_2 .

The ratio of specific heats in the acoustic disturbance is 1.4 at a distance of 10–20 mm from the source of the disturbance.

3. Structure of the Mach Line of a Gas Undergoing Relaxation in the Approximation of Geometrical Acoustics

It is well known (see, for example, [127]), that the system for equations of "relaxational" gasdynamics (i.e., of gasdynamics which take into account the excitation of internal degrees of molecular freedom) can be written in the form

$$\begin{aligned} d\rho/dt + \vec{\nabla}(\rho, \vec{v}) &= 0, \\ \rho(d\vec{v}/dt) + \vec{\nabla}p &= 0, \end{aligned} \quad (3.3)$$

$$\rho(d\xi/dt) = -K\varepsilon_{\xi}, \quad (3.4)$$

$$\rho T(dS/dt) = K\varepsilon_{\xi}^2. \quad (3.5)$$

Here ξ is some relaxation parameter, $\varepsilon(\rho, S, \xi)$ is the internal energy of a unit mass; Eq. (3.4) is the relaxation equation; Eq. (3.5) defines the rate of increase of the entropy (which is different from zero for $(d\xi/dt) \neq 0$) and K is some phenomenological function of state.

The above system of equations describes the state when it is possible to disregard not only the viscosity and "translational" thermal conductivity (i.e., the ordinary thermal conductivity due to translational degrees of freedom), but also those relaxation transfer coefficients which arise on the transport of quanta of internal excitation (see, for example, the discussion of relaxation thermal conductivity in [123, 124]).

On the assumption of validity of "pure" relaxation, i.e., of describing the physical situation by Eqs. (3.3)–(3.5), several authors (for example, [14, 127]) have made a study of the structure of the Mach line in media undergoing relaxation.

/69

It was shown that in these media the Mach line "spreads" into an entire region (namely, cone AOB in Fig. 32). It was also clarified in these studies that in cases of $(x, y) \rightarrow 0$ and $(x, y) \rightarrow \infty$ the structure of the disturbance region (produced by a source in $x = y = 0$) is such, that there exists a clearly expressed maximum of disturbance, localized along the frozen Mach line (line OA, Fig. 32) and accordingly along the "equilibrium" Mach line (the latter being line OB). Let us clarify these assertions. For this we consider the character of the function $\rho_{\nu_0}(x)$ ($\rho_{\nu_0}(x) = \rho(x, y_0)$ and ρ is the density) for large y_0 ($y_0 \gg l$), $l = \tau (a_\infty/a_0)^2$. This function is represented in Fig. 33, a. It can be seen that after the real discontinuity which passes along the frozen Mach line [125] there starts a region of smooth transition ("washed out discontinuity") into continuous flow behind the disturbance region (to the right of OB). We note concurrently that the amplitude of this discontinuity decreases with an increase in y .

In Fig. 33, b presents function $\partial \rho_{\nu_0}(x)/\partial x$. The region of values of (x, y) in which $\rho'_x(x, y) \neq 0$, can be called the region with nonzero disturbance strength*. In particular, when $y_0 \rightarrow \infty$ the greatest disturbance strength passes along the equilibrium Mach line.

/70

When $y_0 \rightarrow 0$, function $\rho'_{\nu_0}(x)$ approaches a θ -shaped shock

$$\begin{aligned} \rho_{\nu_0}(x) &\cong \theta[x - x_\infty(y)], \\ y_0 &\sim 0 \\ \theta(z) &= \begin{cases} 1, & z > 0 \\ 0, & z < 0, \end{cases} \end{aligned} \quad (3.6)$$

here $x_\infty(y)$ is the equation of the frozen Mach line.

Thus, relaxation gasdynamics does not allow the concept of a Mach line as a one-dimensional region along which the entire disturbance is transported. Nevertheless, the structure of the Mach line for large y_0 (Fig. 33) is such that it is possible to give an averaged description of the disturbance region by means of some "effective" Mach line, as a region along the disturbance is most effective in one sense or another. For example, it is possible to define the

*For clarity we will somewhat smooth out the front of the disturbance along the frozen Mach line. This does not effect the validity of the subsequent presentation.

effective Mach line as a line along which the maximum of the disturbance is transported (inside AOX)

$$x_{\text{ef}}(y) = \max_x \rho'_x(x, y) \quad (3.7)$$

$$(x > x_{\infty}(y)).$$

As previously, the effective Mach line thus defined coincides at large distances from the source of the disturbance with the equilibrium Mach line. It is also possible to define the effective Mach line as the locus of "centers" of the disturbance (for each given y)

$$x_{\text{ef}}(y) = \frac{\int x p'_x(x, y) dx}{\int p'_x(x, y) dx} \quad (3.8)$$

When thus defined the effective Mach line will everywhere lie above its equilibrium counterpart. This can be shown by using Fig. 33, b (the disturbance across the front of the Mach line is not shown in the figure). In fact, the fact that the amplitude of the shock across the front of the disturbance is finite is responsible for the fact that x_{ef} is displaced somewhat to the left of the point corresponding to maximum disturbance along the equilibrium Mach line.

Reference [126] uses still another definition of the effective Mach line, which is quite close to definition (3.8). Use is made there of the approximation of geometric acoustics. In accordance with this the "velocity" (dy_{ef}/dx) with which the effective "center" of the disturbance (represented in the form of a wave packet) propagates was equated to the group velocity

$$dy_{\text{ef}}(x)/dx = (d\bar{\omega}/d\bar{R}). \quad (3.9)$$

Here $\bar{\omega}$ and \bar{R} are usually expressed in terms of eikonal ψ of field ρ

$$\begin{aligned} \rho &= A e^{i\psi}, \\ \bar{\omega} &= -(\partial\psi/\partial x), \\ \bar{R} &= (\partial\psi/\partial y). \end{aligned} \quad (3.10)$$

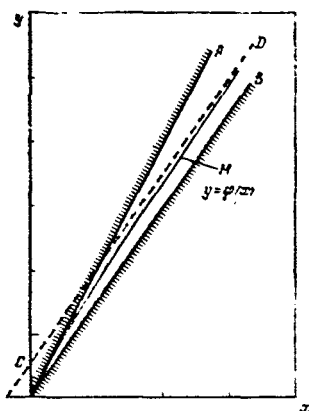


Figure 32. Effective Mach Line (M); Line OA Represents the Frozen and Line OB the Equilibrium Mach Line.

In fact, the result of operating this operator on $\exp(i\omega x)$ will be expressed in the form $[v/a(\omega)]\exp(i\omega x)$, where $a(\omega)$ is the known complex speed of sound in the gas undergoing relaxation (see, for example, [68]).

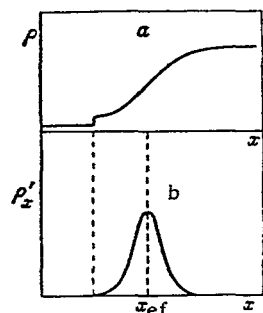


Figure 33. "Section Through the Disturbance Region Far From the Source.

Mach line in a medium undergoing relaxation

The starting equation for solving the above problem is

$$\begin{aligned} [(\hat{M}^2 - 1)\partial^2/\partial x^2 - \partial^2/\partial y^2]\rho(x, y) &= 0. \\ \hat{M}^2 - 1 &= (M_0^2 - M_\infty^2)\hat{l} + (M_\infty^2 - 1), \\ \hat{l} &= [1 + l(\partial/\partial x)]^{-1}, \\ \hat{l}\rho(x) &= \int_0^\infty [\exp(-z/l)/l]\rho(x-z)dz, \end{aligned} \quad (3.11)$$

i. e., the Prandtl-Glauert equation for a gas undergoing relaxation in the integral form [126]. This equation (in another, nonintegral form) was used in many other studies, for example [125]. Operator \hat{M} in Eq. (3.11) can be called the "operator Mach number."

From here on we restrict ourselves to the region of hyperbolic equation (3.11), i. e., the region of $M_\infty > 1$. This limitation is not excessively restrictive, since the majority of experimental work is performed in namely this region.

The equation defining the shape of the effective Mach line can be derived from Eq. (3.11) in the approximation of (3.9) and (3.10). As a result we get

$$(\hat{M}^2 - 1) \left[\frac{dy_{ef}(x)}{dx} \right]^2 = 1. \quad (3.12)$$

Direct solution of the above equation (in region $M_\infty > 1$) yields the following shape of the effective

/72

$$[y'_x(x)]^2 = [1/(M_0^2 - 1)] + qe^{-px} \quad (3.13)$$

when $\tau > 0$ and

$$[y'_x(x)]^2 = [1/(M_0^2 - 1)] \quad (3.14)$$

when $\tau = 0$, with q and p which enter Eqs. (3.13) and (3.14) defined as

$$\begin{aligned} p &= [(M_0^2 - 1) / (M_\infty^2 - 1)] (1/l), \\ q &= [1 / (M_\infty^2 - 1)] - [1 / (M_0^2 - 1)]. \end{aligned} \quad (3.15)$$

Let us discuss the solution obtained. First of all, it follows from (3.13)-(3.15) that in the limiting cases ($x \rightarrow 0, x > 0$) and ($x \rightarrow \infty, x > 0$) the direction of the Mach line coincides asymptotically with the directions of the frozen and equilibrium Mach lines.

The effective Mach line proper (M in Fig. 32) approaches, when $x \rightarrow \infty$, some straight line, which is parallel to the equilibrium Mach line and lies above it (CD).

Thus, in the approximation of (3.9) and (3.10) the relaxation structure of the Mach line is described by averaging, i.e., by means of an (one-dimensional) effective Mach line. This latter line can be interpreted as the path of some "quasiparticle", which is comparable to field ρ in the geometric acoustic approximation defined by Eqs. (3.9) and (3.10). In the beginning (at $x \sim 0$) the velocity of this quasiparticle is $(1 / \sqrt{M_\infty^2 - 1})$, then (as $x \rightarrow \infty$) a part of its translational energy is converted into excitation of internal degrees of freedom and the velocity drops to $(1 / \sqrt{M_0^2 - 1})$. However, this velocity is nowhere lower than the latter expression for which reason the path of this quasiparticle lies above the equilibrium Mach line.

Further, as $\tau \rightarrow 0$ we obtain an equilibrium Mach line, and when $\tau \rightarrow \infty$, we get a frozen Mach line. In conjunction with this we shall dwell briefly on the frequently discussed assertion that lines of propagation of small disturbances do not exist in relaxation acoustics (see [14, 115]). In fact, the characteristics of Eq. (3.11) are defined as

$$\frac{dy}{dx} = \begin{cases} \pm (1 / \sqrt{M_\infty^2 - 1}), & \tau > 0, \\ \pm (1 / \sqrt{M_0^2 - 1}), & \tau = 0, \end{cases} \quad (3.16)$$

i.e., for an as small as desired (but nonzero) τ the characteristics differ by a finite value from the equilibrium characteristics. This takes place not only in relaxation gasdynamics; this effect is sometimes counted among the "asymptotic" paradoxes of hydrodynamics.

The correct interpretation of this paradox, in our opinion, consists in the fact that a discontinuity at $\tau = 0$ would have only been paradoxical for an effective Mach line. Actually the "center" of the disturbance energy is transported along the effective Mach line, and not along the characteristic. The characteristics, on the other hand, define the forward front of the disturbance and in this sense determine the velocity of propagation of the "signal" as a quantity which does not depend on its strength.

Let us now briefly discuss the limits of applicability of the solution obtained.

1. Within the limits of starting equation (3.11) the solution obtained is valid for any $M_\infty > 1$. However, actually when $(M_0, M_\infty) \sim 1$ we should have immediately taken into account nonlinear corrections to Eq. (3.11), as in the case of the ordinary Prandtl-Glauert equation. This limitation under conditions of our experiment using supersonic flow velocities was not of substance.

2. It was already mentioned previously that the validity of the starting system of equations (3.3)–(3.5) and, consequently, also of Eq. (3.11) is limited to the region of pure relaxation and disregarding the additional (relaxation) parts of the transport coefficients. The effect of increasing the thermal conductivity due to relaxation is of particular interest [123, 124].

3. Solution (3.13)–(3.15) assumes that there exists only one relaxation time. In the meantime the establishment of thermodynamic equilibrium behind an incident shock wave (as that of propagation of small disturbances) has under our conditions at least two relaxation times: the time (τ_r) of rotational relaxation and the time (τ_v) of vibrational relaxation.

If, as usual, $\tau_r \ll \tau_v$ and there is practically no interaction between rotation and vibrations, then the effect of τ_r can be approximately estimated using (3.13)–(3.15) for frozen vibrations. Then we will get an estimate of the starting shape of the effective Mach line. Usually τ_r is very small, for which reason also the rotational equilibrium is achieved at a very small distance from the source.

CHAPTER 4

REFLECTION OF NORMALLY INCIDENT SHOCK WAVES IN REACTING GASES

1. Unsteady Propagation of a Reflected Shock Wave in a Reacting Gas

If the reactions taking place behind a reflected shock wave are nonequilibrium, /74 then their development with time may introduce quantitative features into the process of reflection of the wave. A reaction which does not succeed in reaching equilibrium in gas regions near the front of the reflected shock wave develops in gas regions near the end. These are heated by the reflected wave before others. This produces changes in time in the boundary condition at the reflecting surface, for which reason on the propagation of the reflected wave becomes unsteady. The study of propagation of reflected waves in reacting gases is of great interest from this point of view. In addition, measurement of flow variables behind reflected shock waves and the velocity of propagation of the reflected wave may yield information on the total rates of relaxation processes which take place in the test gas at elevated temperatures.

However, phenomena produced by bifurcation and energy losses attendant to reflection in a shock tube strongly distort the pattern of unsteady propagation of the reflected wave and also modify the variables of the heated gas (see Chapter 2).

In the present chapter we present studies of changes of the reflected wave's velocity. The flow variables behind the reflected shock will be determined theoretically. But before considering in detail the changes in the velocity of the reflected wave, let us determine the accuracy of determining the flow variables using the laws of conservation of energy on the condition that the gas at the reflecting surface is at rest.

Measurements of the density behind a reflected wave performed by Gardiner and Kistiakowsky [128] show that a distance of 0.5-5 from the plane of reflection, /75 within the limits of experimental accuracy (2%) the density after the passing of reflected waves are in agreement with the values calculated on the basis of velocities of incident waves, applying the conservation laws to them. Further, during 350 microseconds the density increases by 5%.

Strelov [129] has established by using an interferometer that in argon with $M = 2$ the density behind the reflected wave coincides with the theoretical value, while at $M = 5$ it exceeds it by 5% (the experimental accuracy was 2%).

It was shown in [130-137] that in CO_2 , N_2 and Ar for an incident shock with $M < 3$ the density remains unchanged up to the time when the reflected wave meets the contact surface. Here the density fluctuation is 1-2%. For incident waves with $M > 3$ the density behind a reflected shock is equal to the theoretical within 2-3%. Then an increase in density with time is observed in a given shock-tube cross section. The absolute deviation of the density of the gas behind a reflected wave from the theoretical value increases with an increase in the

Mach number and reaches 7 and 20% for CO_2 ($M = 4$ and $M = 6$), respectively.

Skinner [132] measured the pressure behind a reflected wave and has established that it is found to first be somewhat lower than the theoretical value and then linearly increases with time. The same was reported in [133]. The increase in pressure behind the reflected wave with time is attributed in [134] to the effect of waves created by the increasing boundary layer along the entire shock tube attendant to the interaction with the reflected wave. Experimental observations are in satisfactory agreement with those calculated theoretically. Authors of [135] have observed a slow increase in pressure behind the reflected wave and attributed it to the effect of the boundary layer.

In the Institute of Physics of the USSR Academy of Sciences [136] there was measured the temperature of N_2 , O_2 , CO_2 and Ar behind a reflected shock by spectral line reversal. The results of these measurements were compared with those calculated using the one-dimensional gasdynamics theory. It was also assumed that the state of the gas behind the reflected wave in the point of observation is determined by the velocity of the incident wave in this point. It was discovered that the theoretical and experimental results are in agreement within the $\pm 5\%$ experimental error. In addition, still another important conclusion was reached in examining the test gases in the series Ar- N_2 - air - O_2 - CO_2 (i. e., mono-, di, and poly-atomic gases). According to studies by Mark, Strellov and Cohen, the more intense bifurcation in this series results in an increasingly smooth increase in the temperature behind the front of the reflected wave. This was demonstrated experimentally in the Institute of Physics.

It is also of interest that the gas behind the reflected wave is not at rest, but some velocity distribution from the end [of tube] to the wave exists. However, it does not exceed 2% of the flow velocity behind the incident wave [137]. /76

This survey of experimental data concerning the correctness of determining the state variables of the gas behind the central part of a reflected wave based on calculations using the conservation laws leads to the conclusion that the state of the gas immediately behind a reflected wave is in agreement with that calculated theoretically within 5-8%. The accuracy in calculating the state of the gas at the butt [of tube] is much lower, amounting to 20%.

The velocity of the reflected wave was measured by the authors of [104, 144, 145]. Their results were then compared with theoretical values obtained by solving conservation equations for a plane shock, adiabatically reflected from a perfectly rigid wall. The following was observed: as the reflected wave moves away from the wall, its velocity in some cases is variable, first decreasing and then increasing near the contact surface. The slowdown is attributed to the effect of relaxation processes, while the acceleration - to inhomogeneity of the gas flow behind the incident wave due to the development of the boundary layer.

The velocity of the reflected wave in the immediate vicinity of the [tube] end is in satisfactory agreement with the theoretical values only for low Mach numbers

of the incident wave ($M < 4$). In the case of higher M , the scatter of the experimental points increases, and the deviation from ideal behavior is found to be different for different gases. The greatest deviation (about 30%) is observed for argon [139, 129, 141]. In argon with a Mach number of the incident wave higher than 5 a subsequent acceleration of the reflected wave is observed. In nitrogen and oxygen the experimental velocity of the reflected wave is found to be lower than the theoretical value by about 1-7%. This reduction is attributable to the effect of losses attendant to reflection.

On the basis of the hypothesis that the velocity of the reflected wave is a function of the state of the gas behind it, some authors have used a reflected wave for studying the kinetics of chemical reactions [104, 138, 143, 140, 144]. The authors of [143] have been able to determine the energy of molecular dissociation for N_2 and CO on the basis of the velocity of the reflected wave.

The method of the reflected shock wave for studying the relaxation of O_2 and N_2 molecules was used most comprehensively by Strelov and Cohen [104]. The relaxation time for exciting vibrations of N_2 and O_2 molecules was studied by Blackman [146] using an incident shock wave. The calculations presented in [104] which were based on Blackman's data show that the reflected wave should be decelerated near the end wall of the tube due to vibrational relaxation of the gas behind the wave. The Strelov-Cohen experiment showed that the reflected wave is actually slowed down and that the deceleration time is in agreement with that precalculated. /77

The relationship between the relaxation time and the time of reaching a shock-wave velocity close to that on equilibrium was obtained by Spence [18]. He has considered the unsteady-state propagation of a shock wave ahead of a piston in a gas undergoing relaxation by the method of linearized characteristics. The problem of reflection of a shock wave from a flat wall differs from that of propagation of a wave ahead of a piston by the fact that the velocity of the piston is assumed to be zero, the initial flow comes in with the velocity of the piston. In solving the problem of propagation of a shock wave ahead of a piston, Spence examined the equations of motion of a gas undergoing relaxation in the Lagrangian

coordinates $h = \int_{x(0,t)}^{x(h,t)} \rho dx$:

$$\begin{aligned} \frac{\partial u}{\partial t} &= - \frac{\partial p}{\partial h}, \\ \frac{\partial u}{\partial h} &= \frac{\partial}{\partial t} \left(\frac{1}{\rho} \right), \\ \frac{dE}{dt} + p \frac{\partial}{\partial t} \left(\frac{1}{\rho} \right) &= 0. \end{aligned} \tag{4.1}$$

The equation in the characteristic form is written as

$$\frac{a}{\gamma p} \left(\frac{\partial}{\partial t} \pm \rho a \frac{\partial}{\partial h} \right) p \pm \left(\frac{\partial}{\partial t} \pm \rho a \frac{\partial}{\partial h} \right) u = - \frac{E}{a} \frac{dx}{dt}, \quad (4.2)$$

where a is the frozen speed of sound and α is the degree of dissociation of the gas

$$a^2 = \gamma(x) \frac{p}{\rho}.$$

The reaction rate $d\alpha/dt$ can be obtained if the relationship $\alpha(t)$ is known. If the reaction does not introduce appreciable changes into the state of the medium, then

$$\alpha(t) = \alpha_0 \tanh \frac{t - t_0}{2\tau_0},$$

where t_0 is a constant of integration, α_0 is a constant characterizing the time for reaching degree of dissociation α_0 , which is close to that at equilibrium.

It is assumed in the solution that the boundary conditions which are satisfied by the variable flows immediately behind the shock waves are applicable at the undisturbed path of the wave $X = U_0 t$, where U_0 is the shock wave velocity, if there is no dissociation between the wave and the piston. Then the Lagrangian coordinate $h_s(t)$ of the shock wave, equal to the mass of the gas which flowed through the shock wave during time t , is

$$h_s(t) = \rho (U_0 - u_0) t,$$

where u_0 is the piston velocity.

After substituting the expression for α and linearization, Eq. (4.2) takes on the form

$$\left(\frac{\partial}{\partial t} \pm \rho_0 a_0 \frac{\partial}{\partial h} \right) \left(\frac{p}{\gamma_0 p_0} \pm \frac{u}{a_0} \right) = - \left(\frac{\alpha_0}{2\tau_0} \right) \left(\frac{E_0}{a_0^2} \right) \rho \operatorname{ch}^2 \left\{ \frac{t - t_0(h)}{2\tau_0} \right\}.$$

The general solution of this equation

$$\frac{u - u_0}{a_0} = A \left[f \left(t - \frac{h}{\rho_0 a_0} \right) + g \left(t + \frac{h}{\rho_0 a_0} \right) - \tanh \left\{ \frac{t - t_0(h)}{2\tau_0} \right\} \right], \quad (4.3)$$

$$\frac{p-p_0}{\gamma_0 p_0} = A \left[f \left(t - \frac{h}{\rho_0 a_0} \right) - g \left(t + \frac{h}{\rho_0 a_0} \right) - M \operatorname{th} \left\{ \frac{t - t_0(h)}{2\tau_0} \right\} \right], \quad (4.4)$$

where f and g are arbitrary functions, while $M = \frac{U_0 - u_0}{a_0}$,

$$A = - \frac{\alpha_0 E_0}{a_0^2} \frac{M}{1 - M^2}.$$

When boundary conditions $h = h_g(t)$ are substituted into Eqs. (4.3) and (4.4), the values of u and p become equal to these gas variables immediately behind the shock, when these are determined on the basis of the conservation laws. The use of this boundary condition across the shock makes it possible to eliminate the arbitrary function g , while function $f(t)$ is found from the boundary condition at the piston where $u = u_0$ for all the t .

The expression for $f(t)$ is given by the functional equation

$$f(t) + v f(\lambda t) = \operatorname{th} \frac{t}{2\tau_0}, \quad (4.5)$$

where v and λ are functions of the Mach number of the flow.

For the case of a shock wave reflected from a rigid wall ($u_0 = 0$), the Mach number of the flow behind the wave is u_0/a_0 . When passing through the front of the reflected wave γ may be regarded as unchanged, since the active degrees of freedom have already been excited in the incoming flow behind the incident shock wave, while the unactive degrees of freedom are not excited immediately behind the shock due to lack of time. Analyzing the boundary conditions for this case we get the following values of λ and v

$$\lambda = \frac{1-M}{1+M},$$

$$v = \left[\left\{ 1 - 2 \left(\frac{\gamma-1}{3-\gamma} \right) M \right\} / \left\{ 1 + 2 \left(\frac{\gamma-1}{3-\gamma} \right) M \right\} \right] \lambda^2$$

The time needed for the velocity to reach its limiting value is, by definition, infinity ($t = \infty$, $U = U_\infty$), however, analysis of functional equation (4.5) performed in [18] shows that $f(t)$ come quite close to the equilibrium value during a time $\tau_s = \int_0^\infty [1 - F(t)] dt$. This time is a function of τ_0 , the relaxation time of the reaction

/79

$$\tau_s = \tau_0 \frac{2 \ln 2}{1 - M^2} \left\{ \frac{1 + \frac{3\gamma - 1}{3 - \gamma} M^2}{1 + 2 \frac{\gamma - 1}{3 - \gamma} M^2} \right\}. \quad (4.6)$$

Analysis of experimental and theoretical data on the reflection of shock waves shows that, if the time of the relaxation process is commensurable with the time of propagation of the wave, then it is possible to observe nonsteady propagation of the reflected wave and to determine the relaxation time by the relationship governing the deceleration of the reflected wave. Here it is necessary to take into account corrections introduced into the reflected wave's velocity by the energy losses occurring on reflection.

2. Study of the Nonsteady Propagation of a Reflected Wave in CO₂ Undergoing Relaxation

Comparing the velocities of a reflected wave in CO₂ for initial pressures p_0 of 3 and 12.7 mm of Hg, on different assumptions on the thermodynamic state of the gas behind the incident and reflected shock waves (Table 4.1), we see that the velocities obtained on the assumption of complete equilibrium (1) differ appreciably from the values calculated without taking molecular dissociation into account (2), starting with $M = 8$ of the incident wave, to values calculated on the assumption of a constant ratio of specific heats ($\gamma = 1.3$) when passing through the shock (3), starting with $M = 4$.

TABLE 4.1. VELOCITY OF A REFLECTED WAVE IN CO₂ (m/sec)

M_0	1		2	3
	$p_0 = 3$ mm of Hg	$p_0 = 12.7$ mm of Hg	$C_p (T)$	$\gamma = 1.3$
4	240	240	270	320
6	270	270	280	450
8.5	275	290	350	570
11	305	320	500	780

To discover the effect of nonequilibrium processes in the gas on the velocity of a reflected shock wave, experiments were performed in CO₂ for $M = 4-12$ of the incident wave with an initial pressure $p_0 = 12.7$ and 3 mm of Hg, using the UT-2 facility.

A typical scan of the schlieren pattern of the reflection is shown in Fig. 34. It was assumed that the velocity of the reflected wave is equal to the velocity of an average disturbance on the scan. In the case of $M < 8$ the velocity of the reflected wave is constant, while when $8 < M < 12$

it is variable. The wave slows down at about 8-12 mm from the end of the tube, while near the contact surface its velocity increases sharply. The latter takes place due to inhomogeneity of the variables in the plug behind the incident wave (Chapter 3).

The results of measuring the velocity of the reflected shock wave are presented in Figs 35 and 36. Curve 1 corresponds to the case of equilibrium dissociation of the gas behind the incident and reflected shock waves: curve 2 of $C_p (T)$

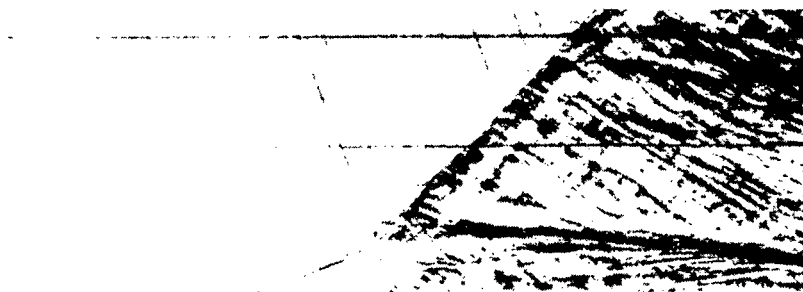


Figure 34. Photographic Scan of the Schlieren Pattern of a Wave Reflected in CO_2 ; $p_0 = 12.7$ mm of Hg, $u_0 = 2240$ m/sec.

is calculated on the assumption of equilibrium excitation of molecular vibrations, without considering dissociation; curve 3 ($\gamma = 1.3$) assumes that the gas is ideal. The experimentally determined velocities of the reflected wave for $M < 8$ lie near the curve of $C_p(T)$, while for $M > 8$ the velocities measured directly at the tube's end lie near this curve and below it, while the velocities after deceleration lie near the curve corresponding to complete equilibrium in the system, and below. The fact that the velocity of reflected waves after deceleration obtained in some experiments is below the equilibrium velocity is attributable to energy losses on reflection. As was shown in Chapter 2, the values of D_2 on assumption of losses are lower than the ideal theoretical values by 10%. Hence it cannot be claimed that the velocity after deceleration corresponds to the state of total equilibrium of the gas behind the reflected wave. The measured time between the instant of reflection and the start of deceleration points only to the fact that the dissociation reaction at the tube end has not as yet reached the equilibrium extent, i. e., the relaxation time of the gas behind a reflected wave is greater than that measured.

It is interesting to note that the velocity of a reflected wave in CO_2 measured under conditions when losses for interaction between the reflected wave and the boundary layer have been eliminated, was found to be 10-20% higher than the values calculated on the assumption of frozen dissociation and equilibrium excitation of vibrations (Fig. 37). These experiments were performed by R. I. Soloukhin [140], using initial data corresponding to those at which nonsteady propagation of the reflected wave was observed ($p_0 = 12.7$ mm of Hg, $M_0 = 2-10$). To eliminate the interaction between the reflected wave and the boundary layer, the reflecting butt was placed into the shock tube in such a manner that its ends were not in contact with the tube walls. Under these conditions the propagation of the reflected wave was not affected by the state of the gas at the walls during the time for which no rarefaction waves produced due to outflow of gas through the gap formed between the butt and the shock-tube walls arrived in the central part of the wave. This time was found insufficient for observing the deceleration of the reflected wave. The increased reflected-wave velocities observed by Soloukhin

point to the fact that the velocities measured in our experiment are somewhat on the low side due to losses for interaction between the reflected wave and the boundary layer, and that during the first moments after reflection in CO_2 under the conditions of our experiments the molecular vibrations have not been completely excited.

Measurement of the time in our experiments during which the velocity of the reflected wave with $p_0 = 3$ mm of Hg increased was possible only for $M > 10$, since the pressure behind the shock is higher for larger velocities and the schlieren photographs become clearer. For an initial pressure of 12.7 mm of Hg it becomes possible to follow the change in the reflected-wave velocity for $M_0 = 8-10$. Figure 38 shows the path taken by a reflected shock wave, constructed by measuring the wave's coordinates on a photoscan.

At the first section the reflected wave propagated with continuous deceleration from the initial velocity (curve 1) to the equilibrium velocity (curve 2), then on the following section (curve 3) the velocity becomes greater due to variation in the variables of the incoming flow at the contact surface. The time for reaching the equilibrium velocity of the reflected wave can be measured within 20%.

If the high reflected-wave velocities near the butt are attributable to the non-equilibrium composition of the gas with temperature T'_2 immediately behind the reflected shock, then the same high velocity should also be observed when the front moves away from the butt, since the front moves all the time through fresh gas. Deceleration of the reflected wave can be produced by changes in the boundary layer at the butt, after the dissociation in the layer at the butt reaches its equilibrium value, and the temperature acquires its equilibrium value T_2 .

/83

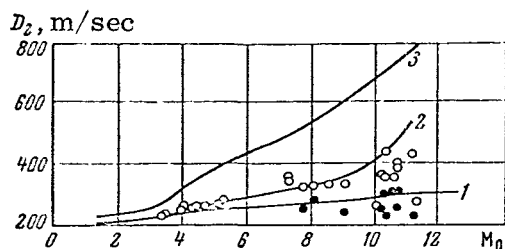


Figure 35. Velocity D_2 of a Reflected Shock Wave as a Function of M_0 , the Mach Number of the Incident Wave. Initial Pressure $p_0 = 3$ mm of Hg.

o—Velocity of Reflected Shock Wave in Immediate Vicinity of the Butt;
o—Same as Before After Deceleration.

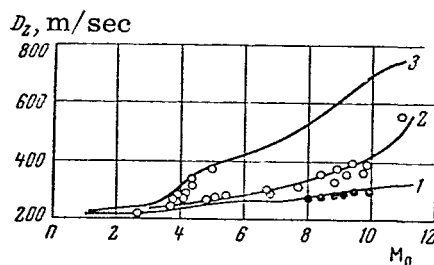


Figure 36. Velocity D_2 of a Reflected Shock Wave as a Function of M_0 , the Mach Number of the Incident Wave. Initial Pressure 12.7 mm of Hg.

The Notation is the Same as in Fig. 35.

/82

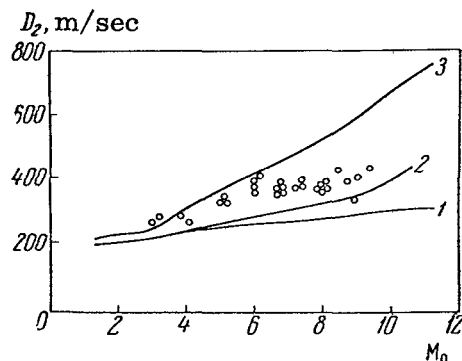


Figure 37. Velocity of a Shock Wave in CO₂ Reflected From an Insertable Butt.

The Notation is that of Fig. 35.

of the reflected wave. Then the time needed for establishing the equilibrium velocity of the reflected wave can be used to determine the time of establishing the equilibrium concentrated in the gas layer near the butt, which was the first to be stopped by the reflected wave.

Let the composition of the gas at the butt reach its equilibrium value during a time τ_0 after reflection of the wave which propagates relative to the butt with a velocity D_2 . When the first signal about the changed state at the butt, which moves with velocity a , will reach the reflected front at the time τ_s , which is equal to $\tau_0 + t_1$ (t_1 being the time needed by the signal to overtake the reflected shock). The relationship between these times can be easily obtained by equating the expressions for the front's coordinates at the time of meeting τ_s .

$$\begin{aligned} D_2 \tau_s &= a_2 t_1, \\ \tau_s &= \tau_0 + t_1. \end{aligned}$$

Then the time needed for establishing the equilibrium concentration will be expressed in terms of the time needed by the first signal to reach the reflected shock as follows

$$\tau_0 = \tau_s (1 - D_2 / a_2); \quad D_2 / a_2 = M. \quad (4.7)$$

The maximum signal velocity a_2 is apparently equal to the frozen speed of sound under conditions prevailing behind a reflected shock wave (Chapter 3). The experimentally determined values of τ_s range from 30 to 7.5 μsec (it should be noted that due to the fact that this transition is smooth, the time is measured to approximately within 20%). These data were used for calculating τ_0 , as well as $\tau_0 p$ reduced to atmospheric pressure.

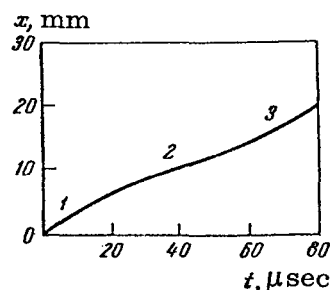


Figure 38. Coordinate x of a Reflected Wave in CO₂ as a Function of Time.
 $M_0 = 8.1$, $p_0 = 12.7$ mm of Hg.

We now estimate the shortest time during which a change in the state of the gear near the butt can effect the velocity

The time $\tau_s F$ of establishing equilibrium velocity of the reflected wave and the time τ_0 [sic] for establishing equilibrium concentration of CO_2 are given below

u_0 , m/sec . . .	2040	2180	2265	2400	2420	2580
M_0	7.67	8.1	8.45	8.9	9.05	9.6
D_2 , m/sec . . .	280	290	290	300	300	320
T_2 , °K	2700	2900	3000	3200	3200	3300
T_2' , °K	3800	4300	4600	4900	5000	5500
P_2 , atm	14.0	17.0	19.0	21.0	22.0	26.0
a_2 , m/sec . . .	880	920	960	1010	1020	1080
$(a_2)_\infty$, m/sec . .	1000	1060	1100	1130	1150	1200
τ_s , μsec	30	28.2	8.3	12.0	7.6	8.3
τ_0 , μsec	21.6	20.5	6.1	8.8	5.6	6.1
$\tau_0 P$, $\mu\text{sec} \cdot \text{atm}$	300	350	115	185	123	157

/84

The relationship between the relaxation time and the time for obtaining equilibrium velocity of a reflected wave can be determined more exactly from Eq. (4.6) derived by Spence. This formula uses the ratio of specific heats γ , which has different values across the front and near the piston. However, calculations using this expression show that the ratio τ_s/τ_0 depends little on the value of γ when the latter is in the range from 1.3 to 1.15.

Applying Eq. (4.6) to the measured times for establishing equilibrium velocity of the reflected wave in CO_2 we see, that τ_0 the dissociation relaxation time is by approximately 60% lower than the time τ_s of establishing equilibrium velocity of the wave

M_0	7.67	8.1	8.45	8.9	9.05	9.06
u_0 , m/sec	280	290	290	300	300	320
a_0 , m/sec	1000	1000	1100	1130	1150	1200
τ_s/τ_0 ($\gamma = 1.3$)	1.66	1.65	1.63	1.63	1.62	1.63
τ_s/τ_0 ($\gamma = 1.15$)	1.64	1.63	1.61	1.61	1.60	1.61
τ_s/τ_0 from (4.7)	1.39	1.38	1.36	1.36	1.35	1.36

The values of τ_s/τ_0 , determined on solving the problem of flow of gas undergoing relaxation ahead of the piston, is only by 15% higher than the value obtained from simple considerations concerning the propagation of elementary disturbances with the speed of sound from the butt to the shock wave ($\tau_s/\tau_0 = 1/(1-M)$). The dependence of time of establishing equilibrium dissociation on the temperature of the gas behind a reflected shock is shown in Fig. 39. Here T_2' denotes the temperature across the reflected shock, calculated on the assumption of frozen dissociation and excited rotational and vibrational degrees of molecular freedom; $\tau_0 P$ are the times of dissociation relaxation τ_0 reduced to atmospheric pressure, recalculated from experimental values of τ_s using Eq. (4.7).

The relaxation times plotted in Fig. 39 were obtained indirectly. It is of interest to compare the relaxation time thus obtained with some results obtained

by other methods. In [136] the temperature of the CO_2 was measured behind the reflected wave under conditions reproducing those of our experiments. The temperature behind a reflected wave in CO_2 for an incident wave velocity of 2100 m/sec, $p_0 = 12$ mm of Hg at a distance of 10 mm from the butt after the passing of the reflected shock was 3350°K , and after $13 \pm 5 \mu\text{secs}$ it dropped to 2600°K . The first value corresponds to the temperature behind the reflected shock wave with excited vibrations and frozen dissociation, while the second is for equilibrium temperature calculated on the basis of the velocity of the incident wave at the butt. The time needed by the temperature to reach its equilibrium value, reduced to atmospheric pressure, is about $200 \pm 70 \mu\text{secs}$.

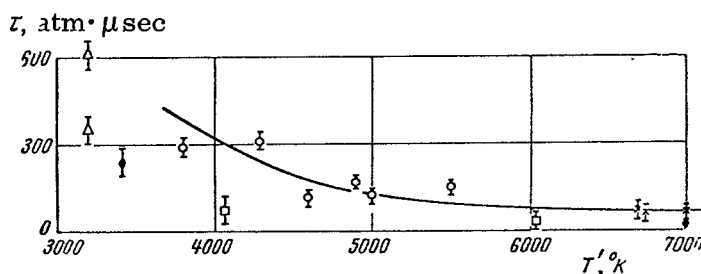


Figure 39. The Relaxation Time in CO_2 as a Function of the Temperature ($T_2' \text{ K}$ is the Temperature For the Case of Nonequilibrium Dissociation).

O— $p_0 = 12.7$ mm of Hg; x— $p_0 = 3$ mm of Hg; +—From [136]; Δ—From [142].

The time for establishing equilibrium temperature at $T = 7000^\circ \text{K}$ ($M = 11$, $p_0 = 12.7$ mm of Hg), according to [146] is not more than $6 \mu\text{secs}$ ($6 \mu\text{secs}$ is the time needed for establishing reliable readings of the temperature-measuring apparatus in the given experiments). This time, reduced to atmospheric pressure, is not more than $280 \mu\text{secs}$.

Some information on the dissociation relaxation time can be obtained by measuring the concentration of CO_2 and the temperature behind the incident wave, which were determined on the basis of ultraviolet absorption in [147]. For $M_0 = 10.5$, $T_2 = 3320^\circ \text{K}$, and $p_0 = 0.36$ atm no composition or temperature changes were recorded along the entire plug up to the contact surface ($t = 25 \mu\text{secs}$). For $M_0 = 12.5$, $p_0 = 0.5$ atm and $T_2 = 4050^\circ \text{K}$ a region was observed behind the front, which corresponded to a drop in the temperature and CO_2 concentration during $15 \mu\text{secs}$ of laboratory time. This time reduced to $7 \mu\text{secs}$ for $M_0 = 14.8$. The time of existence of these inhomogeneous regions reduced to atmospheric pressure,

in the coordinate system moving with the gas particles is 75 μ secs at $T = 4050$ and 21 μ secs at $T = 6000^\circ$ K. On the basis of results obtained by the present authors and in [136, 147] it can be concluded that the dissociation relaxation time for CO_2 behind a shock wave at temperatures of $3000-6000^\circ$ K reduced to atmospheric pressure, is of the order of $3-1 \cdot 10^{-4}$ secs. /86

These results pertain to dissociation of CO_2 with a 2% content of water vapor. Of interest for gasdynamic studies is the relaxation time in moist CO_2 , since flows of this gas practically always take place in the presence of water vapor.

The relaxation of dissociation and vibrations at high temperatures has an appreciable effect on the flow of CO_2 and, in particular, on the state of the gas behind a shock which is produced in flows about bodies. The determined dissociation relaxation times can be used to determine the distances at which equilibrium variables of CO_2 are established behind a normal shock. The results obtained for a normal shock give an idea about the state of the gas behind a detached shock which is produced in the flow about a blunt body, for example, when a space ship enters the atmosphere of the planet Venus. At atmospheric pressure behind the shock, when the velocity of the incoming flow is 4 kg/sec equilibrium behind the shock wave is established at a distance of 3 cm from the shock front, for a flow velocity of 3 kg/sec this distance is 10 cm, while at 2.5 km/sec equilibrium is not established at a distance greater than 15 cm.

The gas temperature in the above region ranges from T'_2 at the front corresponding to frozen dissociation, equilibrium values. The difference between these temperatures is several thousand degrees.

3. Determining The Dissociation Relaxation Time of Mixtures of CO_2 With N_2 at $T = 1000-3000^\circ$ K On The Basis of Nonsteady Propagation of a Reflected Shock Wave

Experiments with reflected shock waves in a mixture of CO_2 and N_2 were performed to determine the effect of diluting strongly dissociating CO_2 by N_2 which does not dissociate at these temperatures [150]. The experiments were performed using the UT-2 facility. The initial pressure was 12 mm of Hg, the incident-wave velocity ranged from 1700 to 2500 m/sec. As in the case of pure CO_2 , it was observed that for incident waves with $M < 8$ the reflected wave undergoes a deceleration, which in this case was attributed to the development molecular dissociation /87 in CO_2 behind the reflected wave. The experimental results are given in Fig. 40.

The velocity of the reflected wave immediately after reflection, on the other hand, exceeds the value precalculated on the assumption of complete equilibrium behind the reflected wave (curve 1), and approaches the curve obtained on assumption of frozen dissociation (curve 2), and in several cases ($u_0 = 1800-1900$ m/sec) even exceeds it. This shows that the gas at the butt is not in equilibrium. The velocities after deceleration lie somewhat below curve 1. The time needed by the velocity of the reflected wave to reach its equilibrium value was measured to within about 40%.

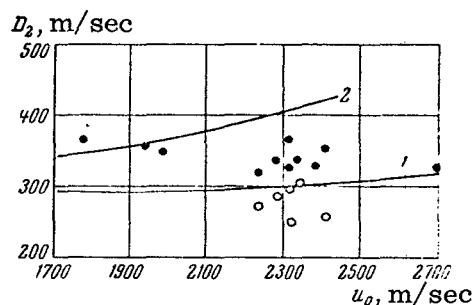
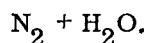


Figure 40. Velocity D_2 of Reflected Wave as a Function of u_0 , the Velocity of the Incident Wave, in a Mixture of 74% CO_2 + 24%



o—Velocity of Reflected Shock Wave After Deceleration; o—The Same at the Butt.

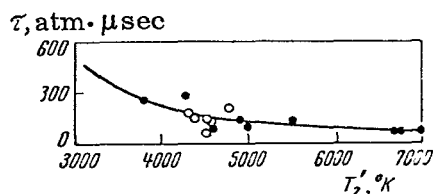


Figure 41. Comparison of τ the Relaxation Time in CO and in a CO_2 - N_2 Mixture as a Function of the Nonequilibrium Temperature of the Gas, $T^\circ \text{K}$.

●— CO_2 ; ○— N_2 - CO_2 Mixture.

The values of dissociation times τ_0 calculated on the basis of measured τ_s are presented below

$T_2 \text{ eg}$	2900	2950	3350	2700	2630	2500	3050	2900	3000	3000	2900
$u_0, \text{ m/sec}$	2150	2200	2550	1800	1750	1590	2200	2100	2150	2150	2030
$p_2, \text{ atm}$	14					7.1	15.7	12.6	14.0	14.5	12.3
$D_2 \text{ theo}$	305	310	320	300	290	285	300	295	305	305	295
$a_2, \text{ m/sec}$	1150	1180	1290	1020	995	910	1180	1130	1150	1160	1120
M_2	0.32	0.28	0.25	0.34	0.36	0.40	0.30	0.30	0.28	0.29	0.28
$T_2', ^\circ \text{K}$	4570	4800	5700	3500	3400	2850	4800	4400	4570	4600	4300
$\tau_0, \mu\text{sec}$	6.1	—	—	—	—	—	14.8	13	11.6	11.5	16.5
$\tau_0 p, \mu\text{sec} \cdot \text{atm}$	85	—	—	—	—	—	232	164	162	167	202

The dissociation time $\tau_0 p$, reduced to atmospheric pressure is shown in the last line. This value is shown by triangles in Fig. 41, as a function of temperature T_2' pertaining to the initial state of the gas behind the reflected wave (without dissociation). The same graph denotes by dots the values of the dissociation relaxation time for CO_2 without nitrogen [148]. It can be seen from the graph that the time for establishing equilibrium composition in moist CO_2 mixed with 25% of N_2 is of the same order for the time of establishing equilibrium dissociation in moist CO_2 without N_2 . /88

4. Effect of Nonequilibrium Ionization on the Propagation of a Reflected Shock Wave in Argon

As was noted in earlier works [104], the observed velocity of a reflected shock in argon is smaller than the theoretical equilibrium values, which is attributable to energy losses attendant to reflection of the wave from the tube's end. It was discovered on examining scans of schlieren patterns of reflection in argon that the velocity of the reflected wave under some regimes is not constant. This velocity decreases from its values at the end, which exceed those at

equilibrium, to the lower values at the contact surface. Apparently, the reduction in the wave's velocity is attributable to changes in boundary conditions at the tube's end, where the state of the gas changes as equilibrium ionization is established. It can vary partially also because of losses.

In order to analyze the effect of the nonequilibrium ionization process on the velocity of the reflected wave, we have compared ΔD_{ex} , the observed change in the reflected-wave velocity, with the theoretical change in the velocity of a reflected wave on transition from the state with frozen ionization of equilibrium ionization of argon behind the reflected wave. The theoretical data for the initial pressure $p_0 = 10$ mm of Hg were taken from [45], while the theoretical data for initial pressures of 5 and 1 mm of Hg were interpolated from data for 10 and 0.8 mm of Hg. Below are presented the equilibrium variables for argon behind incident and reflected waves for $p_0 = 0.8$ mm of Hg and $T_0 = 293^\circ \text{K}$

M_0	7	8	8.5	9	9.5	18
u_0 , m/sec . .	2240	2540	2710	2840	3000	5720
T_1 , $^\circ\text{K}$. . .	4800	6000	6700	7200	7900	12000
p_1 , atm . . .	0.065	0.085	0.095	0.108	0.12	0.50
ρ_1 , g/cm ³ . .	$6.5 \cdot 10^{-6}$	$6.8 \cdot 10^{-6}$	$6.8 \cdot 10^{-6}$	$7.2 \cdot 10^{-6}$	$7.3 \cdot 10^{-6}$	$17.4 \cdot 10^{-6}$
x_e	$0.16 \cdot 10^{-5}$	$0.76 \cdot 10^{-4}$	$0.55 \cdot 10^{-3}$	$0.4 \cdot 10^{-3}$	$0.35 \cdot 10^{-2}$	0.14
M_0	7	8	8.5	9	9.5	18
T_2 , $^\circ\text{K}$. . .	9000	10000	10000	10500	11000	14000
p_2 , atm . . .	0.32	0.47	0.53	0.61	0.75	5.0
ρ_2 , g/cm ³ . .	$17 \cdot 10^{-6}$	$22 \cdot 10^{-6}$	$24.8 \cdot 10^{-6}$	$27 \cdot 10^{-6}$	$31 \cdot 10^{-6}$	$146 \cdot 10^{-6}$
x_e	0.025	0.028	0.0282	0.016	0.005	0.158
n_e , 1/cm ³ . . .	$6.45 \cdot 10^{15}$	$0.91 \cdot 10^{16}$	—	$1.93 \cdot 10^{16}$	$3.2 \cdot 10^{16}$	$4.1 \cdot 10^{17}$
D_2 , km/sec .	0.45	0.33	—	0.27	—	—

The observed reduction of the velocity of a reflected wave is compared below with the calculated reduction in velocity when passing from the frozen to the equilibrium state in argon:

/89

M_0	7.64	7.1	6.8
p_0 , mm of Hg . .	5	10	1
D_{20} , m/sec . . .	1065	1065	875
D_{2k} , m/sec . . .	880	935	740
$(\Delta D_2)_{\text{exp}}$ m/sec .	185	80	135
$(\Delta D_2)_{\text{theo}}$ m/sec .	220	160	120

It should be noted that the final shock-wave velocities were somewhat lower than the theoretical equilibrium values.

The relationship between the time required for changing the velocity of the reflected and with the time required for changing the boundary condition at the shock-tube end is determined by considering the flow of a gas between a piston and a shock wave in a gas undergoing relaxation [18, 111].

The relationship between the time for changing the shock wave velocity τ_s and the ionization time τ_0 behind a reflected wave in argon

M_0	7.4	7.1	6.8
T_2' °K	12 900	11 800	11 800
T_2 °K	10 000	10 000	8 800
p_2 , mm of Hg	2 000	3 500	300
$M_s = D_s/a_0$	0.60	0.59	0.50
τ_s/τ_0	1.9	1.6	1.8

It follows from the above data that the velocity of the reflected wave changes during a time which is almost two-fold greater than the time for changing the degree of ionization. Nonsteady propagation of the reflected shock wave was observed under the above conditions over the entire path, up to interaction with the contact surface, i. e., during approximately 100–200 μ secs. It may be concluded from this that nonequilibrium ionization exists under these conditions for more than 50–100 μ secs.

It was established by measuring the ionization rate behind an incident shock that the ionization time for argon at 10^4 °K is 25 μ secs in the laboratory system of coordinates up to pressures of 1 atm behind the shock wave [149]. The time reduced to a pressure of 4,5 atm and a coordinate system moving with the gas is approximately 100 μ secs. Extrapolation of data of [149] to conditions behind a reflected shock wave thus shows that during the time the reflection process is observed until the reflected wave meets the contact surface the ionization of argon does not reach its equilibrium value and the reflected wave propagates attendant to continuously varying boundary conditions at the end, which affects the change in the velocity of the reflected shock wave.

CHAPTER 5

REFLECTION OF OBLIQUE INCIDENT SHOCK WAVES IN A REACTING GAS (MACH REFLECTION)

1. Irregular Reflection of Shock Waves in an Ideal Gas

The reflection of shock waves from an inclined surface can produce two wave configurations, depending on the reflection conditions. The simplest configuration is regular reflection.

The shock wave, moving with speed u_0 , is incident on the solid surface at an angle ω_1 . In the coordinate system moving with the wave the gas flows into the latter with a velocity $u_0 \operatorname{cosec} \omega_1$ and is deflected through an angle l . Since subsequently to this the flow should be parallel to the wall, a reflected wave is formed which will turn the flow in the opposite direction through the same angle l .

Specifying the incident angle ω_1 and the shock wave strength defines uniquely the state of the gas in the region between the incident and reflected waves. The strength and position of the reflected wave is determined by the equation of the shock polar (curve). But, for a given angle of turning of the flow the shock polar defines two different shock waves, those of the weak and those of the strong family. As is shown experimentally, the reflected wave belongs to the weak family of waves. This means that in the limit, when approaching incident waves with infinitesimal strength, the strength of the reflected wave also tends to zero, and the angle of reflection approaches the angle of incident, which is actually observed in acoustics. When $\omega_1 \rightarrow 0$, the reflected wave of the weak family is transformed into a wave with which we dealt on normal incidence of a shock wave onto a solid body.

It follows from the properties of the shock polar that regular reflection is by no means always possible. For a given incident-wave strength there exists a limiting angle ω_k ; regular reflection is not possible when $\omega_1 > \omega_k$. For an infinite incident-wave strength this angle approaches $\arcsin 1/l$, i.e., for gases with $l = 1.4$, $\omega_k = 40^\circ$. For waves with infinitesimal strength $\omega_1 \rightarrow 0$, i.e., regular reflection is possible for any angles of incidence.

/91

On reflection of shock waves ω_1 , the angle of incidence, is not identical with angle of reflection ω_2 , which may be both greater and smaller than ω_1 . For a some angle of incidence $\omega_1^* = 1/2 \arccos \gamma - 1/2$, $\omega_1 = \omega_2$. When $\omega_1 > \omega_1^*$, $\omega_2 < \omega_1$, when $\omega_1 < \omega_1^*$, $\omega_2 > \omega_1$. Angle ω_1^* is independent of the strength of the incident wave.

In cases when regular reflection is impossible, the incident A and reflected AR waves move away from the wall (Fig. 42) and a third shock wave is formed;

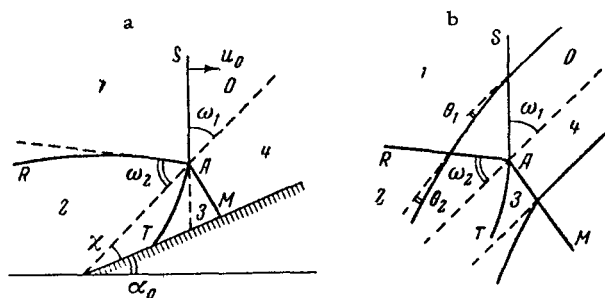


Figure 42. Schematic of Mach Reflection.

a—In the Coordinate System Tied to the Stationary Wall; b—in the Coordinate System Tied to the Triple Point.

it is termed the Mach wave AM. The gas near the wall passes only through one wave, while far from the wall it passes through both the incident and reflected wave. Consequently, there should exist a contact discontinuity, emerging from the "triple" point, i. e., line AT. This wave reflection pattern is called Mach reflection (named after the physicist Mach who has first observed this phenomenon).

The Mach reflection phenomenon is so complex that up to present no theory is available for calculating, even in the case of an ideal gas, the entire flow field and which would have given satisfactory agreement with experimental results in the entire range of Mach numbers of the incident wave and for all angle of the reflecting surface.

Theoretical study of the reflection is difficult not only because we are dealing with a nonlinear problem, but also due to the fact that the entropy of the system is changing and that the motion is of the vortex-flow type.

The first method of obtaining a solution consists in linearizing the basic equations of motion on the assumption that the incident shock is weak. In this case the change in entropy is a third-order infinitesimal as compared with the incident shock strength and it can be disregarded. This method was first used by Sommerfeld [151].

/92

A second method consists in considering an incident shock of arbitrary strength and assuming that the obstacle introduces only small disturbances into the homogeneous flow behind the shock. This method was developed by Lighthill [152] and Ting and Ludloff [153, 154] and is used successfully by many other authors [155, 156].

The above approaches yield results in satisfactory agreement with experimentally obtained data [155, 157].

A more complex case of Mach reflection, i. e., that occurring when the variables of the medium undergo sharp changes at relatively small distances

(so-called short waves), was studied by Ryzhov and Khristianovich [158, 159]. The case of Mach reflection considered by them takes place at close-to-critical angles of incidence.

The majority of experimental studies of Mach reflection pertains to weak waves with $M < 3-4$. Studies in this range of Mach numbers have yielded the following relationships for long shock waves [160-164]:

- a) the triple point moves along a straight line inclined at a constant angle to the reflecting surface;
- b) angle χ for an constant-strength incident wave increases with an increase in the angle of the reflecting surface;
- c) the motion of the triple wave configuration is self-similar.

The angles between waves in the Mach configuration is determined satisfactorily from the three-shock theory. In the general form this theory makes it possible to describe the flow of the gas in all the angular regions which are formed by the interacting waves. A detailed solution of the problem of wave interaction can be found, for example, in [165] for the steady-state case. For solving the problem of the Mach configuration, i.e., for the quasi-steady case, this theory was used in [162, 166]. Let us consider the pattern of the Mach reflection (Fig. 42, a). For this it is convenient to use a coordinate system tied to the triple point, since in this system the reflection can be regarded as quasi-steady. Then the triple configuration can be examined without reference to the reflecting surface (Fig. 42, b). The location of shock waves in such a configuration will depend appreciably on the direction of the incoming flow. In the coordinate system in which the triple point is at rest the direction of the incoming flow is determined by angle ω_1 . The flow of the gas in the close vicinity of the triple point is depicted schematically in Fig. 42, b.

The Mach reflection in the coordinate system tied to the triple point is similar to regular reflection when the latter is produced by a surface passing through the line of motion of the triple point perpendicular to the figure. By analogy with regular reflection we shall also term angles ω_1 and ω_2 in the Mach reflection as angles of incidence and reflection, respectively. In comparing with experimental results resort is had to the fact that the angle of incidence is related to the angle of motion of the triple point and the angle that the reflecting surface makes with the shock wave (wedge angle) by the relationship

$$\omega_1 = 90^\circ - (\chi + \alpha_0).$$

Angles ω_1 and ω_2 in the Mach reflection are related to angles of incidence and reflection on regular deflection by the expressions

/93

$$\omega_1^{\text{Mach}} = \omega_1^{\text{reg}} - \chi,$$

$$\omega_2^{\text{Mach}} = \omega_2^{\text{reg}} + \chi.$$

We now denote by ρ , u , p , T , μ , and H the density, velocity, pressure, temperature, molecular weight and enthalpy of the gas, respectively; by 0 - the state ahead of the shock (Fig. 3); by 1 the state behind the incident shock wave; by 2 is the state behind the reflected wave; by 3 the state behind the Mach wave, and by 4 the state ahead of the Mach wave, which is the same as state 0. The gas variables in region 1 are determined on the basis of velocity u_0 by the method described in Chapter 4.

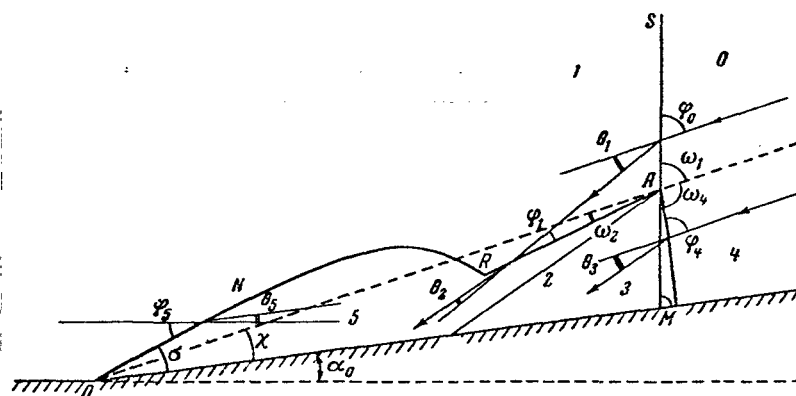


Figure 43. Schematic Depicting the Reflection of a Shock Wave.

Let us consider a coordinate system tied to the triple point. In this system the gas "flows" into the incident wave with the velocity $u_0/\sin\omega_1$ at the angle $\varphi_0 = \omega_1$. The incident wave deflects the flow passing through it by angle θ_1 . The value of this angle is determined from the continuity equation

/94

$$\frac{\tan(\varphi_0 - \theta_1)}{\tan \varphi_0} = \frac{\rho_0}{\rho_1}, \quad \theta_1 = \arctan \left[\frac{(1 - \rho_0/\rho_1)\tan\varphi_0}{1 + \rho_0/\rho_1 \tan^2 \varphi_0} \right].$$

The velocity of the gas behind shock wave AS in the coordinate system tied to the triple point is

$$\bar{u}_1 = \sqrt{u_1^2 + u_0^2 \cot^2 \varphi_0}.$$

Let us consider the shock polar in coordinates p_2, θ_2 for the reflected wave. Let the reflected wave be situated at angle φ_1 to the flow coming in with velocity \bar{u}_1 , then the normal component of the flow velocity will be $\bar{u}_{1n} = \bar{u}_1 \sin \varphi_1$

We write the conservation equations at the reflected wave

$$\begin{aligned} \rho_1 \bar{u}_{1n} &= \rho_2 \bar{u}_2, \\ \rho_1 \bar{u}_{1n}^2 + p_1 &= \rho_2 \bar{u}_2^2 + p_2, \\ H_1 + \frac{\bar{u}_{1n}^2}{2} &= \frac{\bar{u}_2^2}{2} + H_2, \quad \theta_2 = \arctan \left[\frac{\left(1 - \frac{\rho_1}{\rho_2}\right) \tan \varphi_1}{1 + \frac{\rho_1}{\rho_2} \tan^2 \varphi_1} \right]. \end{aligned}$$

Solving this system by the same trial-and-error method as for the case of the incident wave, we will get for a number of values of \bar{u}_{1n} values of p_2 and θ_2 , i.e., the shock polar in the $p_1\theta_1$ plane, whose points represent possible values of the pressure ratio p_2/p_1 attendant to passing through the reflected wave and the deflection $\theta = \theta_2 - \theta_1$ of the flow in region 2.

Let us now construct the shock polar for the Mach wave. If this wave is situated at angle $\varphi_1 = 180^\circ - \omega_1$ to the incoming flow, then the normal component of the velocity to the Mach wave

$$u_M = u_0 \frac{\sin \varphi_1}{\sin \omega_1}.$$

The conservation equations at the Mach wave will be written as

$$\begin{aligned} \rho_0 u_M &= \rho_3 u_3, \\ \rho_0 u_M^2 + p_0 &= \rho_3 u_3^2 + p_3, \\ \frac{u_M^2}{2} + H_0 &= \frac{u_3^2}{2} + H_3, \\ p_3 &= \frac{\rho_3 R T_3}{\lambda_{13}}. \end{aligned}$$

Solving this system by the trial-and-error method, we find the values of p_3 and ρ_3 for the given u_M . The angle θ_3 of flow deflection is found from

$$\tan \theta_3 = \frac{\tan \varphi_1 (1 - \rho_0 / \rho_3)}{1 + \rho_0 / \rho_3 \tan^2 \varphi_1}$$

/95

By specifying different values of u_M it is possible to construct the shock polar for the Mach wave in the coordinates $p_3\theta_3$. In order to find the sought solution, one must satisfy the compatibility conditions which require that the pressures be equal and the flows be parallel in regions 2 and 3

$$p_2 = p_3, \theta_3 = \theta_1 - \theta_2.$$

These conditions are satisfied at the point of intersection of shock polars for the reflected and the Mach wave.

All the angles of the Mach configuration are determined from

$$\sin \varphi_1 = \frac{\bar{u}_{1n}}{u_1}, \quad \omega_2 = \varphi_1 - \theta_1,$$

$$\sin \varphi_4 = \frac{u_M}{u_0} \sin \omega_1, \quad \omega_4 = 180^\circ - \varphi_4.$$

It should be noted that the three-shock theory examined above presupposes uniformity of flow in regions bound by the shock waves. This means that: 1) all the intersecting discontinuities are straight lines and 2) the flow parameters do not depend on the distances from triple point A and that these variables are constant in each of the regions bound by the discontinuities.

Let us now compare results obtained on application of the three-shock theory with experimental data (Fig. 44) [162]. The curves were calculated for two incident-wave strengths: $x = p/p_1 = 0.8$ and $x = 0.2$. The experimental data obtained in the shock tube pertain to regular reflection (circles) and to Mach reflection (crosses).

For strong shock waves (●) with pressure gradients across the wave of 0.2 there is no disagreement with theory. In the case of the weaker shock wave with $x = 0.8$ the deviation from the theoretical case is quite appreciable (○). In a weak incident wave the transition from regular to Mach reflection is continuous, while according to theory the angle of reflection should change in a quite large step. In addition, the angles proper differ appreciably. Smith [167] showed that satisfactory agreement between theory and experimental data is obtained for shock waves with $x \leq 0.4$ with substantial deviations appearing as early as for $x \geq 0.5$.

It thus turns out that the three shock theory is valid only for strong shock waves. A successful explanation of the paradox observed in the Mach reflection is given in [168]. The principal ideas expressed there are most conveniently analyzed using shock polars in the p, θ plane, where p is the pressure and θ is the angle of flow deflection.

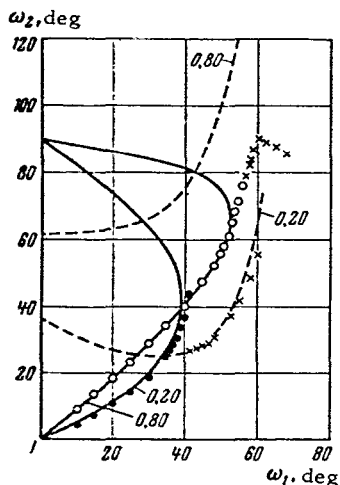


Figure 44. Comparison of Theoretical and Experimental Relationships of Reflection Angles ω_2 to Angles of Incidence ω_1 on Regular and Mach Reflection [162], Calculated According to the Three-Shock Theory (Dashed Curves) and According to the Theory of Regular Reflection (Solid Curves).

Figure 45 depicts the shock polar for regular reflection. The pressure behind the reflected shock wave, divided by the constant pressure ahead of the incident wave is laid off on the coordinate axis, while angle θ , defining the deflection of the flow from its initial direction is laid off on the abscissa. Curve ABCDA is the shock polar corresponding to one Mach number of the incoming flow. If the strength of the shock wave and its inclination is specified, then we have on the shock polar one point which defines the state of the gas (p, θ), in a region behind the shock wave. Let this point be point I and lie in the supersonic region. Point I can then serve as the initial state for drawing a second shock polar IRER'FLI. The state of the flow behind the reflected shock wave corresponds to one point on this polar. It is obvious that the gas flow behind the reflected wave should be parallel to the surface of the wall, i.e., the angle of deviation should be zero. This condition is satisfied by points R and R'. The state defined by point R' corresponding to a high pressure usually is not realized, since it pertains to a family of strong waves.

/97

Let now the strength of the incident wave increase, but the Mach number of the incoming flow remain the same, i.e., only the angle of incidence (ω_1) changes. This means that point I

moves away from point A. The reflected wave becomes weaker. The shock polar corresponding to the reflected wave will not intersect the abscissa axis and points R and R' will go out of existence. There is no regular reflection (Fig. 45,b) and we have the case of Mach reflection. In this reflection of the flow behind the triple point is divided by the contact discontinuity into two regions. The region in which the gas passes through two shock waves - the incident and the reflected, is defined by one point on the secondary shock polar, while the region through which the gas passes through only one wave, i.e., the Mach wave is defined by one point on the primary polar. Since both these states have common streamlines, common contact surface and the same pressure, the flow behind the triple point is represented by the point of intersection of the primary and secondary shock polars, i.e., by points M and M'. Since the Mach wave should be perpendicular to the reflected surface, the flow immediately behind the wave is represented by segment MC on the first shock polar in the steady-state case.

Now we consider the intermediate case, near the point of transition from regular to Mach reflection. The shock polars for these cases are shown in Fig. 46. Here point C corresponds to the base of the Mach wave, while points R and M correspond to the state of the flow behind the reflected shock wave in the

/98

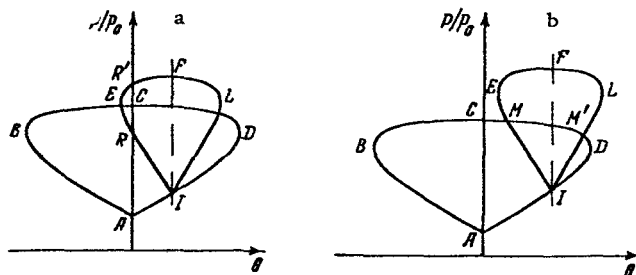


Figure 45. Shock Polars in the p/p_0 , θ Plane for Regular (a) and Mach (b) Reflections.

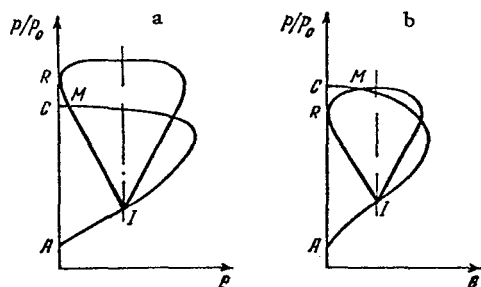


Figure 46. Shock Polars in the p/p_0 , θ Plane for Regimes Close to Those of Transition from Regular to Mach Reflection:

a—Supersonic Flow Behind the Point of Intersection; b—Subsonic Flow Behind the Point of Intersection.

found from the the theory of reflection of shock waves; the Mach number of the flow ahead of the front is 3.203, the pressure ratio across the incident wave is $p_0/p_1 = 0.433$, the angle between the incident wave and the reflecting surface should be 41.5° .

The first type of transition (a) takes place when the strength of the incident wave is higher than that for the steady-state Mach reflection. The second type of transition (b) takes place for weaker waves.

In case (b) the angle between the reflected shock wave and the reflecting surface will vary continuously on transition from regular to Mach reflection, while in the second case the angle of reflection should change in stepwise fashion. This is verified by data of Fig. 44. The case with $x = 0.20$ is for the first and that of $x = 0.80$ is for the second type of transition.

regular and Mach cases, respectively. The principal difference between cases a and b consists in the following. In the first case point M is situated on the weak branch of the shock polar, while in the second case it is on the strong branch. We note that the for the shock polars under consideration the point of maximum flow deflection is close to the sonic point. For this reason it is possible to assume with a quite negligible error that on transition to Mach reflection the flow behind the Mach wave is either supersonic (a), or subsonic (b). It is called steady-state Mach reflection when CMR becomes a single point. On steady-state Mach reflection the Mach wave is a straight line perpendicular to the wall, the flow here is sonic. The condition for steady-state reflection is easily

Let us further consider what takes place near the point of transition in region CMR. If the flow in the region behind a reflected shock wave is supersonic, its state is determined solely by the local conditions and is not affected by disturbances which arise downstream of the flow. Hence the only inhomogeneity in regions bound by discontinuities in this case can only be rarefaction waves of the Prandtl-Mayer type flow. However, as is shown in [162], this kind of flow should not exist when the flow is supersonic. Kawamura showed that the curvature of the reflected wave and of the Mach wave is infinitesimal near the triple point. Thus, the flow in regions behind the triple point is homogeneous and the flow should be defined by the three-shock theory. This is verified by experiments.

In the case when the flow behind the reflected wave is subsonic, everything becomes more complicated. In this case pronouncedly inhomogeneous flow takes place in region CMR. In a real flow this region on the p, θ diagram will have corresponding to it a highly compressed region or one singular point immediately after transition to Mach reflection.

The experimentally measured angles will not correspond to point M but rather to point R. We will have an apparently continuous variation of the magnitudes of reflection angles on transition from regular to Mach reflection, since smaller angles of reflection will be measured.

/99

Thus, two kinds of transition from regular to Mach reflection are possible. The first takes place when the flow behind the reflected wave is subsonic. In this case the angle of reflection increases continuously on transition to Mach reflection. This case contradicts the three-shock theory. The second kind of transition is that when the flow behind the reflected wave is supersonic. In this case the angle of reflection undergoes a stepwise change and its value is in agreement with that calculated by the three-shock theory. Steady-state Mach reflection serves as the transition state from the first to the second kind.

The experiments performed by Kawamura in a shock tube supply sufficiently convincing proof of the above assertions.

Thus, the use of the three-shock theory is possible if the angle of motion of the triple point is determined experimentally, i.e., this theory is only a method for describing the flow pattern. Work done by Whitham [169] and Cabannes [170] makes it possible to calculate, with some simplifying assumptions, the reflection of shock waves of any strength from a wedge with an arbitrary wedge angle. Whitham has based his deliberations on the following assumptions. The disturbances in the flow which are produced by some or other phenomena, for example, change in the tube's cross section, are regarded as waves propagating through the shock. These disturbances, which increase the Mach number of the shock, can become a discontinuity in the same manner as a plane compression wave becomes a shock. This shock, which propagates through the original shock is called a double shock. Actually this is a discontinuity in the Mach number and the inclination of the shock being considered. On Mach reflection this double shock is the trace of the triple point.

For small angles θ it is possible to compare this theory with the linear theories of Lighthill [152], Ting and Ludloff [153]. Comparison shows that Whithem's method is suitable for strong shocks with $M > 2$; its application to weak shocks requires caution.

A different calculation of Mach reflection of shock waves of arbitrary strength is given by Cabannes [170]. It is based on the following assumptions.

1. The mutual position of waves in the vicinity of the triple point can be determined by equations of shock polars, i. e., it is possible to apply to each of the shocks the laws of conservation satisfying compatibility conditions.
2. The configuration which is realized from among all those possible which satisfy the compatibility conditions is that in which the Mach wave is perpendicular to the reflecting surface.
3. A basic requirement is that requiring all the shock waves comprising the Mach configuration to be rectilinear. This theory is basically the three-shock theory, supplemented by the requirement specified in item 2. Item 2 orients the three-wave configuration relative to the reflecting surface. The ensemble of these assumptions thus makes it possible, for a given wave strength and angle α_0 of the wedge to determine angle χ and all the other angles near the triple point.

/100

Cabannes has solved this problem for a constant γ of the gas on passing through the shock, assuming it to be 1.4 ahead and behind the shock.

The Cabannes and Whithem theories are in the greatest disagreement for small θ for large θ they yield practically identical results. In addition, unlike Whithem, Cabannes has obtained a θ_{\max} , above which regular reflection should ensue.

When dealing with increasingly higher incident-wave strengths the problem arises of the effect of variable γ on the mode of Mach reflection. We know of, for example, work by White [172, 173] where he has observed changes in the wave configuration on irregular reflection in CO_2 , for which excitation of molecular vibrations and dissociation take place at sufficiently low temperatures. In this case one cannot use theories for $\gamma = \text{const}$.

2. Experimental Study of Irregular Reflection of Strong Shock Waves

To determine the effect of real properties of a gas attendant to irregular reflection of waves, studies were made of the reflection of strong shock waves in CO_2 , air, nitrogen and argon [175, 176]. In CO_2 excitation of molecular vibrations and dissociation are quite perceptible at sufficient low temperatures, when M_0 of the incident wave do not exceed 7-8. In air and nitrogen these effects at the same Mach numbers are less pronounced.

The experiments were performed with the UT-2 shock tube. A wedge with a vertex angle of α_0 was placed into the test section. In the majority of cases the wedge was raised above the lower wall of the tube. The process was visualized by the schlieren method. It was photographed by the SFR-L camera and the FR-185 photorecorder, which made possible obtaining time scanning of the process.

The vertex angles of the wedge were 10, 24, 28, 32 and 36°. The initial pressure p_0 ahead of the incident wave was usually 12.7 mm of Hg = $1.68 \cdot 10^4$ dynes/cm².

The angles between all the waves comprising the Mach configuration were measured on the photographs and their variation in time was checked. The shock wave velocity was measured from the photographs and at the same time by means of piezoelectric pickups placed along the tube.

A sequence of frames of diffraction of shock waves in CO₂ on a wedge with a vertex angle of 24° is shown in Fig. 47, a. The wave velocity was $u_0 = 1900$ m/sec, which corresponds to $M_0 = 7.2$, and the initial pressure was 12.7 mm of Hg.

/101

The picture of reflection of a shock wave from a wedge with the same angle of opening for a wave propagating in N₂ with $u_0 = 2100$ m/sec ($M = 5.9$) for the same initial pressure is shown in Fig. 47, b. Beneath the photographs are shown schematics which clarify the location of waves in the Mach configuration. The wave moves from left to right. SA is the undisturbed part of the incident wave, AM is the Mach wave, ARNO is the reflected wave AT is a tangential discontinuity, and L is the time mark. Point R denotes a break of the reflected wave in CO₂. The time between successive frames was 4 μ secs.

/102

The knife edge of the IAB-451 instrument is vertical, for which reason the density gradients in the vertical direction of the knife edge are less discernible than in the horizontal direction.

The photographs taken in CO₂ show clearly that the reflected wave has a break. A new shock wave is formed at the break, i. e., a second triple point is formed. The reflected wave is situated below the path of motion of the triple point. The Mach wave changes its inclination on passing from the triple point to the surface of the wedge.

The instability of the tangential discontinuity is clearly expressed. In nitrogen the tangential discontinuity curls up into an eddy. It is particularly clearly seen in the third-fourth frames (Fig. 47, b). This type of instability was noted in [171, 96, 176] on diffraction of shock waves in a cylinder. In CO₂ at the vertex near the triple point one can see sharp fluctuations of the tangential discontinuity. Their amplitude increases gradually as one moves away from the triple point and an angular region is formed.

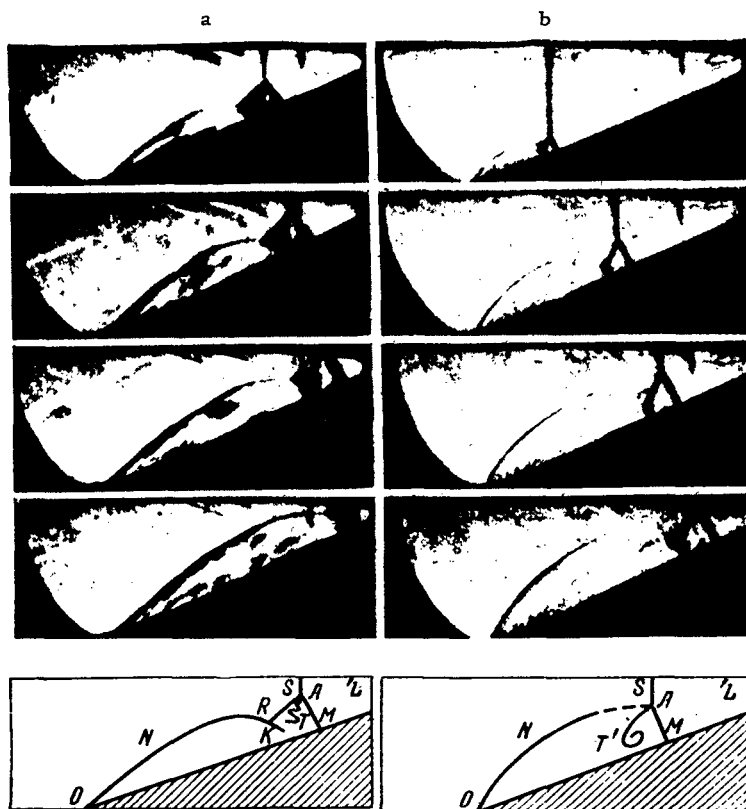


Figure 47. Irregular Reflection of Shock Wave from a Wedge With $\alpha_0 = 24^\circ$ in CO_2 (a) and N_2 (b).

Mach reflection was observed during a short time interval, limited by the time during which the shock wave passed along the wedge. For a wave with $u_0 = 2$ km/sec this time is not more than $30 \mu\text{secs}$. During this time the process is self-similar, the accuracy being 3%.

The self-similarity of the pattern in the range of Mach numbers under study made it possible to use photographing scanning in time and to calculate the angles in the Mach configuration from the photographs thus obtained (Fig. 48). As long as the shock wave propagates from the forward edge of the wedge to position 1, only one point on the wave is seen through the slot. On the scan the wave "draws" line SA. The wave velocity u_0 is determined on the basis of the angle of this line.

After the triple point intersects the slot, the Mach and the reflected waves appear in the field of vision and, consequently, line AS forks out (position 2). If the reflected wave has a break with its associated second triple point, then when the point of break appears in the slot the line on the scan will break at point R (position 3). If another wave exists at the point of break, then a new line will appear on the scan starting from point R and directed toward the trace of the Mach wave.

A through hole d was made in the body of the wedge near the upper facet on the level of the slot. It is recorded on the film as a lighted line d' , parallel to the edge of the film. This line served as a distance marker. Knowing the position of waves relative to the marker we know their location relative to the nose of the wedge during any time instant. This makes it possible to obtain from the scan the angles at which the triple points move

$$\operatorname{tg}(\chi + \alpha_0) = \frac{a}{b - AA'},$$

$$\operatorname{tg}(\chi_1 + \alpha_0) = \frac{a}{b - RR'}.$$

From the above formulas angle χ is determined to within 4%. The results were processed with a tool-maker's microscope on which lengths of segments could be measured to within 0.01 mm.

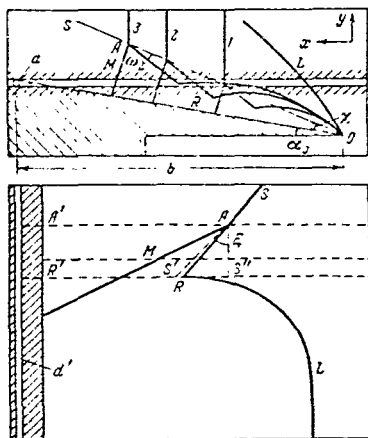


Figure 48. Schematic Diagram of the Study of Mach Reflection and Diffraction of a Shock Wave on a Wedge Using Photoscanning.

The scans can also be used to decide whether the reflected wave is located below or above the path of the triple point, i.e., to determine the sign of angle ω_2 (for the angle designation see Fig. 43). If the reflected wave past the triple point is directed along AO, the line of motion of the triple point, then the trace of its motion on the scan is denoted by straight line AS". When ω_2 is positive the trace of the motion will lie to the right of line AS", for a negative ω_2 it lies to its left. The absolute value of ω_2 is obtained from the scans (if it is taken into account that self-similarity of motion is verified by experiment) using the expression

$$\omega_2 = \arctan \left[\frac{-(RR' - S'R')K + u_0 \cdot I'R'}{u_0 \cdot A'R' \operatorname{tg}(\chi + \alpha_0)} \right] - \omega_1,$$

where K is the reduction factor.

These experiments show the following.

1. For all the gases that were studied the reflected wave has a break in the case of high M_0 ; the magnitude of the break depends on the kind of gas. Figure 49 shows scans of reflection in CO_2 and air. For the same shock-wave velocity in CO_2 and air the break in CO_2 (a) is sharply expressed and angle ω_2 is negative. In air (c) the break is barely noticeable, angle ω_2 remains positive; the break

becomes increasingly more pronounced with an increase in wave velocity. Figure 49, b shows a scan of reflection in CO_2 for a shock wave velocity of $u_0 = 960$ m/sec. Angle ω_2 is positive. As the velocity is increased to 1500 m/sec (a) ω_2 becomes negative. Figure 49, b shows a scan of reflection in air for $u_0 = 1170$ m/sec. The break in the reflected wave is very weakly expressed. The pattern is close to that of ordinary Mach reflection.

/104

2. When the incident-wave velocity is increased a new wave forms at the break and it then moves after the Mach wave (Fig. 49, a-c).

3. Features Peculiar to Mach Configuration in a Real Gas

As was pointed out in Section 1, the available methods for calculating irregular reflection require the satisfaction of the following conditions: rectilinearity of waves emanating from the triple point, homogeneity of flow in the regions between them, perpendicularity to the reflecting surface of the Mach waves, as well as the requirement that the ratio γ of specific heats remain constant.

It is seen from Fig. 47 that on reflection of a shock wave moving in CO_2 at $u_0 = 2000$ m/sec the Mach wave is not a straight line. And even if its base is perpendicular to the surface of the wedge, these conditions are not satisfied near the triple point. Hence in our subsequent calculations of the Mach configuration we shall use experimental values of χ

/105

When applying the three-shock theory to the study of wave configuration reference should be had to the formation of an angular vortex region instead of the tangential discontinuity. This problem was studied in detail in [102]. It is shown there that formation of this angular region shifts the values of angles between the waves forming the triple configuration by $1-2^\circ$, which is within the limits of experimental error. Hence when using the three-shock theory we have considered the tangential surface as the classical tangential discontinuity.

The physical and chemical transformations behind the fronts of strong shock waves were taken into account as follows. The state of the gas and the location of shock waves in the vicinity of point A were calculated on the basis of the three-shock theory (Section 1), while the enthalpies of the gas $H = H(T, p)$ were taken according to the assumed degree of physical and chemical transformations (see Appendix 5). Since the time of existence of the entire configuration in our experiments was small and commensurable with the relaxation times, calculations were made on several assumptions.

/106

Version I. The gas behind the incident as well as behind the reflected and Mach waves is in complete thermodynamic equilibrium, i. e., molecular vibrations of the gas are excited and dissociation takes place. The values of H and μ under this version were taken from tables (see Appendix).

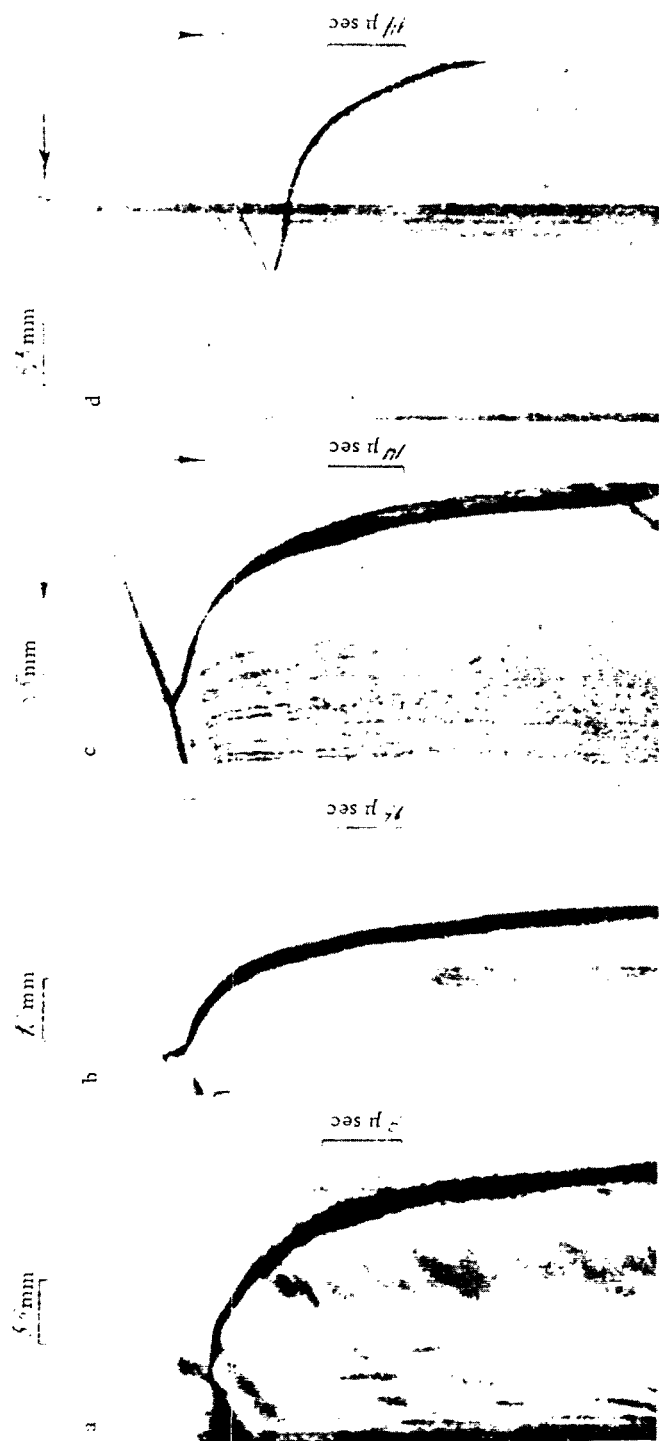


Figure 49. Photographic Scan of Mach Reflection of a Shock Wave from a Wedge With Vertex Angles $\alpha_0 = 32$ and 24° .
a— CO_2 , $u_0 = 1500$ m/sec, $\alpha = 32^\circ$; b— CO_2 , $u_0 = 960$ m/sec, $\alpha = 32^\circ$; c—Air, $u_0 = 1440$ m/sec, $\alpha = 32^\circ$; d—Air, $u_0 = 1170$ m/sec, $\alpha = 24^\circ$.

Version II. In the CO_2 and nitrogen molecular vibrations were excited while there was no dissociation. In air the oxygen molecules dissociated and molecular vibrations were excited in the N_2 . There was no dissociation in N_2 . The values of H were taken from [118, 119].

Version III. No physical or chemical transformations took place in the test gas. The ratio of specific heat in the gas behind the wave remained the same as ahead of the wave.

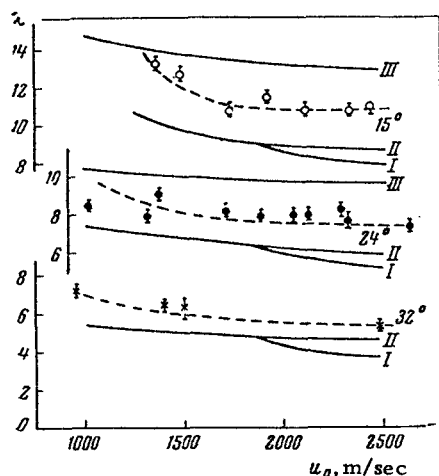


Figure 50. Experimental and Theoretical Curves of χ and Angle at Which the Triple Point Moves, as a Function of u_0 , the Incident-Wave Velocity, in CO_2 .

Experimental curves of $\chi(u_0)$ for three values of the wedge angle are given in Fig. 50. For comparison theoretical curves of $\chi(u_0)$, obtained by the method of shock polars and taking into account the fact that γ changes on passing the shock are also plotted there (Versions I, II and III). These curves show that the three-shock theory does not suffice for precalculating the angle at which the triple point moves.

A comparison of experimentally determined reflection angles ω_2 with those obtained from the three-shock theory as a function of u_0 , the incident-wave velocity for a constant wedge angle $\alpha_0 = 24^\circ$ in argon, air and CO_2 is presented in Fig. 51. The values of ω_2 as a function of u_0 and of angle ω_1 were calculated

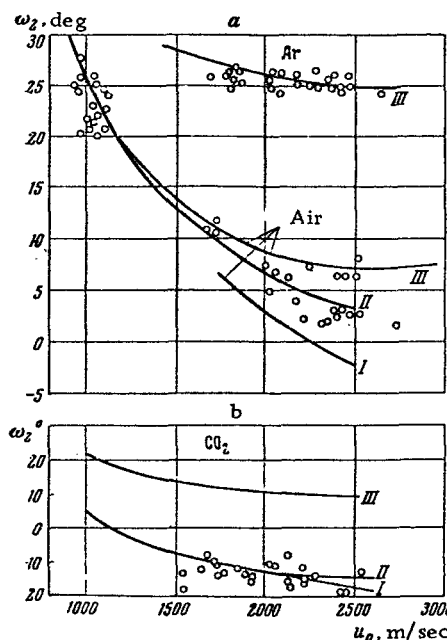


Figure 51. The Angle of Reflection ω_2 as a Function of the Incident-Wave Velocity in Argon, Air and CO_2 on Different Assumption With Respect to the State of the Gas Behind the Shock Wave.

/107

theoretically. Angles ω_2 and $\omega_1 = 90 - (x + \alpha_0)$ for u_0 were obtained experimentally.

In argon (Fig. 51, a) the experimentally obtained values of ω_2 are in agreement with curve III, since no physical or chemical transformations take place in argon under the conditions under study. In air in the range of incident-wave velocities of 900–1200 m/sec the points lie on curve III. In the velocity range of 1800–2500 m/sec the relaxation time for exciting molecular vibrations in O_2 and N_2 and the dissociation time for O_2 is shorter than the time during which the gas is in the heated state, while the dissociation relaxation time for N_2 is much greater. The points cluster around curve II. In CO_2 (Fig. 51, b) up to velocities $u_0 = 1800$ m/sec the experimental values of ω_2 lie near the curve taking into account excitation of internal degrees of freedom. Consideration of dissociation in high-velocity incident waves modifies the value of ω_2 within limits of experimental error. Due to the fact that one of the relaxation times is shorter and the other is longer than the process under study proper, the process of reflection in the velocity range under study is self-similar. It is probable that in the case of even higher velocities this self-similarity ceases to exist if the time during which the gas is in the hot state is comparable with the dissociation relaxation time.

Comparison of experimental with theoretical data (calculated with consideration of possible physical and chemical transformations) in the form of the curve of $\omega_2 = f(\omega_1)$ for a constant incident-wave velocity and different wedge angles is presented in Fig. 52. Curve I and experimental points (●) are from [162] for a velocity of the wave in air of $u_0 = 364$ m/sec. The experimental points lie by approximately 60° below. The experimental data obtained for Ar (o) and CO_2 (Δ) are in good agreement with theoretical results. The theoretical curves II for Ar become a single curve starting with velocity of 1600 m/sec and above. The curve III for CO_2 is presented for a velocity of 1900 m/sec.

In order to show the effect of physical and chemical transformations, it is convenient to use the concept of effective ratio of specific heats γ_{ef} [7]. The enthalpy of a gas undergoing physical and chemical transformations is a complex function of the temperature. Similarly to the case of a gas with constant specific heat we can introduce the expression

/108

$$h = \frac{\gamma_{ef}}{\gamma_{ef} - 1} \frac{p}{\rho},$$

where h is the specific enthalpy, p is the pressure and ρ is the density. This approximation makes it possible to use for complex calculations the Hugoniot [shock] relation, in which we now use the effective ratio of specific heats. Calculations were made for the triple configuration which is produced by a wave incident on a wedge when the former moves with a velocity of 1.9 km/sec for

different values of γ_{ef} . The relationships $\omega_2 = f(\omega_1)$ are presented in Fig. 52.

Thus, reflection angle ω_2 is very sensitive to variations in γ_{ef} . A moderate change in γ_{ef} appreciably increases the angle between the incident and reflected waves. For $\gamma_{ef} = 1.05$ angle ω_2 is negative for all values of the angle of incidence. If the gas is assumed to be ideal ($\gamma = 1.66$ and 1.4) angles ω_2 are always positive.

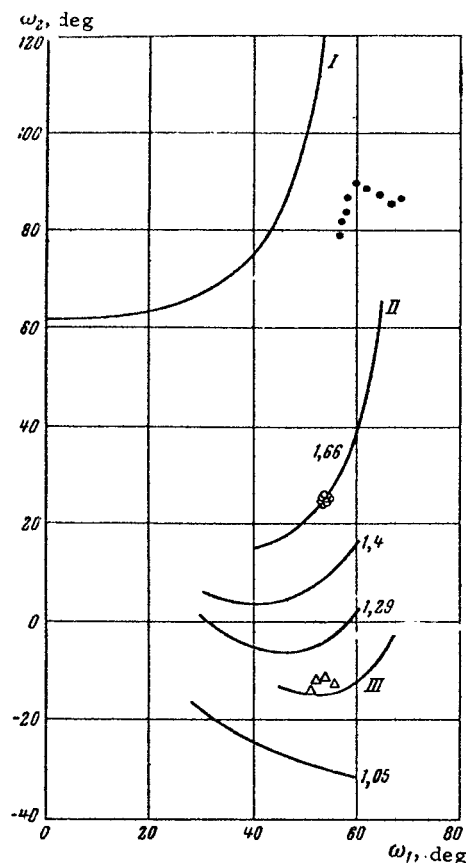


Figure 52. Curve of Angle of Reflection ω_2 vs Angle of Incidence ω_1 for Different γ_{ef} .

angles ω_2 are displaced toward the positive range.

Comparison of experimentally and theoretically obtained values of reflection angles $\omega_2 = \omega_2(\omega_1, u_0)$ validates the application of the three-shock theory modified so as to take into account variations in the γ of the gas for calculating irregular reflection of strong shock waves in the vicinity of the triple point. Since the

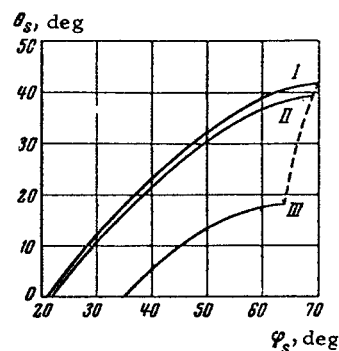


Figure 53. Angle θ_s of Flow Deflection in the Attached Wave as a Function of its Angle of Inclination φ_s to the Initial Direction of Flow, for Different Degrees of Physical and Chemical Transformations in the Gas Behind the Incident and Attached Waves.

For wave velocities of about 1800–2000 m/sec in CO_2 the state of the gas behind the reflected and the Mach waves corresponds to $\gamma \cong 1.18$, in air to $\gamma = 1.4$ and in argon to $\gamma = 1.66$. This is precisely the reason why the double configuration appears first in CO_2 .

It should be noted that as ω_0 becomes smaller, i.e., as ω_1 becomes larger,

pattern of wave diffraction on the wedge is composed of Mach reflection and of supersonic flow about the wedge angle, it is required that the reflected wave become an attached wave (see Fig. 53).

Calculations made for a wave at the forward edge of the wedge show that consideration of physical and chemical transformations also yields a sharp reduction in the angle of the attached wave and increases the speed at which the detached wave becomes an attached wave on increasing the wave velocity.

Figure 53 shows results of calculations for an oblique shock in CO_2 for different assumptions on the thermodynamic state of the gas behind the incident wave and the attached shock ($u_0 = 1900$ m/sec). Version III is for $\gamma = 1.4$, version II corresponds to consideration of excitation of molecular vibrations with the dissociation frozen, while version I assumes equilibrium dissociation and vibrations. Angle φ_3 is the angle made by the oblique shock with the initial direction of flow, while angle θ_3 is the angle through which the flow turns on passing through the shock; obviously it is equal to the wedge angle α_0 (see the schematic of Fig. 43). The values of the wedge angle for which the attached shock becomes detached are shown by the dashed line.

In an ideal gas with $\gamma = 1.4$ no attached shocks exist for $\alpha_0 > 18^\circ$. For version I, which takes into account all the molecular transformations possible at the given temperature, the limiting angle for detachment of the shock from the nose of the wedge body is 42° . This means that the change in the ratio of specific heats brought about by chemical and physical transformations changes appreciably the gas-dynamic process attendant to flow of hot gas about a wedge. Thus, when an ideal gas heated by a shock wave flows past the wedge at $u_0 = 1900$ m/sec (version III), a detached wave is formed; conversely, an attached wave is formed in a gas with vibrational molecular levels excited.

/110

The variation in ω_2 as a function of the extent of physical and chemical transformations is more pronounced than that in the angle of attached wave. In this case conditions no longer exist for smooth transition from the reflected to the attached wave, a break forms and consequently, a secondary Mach wave is formed. For negative ω_2 smooth transition is also impossible in the case when the forward edge of the wedge is removed to infinity, i.e., a Mach reflection will take place without receiving a disturbance signal from the forward edge. A Mach wave must inevitably be produced when $\omega_2 < 0$.

In the case of $\omega_2 > 0$, it is geometrically possible to have a smooth joining of the attached and reflected waves. However, as is shown experimentally, this kind of transition does not always occur and a break does form in the reflected wave. The point at which the secondary break forms can be estimated as follows. In the coordinate system moving with the triple point the gas velocity behind the reflected wave is always supersonic. Let us find the boundary of the effect of signals which disturb the region behind the reflected wave. Along the tangential discontinuity line we lay off velocity u_2 and find the point of intersection of the reflected wave with a circle of radius c_2 . We determine the difference $\chi_1 - \chi_2$.

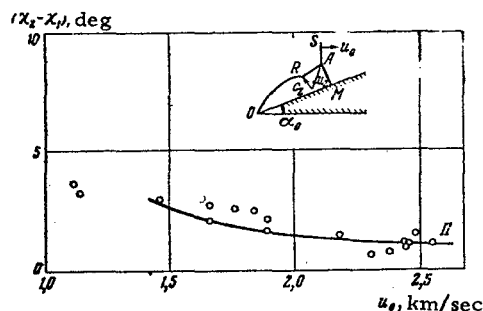


Figure 54. The Difference $\chi - \chi_1$, Between Angles at Which the First and Second Triple Points Move, as a Function of the Incident-Wave Velocity.

It may be assumed that the break on the reflected wave which is due to the need for joining the processes of reflection and flow past the vertex of the wedge will take place in point R (Fig. 54) which defines the region of influence of angular signals in the gas flow behind the reflected wave. The region of influence was calculated for version II in air. The theoretically calculated data were compared with the experimentally obtained values of $\chi_1 - \chi_2$ (Fig. 54). It can be seen that the experimental points lie on the theoretical curve. Knowing the position of the second triple point it is possible to determine from the three-shock theory the direction and strength of the secondary Mach wave in the vicinity of the second triple point.

The variation in the ratio of specific heats γ in a gas heated by a shock wave results in appreciable changes not only of the Mach configuration proper. It also affects the transition from regular to Mach reflections.

/111

Calculations show that excitation of internal degrees of freedom in the gases under study displaces the limiting angle of transition of regular into Mach reflection by 1-3°, increasing the range of regular reflection.

4. Variation in the Pressure and Temperature of the Wedge Surface

In an ordinary Mach configuration the gas pressure drops from the Mach wave in the direction of the wedge nose. In a double configuration the pressure distribution should be different due to the appearance of the secondary Mach wave. In order to calculate the pressure on the surface it is not enough to know the strength of the secondary wave in the vicinity of the second triple point, since the compression wave, or shock wave which emanates from the second triple point interacts with the tangential surface of the discontinuity and the boundary layer which develops behind the incident wave. Its strength changes. In order to determine the strength of the secondary Mach wave on the surface of the wedge, the pressure was measured by rapid-response pickups. At the same time a platinum resistance thermometer was used for measuring the temperature of the wedge surface. The pressure and heat flux pickups recorded a sharp rise in the pressure and temperature on the wedge surface. Estimates made on scanning of the instant of this rise show that the rise takes place when the region of the tangential discontinuity and the secondary Mach wave pass past the sensors. Figure 55 shows pressure oscillograms and the temperature recording for the wedge surface for a wave reflected in air from a wedge with a vertex angle of 24°. The wave velocity was 2400 m/sec. The pressure behind the Mach wave first increases, then remains constant again increases and then remains approximately constant until the reflected wave from the upper part of the tube arrives.

This means that apparently the secondary Mach wave increases the pressure behind the primary Mach wave to the pressure behind the attached wave. An additional pressure increase starts to appear at incident-wave velocities of about 900 m/sec. The pressure increases with an increase in the incident-wave velocity.

The additional increase in the wedge-surface temperature, which is recorded by the resistance thermometer, is observed in weaker waves when the pressure rise is not as yet recorded. In air the additional rise in wall temperature is observed for shock-wave velocities of about 635 m/sec. Apparently the surface temperature increase is a result of turbulization of the contact surface, as well as of the increase in the temperature and velocity of the gas behind the secondary shock wave. The resolving power of the apparatus used did not suffice for separating these two factors in time.

/112

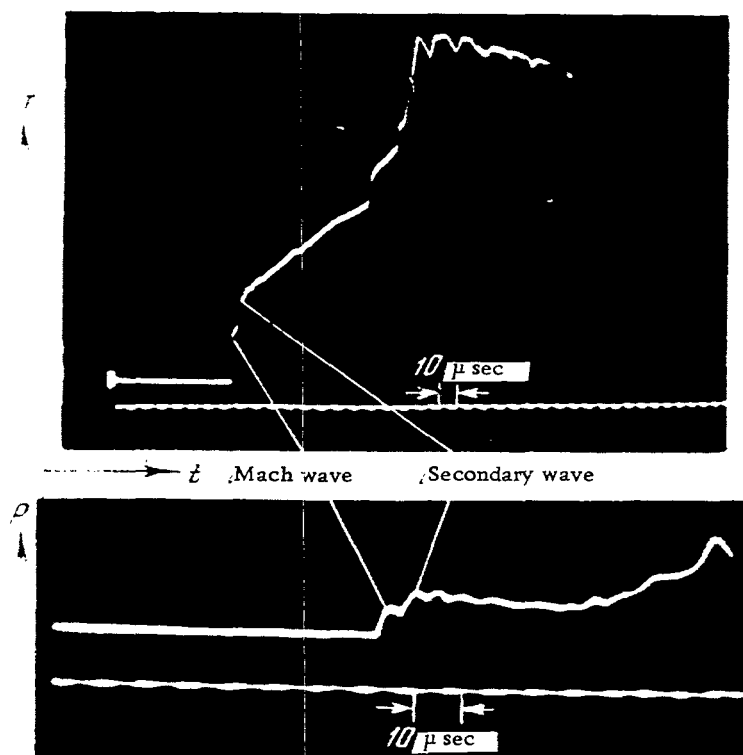


Figure 55. Oscillogram of the Pressure and Temperature Variations at the Surface of the Wedge with Time in CO_2 for $u_0 = 2330$ m/sec, $p_0 = 12.7$ mm of Hg; Wedge Angle $\alpha_0 = 24^\circ$.

Thus, as the shock-wave velocity increases, the diffraction at the wedge result in transition to the double Mach configuration, which is accompanied by appearance of a secondary Mach wave, which propagates over the surface of the wedge right behind the first Mach wave. This secondary Mach wave increases the pressure on the surface of the wedge and increases the heat flux into the surface. The appearance of the double Mach configuration is due to physical and chemical processes behind the shock waves and, consequently to changes in γ the ratio of specific heats. As the incident-wave velocity is increased a supersonic region appears behind the reflected wave and the angle between the incident and reflected waves starts increasing. The wave at the nose of the wedge becomes attached and the pressure behind it starts exceeding the pressure behind the Mach wave. Then a secondary Mach wave must appear and in it the pressure increases behind the first Mach wave to that behind the attached wave.

/113

It is probable that the steady-state Mach configuration, obtained on interaction between two shock waves, should also change in the case of strong waves. A double Mach disk should form if the physical and chemical reactions reduce the ratio of specific heats and increase the flow velocity to the point where angle ω_2 in calculations using the triple-shock theory will become negative.

REFLECTION AND REFRACTION OF DETONATION WAVES

Propagation of shock waves in a medium capable of exothermal reactions differs qualitatively from the propagation of shock waves in a medium with endothermic reactions. A shock wave which is accompanied by a reaction with generation of heat cannot propagate in a steady-state manner if its velocity is lower than the velocity of the Chapman-Jouguet detonation wave. If in a medium in which exothermal reactions are possible a shock wave propagates at a moderate speed, then a reaction which starts at some distance behind it will result in the formation of compression waves which overtake the shock wave and amplify it. In this case a detonation wave is formed which moves at a speed which is first higher than the speed of Chapman-Jouguet detonation, and then, in the absence of a maintaining gas flow will slow down to the steady-state velocity of the Chapman-Jouguet wave. In addition, the propagation of this wave proper is unsteady at distance of the order of a front thickness, since the structure of the front of such a wave is multidimensional. The one-dimensional wave is unstable. A random temperature increase in any region of the shock-wave front is accompanied by production of local ignition nuclei and transverse shock waves, which propagate through the wave front, thus forming a highly complex multi-front structure, which is observed in practically all cases of propagation of detonation waves.

It is obvious that the structure of a detonation wave and the laws governing its propagation are appreciably affected by the boundary conditions which determine the flow variables behind the detonation wave. This takes place as a result of the effect on the detonation-wave front of purely gasdynamic phenomena (expansion or compression of the gas, acceleration or deceleration of the flow, etc.), as well as a result of variation in the rates of chemical reactions behind the detonation wave attendant to changes in the gasdynamic properties of the gas flow. From this point of view it is of interest to examine some experimental data on the formation and propagation of detonation waves under various conditions.

/115

1. Effect of Boundary Conditions on the Onset of Detonation

When flame propagation in tubes takes place under certain specific conditions, the combustion process is transformed into detonation as a result of the appearance of a series of shock waves ahead of the flame front.

The process of formation of shock waves ahead of the flame front at the first stage of the latter's propagation, when the pressure is the products of combustion is higher than that ahead of the flame front, can be examined on the basis of the known Hugoniot solution to the problem of shock-wave formation ahead of an accelerating piston [180, 181].

The relationship between velocity v and acceleration dv/dt of the piston and the point of formation of the shock wave is given by

$$X = \frac{2a^2 \left(1 + \frac{\gamma-1}{2a} \frac{v}{a} \right)^{\frac{2\gamma}{\gamma-1}}}{(\gamma+1) \frac{dv}{dt}}, \quad (6.1)$$

where a is the speed of sound.

Comparison of experimentally measured distances from the point of origin of a shock wave to the butt of the tube with theoretical values of X for different relationships governing the acceleration of the flame shows that the Hugoniot relation is suitable for calculating the point of formation of the shock wave ahead of the flame front. However, it is obvious that the motion of a flame cannot be completely identified with the motion of a piston in a tube, since a flame, unlike a piston, propagates through the gas and, consequently, is not a nontransparent piston. In addition, as can be seen from instantaneous photographs, the flame front is not plane. To clarify the characteristics of gas motion ahead of a flame front Salamandra has studied the propagation of artificially-created density inhomogeneities ahead of a flame front [182]. These inhomogeneities were produced by heating a thin wire and went into motion together with the surrounding medium. The results of this study showed that as long as the inhomogeneities are at a sufficiently large distance from the flame front they move without changing shape. Only near the flame front is it possible to discern some distortion of the inhomogeneity, which reflects the appearance of a velocity distribution near the flame front. The relationship between the rate at which the inhomogeneities moved and the flame velocity was determined from scans of schlieren patterns. By comparing v_{fl} , the velocity of the flame that sent out the disturbance, with v_g , the velocity of the gas set into motion by this disturbance, it is possible to judge about the ratio between these velocities. At the initial time of mixture ignition, as long as the flame does not cover the tube cross section, the velocity of the gas ahead of the flame front is appreciably lower than the flame velocity. After the flame covers the entire tube cross section, the gas velocity increases and on further propagation of the flame the ratio v_g/v_{fl} becomes constant.

/116

It follows from Salamandra's experiments that the gas motion arising ahead of the accelerating flame under experimental conditions is 0.8 of the rate of flame propagation. In this sense the flame acts as a semitransparent piston. Hence the point of formation of the shock wave ahead of the flame should be calculated using the experimentally obtained gas velocity and the law governing its acceleration, which is the same as the relationship governing the propagation of the flame.

However, it follows from Eq. (6.1) that the location at which the discontinuity takes place is affected primarily by the law governing the acceleration of the piston, rather than the absolute velocity of the gas at the boundary with the piston, since at subsonic velocities the term depending on the gas velocity comprises a small correction to unity. Hence the results of calculations made in [181] are in satisfactory agreement with experimental results.

The velocity field measured experimentally ahead of the accelerating flame corresponds to the velocity distribution obtained from calculating the gas variables ahead of the flame by the method of characteristics. Measurements of the pressure field ahead of the flame made by Oppenheim are also in agreement with the calculated pressure field obtained by considering the disturbances ahead of the flame as simple waves [179].

The experimental and theoretical determination of the velocity field in the gas contained in the region between the shock wave and the flame front, which was performed by Salamandra, shows that the shock-wave front and the flame front are a single system, since the flow behind the shock wave is affected by the velocity changes of the flame front. If the flame slows down after the shock wave has formed, then a rarefaction wave is produced, which reduces the flow velocity of the gas behind the shock wave. This rarefaction wave overtakes the shock wave and weakens it. If the flame continues accelerating after the shock wave has formed, then the disturbances sent out by the flame amplify the shock wave.

States with the most variagated distribution of variables in the region between the shock wave and the flame front arise, depending on the flame's acceleration. A gas flow with constant pressure and temperature may take place only as a particular case.

/117

At the time instants preceding detonation a gas flow with a temperature close to that of ignition is formed ahead of the flame front.

If the gas particles remain in the heated state for a sufficiently long time period, then the mixture between the shock wave and the flame front ignites and a detonation wave is formed. The instant of ignition and of transition to detonation was studied in [183-185]. It was shown that in undiluted mixtures the detonation wave is formed by formation of ignition nuclei, their combination and interaction of the compression waves produced attendant to this with the shockwave front. A more uniform state of the combustible mixture is obtained when it is ignited behind shock waves reflected from the end of the tube. In this case the time that passes from the instant of reflection of the shock wave and to the formation of the ignition nuclei can be identified with the reaction induction period. This process was studied in details in [186-190]. It was established that for highly diluted mixtures ignition behind a reflected wave takes place by formation of a combustion wave uniformly over the entire tube cross section, while for rich mixtures this takes place by nucleate ignition. Figure 56 shows high-speed photographs of the reflection of a shock wave from the end of a shock tube in a mixture of $2\text{H}_2 + \text{O}_2$. One can see the formation of a nucleus behind the reflected shock wave and then the formation of detonation wave. It is noted in [190] that the ignition mechanism depends not only on the chemical composition of the mixture, but also on the fact whether it was preheated. Changes were recorded in the mechanism of ignition of the $0.1 \text{ H}_2 + 0.1 \text{ O}_2 + 0.8 \text{ A}$ mixture depending on whether it was ignited behind a reflected wave (i.e., preheated) or behind an incident shock wave. Here the temperature and pressure were identical in both cases.

If the gasdynamic conditions of the flow are such that the time during which the gas resides behind the shock wave is less than the induction time of the mixture then there is no ignition and the gas behind the shock wave behaves as an inert medium. These conditions are created, for example, on deceleration of a supersonic flow of a reaction-capable gas by an obstacle. Figure 57 shows a sequence of frames of flow of $4\text{H}_2 + \text{O}_2$ past a hemisphere placed in a shock tube [191]. When the shock wave moved at $M = 2.62$, the temperature behind the incident wave was 656°K , the gas velocity was 870 m/sec and the Mach number of the flow behind the incident wave was 1.24. When such a flow takes place about an obstacle, the gas behind the detached shock wave is decelerated, which is accompanied by additional increases in temperature and pressure. Calculations show that when the gas is fully stagnated the temperature behind the shock may be as high as 870°K . In the regions behind the detached shock wave, where the gas velocity is half of the initial velocity behind the shock wave the temperature is 845°K .

/118

Under these conditions ignition did not take place when the flow was decelerated by an obstacle. At the same time, when shock waves were reflected from the end of a shock tube ignition took place at these and even at lower temperatures (see Fig. 56). The ignition delays determined behind a reflected wave in $4\text{H}_2 + \text{O}_2$ mixture were 5–100 μsecs for temperatures of $860\text{--}790^\circ\text{K}$.

The time during which the gas sojourns in the high-temperature region behind the detached wave ahead of the body past which flow takes place can be determined by assuming that the dimension of the high-temperature region behind the detached shock in the direction of the gas motion is equal to the distance from the shock to the forward edge of the body, and by assuming that the gas flows in this zone with the speed equal to half the flow velocity behind the shock. For a half sphere the distance from it to the shock under conditions of the given experiment is 1.5 mm [191], for a wedge with a half opening angle of 10° for $M = 1.2$ the distance from the shock to the forward edge is 2 mm [193]. Consequently, the time during which a given volume of gas is situated in the high-temperature zone between the wave and the sonic line for gas flow velocities of $u \geq 400$ m/sec is not more than 5 μsecs for both the half sphere and wedge. Thus, the time during which the gas is held at high temperature in these experiments was found to be less than the ignition delay time, which was responsible for the fact that the mixture did not ignite.

If the flow regime is selected so that the time during which the gas sojourns behind the detached wave is greater than the ignition delay time, then it is possible to observe the phenomenon of period ignition of gas. After ignition, the shock wave maintained by the combustion starts to propagate upstream. The detonation wave which is produced in this manner is damped out due to expansion at flanks and a result of radial expansion behind the wave and again becomes a shock wave, which is carried down by the flow to the initial position at the decelerating surface and the process is again repeated. This process was observed by R.I. Soloukhin [194] in a mixture of ethyl alcohol, air and oxygen at an initial pressure of 0.05 atm and with incident shock-wave velocities of 1420–1460 m/sec. If the flow is arranged so that the detonation wave produced on ignition behind the detached wave is not accompanied by a rarefaction wave, then it propagates up

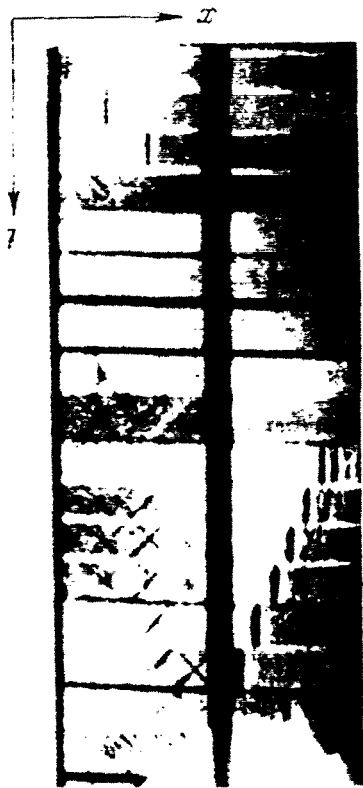


Figure 56. Onset of Detonation on Ignition of a $2\text{H}_2 + \text{O}_2$ Mixture Behind a Reflected Shock Wave.

and down stream from the decelerating obstacle. Such a flow was observed, for example, on propagation of a shock wave in a duct with a concave angular depression in a $\text{H}_2 + \text{O}_2$ mixture [195, 47].

The above examples of the origin of detonation show that the mechanism of detonation-wave formation is determined by the flow variables behind the shock wave and the kinetics of the chemical reactions behind them. Even if the heat generation as a result of the chemical reaction behind the shock wave takes place at a sufficiently high rate, detonation is established depending on the law governing the variation in gas parameters behind the shock wave. If, however, the shock wave is not sufficiently strong, then the temperature across the shock front does not suffice for a rapid heat generation. Ignition takes place at some distance from the front. In this case the development of the process also depends on the conditions of gas flow behind the shock wave. If the flow is arranged so that there is no rarefaction wave behind the shock wave (for example, in a shock tube or behind a reflected shock wave), then there are produced reaction nuclei, and these interact with the shock wave to produce detonation. If, however, the shock wave is followed by a rarefaction wave, then conditions for development of ignition nuclei are not as good due to the temperature reduction, and detonation may not set in.

/120

2. Detonation Wave Structure

The propagation of a shock wave in a mixture capable of exothermal reaction is unsteady and results in the formation of a detonation wave, i.e., of a system consisting of a shock wave and a combustion zone. The structure of the detonation wave in the one-dimensional approximation, taking into account finite rates of chemical reactions in the combustion zone was considered by Ya. B. Zel'dovich [6].

In the coordinate system moving with the wave the detonation wave in the one-dimensional theory has the following form. A relaxation zone, in which molecular vibrations are excited and in which the chemical reaction occurs is situated behind a shock wave in which are excited translational and rotational degrees of freedom of the molecules of the consumed gas. The gas velocity in this zone is subsonic, increasing gradually attendant to the generation of the heat of reaction. The subsequent state of the gas depends on the conditions of flow behind the detonation wave. In the presence of a piston which maintains the gas flow, the

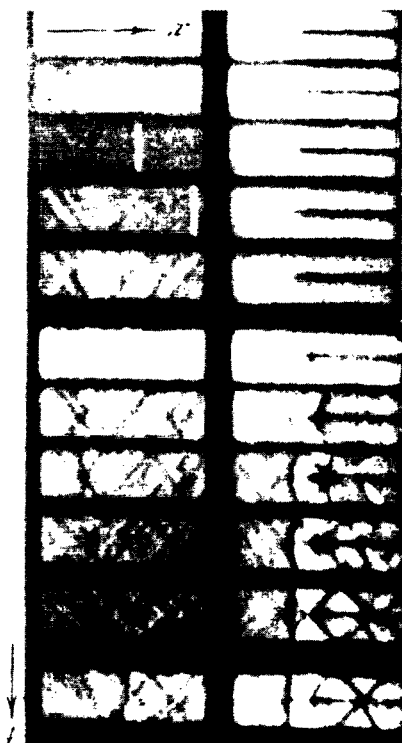


Figure 57. Flow of a $4\text{H}_2 + \text{O}_2$ Mixture Past an Obstacle in a Shock Tube.

gas velocity remains subsonic. When a driving piston is not present, the detonation wave is converted into a self-sustaining detonation. The gas velocity increases to the speed of sound in the plane in which the chemical reaction is completed, i.e., in the Chapman-Jouguet plane. This is followed by an unsteady rarefaction wave, which does weaken the detonation wave, since its leading front propagates with the speed of sound.

In the laboratory [stationary] coordinate system the detonation velocity in the Chapman-Jouguet plane is equal to the sum of the speed of sound and the velocity of the gas flow behind the detonation wave (Chapman-Jouguet condition). Since sound in a medium undergoing relaxation, which is here represented by the hot gas, may propagate at any speed (see Chapter 4), the question arises: what is the speed of sound relative to which the Chapman-Jouguet condition is satisfied? Since the leading front of the rarefaction wave propagation with the frozen speed of sound, it has been concluded by a number of authors that the Chapman-Jouguet conditions should be satisfied with respect to the equilibrium speed of sound [196, 198].

/121

It was found in considering the stability of the one-dimensional configuration that in the majority of cases the one-dimensional system consisting of the shock wave and the combustion zone is unstable. This instability and complex multidimensional structure of the detonation front were verified experimentally. This problem is considered in detail in [32-34]. Different theoretical models of the onset of instability and of the detonation-wave structure are presented in [178, 210]. Instability is due to the high temperature dependence of the reaction rate in the wave. Multidimensionality of the detonation front structure is observed in practically all the mixtures that were studied for Chapman-Jouguet waves and for somewhat overcompressed detonation waves. Since highly overcompressed waves (when the energy generated in the process of the reaction does not make a perceptible contribution to the energy balance) are analogous to shock waves, then their structure is close to one-dimensional. Experiments show satisfactory agreement with calculations made on the one-dimensional theory with variables across fronts of high overcompressed waves [199, 201]. In addition, one-dimensional detonation can be obtained as a transient regime attendant to expansion of an overcompressed wave in a nozzle [202].

The instability of the one-dimensional system consisting of a shock wave with a combustion plane is responsible for the fact that a disturbance produced in the Chapman-Jouguet plane is amplified, transferred in the plane of the shock, distorts its surface, and produces transverse waves. The entire front surface breaks up into cells, whose dimensions are, by order of magnitude, equal to the length of the reaction zone in the one-dimensional model. The size of the inhomogeneities in the front depends on the reaction rate and is characteristic for the given explosive mixture.

It was determined experimentally that when the dimensions of the tube cross section correspond to the width of one zone, spin detonation takes place in the tube. The structure of an individual cell thus corresponds to the structure of the front in spin detonation, i.e., a system of three-shock configuration of waves. Spin detonation was studied in detail in [203-205].

When the number of cells on the detonation front is large, each three-shock configuration moves along a spiral, colliding with other configurations, breaking up and reforming again. The pattern of the motion of transverse wave along the detonation-wave front was studied in [206-210, 244]. As a result of this complex structure, a large number of disturbances is observed in the flow of the consumed gas behind the self-sustaining detonation wave. "Trails" situated along the tube axis extend from each cell on the wave front into the consumed gas. Collisions between triple configuration produce compression waves which propagate back into the consumed gas, i.e., detonation waves are formed. In addition, as is shown in Chapter 5, tangential discontinuities in triple configuration are unstable. They curl into eddies. Hence the existence of three-shock cells in the front should produce turbulence. The inhomogeneous structure of detonation waves is well seen on photographs taken by the Töpler method (Fig. 58). The figure shows frames of a wave propagating in the $\text{CH}_4 + 2\text{O}_2$ mixture initially at atmospheric pressure. The wave moves from left to right. The tube is square and has a cross section of 3 x 3 cm. The photographs were taken for different position of the knife edge in the IAB-451 instrument [211]. Figure 58, a depicts disturbances produced by slots in the chamber wall. The exposure time was 0.5 μsecs . For this exposure time, reduction factor of 8 and detonation-wave velocity of 2.37 km/sec the blurring of the wave's image on the film should not exceed 0.15 mm, i.e., the thickness of the black line on the picture (2.5 mm as actually measured) corresponds to the width of the zone with transverse shock waves. The ensemble of pressure gradients in the reaction zone is so large, that for any position of the knife edge of the IAB-451 the beam goes past the limits of the diaphragm and produces illumination on the negative. Estimates of the thickness of the reaction zone made for methane-oxygen and hydrogen-oxygen mixtures on the basis of schlieren photographs agree with estimates made by other methods. The width of the zone is, by order of magnitude, equal to the distance between "trails" arranged parallel to the axis of the tube.

/122

/123

When the initial pressure is reduced, the sizes of cells in the front increase and the distance between the "trails" becomes larger. The motion of these "trails" is quite well seen on frames of the reflection of a detonation wave from a tube butt at a pressure $p_0 = 200$ mm of Hg (Fig. 67). Disturbances traveling up and down stream should be shaded differently for a given knife-edge position.

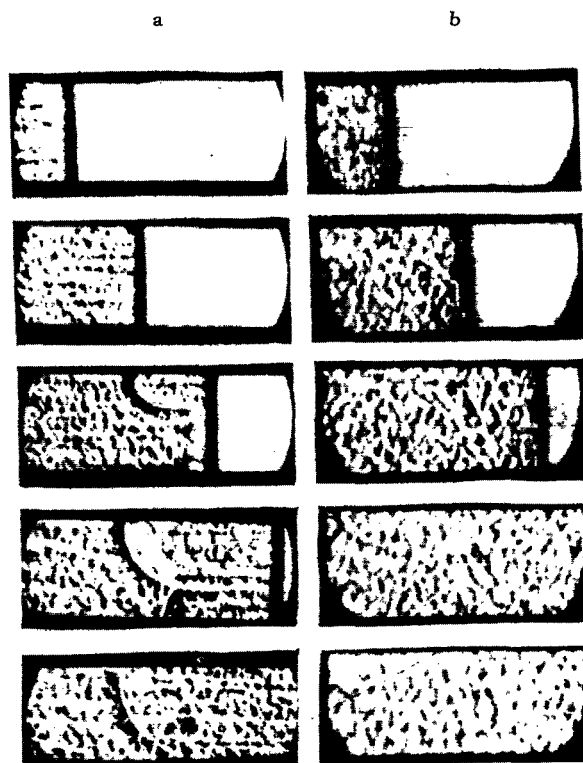


Figure 58. Detonation Wave in a $\text{CH}_4 + 2\text{H}_2$ Mixture. The Knife Edge of the IAB-451 Instrument is Introduced from the Left (a), from the Right (b).

Waves propagating upstream are dark, while those moving downstream are light.

The consumed gas situated behind the wavefront is inhomogeneous. The disturbances become washed out and exist at an appreciable distance from the front.

Inhomogeneities in the gas behind the front may be produced by oscillation of gas in the trails and as a result of turbulence, which develops due to the curling up into eddies of the contact discontinuities of triple configuration in the front. The turbulent disturbances should propagate together with the gas flow. In our experiments the disturbances in the consumed gas move from the front at the speed of sound, i. e., the disturbances behind the front are not turbulent disturbances, but sonic waves (Fig. 58 and subsequent figures).

Figure 59 shows scans obtained from a wave moving in a stoichiometric mixture of methane with oxygen at initial atmospheric pressure [211]. The upper scan is that of normal reflection of a deflection wave from the end of the tube. In addition, a scan is shown of the self-luminosity and a schematic of

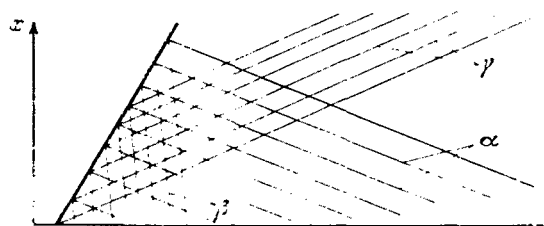


Figure 59. Scans of the Motion of a Detonation Wave in $\text{CH}_4 + 2\text{O}_2$.

the interface. Retonation waves originate at the front proper and a large distances from it move at the speed of the forward front of the reflected rarefaction wave, i. e., with the speed of sound relative to the flow.

Due to the inhomogeneous structure of the detonation front, the state of the products of combustion in the plane where chemical reactions have been completed should differ from the state calculated from the one-dimensional theory using the Chapman-Jouguet condition.

The gas passes the reaction zone with its systems of triple configurations and then moves along the axis of the tube in such a manner that if this zone is excluded it is possible to apply the conservation laws and examine the change in the state of the gas which is introduced by consideration of three-dimensional disturbances in the reaction zone. Due to the inhomogeneous structure of the detonation front the end condition of the combustion products and the Chapman-Jouguet condition should change. References [200, 217, 218] have considered the structure of a detonation wave, taking into account three-dimensional disturbances which have been designated as "turbulence" in the reaction zone. It is assumed that the tube is sufficiently wide, i. e., that we are dealing with a one-dimensional case.

disturbances which arise in the consumed gas. The trails, which are situated almost parallel to the axis, produce β traces on the scan. γ lines are obtained due to the motion of heated gas volumes. The inhomogeneities in the flow of consumed gas behind the front produce on the schlieren photograph streaks α directed away from the front; these apparently originate on the wave front. These so-called retonation waves were observed on scans in [214, 215, 221]. Retonation waves apparently arise as a result of ignition of the gas at the instant of collision of transverse disturbances. In spin detonation, when one head of the spin (one transverse wave) moves along a spiral path and collisions are absent, there are no retonation waves [33, 216]. Retonation waves propagate with the speed of sound in the flow of consumed gas. Figure 60 shows a scan obtained as a result of refraction of a detonation wave from a combustible mixture of $\text{CH}_4 + 4\text{O}_2$ to a mixture of $\text{CH}_4 + 2\text{O}_2$. Here a reflected rare-

faction wave, whose leading front propagates in the flow of consumed gas with the speed of sound, appears at



Figure 60. Scan of the Refraction of a Detonation Wave on Passing from a $\text{CH}_4 + 4\text{O}_2$ to a $\text{CH}_4 + 2\text{O}_2$ Mixture.

It is shown that at the end of the reaction zone we should get a condition which lies on the Hugoniot curve calculated without consideration of losses, but corresponding to higher velocities than the Chapman-Jouguet velocity. It is possible to obtain states corresponding to the given higher velocity, which would be situated on the overcompressed as well as undercompressed parts of the Hugoniot curve. In the above references no consideration was given to the energy transmitted to the trails and retonation waves, and the energy spent for forming of eddies upon disintegration of tangential discontinuities.

In order to establish the quantitative changes in the state of the gas in the Chapman-Jouguet plane due to multidimensionality of the reaction-zone structure it is necessary to consider experiments for determining the gas variables in which an extrapolation was made for an infinite tube diameter, or those performed in wide tubes. The detonation rates of stoichiometric mixtures of ethylene and propane with oxygen with different admixtures of nitrogen were measured in tubes of different diameter and up to 50 m long [212, 213, 224-226]. It was found that detonation propagates with a velocity which is constant to within 0.1%. The detonation rates reduce to an infinite diameter increase the theoretical values by 0.2-0.3%.

/126

The measured pressure ratios in a $\text{C}_2\text{H}_2, \text{O}_2, \text{Kr}$ mixture [199] were 1.70 including a correction for the tube diameter, the theoretical value being 1.78. The pressures measured in $\text{H}_2\text{-O}_2$ mixtures of different composition in a tube 10 cm in diameter differed from the theoretical values by not more than 6% [222]. Greater deviations from theoretically calculated than those attributable to inhomogeneity of the front structure are contributed to the experimental results by losses in friction and heat transfer from the wall of the tube. Differences between experimental and theoretical values are also possible because the regime is sometimes unsteady due to insufficient tube length.

A number of authors has observed the so-called double detonation waves [200, 220, 222]. A shock wave moves at some distance behind a detonation wave at a speed only somewhat lower than that of the latter. The origination

of these waves was attributed in [200] to unsteady transition from an over-compressed to a Chapman-Jouguet wave. When detonation occurs in a tube the wave first moves at somewhat higher velocities, and then is gradually slowed down. Transition to the steady-state velocity does not take place with gradual slowing down of the wave, but attendant to separation of compression waves which move behind the detonation waves, and at slower speeds. It is possible that this phenomenon is also related to energy lost in heat transfer through the tube walls. In narrow ($d = 1.5$ cm) tubes an entire system of compression waves following the detonation wave is produced [223]. In our experiments with methane-oxygen mixtures double waves were produced under a number of regimes is the mixture was ignited by a spark from the SFR-L instrument. At atmospheric pressure detonation in the $\text{CH}_2 + \text{O}_2$ mixture took place at a distance of 50-60 cm in a

3 x 3 cm tube. Only one wave was observed at a distance of 214 cm from the point of ignition. At a distance of 230 cm a compression wave was seen moving behind the detonation wave. At a distance of 350 cm from the point of ignition the distance between these waves started increasing. When the initial pressure was reduced, the point of origin of the second compression wave was displaced from the ignition point. Figure 61 shows a sequence of frames obtained at a distance of 350 cm from the point of ignition. The secondary waves show up as thin lines on the scans. It can be seen from the frames that the secondary waves are blurred and distorted. The fact that these waves are actually compression waves is verified by schlieren photographs. The detonation wave arrives in the field of vision 2800 μsecs after ignition. When the ignition energy was increased (when it was produced by discharging an 180 mmf capacitor charged to 2 kV) a single wave, moving at constant velocity on the segment from 250 to 400 cm was observed at distances from 214 to 4000 cm from the point of ignition. At the 350 cm distance the wave was observed 1630 μsecs from the instant of ignition, i. e., in this case the pre-detonation segment was much shorter than when the mixture was ignited by a spark from the SFR-L. It is probable that in this case, due to the high overcompression of the wave, transition to the steady state should take place at a greater distance from the ignition point. Studies of wave refraction and reflection were performed using these detonation waves. It is shown in the following paragraph that the pressure in such a way exceeds by 15-20% the pressure calculated for the Chapman-Jouguet detonation.

/127

Deviations from theoretical values also arise due to losses in friction and heat transfer at the tube walls. Heat transfer and friction losses at walls result in the appearance of boundary layers in the flow behind a detonation wave and of rarefaction waves, which propagate from the wall radially toward the axis of the tube in the same manner as this takes place for shock waves. If the reaction zone is sufficiently large, these processes may affect the progress of chemical reactions in the zone proper. The problem of Chapman-Jouguet condition for waves moving in tubes of finite size and of variables which are attained in this case in the Chapman-Jouguet plane was solved by Zel'dovich and Fay [219, 198]. Here the point depicting the final state lies on an isentrope corresponding to the total energy loss. It is possible to make a transition to an infinite diameter by extrapolating the curves of the variables under study relative to $1/d$ to zero, where d is the tube diameter. Linearity of these extrapolation was proven experimentally in [224, 225]. These experiments show that the flow variables vary perceptibly due to losses. Measurements of

detonation rates in narrow tubes yield values by 1-3% lower [224, 227]. Pressures in a 1.5 cm tube in experiments [222] are by up to 20% lower than experimental values.

Greater disagreement with theoretical values is exhibited by the velocity of retonation waves. Detonation wave velocities D and retonation wave velocities $(a_1 - v_1)$, where v_1 is the gas velocity behind the front of detonation waves in the laboratory [stationary] coordinate system were measured from scans. Our experiments were performed in three square tubes: $3 \times 3 \text{ cm}^2$ and 5 m long; $5 \times 5 \text{ cm}^2$ and 6 m long, $7.2 \times 7.2 \text{ cm}^2$ and 8.3 m long.

/128

Stoichiometric mixtures of commercial methane and hydrogen with medicinal oxygen were prepared in gasometers above water by volume and were inter-mixed for several days. Then they were ignited by discharges from a 180 mmf capacitor charged to 2 kV. The detonation wave was produced at distances of 40-60 cm from the point of ignition at an initial pressure of 1 atm. In the narrowest tube at a distance of 1.5 m from the point of ignition the detonation-wave velocity was above its steady-state wave. Starting with distances of 2.5 m the detonation-wave velocity became constant within $\pm 50 \text{ m/sec}$, which is within the limits of experimental error. Below are presented values of velocities measured at distance 1 from the point of ignition, and values extrapolated linearly to an infinite tube diameter ($1/d = 0$)

	CH ₄ +2O ₂			2H ₂ +O ₂		
Experimental variables	3×3 cm ² , l=400 cm	7.2×7.2 cm ² , l=800 cm	$\frac{1}{d}=0$	5×5 cm ² , l=500 cm	7.2×7.2 cm ² , l=800 cm	$\frac{1}{d}=0$
D, m/sec	2290±50	2350±50	2400	2750±50	2820±50	2850
(a ₁ -v ₁), m/sec	440±70	370±40	320	520±30	505±20	450

The detonation rate almost does not change within the limits of experimental error when varying the diameter, the quantity $(a_1 - v_1)$ differs from its value for an infinite diameter by 30% in the case of CH₄ + O₂.

The calculation of the detonation rate and the variables behind the detonation wave for a stoichiometric mixture of hydrogen with oxygen was taken from [228]. The wave variables in the methane-oxygen mixtures were calculated using data on the thermodynamics of combustion products, obtained by I. S. Pleshanov in the G. M. Krzhizhanovskiy Power Engineering Institute of the USSR Academy of Sciences. Below are presented variables for the detonation isentrope for a CH₄ + 2O₂ mixture at an initial pressure of $p_0 = 1 \text{ atm}$ and initial temperature of $T_0 = 293^\circ\text{K}$

D, km/sec	10.03	2.437	2.393	2.395	2.61
p ₁ atm	15	25	28	30	50
T ₁ , °K	3484	3670	3708.7	3729.8	3917.8
x	0.983	0.630	0.571	0.536	0.345
p ₁ , g/cm ³	1.102·10 ⁻³	1.734·10 ⁻³	1.916·10 ⁻³	2.039·10 ⁻³	3.169·10 ⁻³

v_1 , km/sec . . .	0.127	0.900	1.029	1.108	1.712
a_{1e} , km/sec . . .	1.236	1.280	1.290	0.296	1.389
a_{1f} , km/sec . . .	1.280	1.322	1.332	1.337	1.387
a_{1ff} , km/sec . . .	1.368	1.413	1.423	1.429	1.488
$a_{1e}-v_1$, km/sec	1.109	0.380	0.261	0.187	-0.372
v_1-v_1 , km/sec	1.152	0.422	0.303	0.229	-0.33
$a_{1ff}-v_1$, km/sec	1.24	0.512	0.394	0.320	-0.224
μ_1	21.42	21.17	21.11	21.08	20.64

/129

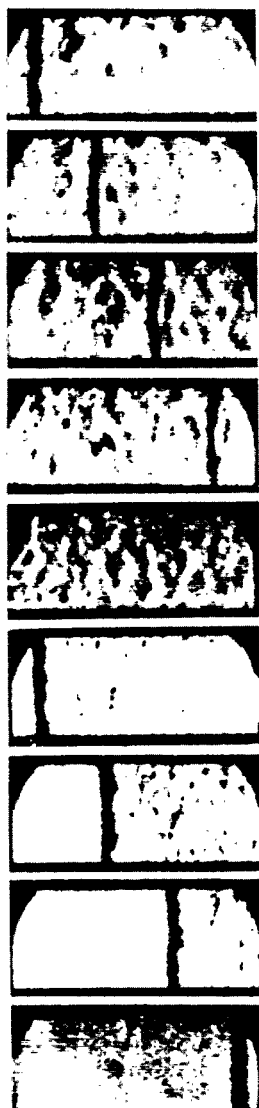


Figure 61. Double Waves in a $\text{CH}_4 + 2\text{O}_2$ Mixture.

Here D is the wave velocity, p , T , ρ and μ are the pressure, temperature, density and molecular weight in the combustion products, respectively; $x = \rho_0/\rho_1$, v is the gas velocity in the laboratory [stationary] coordinate system, a is the speed of sound in the combustion products, subscript e pertains to equilibrium speed of sound, subscript f pertains to the speed of sound calculated on the assumption of frozen dissociation, but excited vibrations attendant to the passage of the acoustic wave, subscript ff pertains to the speed of sound calculated on the assumption that there is no dissociation or excitation of vibrations in the acoustic wave.

The equilibrium speed of sound was determined for the given composition of combustion products from

$$a_e = \sqrt{\frac{\gamma_1 R T_1}{\mu_1} \frac{1 + T_1 \frac{1}{N} \left(\frac{\partial N}{\partial T} \right)_v}{1 + T_1 \frac{1}{N} \left(\frac{\partial N}{\partial T} \right)_p}}, \quad (6.2)$$

where

$$\begin{aligned} \frac{1}{N} \left(\frac{\partial N}{\partial T} \right)_p &= \sum_i \frac{1}{N} \left(\frac{\partial N_i}{\partial T} \right)_p, \\ \frac{1}{N} \left(\frac{\partial N}{\partial T} \right)_v &= \sum_i \frac{1}{N} \left(\frac{\partial N_i}{\partial T} \right)_v, \end{aligned}$$

γ is the ratio of specific heats c_p/c_v for the reacting gas.

$$c_p = \frac{1}{\mu_1} \left[\sum_i c_{pi} X_i + \sum_i H_i \frac{1}{N} \left(\frac{\partial N_i}{\partial T} \right)_p \right],$$

$$c_v = \frac{1}{\mu_1} \left[\sum_i c_{pi} X_i - R + \sum_i H_i \frac{1}{N} \left(\frac{\partial N_i}{\partial T} \right)_v - RT \sum_i \frac{1}{N} \left(\frac{\partial N_i}{\partial T} \right)_v \right],$$

where H_i is the molar enthalpy of the components, and N_i is the number of atoms of the given type

$$X_i = \frac{p_i}{p} = \frac{N_i}{N}.$$

The summation was taken over all kinds of atoms. The values of a_f and a_{ff} were determined from

$$a_f = \sqrt{\frac{\gamma_f R T_1}{\mu_1}},$$

where γ_f and γ_{ff} are the ratios of specific heats in the combustion products for a known frozen composition. The enthalpies of components in these calculations were taken from tables of [118].

/130

From the values of the detonation isentrope thus obtained were calculated variables in the Chapman-Jouguet point, if it is defined as a point where the velocity of the combustion products relative to the detonation front is equal to the equilibrium speed of sound. Below are presented values of gas variables in the Chapman-Jouguet plane for a $2H_2 + O_2$ mixture, taken from [228] for the

"equilibrium" Chapman-Jouguet condition

	$CH_4 + 2O_2$	$2H_2 + O_2$
D , km/sec	2.392	2.846
p_1 , atm	29.7	18.80
x	0.541	0.543
v , km/sec	1.097	1.54
T , °K	3725.7	
μ	21.09	
$(a_{1e} - v_1)$, km/sec . . .	0.198	0.240
$(a_{1f} - v_1)$, km/sec . . .	0.239	0.357
$(a_{1ff} - v_1)$, km/sec . . .	0.331	0.457

Comparison of theoretical values of $(a_1 - v_1)$ with experimental quantities shows, first, that the speed of sound in the consumed gas relative to the flow velocity in small-diameter tubes differs appreciably from that theoretically calculated.

It should be taken into account in comparing theoretical with experimental data that measurements in the 3 x 3 cm were made at a distance of 400 cm from the point of ignition. The wave was somewhat overcompressed (see Section 3), although its velocity was constant within the limits of experimental error at distances of 250 cm from point of ignition. It follows from the table of variables of the detonation isentrope that displacement of the point depicting the final state into the overcompressed region results in reducing the magnitude of $(a_1 - v_1)$, consequently, this quantity measured at a distance of 400 cm can only be lower than the steady-state value. Consequently, it is impossible here to calculate the gas variables behind the detonation wave using conservation equation, i.e., without consideration of losses. The point depicting the final state does not lie on the equilibrium Hugoniot curve.

Secondly, comparison of experimental data reduced to an infinite diameter with those obtained by calculation shows that velocity $(a_1 - v_1)$ is identical with that calculated on the assumption of a speed of sound with frozen dissociation and vibrations. This corresponds to an effective ratio of specific heats of $\gamma = 1.39$ for the $\text{CH}_4 + 2\text{O}_2$ mixture. The fact that acoustic sonic waves propagate with speeds frozen with respect to dissociation and vibrations is in agreement with results presented in Chapter 4. The acoustic waves move at the same speeds as the forward front of the rarefaction wave. It is known that this front should propagate in a gas undergoing relaxation with a velocity frozen relative to excitation of vibrations during a time period of the order of the vibrational relaxation time. It was shown in [229, 230] in which a centered rarefaction wave in oxygen undergoing relaxation was studied, that distances, determined experimentally by the schlieren method, at which the forward front of the rarefaction wave moves with frozen speed of sound are by order of magnitude greater than those expected on theoretical considerations. The time of 30 μsecs during which the rarefaction wave moved in our experiments at a constant frozen velocity is approximately exactly ten-fold longer than the time which can be obtained by estimating various relaxation times for a gas behind a detonation wave.

/131

It is interesting to note that in experiments performed by Bone and Fraser [231] in a moist mixture of $2\text{CO} + \text{O}_2$ were obtained the following: $D = 1760$ m/sec, $v = 780$ m/sec and $a_1 - v_1 = 320$ m/sec. While D and v_1 agree with theoretical values, the magnitude of $a_1 - v_1$ exceeds somewhat even the value calculated on the assumption of frozen dissociation and vibrations. Apparently, this increase, as in the case of $\text{CH}_4 + 2\text{O}_2$, takes place due to the effect of a finite tube diameter. The fact that the forward front a rarefaction wave propagates at a speed corresponding to $\gamma = 1.39$ is used in the following section for determining the flow variables behind detonation waves in narrow tubes.

3. Effect of Variation of Tube Cross Section on the Detonation-Wave Structure

When the cross sectional area of the tube is increased, the steady-state detonation wave may either be damped out or become a spherical detonation

wave [233, 236]. The detonation wave may disintegrate attendant to a sharp reduction in the pressure behind the wave, since the processes taking place across the detonation-wave front are related to the state of the consumed gas.

We consider the two-dimensional case of diffraction of a detonation wave in a mixture of CH_4 and 2O_2 [234, 235]. The detonation wave propagated through a square tube $3 \times 3 \text{ cm}^2$ in cross section. At 4 m from the closed end was placed the viewing section, with optical glass inserted in two of its walls flush with the metal walls. The two other walls of the section had slots into which metal inserts of various shape could be placed so that the detonation wave could be forced to flow past angles of 65° , 90° and 115° . In a number of cases the wave was made to simultaneously flow past wedges placed from top and bottom. Figure 62 shows a sequence of frames of the flow of a detonation wave past a 90° angle. The exposure time of each frame was $0.5 \mu\text{secs}$, the frames succeeded one another at $4 \mu\text{sec}$ intervals, and the initial pressure was 1 atm. The shadowgraphs were taken by the SFR-L high-speed camera. An IAB-451 instrument with standard knife edge was used. This edge was placed vertical, perpendicular to the tube axis.

/132

In the flow about the wedge the incident wave propagates into the region behind the wedge, and its strength varies along the front. The lowest strength is in those points of the front which move along the side of the wedge. A pressure reduction, i.e., rarefaction wave, propagates upstream. The entire pattern has the form shown in Fig. 63.

The pressure in region KBAO, situated between the forward front of the rarefaction wave and the diffracted shock-wave front is not constant. The wave is weakened more extensively with smaller angles δ

We now present ratios of velocities D_w of those parts of the front which move along the wall, to the velocity D of the incident detonation wave as a function of the streamlined angle δ :

$$\begin{array}{cccc} \delta & \dots & 65^\circ & 90^\circ & 115^\circ \\ D_w/D & \dots & 0.32 \pm 0.06 & 0.47 \pm 0.02 & 0.51 \pm 0.05 \end{array}$$

The diffraction process is self-similar. This was checked in the same manner as for Mach reflection in Chapter 5. Figure 64 shows successive positions of the detonation front for a number of rays (1-6) drawn from the vertex of the wedge. On self-similar motion and flow past a 65° angle the points in r, t coordinates should lie on straight lines, which is seen on the graph (r is the distance along the ray). The point of contact between the disturbed and undisturbed parts also moves at a constant angle of $23.6^\circ \pm 1^\circ$. The weakened parts of the detonation front disintegrate. They are overtaken by a shock wave which is separated from the combustion zone.

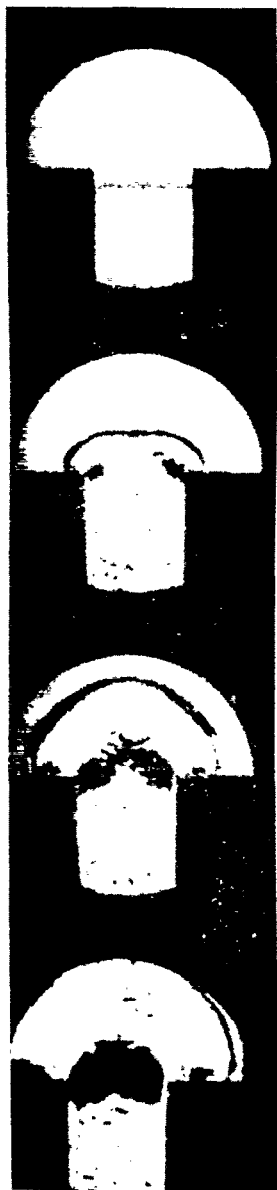


Figure 62. Diffraction of a Detonation Wave Flowing Past a 90° Angle. A $\text{CH}_4 + 2\text{O}_2$ Mixture.

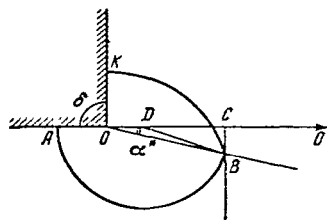


Figure 63. Schematic Diagram of Fronts Attendant to Diffraction Detonation Waves.

KB--Front of Diffracted Wave; AB--Forward Front of Reflected Rarefaction Wave.

The motion is self-similar most probably due to the fact that the detonation wave is not weakened gradually, but rather disintegrates immediately and combustion behind it takes place at a low rate only at the contact surface between the fresh gas (heated by the shock wave) and the consumed gas. Hence the process does not contain quantities which are separately time- or position-dependent. It was found in [206] dealing with dif-

fraction of spin detonation that the detonation wave disintegrates at a low pressure and it was also concluded that combustion at the contact surface propagates at approximately the rate of normal combustion relative to the fresh gas, i. e., with the velocity which is negligible as compared with the velocity of the shock wave and the contact surface. Due to the fact that this process is self-similar, it is possible to estimate from photographs the velocities of individual parts of the front, since in self-similar motion the velocities of individual points of the front will be proportional to vectors dropped perpendicularly from the vertex of the wedge onto the tangent to the front at this point. Then the velocities of the front's segment can be used for determining the flow variables behind these segments. The temperature drops so sharply that reaction cannot take place directly behind the shock wave. In the case at hand the distances from the shock wave to the contact surface behind the weakest segments of the front are insufficient for igniting the gas. The time during which the gas is compressed is less than the induction time. Below are presented the induction times τ for temperatures and pressures behind shock wave moving along the wall, and the times t during which the gas is under compression.

δ , deg	115	90
T , °K.	850	1000
τ , sec	$3.5 \cdot 10^{-4}$	$8 \cdot 10^{-5}$
t , sec	$5 \cdot 10^{-6}$	$9.4 \cdot 10^{-6}$

/134

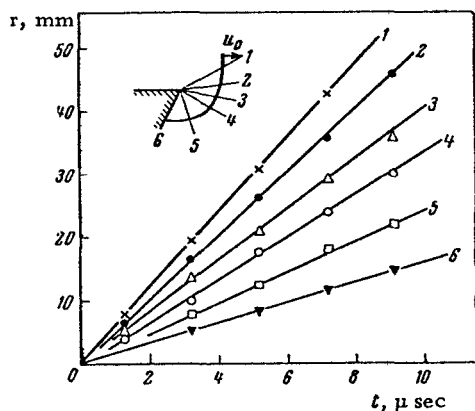


Figure 64. The Position of Individual Points on the Detonation-Wave Front During Diffraction as a Function of Time.

The induction times for methane-oxygen mixtures were taken from [237].

The disintegration of the detonation wave may continue until, as a result of self-similar increase in the distance between the shock wave and the contact surface, the mixture will be held in the region of shock-compressed gas for such a time which is comparable to the induction time. Of course, no interaction between rarefaction waves moving from opposite sides of the tube should not take place during this time. In this case the rarefaction wave which is deflected from the axis of the tube as a rarefaction wave will even more weaken the shock wave and the detonation wave will be completely attenuated. Diffraction experiments were used for determining separation

the flow velocity and the speed of sound in the gas behind a detonation wave.

The point of contact between the undisturbed part of the wave and the diffracted part moves at the same angle α^* for all the angles past which flow takes place (Fig. 63), since this angle characterizes only the variables of the consumed gas. Angle α^* is a function of v_1 , a_1 and D (the flow velocity, speed of sound behind the detonation wave and detonation-wave velocity, respectively).

Segment CB on Fig. 63 is proportional to the velocity of pressure-drop [rarefaction-wave] propagation along the shock. From triangle CDB this velocity is

$$V \sqrt{a_1^2 - (D - v_1)^2}.$$

The tangent of the angle at which the point of contact moves is determined from triangle OCB, since $OD = v_1$

$$\tan \alpha^* = \frac{V \sqrt{a_1^2 - (D - v_1)^2}}{D}. \quad (6.3)$$

Knowing the parameters of the incident wave, it is possible to use this expression for finding $\tan \alpha^*$.

In our case by measuring $OA = a_1 - v_1$, α^* and $OC = D$, we determine the values of D , a_1 and v_1 behind the incident wave

$$\begin{aligned} D &= 2300 \pm 100 \text{ m/sec;} \\ v_1 &= 1100 \pm 90 \text{ m/sec;} \\ a_1 &= 1540 \pm 160 \text{ m/sec.} \end{aligned}$$

It follows from the above values of the variables that $v_1 + a_1 > D$, i.e., the wave is overcompressed. The large errors in this case are due to the fact that the above values were obtained in several experiments performed at distances of 2500 and 3500 mm from the end of the tube.

It was shown in the preceding section that in a 3 x 3 cm tube the state of the gas behind the detonation wave differs from that calculated on the basis of the equilibrium Hugoniot curve. Knowing the values of D_1 , v_1 and a_1 , this conclusion can be verified as follows. Using the conservation equation without consideration of losses and the expression $a^2 = p_1/\rho_1$, for the speed of sound, it is possible to determine the effective value of γ in the expression for the speed of sound if a_1 , v_1 and D are known. The value $\gamma = 1.62 \pm 0.16$ obtained in this manner shows that conservation laws without consideration of losses cannot be used. The point depicting the state of the consumed gas [thus] does not lie on the equilibrium Hugoniot curve.

In [6] the losses attendant to propagation of a detonation wave in a tube were taken into account in the one-dimensional approximation. In this case consideration of losses modifies all the conservation equations with the exception of the continuity equation. Applying the latter equation to our case we get that $\rho_0/\rho_1 = 0.521$. The pressure behind the wave can be obtained from $a^2 = \gamma p/\rho$. We shall assume in keeping with results of Section 2, that the sound near the detonation wave propagates at a speed which is frozen relative to vibrational excitation, i.e., accordingly $\gamma = 1.39$. Then the pressure and temperature behind the wave are $p_1 = 35.6$ atm and $T_1 = 3980^\circ\text{K}$, the equilibrium γ_e in this case being 1.245. Let us consider another version. We assume that the experimentally-calculated speed of sound a_1 is the equilibrium velocity relative to vibrational excitation. This assumption yields: $p_1 = 39.4$ atm, $T_1 = 4200^\circ\text{K}$ and $\gamma_e = 1.265$.

4. Triple Configurations Arising on Refraction of Detonation Waves

The reflection of a detonation wave gives rise to an overcompressed detonation wave due to the increased pressure behind the wave. If a process is brought about in which the pressure undergoes a sharp drop, then, as in the case of diffraction, the detonation wave may disintegrate. This process was obtained on refraction of a detonation wave, i.e., on its passing from one explosive medium to another. This is accompanied by formation of a triple configuration consisting of the detonation wave, a shock wave and a rarefaction wave.

The following setup was used in refraction experiments with detonation waves [211]. A square detonation tube 3 x 3 cm² in cross section was separated,

/136

in its viewing section, into two parts by a thin film, stretched at an arbitrary angle to the axis of the tube. The detonation wave propagated through the and was refracted at the interface between two mixtures. A similar arrangement was used in [232]. The films were made from a nitrocellulose solution (specific weight $d = 1.68 \text{ grams/cm}^3$). The composition of the solution was 100 milliliter of a 2.6% solution of nitrocellulose in an amilocitate-acetone mixture (in the 2:1 ratio), 70 milliliter of toluene and 10 milliliters of diamylphthalate [124].

The film was produced in the following manner. A drop of the solution was deposited on the surface of distilled water, the solvent was evaporated, and this produced a thin film of nitrocellulose on the water's surface. The film after drying was removed by raising a metal ring, previously immersed into the water. Before the experiment the film was moved onto a metal frame on which BF glue was smeared, a second frame was put on top and then these frames were placed in slots of the viewing section. Slits were cut in the optical glasses and the lateral sides of the frame were placed in them. In order that the gases on both sides of the films would not intermix, the slots in the glasses and in the viewing section were sealed by a vacuum cement. On interaction of the wave with the film the incident wave should be distorted due to the fact that the film has a finite mass.

Meyer [239] has performed experimental and theoretical studies of the interaction of the wave with a 0.0425 mm thick cellulose acetate film. The shock wave in the shock tube was incident on the film and the latter was carried away by the flow. Due to the film's inertia, the wave incident upon it was reflected, and the refracted wave was at first slowed down. After some time the refracted wave picked up speed and the reflected wave degenerated into an acoustic signal. In the presence of a film the wave passes, during a given time period, a smaller distance in the tube than in the absence of a film.

The effect of the mass of the film on the refraction process can be estimated by means of parameter δ which is difference between the distance which would be passed, from a given initial point, by a wave in the absence of the film and that passed by the wave when a film is placed in its path.

This distance δ for $t \rightarrow \infty$ is estimated as follows

/137

$$\delta = \frac{\rho_w}{\rho_1} r.$$

Here ρ_w , and ρ_1 are the film and gas densities, respectively, and r is the film thickness.

In our case the film thickness did not exceed 800 Å. This thickness was estimated on the basis of the mass of a drop of the solution and the area it occupied on the water surface. The value of 800 Å is the greatest obtained. Then in our case $\delta = 0.13 \text{ mm}$, i.e., practically, films of this thickness should not affect the refraction process. To check this, we have performed experiments with the tube filled from both ends with the same mixture.

When using a film three-fold thicker than that usually utilized, a weak compression signal, propagating with the speed of sound upstream was reflected from the film. No other changes occurred in the flow and in the detonation-wave velocity.

The films were sufficiently thin in order that the finite mass of the film would not affect the refraction. At the same time they were sufficiently flexible in order not to burst from a moderate distortion. In order to place the frames the tube was evacuated to 0.1 mm of Hg and filled with the mixture, which would ultimately occupy the major part of the tube. Then the frame and the glasses were placed. The tube was equipped with four needle valves, two of which communicated with the atmosphere, while the other two were connected to gas tanks containing the explosive mixtures. The atmospheric valves were opened and then the gas tank valves were gradually and simultaneously opened up. The appropriate mixture was blown through its corresponding part of the tube. The film served as a sensitive pressure gage. It bent in one or another direction as soon as pressures to both sides became different. Four liters of mixture I were blown through the larger part of the tube, which was already almost completely filled with this mixture, while 2 liters of mixture II were blown through the smaller part of the tube, after which only gas I remained in the larger part of the tube and only gas II in the smaller. Then the valves were carefully closed and the mixture was ignited not more than a minute afterwards. It was established by visual inspection using the Töpler [schlieren] method that the gases to both-sides of the film do not intermix, in any case for 5 minutes. Experiments with diffraction of detonation waves were performed for angles of incidence of 0, 30 and 58° with the waves passing from $\text{CH}_4 + 2\text{O}_2$ and $\text{CH}_4 + 4\text{O}_2$ into air, oxygen and methane-oxygen mixtures of different composition. The wave systems arising on refraction into inert and combustible mixtures are shown in Fig. 65. The angle of incidence was $\omega = 58^\circ$. In Fig. 65,b the mixture passed from a $\text{CH}_4 + 2\text{O}_2$ mixture into a $\text{CH}_4 + 4\text{O}_2$ mixture. The inclined line which passes through the frame is the trace of frames between which the film was clamped, 1, 2, 3, 4 are, respectively, the incident wave, forward front of reflected rarefaction wave, rear front of reflected rarefaction wave, the refracted wave; 5 is the wave system obtained as a result of the combined effect of "angular signals" and the development of chemical reaction behind the refracted wave. The angular signals are a result of limiting of the refraction pattern by the side walls. The angular signal may be a compression as well as a rarefaction wave. This depends on the strength of the reflected wave and on the angle at which refraction starts. By varying this angle it is possible vary the angular signal and then to isolate outlines characteristic of the refraction process proper. For each pair of test gases experiments were performed with different angular signals. Figure 65,a shows the passing of a detonation wave into air. In this case the deflected interface, i.e., the contact surface, is well seen. In this case the angular signal can be regarded as the reflection of the refracted wave from the lower wall. This reflection is irregular, since the angle of incidence is close to glancing incidence angle. The region characteristic of the wave-refraction proper is that between the point of intersection of the incident and refracted wave and the triple point of the refracted wave. In this region the wave pattern is stationary in the coordinate system moving together with the point of intersection of all the waves.

/138

/139

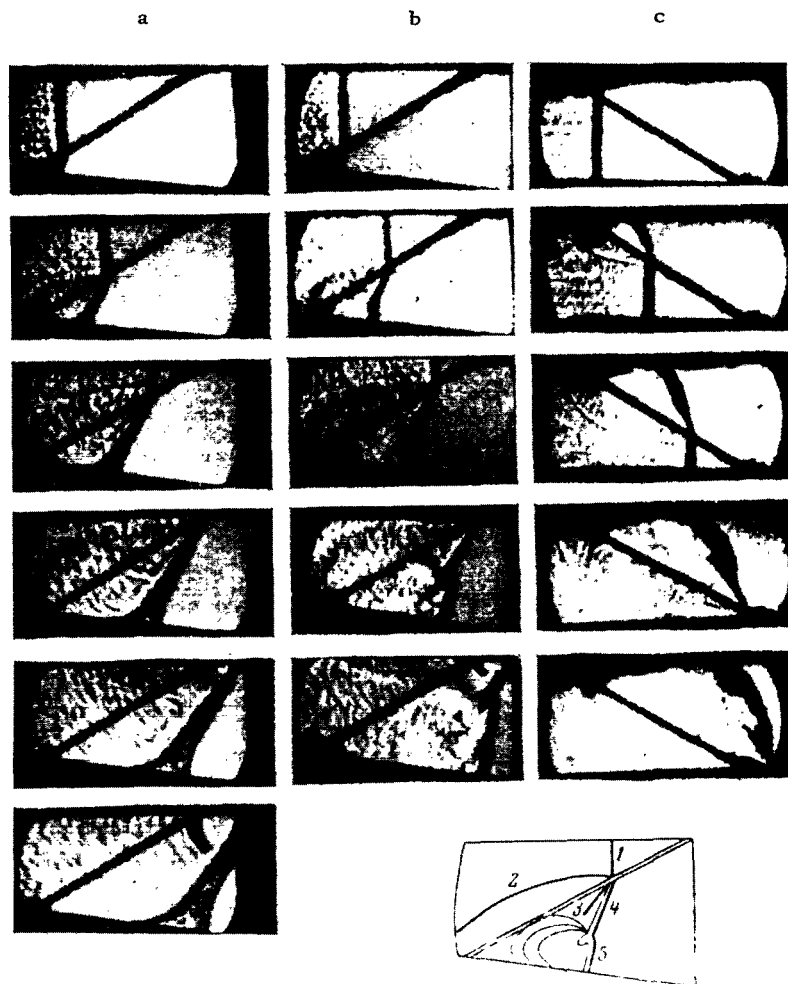


Figure 65. Refraction of a Detonation Wave on Passing From
a $\text{CH}_4 + 2\text{O}_2$ Mixture Into:
a—Air; b— $\text{CH}_4 + 4\text{O}_2$ Mixture; c— $\text{CH}_4 + 3\text{O}_2$ Mixture. Angle
of Incidence 58° .

Figure 65, c shows the reflection of a wave into a $\text{CH}_4 + 3\text{O}_2$ mixture, when the upper plane is deflected through an angle such that the refracted wave moves normal to it. The angle of incidence is $\omega = 58^\circ$. In this case there is no Mach reflection. The disturbances discernible on the photograph characterize the process of transition to detonation in the refracting medium.

It was found that the waves refracted upon passing of a detonation wave in a reacting medium were shock waves. Passing was studied into mixtures with higher as well as lower detonation rates. The detonation rates of the mixtures

used were*

$\text{CH}_4 + \text{O}_2$	2637
$\text{CH}_4 + 1,5\text{O}_2$	2531
$\text{CH}_4 + 2\text{O}_2$	2392
$\text{CH}_4 + 3\text{O}_2$	2046
$\text{CH}_4 + 4\text{O}_2$	2067

If the refraction of the detonation wave would have immediately sent into the second medium a Chapman-Jouguet wave, then its inclination could be easily found from the law of sines. The refraction angles ω_4 (Fig. 66) should be assumed to be as follows (for an angle of incidence of 58°)

Mixture	$\text{CH}_4 + 4 \text{O}_2$	$\text{CH}_4 + \text{O}_2$
ω	$47^\circ 12'$	$61^\circ 02'$

Had the refracted wave been overcompressed, angles ω_4 would have been even larger. In all experiments the refraction angles were smaller. Calculations presented below on the assumption that a shock wave propagates in the second medium without chemical reactions agree with experimental results. Transition to detonation behind the refracted wave takes place by nucleate ignition with formation of a series of shock waves, which are quite noticeable in Fig. 65, c. This figure also shows the development of detonation and the changes produced by this in the inclination of the refracted wave. The velocity of the refracted wave in the second medium approaches the steady-state detonation rate. The ignition delay can be determined from similar frame sequences by measuring the greatest distance between the shock wave and the contact surface before the reaction starts.

/140

We now determine the ignition delay in a $\text{CH}_4 + 3\text{O}_2$ mixture (Figs. 65, c and 66). Here $\omega_4 = 34^\circ 30'$; we determine the corresponding velocity of the gas behind the shock wave $v_1 = D - u_1$, i. e., that velocity with which the gas particles embraced by the shock wave move.

The greatest distance between the refracted wave and the contact surface at which the gas does not as yet ignite is 2.7 ± 0.2 mm. Then the ignition delay will be $\tau = 10.8 \mu\text{secs}$. The pressure behind the shock wave then was $p_1 = 26.68$ atm, and the temperature was $T_1 = 1176^\circ\text{K}$.

The time of transition of steady-state detonation rates in the second medium depends on the strength of the refracted wave, consequently, on the angle of incidence of the detonation wave and on the difference in steady-state detonation rates

*These rates were calculated by the present authors and also obtained from [238].

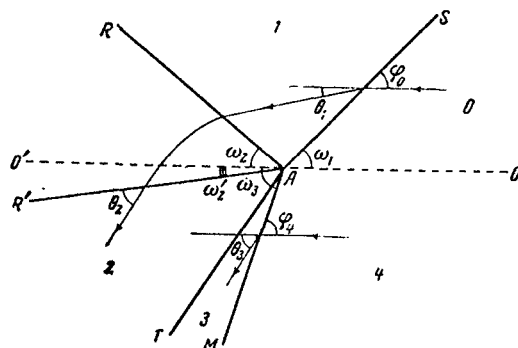


Figure 66. Schematic of the Position of Waves for Refraction of a Detonation Wave at the Interface of Two Media.

SA is the Incident Wave; AM is the Refracted Wave.

of both mixtures. When the angle of inclination is reduced, the strength of the passing wave increases and the transit time is correspondingly reduced.

/141

Figure 60 shows a scan of passing from $\text{CH}_4 + 4\text{O}_2$ to $\text{CH}_4 + 2\text{O}_2$. In this case there is practically no transition period. Practically starting from the interface the detonation rate in the second medium is established. The transition time is also reduced when the difference between the detonation rates of both media is minimized. On passing into a mixture which is far from detonation limits with a large induction time it is possible that the mixture will not ignite during the observation time. The photograph of the passing of a detonation wave from $\text{CH}_4 + 2\text{O}_2$ into a $\text{CH}_4 + \text{O}_2$ mixture is fully analogous to that depicted in Fig. 65, a. The refracted wave is a shock wave, which then underwent Mach reflected at the lower boundary.

In all the cases studied the wave reflected into the consumed gas was a rarefaction wave. The forward and near fronts of this wave are visible in Fig. 65 (lines 2 and 3). The fact that it is a rarefaction wave which is refracted follows not only from the schlieren photograph, but also from the fact that the angle of the reflected wave does not change, irrespective of the medium into which the detonation wave is refracted. This is possible when the velocity of the reflected wave does not depend on that of the refracted wave. This case was obtained for a reflected rarefaction wave.

Calculating Initial Refraction Variables for Detonation Waves at the Interface Between Two Media

The initial refraction variables for detonation waves at interfaces between two media were calculated from the three-wave theory. A schematic of the

fronts attendant to refraction is given in Fig. 66. The triple-shock configuration in the case at hand differs from that of shock waves (see Chapter 5) by the fact that the reflected wave is the rarefaction wave RR'. To calculate the rarefaction wave we write a corollary of Riemann equations [240, 242]

$$\begin{aligned} \theta_2 = & \sqrt{\frac{\gamma_1 + 1}{\gamma_1 - 1}} \left\{ \arctan \sqrt{\frac{2 - x'(\gamma_1 + 1) + (\gamma_1 - 1)M_1^2}{x'(\gamma_1 + 1)}} - \right. \\ & - \arctan \sqrt{\frac{(\gamma_1 - 1)(M_1^2 - 1)}{\gamma_1 + 1}} \left. \right\} + \arccos \frac{1}{M_1} - \\ & - \arccos \sqrt{\frac{x'(\gamma_1 - 1)}{2(1 - x') + (\gamma_1 - 1)M_1^2}}, \end{aligned} \quad (6.4)$$

where

$$x' = \left(\frac{p_2}{p_1} \right)^{\frac{\gamma_1 - 1}{\gamma_1}}; \quad M_1 = \sqrt{1 + \left(\frac{p_1}{p_0} \right)^2 \cot^2 \omega_1 \cdot \frac{D_0}{a_1}}.$$

The notation used is (see Fig. 66): p_i - pressure in region i , M_1 - Mach number in region 1, θ_i - deviation of flow on passing through the wave into region i , D_0 - the velocity of incident detonation wave.

/142

The flow variables in the first medium ahead of the detonation wave are assigned subscript 0, the flow variables in the second medium are denoted by subscript 4, the flow variables behind the incident detonation wave carry the subscript 1, those behind the refracted wave are assigned subscript 3, while those behind the reflected wave are denoted by subscript 2.

For the case of normal incidence of a detonation wave onto the boundary between two media it is most convenient to write shock polars in the p, v plane, where v is the flow velocity behind the wave in the laboratory [stationary] coordinate system. This follows from the fact that the coupling conditions in this case are: equality of pressures behind the refracted and reflected waves and equality of velocities. In the p, v variables the shock polar for a reflected rarefaction wave is written in the form

$$v_2 = \frac{2a_1}{\gamma_1 - 1} \left[1 - \left(\frac{p_2}{p_1} \right)^{\frac{\gamma_1 - 1}{2\gamma_1}} \right] + v_1. \quad (6.5)$$

It was assumed that γ in the rarefaction wave remained constant. Let us consider refraction into air. The refracted wave will be defined by Hugoniot

curves taking into account excitation of molecular vibrations in the gas behind the shock waves. It is assumed that the refracted wave is a Chapman-Jouguet wave with variables determined on assumption of equilibrium speed of sound. We consider rarefaction into air for a normal angle of incidence and for an incidence angle of 58° . The results of calculations are presented below

	$\omega_1 = 0^\circ$	$\omega_1 = 58^\circ$		$\omega_1 = 0^\circ$	$\omega_1 = 58^\circ$
D_2 , m/sec.	2392	2392	D_4 , m/sec.	1588	$\omega_4 = 32^\circ 30'$
p_1 , atm	29.7	29.7	p_2/p_1	24.95	$\omega_2 = 23^\circ 41'$
ρ_2/ρ_1	0.541	0.541	$a_1 - v_1$, m/sec. . .	223	$\omega_2' = -4^\circ 14'$
p_2/p_1	0.85	0.707	$a_1 - v_2$, m/sec. . .	-10	$\theta_2 = 25^\circ 35'$

The [corresponding] experimental values are

	$\omega_1 = 0^\circ$	$\omega_1 = 58^\circ 30' \pm 30'$
D_2 , m/sec.	2390 ± 40	$\omega_4 = 32^\circ 30' \pm 1^\circ$
D_4 , m/sec.	1510 ± 80	$\theta_2 = 24^\circ \pm 1^\circ$
$a_1 - v_1$, m/sec. . .	440 ± 40	$\omega_2 = 37^\circ \pm 3^\circ$
		$\omega_2' = -15^\circ 30' \pm 1^\circ$

For angles of incidence of $\omega_1 = 0^\circ$ and $\omega_1 = 58^\circ$ the greatest difference is found for variables in the reflected rarefaction wave.

We now present results obtained on the assumption that the gas is in a state calculated on the basis of diffraction experiments (see Section 3 of the present chapter). The characteristics in the rarefaction-wave cone correspond [sic] to $\gamma = 1.39$. We also present results of calculations obtained on the assumption that the experimentally determined speed of sound is in equilibrium with respect to vibrations

	$\omega_1 = 0^\circ$	$\omega_1 = 0^\circ$		$\omega_1 = 58^\circ$	$\omega_1 = 58^\circ$
D_2 , m/sec.	2300	2300	D_2 , m/sec.	2300	2300
p_1 , atm	35.6	39.4	p_1 , atm	35.6	35.2
ρ_2/ρ_1	0.52	0.521	ρ_2/ρ_1	0.521	0.521
a_f	1540	a_f 1540	a_{1ff} , m/sec.	1540	a_f 1540
p_2/p_1	0.83	0.81	p_2/p_1	0.61	0.58
D_4 , m/sec.	1520	1540	ω_2	$37^\circ 34'$	$37^\circ 34'$
$a_1 - v_1$, m/sec. . .	440	440	ω_2'	$-11^\circ 34'$	$-15^\circ 11'$
$a_1 - v_2$, m/sec. . .	88	64	ω_4	$35^\circ 36'$	$36^\circ 48'$
			θ_2	$26^\circ 36'$	$30^\circ 12'$

Comparison of experimental with theoretical data shows satisfactory agreement between the two. Both calculations differ by the value of θ . Better agreement with theory is given by the assumption that $\gamma = 1.39$ in the rarefaction-wave cone. In our experiments on refraction into $\text{CH}_4 + \text{O}_2$ there was no reaction behind the refracted wave. The refraction into this mixtures, as well as into $\text{CH}_4 + 3\text{O}_2$ and into $\text{CH}_4 + 4\text{O}_2$, was calculated assuming that no reaction takes

placed behind the refracted wave. The Hugoniot curves in mixtures of CH_4 and O_2 were calculated upon consideration of vibrational excitation in the CH_4 and O_2 molecules. The enthalpies for methane and oxygen were taken from [118]. The calculations were made by assuming a state behind the wave with consideration of losses at the walls and $\gamma = 1.39$. Below are presented theoretical and experimental data on refraction from a $\text{CH}_4 + 2\text{O}_2$ mixture into $\text{CH}_4 + 4\text{O}_2$, $\text{CH}_4 + 3\text{O}_2$ and $\text{CH}_4 + \text{O}_2$ for an angle of incidence $\omega_1 = 58^\circ$.

	$\text{CH}_4 + 3\text{O}_2$	$\text{CH}_4 + \text{O}_2$	$\text{CH}_4 + 4\text{O}_2$
p_2/p_1	0.635	0.58	0.645
$\theta_1 + \theta_2 = \theta$	$26^\circ 05'$	$28^\circ 30'$	$26^\circ 48'$
ω_2	$37^\circ 15'$	$37^\circ 15'$	$37^\circ 15'$
$\varphi_1 = \omega_1$	$31^\circ 45'$	$34^\circ 48'$	$33^\circ 12'$
ω_2'	-11°	-12°	$-10^\circ 24'$
$\omega_{2\text{exp}}$	$34^\circ \pm 2^\circ$	$32^\circ 30' \pm 2^\circ$	$33^\circ 30' \pm 1^\circ 30'$
$\theta_{3\text{exp}}$	$31^\circ \pm 1^\circ$	$27^\circ 30' \pm 2^\circ$	$26^\circ 30' \pm 30'$
$\omega_{2\text{exp}}$	$38^\circ 20' \pm 1^\circ$	$37^\circ \pm 2^\circ$	$37^\circ 30' \pm 2^\circ$
$\omega_{2\text{exp}}$	-15 ± 2	—	$-16^\circ \pm 3$

The above data verify the assertion that the refracted wave is a shock wave.

5. Regular and Irregular Reflection of Detonation Waves

A detonation wave propagating in a narrowing-down duct is reflected in it. In experiments with reflection of detonation waves inserts were placed into the viewing section which form angles with the surface of the wall [57]. A typical pattern of regular reflection of detonation waves is shown in Fig. 67. The study was made in a stoichiometric mixture of CH_4 and O_2 . The angle of incidence was 25° . The waves moved from left to right. There was no bifurcation, as is also the case on normal reflection from the tube end. A scan of normal reflection is shown in Fig. 59. Transition to Mach reflection took place for the $\text{CH}_4 + 2\text{O}_2$ mixture at atmospheric pressure for a wedge angle of more than 35° . For a wedge angle of 35° , i.e., for an incidence angle of 55° , a developed Mach reflection is observed. The triple point moved at an angle of 3° to the surface of the wedge. Figure 68 shows a sequence of frames of Mach reflection from a wedge angle of 20° . The triple point moves away from the wedge surface along a straight line situated an angle $\chi = 6^\circ$. The flow is self similar, i.e., the angles between the waves remain constant.

Calculations of triple configurations of detonation waves were performed by the method of shock polars similar to the manner in which this was done in Chapter 5 in calculating triple configurations of shock waves. To calculate Mach waves which are strong, overcompressed waves, use was made of detonation polars presented in Section 2 of the present chapter. The reflected waves and the shock waves in the consumed gas were calculated by successive approximations using tables of thermodynamic variables for the combustion products of $\text{CH}_4 + 2\text{O}_2$.

/144

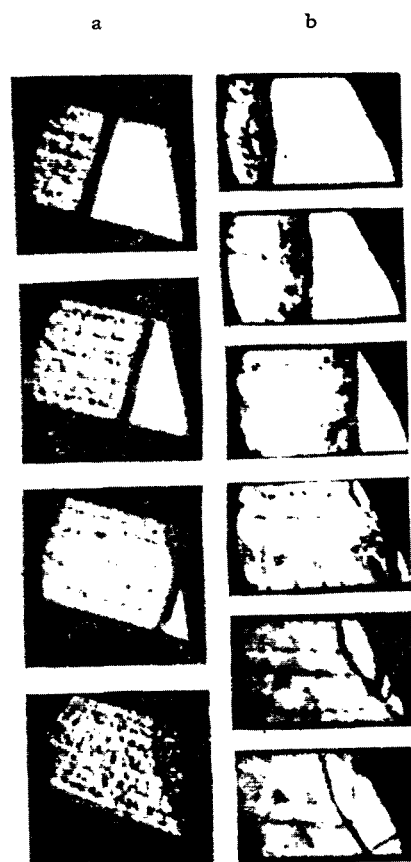


Figure 67. Regular Reflection of Detonation Waves. Mixture of $\text{CH}_4 + 2\text{O}_2$ at $p_0 = 760$ mm of Hg (a) and $p_0 = 200$ mm of Hg (b).

Calculations on the assumption that the Chapman-Jouguet state prevails behind the incident wave yields regular reflection for an angle of incidence of 55° . Transition to Mach reflection should have happened only at an incidence angle of 57° . As a result of this contradiction with experimental results the reflection was [then] calculated for a state determined upon consideration of losses through the tube walls and on the assumption that the acoustic disturbances propagate near the detonation wave with the frozen speed of sound. Calculations made on assumption of a speed of sound near the wave in equilibrium with respect to molecular vibrations, yielded values of ω_2 4-6° on the high side. The results of calculations made for incidence of detonation waves onto wedges with vertex angles of $\alpha_0 = 65$ and $\alpha_0 = 20^\circ$ (Mach reflection) are presented below

	65°	20°
p_0 , mm of Hg	760	760
D , m/sec	2300	2300
v , m/sec	1100	1100
p_1 , atm	35.6	35.6
p_0/p_1	0.521	0.521
ω_1	25	63°

	65°	20°
ω_2	13°44'	51°
ω_4		80°39'
ω_1 exp	25°±1°	63°±1°
ω_2 exp	14°±3°	52°±3°
ω_4 exp		81°±2°

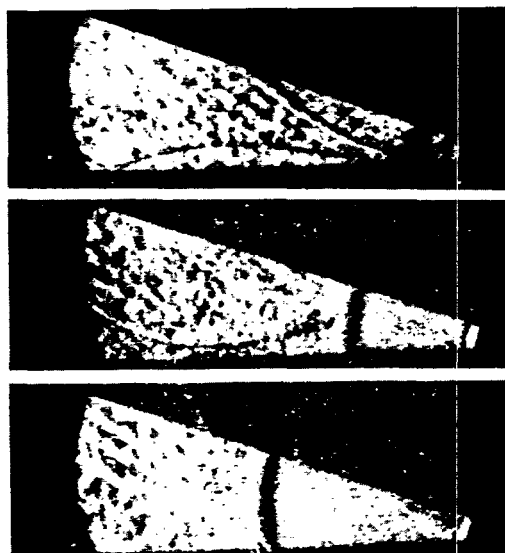


Figure 68. Mach Reflection of Detonation Waves. Mixture of $\text{CH}_4 + 2\text{O}_2$,
 $p_0 = 760$ mm of Hg.

sonic velocities of the gas behind the shock-wave fronts. It is obvious that in the case of overcompressed detonation waves the same Mach configurations should be produced as for shock waves.

Following are the designations of angles in the coordinate system moving with the triple point: ω_1 , ω_2 are angles of incidence and reflection; ω_4 is the inclination of the Mach wave.

The reflected wave belonged to the weak family. Agreement between theoretical and experimental data for the case of $\alpha_0 = 20^\circ$ shows that it is possible to use the data of the one-dimensional theory for calculating configurations with reflected shock waves.

It is interesting to note that angle ω_2 is positive, although the incident-wave velocity and the wedge angle is the same for which double Mach configurations arise on reflection of shock waves. This is a result of the fact that the velocity of the gas behind the detonation-wave front is subsonic, unlike the high super-

/145

IONIZATION STRUCTURE OF SHOCK WAVES IN AIR AND NITROGEN

Air at high temperatures is a complex mixture of gases in which takes place all kinds of reactions: dissociation, recombination, ionization and formation of new molecules. The kinetics of elementary processes taking place behind a shock wave in air was subjected to a thorough study during the last few years, as a result of which sufficient data is available at present for solving gasdynamic problems about the flow of nonequilibrium dissociated air [15, 19, 245, 246]. Calculations show that for $M_0 = 20$ equilibrium temperature behind the shock

wave is established at a distance of the order of 100 mean free paths in undisturbed gas. When the pressure ahead of the shock wave is 1 mm of Hg and $M_0 = 14.2$ close-to-equilibrium temperature behind a normal shock in air is reached at distances of the order of 2.5 cm from the front [245] with $M_0 = 12$ and $p_0 = 1$ mm of Hg. Equilibrium is achieved at a distance of 10 cm from the shock when $M_0 = 10$ and $p_0 = 1$ mm of Hg. The size of the nonequilibrium region behind the shock wave is measured in tens of centimeters [10]. However, the region with temperature which appreciably exceeds that at equilibrium is not larger than 10 cm. For lower shock-wave velocities, the size of this zone is greater, but then the difference between the state across a shock front without dissociation and the equilibrium state decreases sharply. For example, for $M_0 = 7.5$ the temperature in this zone drops by only 300°K. Hence for initial pressure of the order of several mm of Hg the inhomogeneous region produced by dissociation process behind the shock wave is most pronounced for $M_0 = 8-12$.

Ionization process behind a shock wave also take place at a finite rate. This results in the formation of a profile of electron concentrations, whose shape is determined by the ensemble of all the physical and chemical transformations which take place in a shock wave in air.

The ionization structure of shock waves has been studied in a number of theoretical and experimental works [81, 245, 248-255]. However, the shortcomings present in these studies may distort the results appreciably. The main shortcomings are poor space and time resolution of the microwave apparatus used in [253 and 254], as well as they use of shock tubes with very small cross sections (about 1 cm) and short distances from the point where measurements were made to the diaphragm. The last circumstance means that the gas region heated by the shock wave is very short and this results in a fictitious reduction in the time of reaching maximum ionization. This is also shown by the form of absorption oscillogram with a sharp peak and absence of a horizontal equilibrium segment. In addition, the calculations for determining the electron concentration by measuring the high-frequency conductivity were based on classical gaskinetic values of effective frequencies of collisions of electrons with neutral particles, which may produce an appreciable error. This is due to the differences in the gaskinetic and experimentally obtained effective cross sections for elastic collisions of electrons; moreover, due to the fact that these cross sections do not vary smoothly with the temperature but have their maxima and minima. In order to

remove the dependence of results on v and increase the dimensions of the transition regions, the ionization process in some studies [14, 81] were examined at very low initial pressures (0.02-0.2 mm of Hg) and high Mach numbers (14-20).

1. Analysis of the Effect of Easily-Ionized Admixtures on Electron-Concentration Measurements

When considering ionization in various gases, which also includes air, consideration must be given to the possible effect of such easily-ionized admixtures in the test gas as sodium, potassium, etc., which are present in specific concentrations everywhere, i. e., in the atmosphere and in experimental apparatus. This contribution is expressed in an additional quantity of electrons which are formed when the admixtures are heated to relatively low temperatures. In order to estimate the contribution of the ionization of admixtures in our setup, we have studied argon, which is a gas that practically does not ionize up to temperatures of 9000°K. The conductivity of argon heated by a shock wave to 2000-5000°K is attributable to ionization of admixtures. In fact, x_e , the electron concentration in a two component gas mixture in thermodynamic equilibrium is defined as

$$x_e = \sqrt{\frac{1}{p} (x_1 K_{eq1} + x_2 K_{eq2})}, \quad (7.1)$$

where $K_{eq i}$ is the equilibrium ionization constant; x_i is the concentration of i th kind neutral atoms and p is the total pressure.

/148

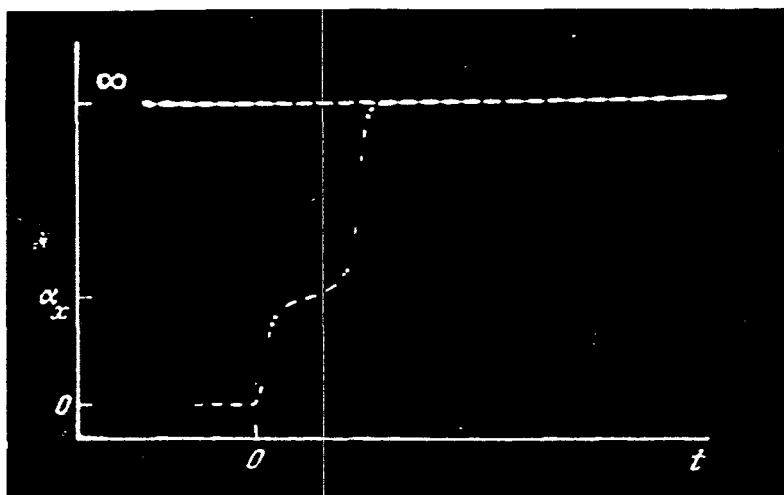


Figure 69. Oscillogram of the Absorption of 3-cm Radio Waves Behind a Shock Wave in Argon.

Since the ionization potential for argon is 15.7 ev, and the potential of sodium, the most prevalent easily-ionized admixture, is 5.1 ev, then their equilibrium constants at $T = 5000^\circ\text{K}$ differ by more than ten orders of magnitude. Consequently, in the above temperature range it is possible to disregard the contribution of the argon proper to the electron concentration, if the admixture concentration is not less than a millionth of a percent.

The experiments were performed in a shock tube. The absorption of radio waves was measured by a single-channel microwave line (version I) operating at a frequency of 10,000 Megacps ($\lambda = 3$ cm). The measurements were made at initial pressures of the argon from 2 to 10 mm of Hg and Mach numbers of the incident wave from 3 to 5. The work was done with pure argon from a tank with an admixture of 0.01% of nitroben and 0.005% of oxygen. A typical oscillogram of radiowave absorption is depicted in Fig. 69. Absorption behind the reflected wave proper has corresponding to it small step α_x . The absorption reaches some equilibrium level, remains constant up to arrival of secondary waves at a time t_{sec} , which waves appreciably increase the gas temperature and pressure. The electron concentrations were calculated from Saha's formula. The effective frequencies of collisions between electrons and argon atoms were calculated on the basis of effective cross section. The temperatures and pressures behind reflected shock waves were calculated for the velocity of the incident wave from ideal-gas formulas.

/149

We write the Saha equation in the form

$$\ln n_e^2 = \ln K + \ln p + \frac{1}{2} \ln T - \frac{\Phi}{kT}, \quad (7.2)$$

where Φ is the ionization potential of a substance which gives an electron concentration n_e for a pressure p and temperature T , and K is some constant which is not a function of p or T .

The dependence of $\ln n_e^2 - \ln p - \frac{1}{2} \ln T$ on T^{-1} which was obtained in a straight line. The tangent of this line yields the ration Φ/k . In our experiments the ionization potential of the admixtures was found to be 5.1 ev (Fig. 70), which corresponds to the ionization potentials of sodium. Experimentally determined values of n_e and Φ can be used for determining the concentration of sodium in the gas. For this we write the Saha equation in the form

$$n_{\text{Na}} = n_e^2 \frac{kT}{K_n}. \quad (7.3)$$

Analysis of data (see Fig. 70) shows that the content of sodium vapor in the argon in the shock tube was of the order of $10^{-4}\%$ [247].

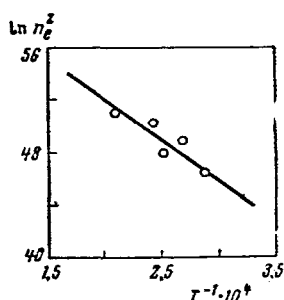


Figure 70. Determination of the Ionization Potential of an Admixture in Experiments With Argon.

It is of interest to compare the electron concentrations in air and argon at the same temperatures and pressures. For example, at $T_2 = 3500^\circ\text{K}$ and $p_2 = 2.7$ atm in argon $n_e \approx 10^{10}$, which in air $n_e \approx 10^{12}$, by two orders of magnitude higher than in argon. This shows that it is possible in our experiments to disregard the effect of admixture ionization in air.

2. Determining of the Time Needed for Reaching Equilibrium Ionization Behind Incident Shock Waves in Air

Ionization processes in air were studied behind incident shock waves for initial pressures of 1-5 mm of Hg and for $M = 8-12$. The absorption of 3.4 and 1.8 cm radiowaves was measured simultaneously. The gas behind the shock front passed in sequence through two probing radio beams situated at about 25 cm from one another. For $M_0 = 9.5$ the time resolution of the 3.4 cm channel was

about 11 μsecs , while for the 1.8 cm channel it was about 6 μsecs . Typical absorption oscillograms for these frequencies are shown in Fig. 71. The time during which absorption increased to a maximum was about 60 μsecs , which is several-fold greater than the resolution time of the apparatus. After maximum absorption level of radiowaves is reached, the experimentally determined electron concentrations agree within the limits of experimental error, with those calculated for equilibrium conditions (Fig. 72) for pressures of 2-5 mm of Hg ahead of the shock front and Mach numbers of 8.5-11. For pressures of 1 mm of Hg a constant absorption level is not reached for M_0 less than 10 in the entire region of the shock-heated gas (about 15 cm for $M_0 = 9$). Figure 73 depicts an

/151

absorption oscillogram for this regime, which is characterized by the fact that the absorption does not reach a constant value and drops sharply due to arrival of cold gas into the test region. However, for $M_0 > 10$, ionization even at $p_0 = 1$

/152

mm of Hg proceeds so rapidly that the electron concentrations succeed in reaching their equilibrium values (Fig. 74). The electron concentrations were calculated on the basis of tabulated values of $K_{eq}(T)$ for ionization of NO [2] and by resort to data on equilibrium temperatures and pressure presented in the Appendix. Since temperature and pressure data in these sources were calculated only for pressures of 1 and 25 mm of Hg, the required variables for intermediate initial pressures were obtained by linear interpolation.

The experimental studies of ionization of air behind an incident shock wave enabled us to determine the time for reaching equilibrium ionization for $M_0 = 8-12$.

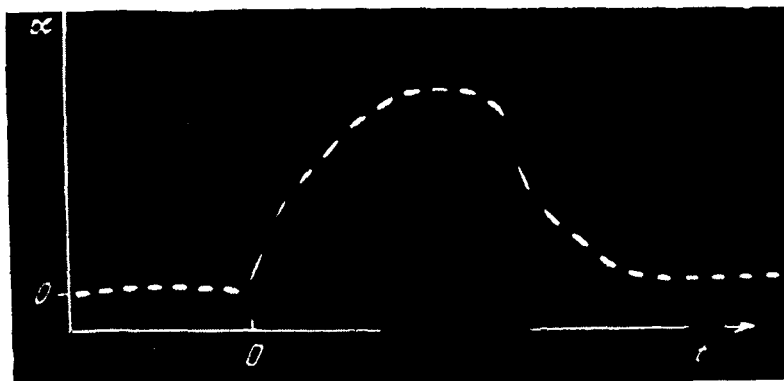


Figure 71. Oscillogram of the Absorption of 3.4-cm Radiowaves Behind a Shock Wave in Air; $p_0 = 3$ mm of Hg, $M_0 = 9.6$

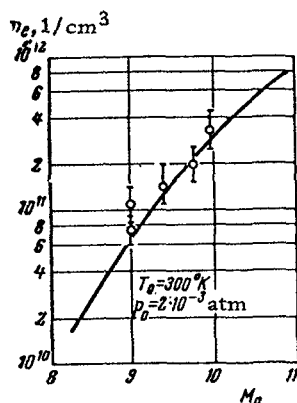
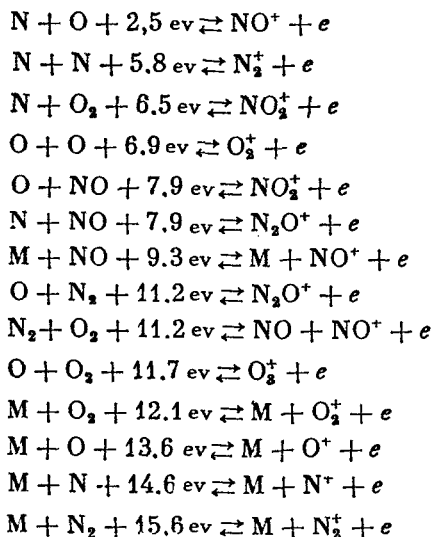


Figure 72. Electron Concentration in Air Behind a Shock Wave as a Function of M_0 for $p_0 = 2$ mm of Hg.

The basic types of ionization reactions are enumerated in [248]



It is also shown in the above reference that all these reactions make important contributions only at high temperatures (approximately 20,000°K). As the temperature is lowered predominance is acquired by collisions between atomic components of the mixtures and at the lowest temperatures considered (about 8000°K) the first of the above reactions takes place most rapidly. This makes it possible to avoid complex machine [computer] calculations in determining the ionization rate of air for comparatively low M_0 [249-252].

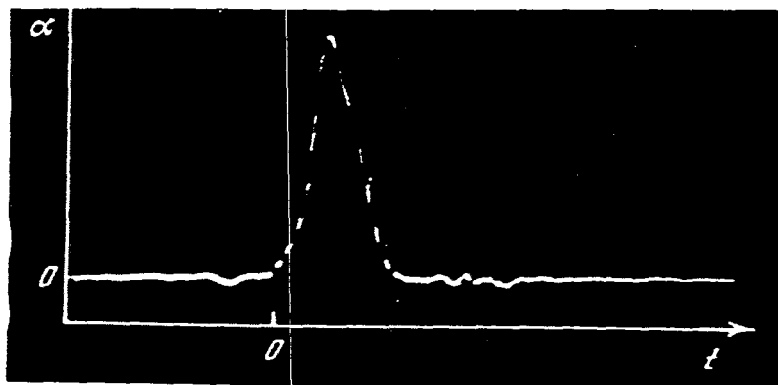


Figure 73. Oscillogram of the Absorption of 3.4-cm Radio-Waves in Air Behind a Shock Wave for $M_0 = 10$, $p_0 = 1$ mm of Hg; the Time Marks are each $10\mu\text{secs}$.

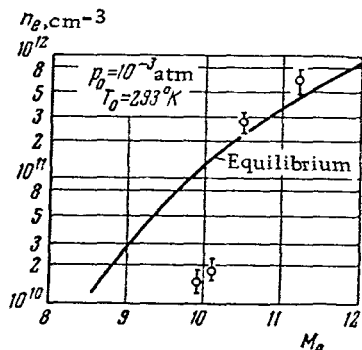


Figure 74. Electron Concentration in Air Behind a Shock-Wave Front as a Function of M_0 for an Initial Pressure of 1 mm of Hg.

Comparison of the time for reaching equilibrium concentrations obtained in our experiments with an approximation calculation for the reaction $N + O \rightleftharpoons NO^+ + e$, is shown in Fig. 75. It should be noted that the data obtained by the present authors are in that range of shock-wave velocities and pressures for which the method suggested by Lin [81] does not apply, since in the radio-wave measurements it is necessary to take account not only the electron concentrations, but also the effective frequencies of collision between electrons and gas particles.

It is also interesting to note that the heated-gas regions in the Mancheimer and Low [253] as well as in the Dvir and Low [254] experiments were also short, due to the very short shock tubes used by them. This was responsible for the fact that ionization equilibrium was not reached over the entire volume of the heated gas up to the boundary with the cold driver gas. Absorption oscillograms presented in studies have, without

exception, a sharp peak and do not have a section with constant absorption. It is therefore quite clear that the times for reaching equilibrium ionization obtained by us for air is 5-10 fold greater than by the above authors.

3. The Ionization Structure of Shock Waves in Nitrogen

/154

The time for establishing equilibrium degree of ionization in nitrogen at 3000-5000°K was determined by absorption of centimeter radiowaves in nitrogen behind an incident and reflected shock waves in a shock tube. The experiments

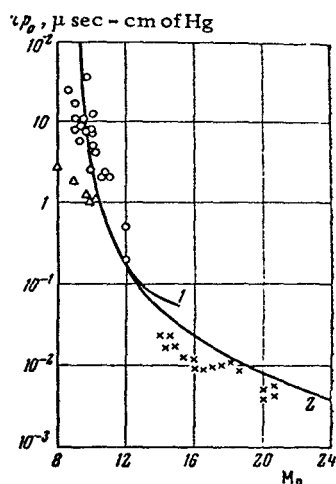


Figure 75. Time for Reaching Equilibrium Ionization of Air Behind a Shock Wave, Referred to an Initial Pressure of 1 mm of Hg, as a Function of M_0 :

1—Calculations for the Reaction $N + O = NO$;
2—Calculations of [248];
Experimental Data:
x—[81]; O—Present
Authors: Δ —[253].

involved simultaneous absorption of 1.6 and 0.8 cm radiowaves directed through the viewing section in two mutually perpendicular directions. The width of the radiowave beams did not exceed 20 mm [256].

The time for reaching the equilibrium degree of ionization in nitrogen was measured at initial pressures of 2 and 5 mm of Hg in the low pressure chamber, with M_0 , the Mach numbers of the incident wave, of 5.5–11.0. The temperature and pressure behind the reflected shock wave, calculated on the basis of conservation laws for an equilibrium composition, are 3000–5000°K and 1–2 atm [257]. A specimen of a radiowave absorption oscillogram is shown in Fig. 76. After the reflected shock wave arrives at the radiowave beam, whose center is situated at 20 mm from the tube's end, gradual absorption of radiowaves is observed for 100 μ secs, and this is followed by a constant level. Further increases in absorption are attributable to the arrival of the secondary wave, produced by interaction between the reflected wave and the contact surface [256]. The reflected wave propagates relative to the shock-tube walls at a speed of 0.5 mm/ μ sec, for which reason the gas behind this wave covers over [passes through] the radiowaves beam during 40 μ secs. This is the resolution time behind a reflected shock wave. It was shown by control experiments in air that bifurcation attendant to shock-wave reflection does not appreciably af-

fect the radiowave absorption. This is apparently attributable to the fact that the shape of the reflected-wave front is distorted only in a narrow region near the front [130]. The observed time interval of increases in radiowave absorption, with correction for the time of resolution, should apparently be ascribed to the time for establishing equilibrium ionization in the nitrogen.

The free electron concentration, measured after reaching the first maximum on the absorption curve is from 10^{11} to 10^{12} cm^{-3} for $M_0 = 5.5$ –6.8 and $p_0 = 2$ mm of Hg. These values of n_e are in satisfactory agreement with theoretically calculated equilibrium values (Fig. 77) [257].

The times for reaching equilibrium thermal ionization in nitrogen, reduced to atmospheric pressure, were 40–800 μ secs (Fig. 78). The experimental values obtained by us behind the reflected wave are depicted here by black dots, while those obtained behind the incident wave are denoted by triangles. For comparison we present the values of ionization time for air, which were found to be shorter than for nitrogen (open circles).

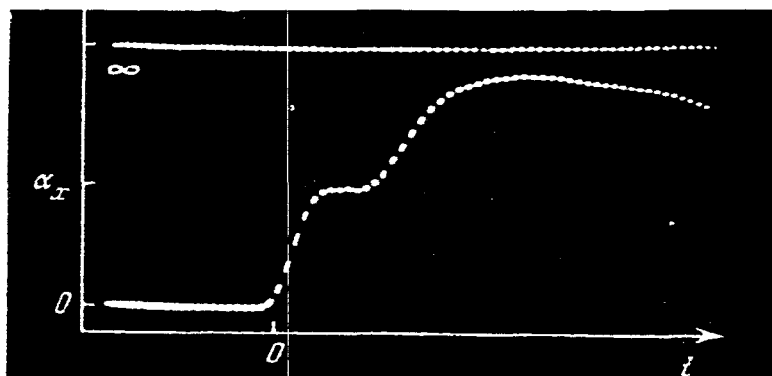


Figure 76. Oscillogram of Absorption of 8-mm Radio-Waves in Nitrogen Behind a Reflected Shock Wave for $M_0 = 6.0$ and $p_0 = 2$ mm of Hg.

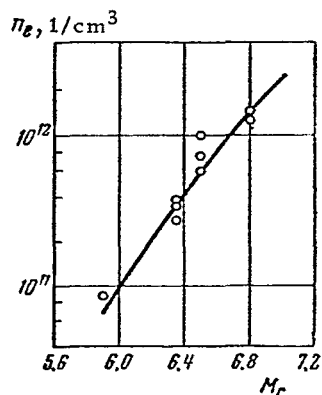


Figure 77. Electron Concentration in Nitrogen Behind the Front of a Reflected Shock Wave as a Function of M_0 for an

Initial Pressure of 2 mm of Hg.

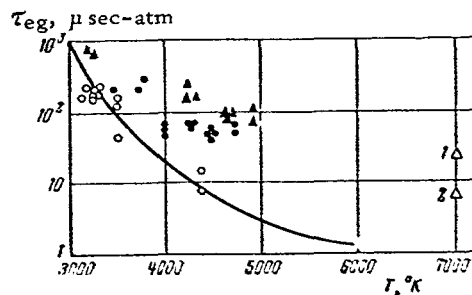
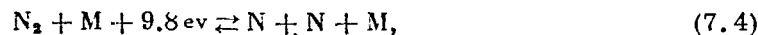


Figure 78. Time for Reaching Equilibrium Ionization of Nitrogen Behind a Shock Wave Front:

The Curve was Obtained Theoretically for Air; 1—Calculations on Assuming Reaction (7.5); 2—Calculations on Assuming Reaction (7.7 [281]) [sic?].

As was shown in [258], the ionization of nitrogen is describable by two reactions



As is known, reaction (7.4) also occurs during ionization of air, hence the difference in the times for reaching equilibrium ionization in nitrogen and air

is attributable to differences in the rates of reactions (7.5) and



Reaction (7.6) has a rate constant of $3 \cdot 10^{-3} T^{-3/2}$, while the rate constant for reaction (7.5) is $1.6 \cdot 10^{-2} T^{-3/2}$, i.e., reaction (7.5) should proceed even faster than reaction (7.6). However, it is shown experimentally that the case is just the opposite.

Let us compare the time $t_m \approx 90 \mu\text{secs}$ for the above case with the time for reaching equilibrium ionization in air at the same temperature of $T = 3800^\circ\text{K}$ and pressure $p = 0.8 \text{ atm}$ as in nitrogen. For air this time is $\tau \approx 20 \mu\text{secs}$. Thus, the time for reaching maximum ionization in nitrogen exceeds 4.5-fold the time in air.

Reference [258] points out still another ionization reaction for nitrogen, attributable to ionization of atoms in the excited metastable state



Calculation of the ionization profile in nitrogen behind a shock wave performed in [258] shows that an appreciable ionization delay occurs in the case of reaction (7.7). This delay is ascribable to the time needed for exciting the nitrogen atoms. It is possible that the long time needed for reaching maximum ionization can be attributed to reaction (7.7).

4. Measuring the Electron Temperature on the Basis of Self Radio-Frequency Radiation of a Gas Behind a Shock Wave

Thermal ionization of a gas is a complex process. It is related to a number of chemical and physical transformations, which serve as the source of free electrons. Due to the absence of electric and magnetic fields, the Maxwellian velocity distribution in an electron gas is established quite rapidly. Nevertheless it is not obvious that the electron temperature during ionization or toward its completion is equal to the temperature of the gas [149, 273]. Thus, a source of fast electrons exists when, while ionizing nitrogen in a gas discharge tube, the discharge is stopped for several hundreds of microseconds (for a pressure of several mm of Hg) [273]. When argon is ionized behind the front of strong shock waves, the electron gas is highly "cooled" since the energy losses for ionization are replenished very slowly due to the great difference in the masses of the electron and argon atoms [149].

/157

The behavior of the electron temperature in some gases was checked experimentally by measuring the coefficients of absorption, reflection and radiation in the 8 mm range of radio frequencies.

The intensity of self radiation of ionized gas is

$$I = I_0 \frac{1-R}{1-Re^{-\delta z}} (1 - e^{-\delta z}),$$

where I_0 is the radiation intensity of a black body.

The radiation temperature T_{rad} is related to the electron temperature T_e by the expression

$$T_{\text{rad}} = T_e \frac{1-R}{1-R(1-K)} K,$$

where $K = 1 - e^{-\delta z}$ is the absorptivity of the gas.

On the other hand, the intensity of the radiation received by a receiver is related to the radiation temperature and the passband of the receiver in the following manner

$$I = kT_{\text{rad}}\Delta f \cdot 10^{-7},$$

where I is in watts, k is the Boltzmann constant and Δf is the passband of the receiver, cps.

Thus, if $K = 1$ and $R = 0$ the gas radiates as a black body and the radiation and electron temperatures are equal.

The radio-frequency wave measurements were made in air, nitrogen and argon. The measurements in air and nitrogen were made behind reflected shock wave, while in argon these were performed behind reflected as well as incident waves. The studies in air were carried out for initial pressures from 3 to 0.5 mm of Hg. The receiving antenna was located laterally to the tube end.

These experiments showed that the intensity of the 8-mm self-radiation of air heated by a reflected shock wave reaches some constant level (Fig. 79) during a time needed for covering over the aperture of the [antenna] horn by the wave-front. For example, for $p_0 = 1$ mm of Hg and $M_0 = 10.2$ this time is about

30 μ secs. The time for achieving equilibrium ionization is about 0.2 μ secs [251]. It is possible that the true time for reaching the radiation maximum is smaller than that obtained by us since the resolution of the apparatus in the given case was quite low (about 25 mm). Using the GSh-7 standard noise source with a noise temperature of 16,600°K we were able to compare the radiation intensity with the radiation temperature.

/158

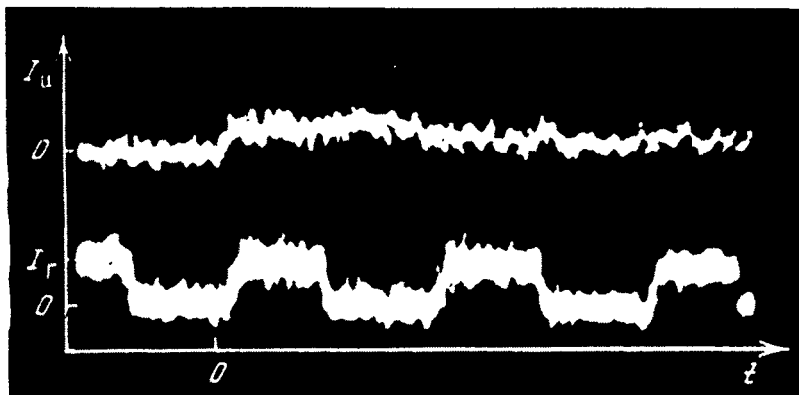


Figure 79. Oscillogram of Self Radiation in the 8-mm Range for Air Heated by a Reflected Shock Wave, for an Initial Pressure of 1 mm of Hg and for $M_0 = 10.3$. The Lower Curve is the Oscillogram of the Calibration Signal.

Since the measured absorption coefficients show that the radio-frequency waves are completely absorbed already for $M = 8.3$, while the coefficient of reflection is low, it is obvious that the radiation and electron temperatures are equal. The gas radiates as a black body (Fig. 80). Figure 80 presents for comparison curves of theoretical equilibrium temperatures of air for three initial pressures (see the Appendix).

It is obvious that in the equilibrium zone behind the front of a reflected wave the electron temperature is the same as the temperature of the gas.

Measurements in nitrogen yield similar results. The only difference here was a somewhat higher reflection coefficient. The equilibrium theoretical values of temperature were taken from [257].

Of the greatest interest, in our opinion, are measurements in argon. Measurements behind incident shock waves were performed in pure argon (with an oxygen content of 0.005%) at initial pressures of 2 and 3 mm of Hg.

Figure 81 shows values of radiation temperatures calculated on the basis of radiation intensities. For $M > 9.7$, i. e., under conditions when the absorption coefficient is zero, conversion of the radiation to the electron temperature using the expression $T_{\text{rad}} = T_e (1 - R)$ shows that T_e is in good agreement with the theoretical equilibrium temperature of the gas.

/159

In experimental measurements of the electron temperature behind incident shock waves a region was discovered in which the self radio-frequency radiation increases gradually. The time of increase for $M = 9-11$ and $p_0 = 1$ mm of Hg is about $60 \mu\text{secs}$, i. e., by an order of magnitude less than the time for reaching the equilibrium degree of ionization [149].

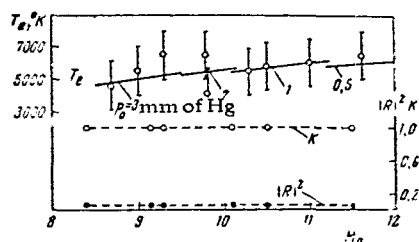


Figure 80. Electron Temperature, Absorptivity and the Coefficient of Reflection of 8-mm Radio-Frequency Waves in Air Behind a Reflected Shock Wave as a Function of M_0 .

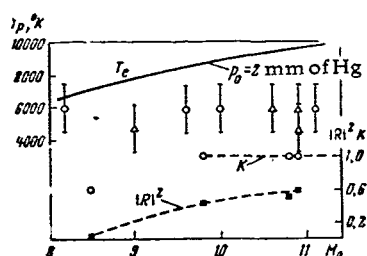


Figure 81. Radiation Temperature, Absorptivity and Coefficient of Reflection of 8-mm Radio-Frequency Waves in Argon Behind an Incident Shock Wave as a Function of M_0 .

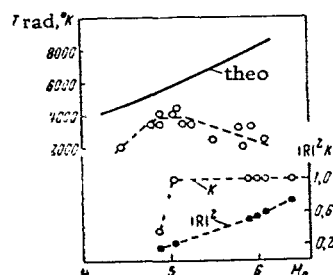


Figure 82. Radiation Temperature, Absorptivity and Coefficient to Reflection of 8-mm Radio-Frequency Waves in Argon Behind a Reflected Shock Wave [as a Function of M_0].

Measurements in argon behind reflected shock waves were made at pressures of 5, 10 and 15 mm of Hg. Figure 82 shows the experiments results. The radiation temperature is very close to the electron temperature only for $M \approx 5$. Then, as the shock-wave strength increases, the self radiation of the hot gas starts to drop and approaches the level noise of the apparatus, i.e., 1500-2000°K. The radiation is as if locked in inside some gaseous "mirror box" and does not go outside, although the gas is heated to very high temperatures. This is apparently attributable to the very small cross section for electron-atom collisions in argon.

5. Cross Section of Elastic Collisions Between Electrons and Neutral Particles In a Gas Ionized by a Shock Wave

/160

An electron moving under the action of an electromagnetic field in a gas loses energy due to collisions with the gas particles. The effective frequency of collisions between the electron and the gas particles depends on the force field of these particles, which scatters the electron. To concretely describe these fields of the particles we introduce the quantity Q , which is called the effective cross section or diameter of collision between electrons and gas particles and is related to ν as follows

$$\nu = \bar{v} \sum_j n_j Q_j,$$

where $v = \sqrt{\frac{8kT_e}{\pi m}}$ is the mean thermal electron velocity, n_j and Q_j are the particle concentrations (per unit volume) and collision cross section for the j th component of the gas (per unit area), respectively.

It was assumed up to the twenties, that this cross section is constant, i.e., its size does not depend on the electron velocity and the kind of gas and it was taken as equal to πa_0^2 , where a_0 is the radius of the particle which was regarded as a solid sphere. This classical cross section was assumed to be $4.4 \cdot 10^{-16} \text{ cm}^2$. However, it was discovered even in the early studies of Ramsauer and Collas which were concerned with measuring the scattering of multi-energy electrons and in those of Townsend and Bailey, pertaining to measurements of the drift of the electron cloud, that this cross section depends on the electron velocity and on the kind of gas particles in which they move (see [259]).

The dependence of the cross section of elastic collisions, during which there is no electron-impact excitation or ionization of the atom or molecule, on the electron velocity was most pronounced for certain substances (argon, for example) with relatively low electron energies (less than one ev) in the form of a sharp minimum. This phenomenon has been called the Ramsauer effect.

Up to the most recent time a large number of studies [260-280] is being devoted to experimental study of the temperature dependence of the collision cross section for different substances.

In examining published experimental data on collision cross sections obtained by different investigators for the same substances one encounters a great amount of disagreement (up to an order of magnitude) and different temperature dependences [267, 276]. Analysis of experimental conditions (as a rule, the measurements were performed in discharge tubes and chambers), performed in [273] shows that the electrons born during the discharge are very "hot", i.e., have temperatures of about hundreds of thousands of degrees. The time needed for "cooling" them to the temperature of the gas is 100-200 μsecs at pressures of several mm of Hg, and not 50 μsecs , as was assumed in [272]. The measurements made during the time when equilibrium is being established will yield a large scatter.

/161

In addition, measurements using the electron cloud drift method have the shortcoming that the velocity distribution of the electrons in the presence of a constant field will not be Maxwellian, with the result that the cross sections measured will be only local in character. For this reason the present author in [256] has measured the effective cross sections in the temperature range of 2500-5000°K, which is of practical importance. The ionized gas was obtained in a shock tube by instantaneous compression behind a shock front. Measurements in a gas heated by a shock wave have a number of advantages over measurements under other conditions, the former being as follows.

1. The thermally ionized gas behind a shock wave front can be divided into two regions, the first of which is the region of nonequilibrium variables, in

which the electron concentration increases from zero to its maximum (equilibrium) value, while the second has a uniform distribution of electron concentrations, of temperatures and pressures (if the shock wave propagates through this region at a constant velocity).

2. The time needed by the gas for reaching ionization equilibrium is known.
3. The temperature and pressure in the equilibrium zone can be calculated for different M_0 of incident waves in different gases with a high accuracy.
4. The electrons behind the shock front acquire a Maxwellian velocity distribution very rapidly (during several μ secs, see [274]) (for this to happen they need only one electron-electron collision), since there are no strong external fields and the temperature and pressure are high ($T = 2000-5000^\circ\text{K}$, $p = 0.01-10$ atm).
5. The cold transition zone (boundary layer) in the direction of propagation of the probing radio-frequency beams at such high pressures behind shock waves is quite small (about 1 mm in nitrogen for $p_0 = 10$ mm of Hg and $M_0 = 5$ [138]). It is of substance that the temperature and pressure of the gas in the shock tube can be measured from the easily determinable shock-wave velocity.

Reference [275] describes spectroscopic studies of temperature along a gas column behind an incident shock-wave front. As a result satisfactory agreement was discovered between experimental data in air, nitrogen and argon with theoretical results in a wide range of shock-wave velocities. A similar conclusion on the temperature of gas behind reflected shock waves in air, oxygen and argon was made in [136] (within the $\pm 2\%$ accuracy of velocity measurements and $\pm 3\%$ accuracy of temperature measurements. Theoretical and experimental results are in agreement).

Thus, accurate information concerning the thermodynamic state of the test gas enabled us with a known confidence (about 30%) to obtain values of effective cross sections on the basis of experimentally measured collision frequencies.

The following values of cross sections were obtained

	$Q, \text{ cm}^2$	$T, ^\circ\text{K}$
Air	$(0.8-1) \cdot 10^{-15}$	3100-3600
Nitrogen	$(0.3-3) \cdot 10^{-15}$	2800-5000
Atomic oxygen	$(1.2-0.8) \cdot 10^{-15}$	3200-3600
Molecular oxygen	$(4-0.8) \cdot 10^{-16}$	2600-3600
Carbon monoxide .	$(0.7-1.0) \cdot 10^{-15}$	2200-4600
Carbon dioxide	$(0.45-0.3) \cdot 10^{-15}$	2600-3600
Argon	$[5 \cdot 10^{-17}$ $3 \cdot 10^{-17}]$	4400 5900

PHYSICAL VARIABLES IN AIR BEHIND A NORMAL SHOCK AND
BEHIND A REFLECTED SHOCK WAVE FOR EQUILIBRIUM
AND FROZEN DISSOCIATION [109]

The state behind an incident shock wave was determined by resorting to conservation laws, written in the coordinate system moving with the shock

$$\begin{aligned}\rho_1 u_1 &= \rho_0 u_0 = a, \\ \rho_1 u_1^2 + p_1 &= \rho_0 u_0^2 + p_0 = b, \\ \frac{u_1^2}{2} + H_1 &= \frac{u_0^2}{2} + H_0 = d, \\ p_1 &= \frac{\rho_1 H_1}{\mu_1}.\end{aligned}$$

- This system of equations was transformed to the form

TABLE 1. TEMPERATURE OF THE GAS BEHIND INCIDENT (T_1 , °K) AND REFLECTED (T_2 , °K) WAVES
AS A FUNCTION OF U_0 FOR DIFFERENT
INITIAL PRESSURES p_0

u_0 , m/sec	10 ⁻³ atm			10 ⁻⁴ atm			10 ⁻⁵ atm			Any	
	T_1 (B)	T_2 (I)	T_2 (II)	T_1 (B)	T_2 (I)	T_2 (II)	T_1 (B)	T_2 (I)	T_2 (II)	T_1 (A)	T_2 (III)
1400	1150	—	2040	—	—	2020	—	—	—	1150	—
1500	1280	—	2260	—	—	2210	—	—	—	1280	—
1600	1410	—	2440	—	—	2350	—	—	—	1410	2600
2000	1950	3000	3000	—	—	2770	—	—	—	1980	3300
2250	2300	3300	—	—	—	—	—	—	—	—	—
2500	2550	3540	3950	2430	3330	—	—	—	—	2840	5560
2750	2780	4110	4000	2610	3860	3690	—	—	—	3350	—
3000	2980	4830	4650	2750	4580	4400	2540	4330	4150	3890	7820
3500	3350	5870	5640	3080	5350	5170	2850	4940	4770	5100	10240
4000	3930	6460	6260	3790	5840	5660	3670	5300	5120	6460	12820
4500	4840	6980	6760	4540	6260	6040	4250	5610	5440	7990	15500
5000	5410	7450	7250	4950	6680	6480	4590	5990	5720	9640	18400
6000	—	—	8330	—	—	7400	—	—	6570	13220	—

Notes. A—there is no dissociation behind the incident wave;
B—equilibrium dissociation behind the incident wave; I—equilibrium dissociation behind the incident and reflected waves;
II—there is no dissociation behind the incident wave while equilibrium dissociation exists behind the reflected wave;
III—there is no dissociation behind the incident and reflected waves.

$$H_1 = \frac{b}{4a^2} \sqrt{b^2 - \frac{4a^2 RT_1}{\mu_1}} - \frac{RT_1}{2\mu_1} = d - \frac{b^2}{4a^2}$$

The state of the gas behind the reflected wave and the velocity of the reflected wave were determined from conservation laws, written in a coordinate system moving with the reflected wave

$$\begin{aligned} \rho_1(v_1 + D_2) &= \rho_2 D_2, \\ \rho_1(v_1 + D_2)^2 + p_1 &= \rho_2 D_2^2 + p_2, \\ \frac{(v_1 + D_2)^3}{2} + H_1 &= \frac{D_2^3}{2} + H_2, \\ p_2 &= \frac{\rho_2 RT_2}{\mu_2} \end{aligned}$$

and reduce to the form

/165

$$D_2 = -\frac{\left(v_1^2 + \frac{RT_1}{\mu_1} - \frac{RT_2}{\mu_2}\right)}{2v_1} + \sqrt{\left[\frac{\left(v_1^2 + \frac{RT_1}{\mu_1}\right) - \frac{RT_2}{\mu_2}}{2v_1}\right] + \frac{RT_2}{\mu_2}},$$

$$v_1 D_2 + \frac{v_1^2}{2} + H_1 = H_2(T_2, p_2)$$

TABLE 2. PRESSURE BEHIND AN INCIDENT WAVE
p₁ (atm) AS A FUNCTION OF u₀ FOR
VARIOUS INITIAL PRESSURES p₀

u ₀ , m/sec	10 ⁻³ atm		10 ⁻⁴ atm		10 ⁻⁵ atm	
	B	A	B	A	B	A
1400	—	1,95·10 ⁻²	—	1,95·10 ⁻³	—	1,95·10 ⁻⁴
1500	—	2,25·10 ⁻²	—	2,25·10 ⁻³	—	2,25·10 ⁻⁴
1600	—	2,60·10 ⁻²	—	2,60·10 ⁻³	—	—
2000	4,05·10 ⁻²	4,05·10 ⁻²	—	4,05·10 ⁻³	—	4,05·10 ⁻⁴
2250	5,20·10 ⁻²	—	—	—	—	—
2500	6,50·10 ⁻²	6,40·10 ⁻²	6,40·10 ⁻³	6,40·10 ⁻³	—	6,40·10 ⁻⁴
2750	8,00·10 ⁻²	7,77·10 ⁻²	8,05·10 ⁻³	7,77·10 ⁻³	—	7,77·10 ⁻⁴
3000	9,50·10 ⁻²	9,20·10 ⁻²	9,65·10 ⁻³	9,20·10 ⁻³	9,70·10 ⁻⁴	9,20·10 ⁻⁴
3500	1,32·10 ⁻¹	1,25·10 ⁻¹	1,33·10 ⁻²	1,25·10 ⁻²	1,35·10 ⁻³	1,25·10 ⁻³
4000	1,75·10 ⁻¹	1,65·10 ⁻¹	1,75·10 ⁻²	1,65·10 ⁻²	1,77·10 ⁻³	1,65·10 ⁻³
4500	2,20·10 ⁻¹	2,10·10 ⁻¹	2,20·10 ⁻²	2,10·10 ⁻²	2,20·10 ⁻³	2,10·10 ⁻³
5000	2,70·10 ⁻¹	2,60·10 ⁻¹	2,75·10 ⁻²	2,60·10 ⁻²	2,75·10 ⁻³	2,60·10 ⁻³
6000	—	4,17·10 ⁻¹	—	4,17·10 ⁻²	—	4,17·10 ⁻³

Notes. A-frozen dissociation; B-equilibrium association.

Commas represent decimal points.

The calculations were made on the following assumptions:

1. The air behind the incident and reflected wave attains equilibrium dissociation. The values of H_2 and μ_2 were taken from tables of thermodynamic functions [1, 2];

2. Internal degrees of freedom are excited behind the incident wave, but no dissociation takes place. Equilibrium dissociation takes place. Equilibrium dissociation is attained behind the reflected wave. Tables of [1, 2, 118, 185] were used.

3. Internal degrees of freedom behind the incident and reflected waves are excited, but dissociation does not take place.

TABLE 3. DENSITY ρ_1 [SIC] (grams/cm³) BEHIND AN INCIDENT WAVE AS A FUNCTION OF u_0 FOR AN INITIAL PRESSURE p_0

u_0 , m/sec	10 ⁻³ atm		10 ⁻⁴ atm		10 ⁻⁵ atm	
	B	A	B	A	B	A
1400	—	5,92·10 ⁻⁶	—	5,92·10 ⁻⁷	—	5,92·10 ⁻⁸
1500	—	6,16·10 ⁻⁶	—	6,16·10 ⁻⁷	—	6,16·10 ⁻⁸
1600	—	6,38·10 ⁻⁶	—	6,38·10 ⁻⁷	—	6,38·10 ⁻⁸
2000	7,26·10 ⁻⁶	7,14·10 ⁻⁶	—	7,14·10 ⁻⁷	—	7,14·10 ⁻⁸
2250	7,86·10 ⁻⁶	—	—	—	—	—
2500	8,74·10 ⁻⁶	7,84·10 ⁻⁶	9,12·10 ⁻⁷	7,84·10 ⁻⁷	—	7,84·10 ⁻⁸
2750	9,64·10 ⁻⁶	8,06·10 ⁻⁶	10,20·10 ⁻⁷	8,06·10 ⁻⁷	—	8,06·10 ⁻⁸
3000	10,50·10 ⁻⁶	8,26·10 ⁻⁶	11,30·10 ⁻⁷	8,26·10 ⁻⁷	12,10·10 ⁻⁸	8,26·10 ⁻⁸
3500	12,20·10 ⁻⁶	8,64·10 ⁻⁶	13,10·10 ⁻⁷	8,64·10 ⁻⁷	14,00·10 ⁻⁸	8,64·10 ⁻⁸
4000	12,80·10 ⁻⁶	8,94·10 ⁻⁶	13,30·10 ⁻⁷	8,94·10 ⁻⁷	13,70·10 ⁻⁸	8,94·10 ⁻⁸
4500	12,90·10 ⁻⁶	9,16·10 ⁻⁶	13,70·10 ⁻⁷	9,16·10 ⁻⁷	14,50·10 ⁻⁸	9,16·10 ⁻⁸
5000	13,60·10 ⁻⁶	9,40·10 ⁻⁶	15,00·10 ⁻⁷	9,40·10 ⁻⁷	16,00·10 ⁻⁸	9,40·10 ⁻⁸
6000	—	9,96·10 ⁻⁶	—	9,96·10 ⁻⁷	—	9,96·10 ⁻⁸

Notes. A-dissociation frozen; B-equilibrium dissociation.

Commas represent decimal points.

Calculations were made for the following conditions

/168

$$u_0 = 1400 - 6000 \text{ m/sec, } p_0 = 10^{-3}, 10^{-4}, 10^{-5} \text{ atm}$$

$$u_0 = 1400 - 3000 \text{ m/sec, } p_0 = 0,033 \text{ atm}$$

$$T_0 = 293^\circ\text{K, } H_0 = 2,904 \cdot 10^9 \text{ ergs/gram.}$$

The results of calculations are presented in Tables 1 through 7, the computational accuracy was 1-2%.

TABLE 4. DENSITY ρ_3 (grams/cm³) BEHIND A REFLECTED WAVE AS A FUNCTION OF u_0 FOR AN INITIAL PRESSURE p_0

u_0 , m/sec	10 ⁻³ atm			10 ⁻⁴ atm			10 ⁻⁵ atm		
	I	II	III	I	II	III	I	II	III
1400	—	2,08·10 ⁻⁵	—	—	2,08·10 ⁻⁶	—	—	—	—
1500	—	2,24·10 ⁻⁵	—	—	2,26·10 ⁻⁶	—	—	—	—
1600	—	2,46·10 ⁻⁵	2,34·10 ⁻⁵	—	2,48·10 ⁻⁶	2,34·10 ⁻⁶	—	—	2,34·10 ⁻⁷
2000	3,35·10 ⁻⁵	3,30·10 ⁻⁵	2,80·10 ⁻⁵	—	3,44·10 ⁻⁶	2,80·10 ⁻⁶	—	—	2,80·10 ⁻⁷
2250	4,00·10 ⁻⁵	—	—	—	—	—	—	—	—
2500	4,81·10 ⁻⁵	4,28·10 ⁻⁵	3,34·10 ⁻⁵	5,32·10 ⁻⁶	—	3,34·10 ⁻⁶	—	—	3,34·10 ⁻⁷
2750	5,49·10 ⁻⁵	4,60·10 ⁻⁵	—	3,08·10 ⁻⁶	4,84·10 ⁻⁶	—	—	—	—
3000	6,00·10 ⁻⁵	4,72·10 ⁻⁵	3,56·10 ⁻⁵	3,70·10 ⁻⁶	4,90·10 ⁻⁶	3,56·10 ⁻⁶	7,56·10 ⁻⁷	5,40·10 ⁻⁷	3,56·10 ⁻⁷
3500	7,43·10 ⁻⁵	5,22·10 ⁻⁵	3,86·10 ⁻⁵	8,54·10 ⁻⁶	5,56·10 ⁻⁶	3,86·10 ⁻⁶	9,84·10 ⁻⁷	5,90·10 ⁻⁷	3,86·10 ⁻⁷
4000	8,58·10 ⁻⁵	5,96·10 ⁻⁵	4,16·10 ⁻⁵	9,64·10 ⁻⁶	6,38·10 ⁻⁶	4,16·10 ⁻⁶	10,60·10 ⁻⁷	6,90·10 ⁻⁷	4,16·10 ⁻⁷
4500	9,31·10 ⁻⁵	6,60·10 ⁻⁵	4,44·10 ⁻⁵	10,70·10 ⁻⁶	7,18·10 ⁻⁶	4,44·10 ⁻⁶	12,50·10 ⁻⁷	7,74·10 ⁻⁷	4,44·10 ⁻⁷
5000	10,80·10 ⁻⁵	7,20·10 ⁻⁵	4,74·10 ⁻⁵	12,56·10 ⁻⁶	7,84·10 ⁻⁶	4,74·10 ⁻⁶	14,70·10 ⁻⁷	8,66·10 ⁻⁷	4,74·10 ⁻⁷
6000	—	8,21·10 ⁻⁵	—	—	8,94·10 ⁻⁶	—	—	9,80·10 ⁻⁷	—

Notes. I-Equilibrium dissociation; II-Frozen dissociation behind the incident wave and equilibrium dissociation behind the reflected wave; III-frozen dissociation. Commas represent decimal points.

TABLE 5. PRESSURE p_2 (atm) BEHIND A REFLECTED WAVE AS A FUNCTION OF u_0
FOR A PRESSURE p_0

u_0 , m/sec	10^{-3} atm			10^{-4} atm			10^{-5} atm		
	I	II	III	I	II	III	I	II	III
1400	—	$1,22 \cdot 10^{-1}$	—	—	$1,22 \cdot 10^{-2}$	—	—	—	—
1500	—	$1,45 \cdot 10^{-1}$	—	—	$1,45 \cdot 10^{-2}$	—	—	—	—
1600	—	$1,72 \cdot 10^{-1}$	$1,74 \cdot 10^{-1}$	—	$1,70 \cdot 10^{-2}$	$1,74 \cdot 10^{-2}$	—	—	$1,74 \cdot 10^{-3}$
2000	$3,00 \cdot 10^{-1}$	$2,95 \cdot 10^{-1}$	$3,06 \cdot 10^{-1}$	—	$2,90 \cdot 10^{-2}$	$3,06 \cdot 10^{-2}$	—	—	$3,06 \cdot 10^{-3}$
2250	$4,10 \cdot 10^{-1}$	—	—	—	—	—	—	—	—
2500	$5,62 \cdot 10^{-1}$	$4,96 \cdot 10^{-1}$	$5,26 \cdot 10^{-1}$	$5,90 \cdot 10^{-2}$	—	$5,26 \cdot 10^{-2}$	—	—	$5,26 \cdot 10^{-3}$
2750	$7,60 \cdot 10^{-1}$	$6,16 \cdot 10^{-1}$	—	$8,02 \cdot 10^{-2}$	$6,05 \cdot 10^{-2}$	—	—	—	—
3000	$10,00 \cdot 10^{-1}$	$7,50 \cdot 10^{-1}$	$8,00 \cdot 10^{-1}$	$10,80 \cdot 10^{-2}$	$7,50 \cdot 10^{-2}$	$8,00 \cdot 10^{-2}$	$11,60 \cdot 10^{-3}$	$7,40 \cdot 10^{-3}$	$8,00 \cdot 10^{-3}$
3500	$15,80 \cdot 10^{-1}$	$10,50 \cdot 10^{-1}$	$11,80 \cdot 10^{-1}$	$17,00 \cdot 10^{-2}$	$10,50 \cdot 10^{-2}$	$11,30 \cdot 10^{-2}$	$18,30 \cdot 10^{-3}$	$10,50 \cdot 10^{-3}$	$11,30 \cdot 10^{-3}$
4000	$21,80 \cdot 10^{-1}$	$14,30 \cdot 10^{-1}$	$15,30 \cdot 10^{-1}$	$22,20 \cdot 10^{-2}$	$18,40 \cdot 10^{-2}$	$15,30 \cdot 10^{-2}$	$22,70 \cdot 10^{-3}$	$14,00 \cdot 10^{-3}$	$15,30 \cdot 10^{-3}$
4500	$27,50 \cdot 10^{-1}$	$18,20 \cdot 10^{-1}$	$19,80 \cdot 10^{-1}$	$28,70 \cdot 10^{-2}$	$18,20 \cdot 10^{-2}$	$19,80 \cdot 10^{-2}$	$30,30 \cdot 10^{-3}$	$14,00 \cdot 10^{-3}$	$19,80 \cdot 10^{-3}$
5000	$35,00 \cdot 10^{-1}$	$23,30 \cdot 10^{-1}$	$25,00 \cdot 10^{-1}$	$38,70 \cdot 10^{-2}$	$23,00 \cdot 10^{-2}$	$25,00 \cdot 10^{-2}$	$41,40 \cdot 10^{-3}$	$22,80 \cdot 10^{-3}$	$25,00 \cdot 10^{-3}$
6000	—	$35,80 \cdot 10^{-2}$	—	—	$35,50 \cdot 10^{-2}$	—	—	$35,20 \cdot 10^{-3}$	—

Notes. I-Equilibrium dissociation; II-Dissociation frozen behind the incident wave and in equilibrium behind the reflected wave; III-dissociation frozen.
Commas represent decimal points.

TABLE 6. VELOCITY D_2 (m/sec) OF THE REFLECTED WAVE RELATIVE TO THE WALL AS A FUNCTION OF u_0 FOR AN INITIAL PRESSURE p_0

u_0 , m/sec	10 ⁻³ atm		10 ⁻⁴ atm		10 ⁻⁵ atm		Any	u_0 , m/sec	10 ⁻³ atm		10 ⁻⁴ atm		10 ⁻⁵ atm		Any
	I	II	I	II	I	II	III		I	II	I	II	I	II	III
1400	—	440	—	436	—	—	—	3000	367	546	543	520	518	496	773
1500	—	453	—	444	—	—	—	3500	620	596	574	553	536	514	865
1600	—	460	—	444	—	—	486	4000	637	612	585	565	538	516	946
2000	464	464	—	434	—	—	568	4500	657	632	600	573	543	524	1016
2250	466	—	—	—	—	—	—	5000	683	656	627	596	570	534	1082
2500	479	476	448	—	—	—	660	6000	—	730	—	660	—	600	—
2750	513	499	486	468	—	—	—								

TABLE 7. FLOW VARIABLES FOR THE GAS BEHIND INCIDENT AND REFLECTED WAVES IN AIR FOR AN INITIAL PRESSURE p_0 of 0.033 atm.

VERSION I

	3.0·10 ³	2.8·10 ³	2.6·10 ³	2.4·10 ³	2.2·10 ³	2.0·10 ³	1.8·10 ³	1.6·10 ³	1.4·10 ³
T_1 , °K	3320		2860	2580	2280	1970	1680	1410	1160
$H_1 \cdot 10^{11}$ ergs/gram	0.37		0.36	0.31	0.26	0.22	0.19	0.15	0.12
μ_1	28.01		28.72	28.89	28.9	28.96	28.97	28.97	28.97
u_1 , m/sec	370		364	356	345	330	314	298	282
$\rho_1 \cdot 10^{-3}$ g/cm ³	0.32		0.28	0.24	0.25	0.24	0.23	0.21	0.20
p_1 , atm	3.2		2.3	2.0	1.7	1.4	1.1	0.9	0.65
p_2 , atm	30.6	2.5	20.0	16.1	12.8	10.1	7.8	5.8	4.1
ρ_2 , g/cm·10 ²	0.17	0.02	0.14	0.13	0.12	0.10	0.09	0.18	0.07
μ_2	25.0	25.7	26.4	27.2	27.9	28.4	28.8	28.9	28.96
T_2 , °K	5360	4850	4420	4030	3670	3300	2920	2500	2100
$H_2 \cdot 10^{-11}$ ergs/gram	0.97	0.85	0.73	0.62	0.53	0.44	0.36	0.29	0.24
D_2 , m/sec	606	574	549	528	513	499	487	469	453

Note: Commas represent decimal points.

PHYSICAL VARIABLES OF CARBON DIOXIDE AND NITROGEN
BEHIND SHOCK WAVES FOR DIFFERENT DEGREES
OF PHYSICAL AND CHEMICAL
TRANSFORMATIONS

Calculations for carbon dioxide were performed on the following assumptions: all kinds of [molecular] vibrations behind the wave have reached their equilibrium state and dissociation took place (version I); all kinds of [molecular] vibrations behind the wave have reached their equilibrium state, but dissociation is not taken into account (version II); there was no dissociation in the gas behind the wave and asymmetric valent vibrations were not excited (version II').

Calculations for nitrogen were made under version II, since the degree of molecular dissociation of nitrogen for the given shock-wave velocities was low.

The enthalpies and molecular weights for version I in CO_2 were calculated on the basis of data of Appendix 3. The enthalpies for version II were taken from tables of [118], and those from version II' were taken from [107].

The calculations were made primarily for a state of the gas ahead of the shock with $p_0 = 1.68 \cdot 10^{-2}$ atm and $T_0 = 293^\circ\text{K}$ for wave velocities from 1000 to 3000 m/sec. The results of these calculations (Tables 8-12) correspond to initial states of a gas with that temperature and pressure which are obtained by passing through a gas at an initial temperature of 293°K of shock waves moving at speeds of $u_0 = 1.0, 1.3, 1.6, 1.9, 2.2, 2.5$ and 2.8 km/sec.

The tables present the ratios of pressure p_1 , temperature T_1 and density ρ_1 behind the wave to the initial pressure p_0 , temperature T_0 and density ρ_0 as a function of the wave velocity u_0 . The initial pressure and temperature are given for version I, while only the initial temperature T_0 is given for version II and II', since in this case the initial temperature of the gas behind the wave is a function of temperature only and the ratios presented in the table depend only on the velocity and the initial temperature. The computational accuracy was 1-2%.

TABLE 8. CARBON DIOXIDE. VERSION I

/170

u_0 , km/sec	$T_0 = 293^\circ \text{ K};$ $p_0 = 0,0163 \text{ atm}$			$1770^\circ \text{ K};$ $0,995 \text{ atm}$			$2120^\circ \text{ K};$ $1,34 \text{ atm}$			$2385^\circ \text{ K};$ $1,75 \text{ atm}$			$2690^\circ \text{ K};$ $2,21 \text{ atm}$		
	T_1/T_0	p_1/p_0	ρ_1/ρ_0	T_1/T_0	p_1/p_0	ρ_1/ρ_0	T_1/T_0	p_1/p_0	ρ_1/ρ_0	T_1/T_0	p_1/p_0	ρ_1/ρ_0	T_1/T_0	p_1/p_0	ρ_1/ρ_0
0,7	—	—	—	1,03	1,33	1,29	1,00	1,22	1,22	1,00	1,04	1,04	—	—	—
0,8	2,08	10,21	4,92	1,07	1,73	1,61	1,03	1,47	1,43	1,02	1,25	1,23	1,066	1,14	1,14
0,9	—	—	—	1,11	2,20	1,97	1,06	1,85	1,74	1,04	1,58	1,51	1,02	1,40	1,35
1,0	2,62	16,14	6,16	1,15	2,72	2,36	1,08	2,28	2,09	1,06	1,97	1,84	1,04	1,74	1,66
1,1	2,93	19,6	6,69	1,19	3,31	2,77	1,11	2,76	2,45	1,08	2,40	2,19	1,06	2,11	1,96
1,2	3,26	23,4	7,17	1,22	3,96	3,21	1,14	3,29	2,83	1,10	2,87	2,55	1,07	2,53	2,30
1,3	3,60	27,5	7,65	1,26	4,67	3,65	1,17	3,88	3,24	1,12	3,38	2,93	1,09	2,96	2,63
1,4	3,97	32,0	8,06	1,30	5,42	4,11	1,20	4,50	3,65	1,14	3,93	3,33	1,11	3,44	2,98
1,5	4,35	36,8	8,46	1,33	6,26	4,59	1,22	5,20	4,13	1,16	4,52	3,74	1,13	3,96	3,25
1,6	4,75	42,0	8,85	1,37	7,14	5,06	1,23	5,94	4,63	1,18	5,15	4,16	1,14	4,52	3,77
1,7	5,19	47,5	9,16	1,41	8,08	5,53	1,27	6,70	5,02	1,20	5,82	4,59	1,17	5,10	4,12
1,8	—	—	—	1,45	9,08	6,03	1,29	7,54	5,54	1,23	6,53	5,02	1,18	5,74	4,56
1,9	6,04	59,2	9,81	1,49	10,16	6,48	1,31	8,43	6,11	1,25	7,29	5,47	1,20	6,39	4,93
2,0	6,42	65,8	10,2	1,52	11,2	6,97	1,34	9,34	6,52	—	—	—	1,22	7,09	5,34
2,1	6,83	72,7	10,6	1,56	12,4	7,47	—	—	—	—	—	—	—	—	—
2,2	7,23	80,0	10,9	1,59	13,6	7,95	—	—	—	—	—	—	—	—	—
2,3	7,58	87,7	11,4	1,63	14,9	8,42	—	—	—	—	—	—	—	—	—
2,4	7,88	95,7	11,8	1,66	16,3	8,89	—	—	—	—	—	—	—	—	—
2,5	8,14	104	12,3	1,69	17,7	9,38	—	—	—	—	—	—	—	—	—
2,6	8,45	113	12,7	1,72	19,2	9,88	—	—	—	—	—	—	—	—	—
2,7	8,70	122	13,2	1,75	20,7	10,3	—	—	—	—	—	—	—	—	—
2,8	8,94	131,5	13,6	1,78	22,2	10,7	—	—	—	—	—	—	—	—	—
2,9	9,16	141	14,1	1,81	23,9	11,1	—	—	—	—	—	—	—	—	—
3,0	9,39	151	14,6	1,84	25,6	11,6	—	—	—	—	—	—	—	—	—

TABLE 9. CARBON DIOXIDE. VERSION II

u_0 , km/sec	293° K					u_0 , km/sec	293° K				
	T_1/T_0	p_1/p_0	u_0 , km/sec	T_1/T_0	p_1/p_0		T_1/T_0	p_1/p_0	u_0 , km/sec	T_1/T_0	p_1/p_0
0,5	1,40	2,78	1,5	4,35	8,46	2,1	7,0	10,35	2,7	10,45	11,5
0,8	2,08	4,92	1,6	4,75	8,85	2,2	7,5	10,6	2,8	11,25	11,60
1,0	2,62	6,16	1,7	5,19	9,16	2,3	8,05	10,81	3,0	12,59	11,90
1,1	2,93	6,69	1,8	5,55	9,55	2,4	8,65	11,0	3,3	14,88	11,21
1,2	3,26	7,17	1,9	6,0	9,83	2,5	9,25	11,16	3,6	17,23	12,56
1,3	3,60	7,65	2,0	6,5	10,11	2,6	9,85	11,33	3,8	19,00	12,72
1,4	3,97	8,06									

Note: Commas represent decimal points.

TABLE 10. CARBON DIOXIDE. VERSION II

/171

u_0 , km/sec	767° K		1055° K		1392° K		1780° K		2220° K		2730° K	
	T_1/T_0	ρ_1/ρ_0	T_1/T_0	ρ_1/ρ_0	T_1/T_0	ρ_1/ρ_0	T_1/T_0	ρ_1/ρ_0	T_1/T_0	ρ_1/ρ_0	T_1/T_0	ρ_1/ρ_0
0.7	1.22	2.45	1.145	1.82	1.02	1.77	—	—	—	—	—	—
0.8	1.31	3.02	1.2	2.30	1.07	2.14	1.07	1.59	1.04	1.30	1.01	1.11
0.9	1.40	3.58	1.26	2.83	1.12	2.57	1.11	1.91	1.08	1.57	1.04	1.34
1.0	1.50	4.15	1.33	3.40	1.17	3.03	1.16	2.27	1.12	1.91	1.08	1.61
1.1	1.61	4.69	1.4	3.95	1.23	3.46	1.21	2.66	1.15	2.26	1.11	1.90
1.2	1.73	5.22	1.48	4.50	1.29	3.92	1.26	3.10	1.20	2.61	1.15	2.19
1.3	1.85	5.73	1.57	4.95	1.36	4.38	1.31	3.50	1.24	2.95	1.19	2.49
1.4	1.98	6.24	1.66	5.48	1.43	4.82	1.37	3.89	1.29	3.31	1.22	2.82
1.5	2.11	6.73	1.76	5.91	1.51	5.25	1.43	4.28	1.33	3.68	1.26	3.16
1.6	2.27	7.14	1.87	6.30	1.59	5.67	1.49	4.68	1.38	4.05	1.30	3.49
1.7	2.44	7.50	1.98	6.70	1.68	6.05	1.56	5.08	1.43	4.41	1.35	3.81
1.8	2.61	7.85	2.11	7.15	1.77	6.46	1.63	5.45	1.49	4.76	1.39	4.14
1.9	2.79	8.20	2.24	7.42	1.86	6.84	1.70	5.81	1.55	5.09	1.44	4.47
2.0	2.96	8.58	2.37	7.80	1.96	7.19	1.78	6.16	1.62	5.43	1.49	4.79

TABLE 11. CARBON DIOXIDE. VERSION II

u_0 , km/sec	293° K		1900° K		2390° K		2965° K		3610° K	
	T_1/T_0	ρ_1/ρ_0	T_1/T_0	ρ_1/ρ_0	T_1/T_0	ρ_1/ρ_0	T_1/T_0	ρ_1/ρ_0	T_1/T_0	ρ_1/ρ_0
1.0	—	—	1.16	2.14	1.11	1.75	1.07	1.44	1.04	1.23
1.1	—	—	1.21	2.49	1.16	2.04	1.11	1.70	1.07	1.45
1.2	—	—	1.26	2.86	1.20	2.35	1.15	1.98	1.11	1.67
1.3	—	—	1.32	3.21	1.25	2.69	1.19	2.27	1.14	1.91
1.4	—	—	1.38	3.57	1.30	3.00	1.23	2.54	1.18	2.16
1.5	—	—	1.45	3.92	1.35	3.33	1.27	2.83	1.21	2.42
1.6	—	—	1.52	4.26	1.40	3.65	1.32	3.12	—	—
1.7	—	—	1.59	4.60	1.46	3.95	1.37	3.40	—	—
1.8	—	—	1.66	4.93	1.53	4.25	1.42	3.69	—	—
1.9	6.49	9.05	1.74	5.25	1.59	4.55	1.47	3.98	—	—
2.0	7.00	9.31	1.83	5.55	1.66	4.83	—	—	—	—
2.1	7.54	9.47	—	—	—	—	—	—	—	—
2.2	8.16	9.69	—	—	—	—	—	—	—	—
2.3	8.81	9.81	—	—	—	—	—	—	—	—
2.4	9.45	9.95	—	—	—	—	—	—	—	—
2.5	10.1	10.1	—	—	—	—	—	—	—	—
2.6	10.8	10.2	—	—	—	—	—	—	—	—
2.7	11.5	10.3	—	—	—	—	—	—	—	—
2.8	12.3	10.4	—	—	—	—	—	—	—	—
2.9	13.1	10.5	—	—	—	—	—	—	—	—

Note: Commas represent decimal points.

TABLE 12 NITROGEN. VERSION II

u , km/sec	293° K		740° K		1030° K		1400° K		1800° K		2270° K		2810° K	
	T_1/T_0	ρ_1/ρ_0	T_1/T_0	ρ_1/ρ_0	T_1/T_0	ρ_1/ρ_0	T_1/T_0	ρ_1/ρ_0	T_1/T_0	ρ_1/ρ_0	T_1/T_0	ρ_1/ρ_0	T_1/T_0	ρ_1/ρ_0
0,7	—	—	1,16	1,50	—	—	—	—	—	—	—	—	—	—
0,8	—	—	1,27	1,84	1,13	1,54	1,04	1,28	1,01	1,11	—	—	—	—
0,9	—	—	1,38	2,17	1,23	1,68	1,11	1,45	1,04	1,24	—	—	—	—
1,0	—	—	1,49	2,49	1,33	1,97	1,16	1,73	1,10	1,35	—	—	—	—
1,1	2,52	3,75	1,62	2,81	1,40	2,33	1,24	1,97	1,16	1,59	1,04	1,21	—	—
1,2	2,83	4,09	1,74	3,16	1,48	2,66	1,32	2,19	1,21	1,85	1,085	1,35	1,035	1,19
1,3	3,15	4,37	1,87	3,46	1,58	2,95	1,40	2,41	1,26	2,11	1,14	1,54	1,075	1,32
1,4	3,5	4,64	2,02	3,73	1,67	3,25	1,49	2,65	1,33	2,34	1,19	1,74	1,12	1,51
1,5	3,9	4,87	2,18	3,99	1,77	3,50	1,56	2,91	1,40	2,54	1,24	1,94	1,16	1,69
1,6	4,3	5,09	2,34	4,23	1,90	3,75	1,65	3,17	1,48	2,74	1,35	2,15	1,21	1,84
1,7	4,7	5,25	2,52	4,45	2,03	3,98	1,73	3,43	1,56	2,93	1,41	2,35	1,26	2,02
1,8	5,15	5,45	2,71	4,64	2,17	4,16	1,82	3,66	1,63	3,15	1,46	2,57	1,30	2,25
1,9	5,6	5,62	2,91	4,81	2,33	4,31	1,91	3,89	1,70	3,39	1,52	2,80	1,36	2,42
2,0	6,1	5,80	3,11	5,01	2,48	4,52	2,03	4,07	1,77	3,63	1,59	3,01	1,42	2,58
2,1	6,6	5,92	3,31	5,20	2,62	4,72	2,16	4,22	1,87	3,77	1,67	3,20	1,47	2,76
2,2	7,15	6,05	3,53	5,37	2,78	4,90	2,28	4,39	1,97	3,95	1,74	3,33	1,52	2,95
2,3	7,72	6,17	3,76	5,52	2,94	5,06	2,39	4,58	2,06	4,12	1,82	3,52	1,58	3,12
2,4	8,3	6,28	4,01	5,63	3,12	5,21	2,52	4,74	2,16	4,30	1,89	3,71	1,64	3,36
2,5	8,95	6,39	4,27	5,74	3,29	5,37	2,65	4,89	2,26	4,47	1,975	3,88	1,70	3,47
2,6	9,55	6,48	4,52	5,88	3,47	5,50	2,78	5,05	2,36	4,62	2,06	4,04	1,77	3,63
2,7	10,22	6,56	4,76	6,02	3,66	5,63	2,92	5,19	2,47	4,77	2,15	4,19	1,84	3,79
2,8	10,85	6,64	5,04	6,12	3,86	5,74	3,07	5,32	2,59	4,90	2,24	4,34	1,91	3,95
2,9	11,55	6,72	5,34	6,20	4,06	5,86	3,22	5,44	2,70	5,04	2,33	4,40	1,98	4,09
3,0	12,25	6,79	5,63	6,29	4,27	5,97	3,37	5,56	2,82	5,17	2,42	4,64	2,08	4,23
	13,0	6,86										4,78	2,13	4,37

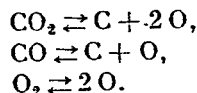
Note: Commas represent decimal points.

APPENDIX 3

EQUILIBRIUM THERMODYNAMIC FUNCTIONS OF CARBON DIOXIDE IN THE TEMPERATURE RANGE OF 1100-4500°K AT PRESSURES OF 0.1-13 ATM

/173

The thermodynamic variables and the carbon-dioxide composition were calculated by a method suggested in [281, 282]. It is assumed that the following reactions take place in carbon dioxide heated to 1000-4000°K



The thermodynamic equations for the system of gases are written as

$$\begin{aligned}\frac{X_{\text{C}}X_{\text{O}}^2}{X_{\text{CO}_2}} &= \frac{K_{p\text{CO}_2}}{P^2}, & X_{\text{CO}_2} + X_{\text{CO}} + X_{\text{O}_2} + X_{\text{C}} + X_{\text{O}} &= 1, \\ \frac{X_{\text{O}}^2}{X_{\text{O}_2}} &= \frac{K_{p\text{O}_2}}{P}, & \frac{X_{\text{CO}_2} + X_{\text{CO}} + X_{\text{C}}}{2X_{\text{CO}_2} + X_{\text{CO}} + 2X_{\text{O}_2} + X_{\text{O}}} &= \frac{1}{2}, \\ \frac{X_{\text{O}}X_{\text{C}}}{X_{\text{CO}}} &= \frac{K_{p\text{CO}}}{P},\end{aligned}$$

where X are the mole fractions of the components, and K_{eq} are the equilibrium constants of the respective reactions.

This system makes it possible to determine the gas composition as a function of temperature and pressure if K_{eq} are known. Knowing the composition of the gas it is possible to find its specific enthalpy and the molecular weight μ .

$$\begin{aligned}h &= \frac{1}{\mu} \sum_n H_n X_n, \\ \mu &= \sum_n \mu_n X_n,\end{aligned}$$

where H_n is the molar enthalpy of the components and μ_n is the molecular weight of the components.

Calculations were performed at temperatures of 1100-4500°K in steps of 200° for pressures of 0.1, 0.5, 1, 2, 3, 5, 7, 9, 11 and 13 atm. Tables 13-19 present the values of h , μ , X_{CO_2} , X_{CO} , X_{O_2} , X_{O} and X_{C} .

The molar fractions of the gas components are presented in the normalized form.

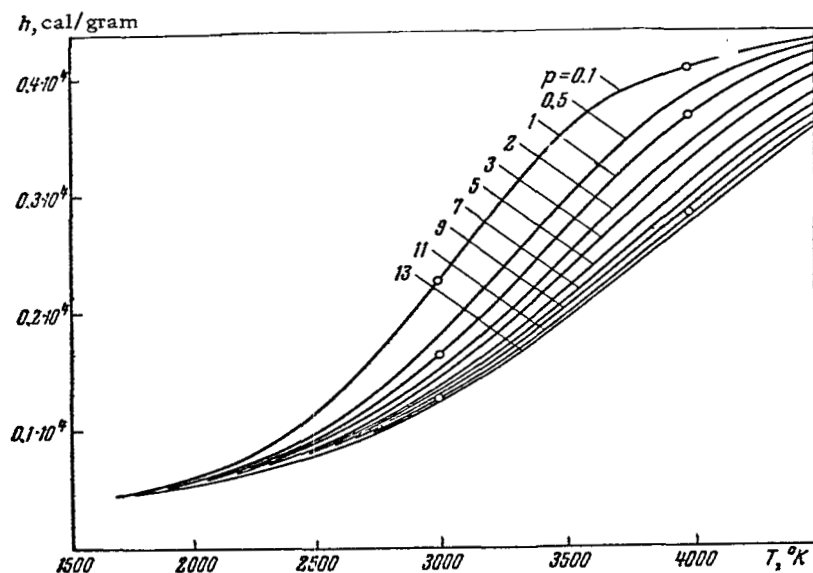


Figure 83.

The curve of $h(T)$ is shown in Fig. 83. The enthalpy of CO_2 under initial conditions ($T_0 = 293.16^\circ\text{K}$) was ± 3.485 cal/gram. The composition and thermodynamic properties of CO_2 were calculated on the basis of thermodynamic functions of its components taken from [118].

The levels at which the components enthalpies were measured, as well as the degrees of dissociation of the principal reactions are shown below

Component	CO_2	CO	O_2	C_2	O	C
Reaction	$-\text{CO}_2 + \text{CO} + \frac{1}{2}\text{O}_2 \rightleftharpoons \text{O}$	$-\text{CO} + \text{C} + \frac{1}{2}\text{O}_2 \rightleftharpoons \text{O}$	$-\text{O}_2 + \frac{1}{2}\text{O}_2 \rightleftharpoons \text{O}$	$-\text{C}_2 + 2\text{C} \rightleftharpoons \text{O}$	58986	263571
Energy dissociation at 0°K , cal/mole	66 767	255 790	117 973	143 170		
H_T , cal/mole	0	66 767	0	—		

Comparison of our data with those of [283], where a larger number of possible reactions was taken into account, with enthalpies for temperatures in steps of 1000°K shows that other gases except for CO_2 , CO , O_2 and O are present in minute quantities and can be disregarded.

The data of [283] are denoted in Fig. 83 by open circles. The disagreement does not exceed 1%.

TABLE 13. ENTHALPY OF CARBON DIOXIDE h, cal/gram

T, °K	P, atm											
	0,1	0,5	1	2	3	5	7	9	11	13		
1700	0,457 3	0,454 3	0,453 3	0,452 3	0,452 3	0,452 3	0,452 3	0,451 3	0,451 3	0,451 3		
1800	0,496 3	0,491 3	0,489 3	0,487 3	0,487 3	0,486 3	0,486 3	0,485 3	0,485 3	0,485 3		
1900	0,542 3	0,531 3	0,527 3	0,525 3	0,524 3	0,522 3	0,521 3	0,521 3	0,520 3	0,520 3		
2100	0,663 3	0,629 3	0,619 3	0,611 3	0,607 3	0,603 3	0,600 3	0,599 3	0,598 3	0,597 3		
2300	0,848 3	0,766 3	0,742 3	0,722 3	0,713 3	0,702 3	0,697 3	0,693 3	0,690 3	0,687 3		
2500	0,113 4	0,963 3	0,914 3	0,873 3	0,854 3	0,932 3	0,820 3	0,811 3	0,805 3	0,800 3		
2700	0,151 4	0,124 4	0,115 4	0,108 4	0,104 4	0,100 4	0,980 3	0,965 3	0,953 3	0,944 3		
2900	0,199 4	0,159 4	0,145 4	0,134 4	0,129 4	0,122 4	0,119 4	0,116 4	0,114 4	0,113 4		
3100	0,251 4	0,200 4	0,182 4	0,166 4	0,158 4	0,149 4	0,144 4	0,140 4	0,137 4	0,135 4		
3300	0,302 4	0,244 4	0,222 4	0,203 4	0,192 4	0,180 4	0,173 4	0,168 4	0,164 4	0,161 4		
3500	0,345 4	0,289 4	0,264 4	0,241 4	0,229 4	0,214 4	0,205 4	0,199 4	0,194 4	0,190 4		
3700	0,375 4	0,330 4	0,306 4	0,281 4	0,266 4	0,250 4	0,239 4	0,232 4	0,226 4	0,222 4		
3900	0,393 4	0,364 4	0,343 4	0,318 4	0,304 4	0,285 5	0,274 4	0,265 4	0,259 4	0,254 4		
4100	0,405 4	0,388 4	0,373 4	0,352 4	0,338 4	0,320 4	0,308 4	0,299 4	0,292 4	0,286 4		
4300	0,414 4	0,405 4	0,395 4	0,379 4	0,368 4	0,351 4	0,340 4	0,331 4	0,324 4	0,318 4		
4500	0,422 4	0,417 4	0,411 4	0,400 4	0,392 4	0,378 4	0,368 4	0,360 4	0,353 4	0,347 4		

Note: Commas represent decimal points.

TABLE 14. MOLECULAR WEIGHT μ

T, °K	p, atm									
	0,1	0,5	1	2	3	5	7	9	11	13
1700	0,439 2	0,440 2	0,440 2	0,440 2	0,440 2	0,440 2	0,440 2	0,440 3	0,440 2	0,440 2
1800	0,438 2	0,439 2	0,439 2	0,439 2	0,439 2	0,440 2	0,440 2	0,440 2	0,440 2	0,440 2
1900	0,436 2	0,438 2	0,438 2	0,439 2	0,439 2	0,439 2	0,439 2	0,439 2	0,439 2	0,439 2
2100	0,428 2	0,433 2	0,435 2	0,436 2	0,436 2	0,437 2	0,437 2	0,437 2	0,438 2	0,438 2
2300	0,412 2	0,423 2	0,427 2	0,429 2	0,431 2	0,432 2	0,433 2	0,433 2	0,434 2	0,434 2
2500	0,386 2	0,406 2	0,412 2	0,418 2	0,420 2	0,423 2	0,425 2	0,426 2	0,427 2	0,428 2
2700	0,353 2	0,381 2	0,391 2	0,400 2	0,404 2	0,409 2	0,412 2	0,414 2	0,416 2	0,417 2
2900	0,317 2	0,352 2	0,365 2	0,377 2	0,383 2	0,391 2	0,395 2	0,398 2	0,400 2	0,402 2
3100	0,285 2	0,321 2	0,336 2	0,351 2	0,359 2	0,368 2	0,374 2	0,378 2	0,381 2	0,384 2
3300	0,258 2	0,293 2	0,309 2	0,324 2	0,333 2	0,344 2	0,351 2	0,355 2	0,359 2	0,362 2
3500	0,240 2	0,269 2	0,284 2	0,300 2	0,309 2	0,320 2	0,327 2	0,333 2	0,337 2	0,341 2
3700	0,230 2	0,250 2	0,263 2	0,278 2	0,287 2	0,298 2	0,306 2	0,311 2	0,316 2	0,319 2
3900	0,225 2	0,237 2	0,248 2	0,260 2	0,268 2	0,279 2	0,286 2	0,292 2	0,296 2	0,300 2
4100	0,222 2	0,229 2	0,236 2	0,246 2	0,253 2	0,262 2	0,269 2	0,275 2	0,279 2	0,282 2
4300	0,221 2	0,225 2	0,229 2	0,236 2	0,241 2	0,249 2	0,255 2	0,260 2	0,264 2	0,267 2
4500	0,221 2	0,223 2	0,225 2	0,230 2	0,233 2	0,239 2	0,244 2	0,248 2	0,252 2	0,255 2

Note: Commas represent decimal points.

TABLE 16. XO_2

T, °K	p, atm									
	0,1	0,5	1	2	3	5	7	9	11	13
1700	0,225 -2	0,132 -2	0,105 -2	0,833 -3	0,728 -3	0,614 -3	0,549 -3	0,505 -3	0,472 -3	0,447 3
1800	0,465 -2	0,273 -2	0,217 -2	0,173 -2	0,151 -2	0,127 -2	0,114 -2	0,105 -2	0,980 -3	0,927 -3
1900	0,886 -2	0,523 -2	0,416 -2	0,331 -2	0,289 -2	0,244 -2	0,218 -2	0,201 -2	0,188 -2	0,178 -2
2100	0,259 -1	0,156 -1	0,125 -1	0,995 -2	0,872 -2	0,738 -2	0,661 -2	0,608 -2	0,570 -2	0,539 -2
2300	0,592 -1	0,370 -1	0,299 -1	0,241 -1	0,212 -1	0,180 -1	0,162 -1	0,149 -1	0,140 -1	0,133 -1
2500	0,107 0	0,719 -1	0,594 -1	0,487 -1	0,432 -1	0,371 -1	0,335 -1	0,310 -1	0,291 -1	0,276 -1
2700	0,154 0	0,116 0	0,994 -1	0,838 -1	0,754 -1	0,656 -1	0,597 -1	0,556 -1	0,525 -1	0,500 -1
2900	0,175 0	0,157 0	0,141 0	0,124 0	0,114 0	0,101 0	0,935 -1	0,878 -1	0,835 -1	0,799 -1
3100	0,157 0	0,177 0	0,171 0	0,159 0	0,150 0	0,138 0	0,130 0	0,123 0	0,118 0	0,114 0
3300	0,111 0	0,168 0	0,178 0	0,178 0	0,174 0	0,167 0	0,160 0	0,155 0	0,150 0	0,146 0
3500	0,638 -1	0,135 0	0,159 0	0,175 0	0,179 0	0,180 0	0,178 0	0,175 0	0,173 0	0,170 0
3700	0,320 -1	0,925 -1	0,124 0	0,152 0	0,164 0	0,175 0	0,179 0	0,181 0	0,181 0	0,181 0
3900	0,153 -1	0,559 -1	0,851 -1	0,117 0	0,135 0	0,154 0	0,164 0	0,170 0	0,174 0	0,177 0
4100	0,746 -2	0,314 -1	0,530 -1	0,815 -1	0,101 0	0,123 0	0,138 0	0,148 0	0,155 0	0,160 0
4300	0,379 -2	0,173 -1	0,312 -1	0,526 -1	0,686 -1	0,913 -1	0,107 0	0,118 0	0,127 0	0,135 0
4500	0,202 -2	0,961 -2	0,181 -1	0,326 -1	0,445 -1	0,633 -1	0,776 -1	0,889 -1	0,982 -1	0,106 0

Note: Commas represent decimal points.

TABLE 17. $X_{\text{CO } 2}$ [sic]

$T, ^\circ\text{K}$	p, atm										
	0,1	0,5	1	2	3	5	7	9	11	13	
1700	0,451 -2	0,264 -2	0,210 -2	0,167 -2	0,146 -2	0,123 -2	0,110 -2	0,101 -2	0,945 -3	0,894 -3	
1800	0,934 -2	0,548 -2	0,435 -2	0,346 -2	0,302 -2	0,255 -2	0,228 -2	0,210 -2	0,196 -2	0,185 -2	
1900	0,178 -1	0,105 -1	0,834 -2	0,663 -2	0,579 -2	0,489 -2	0,437 -2	0,402 -2	0,376 -2	0,356 -2	
2100	0,526 -1	0,314 -1	0,251 -1	0,200 -1	0,175 -1	0,148 -1	0,133 -1	0,122 -1	0,114 -1	0,108 -1	
2300	0,122	0,753 -1	0,607 -1	0,487 -1	0,428 -1	0,364 -1	0,326 -1	0,301 -1	0,282 -1	0,267 -1	
2500	0,229	0,149	0,122	0,997 -1	0,882 -1	0,754 -1	0,679 -1	0,628 -1	0,590 -1	0,559 -1	
2700	0,353	0,250	0,210	0,175	0,156	0,135	0,123	0,114	0,108	0,102	
2900	0,455	0,357	0,312	0,268	0,243	0,214	0,196	0,183	0,174	0,166	
3100	0,510	0,447	0,406	0,362	0,335	0,302	0,280	0,265	0,253	0,243	
3300	0,524	0,502	0,476	0,441	0,417	0,386	0,364	0,347	0,334	0,323	
3500	0,519	0,524	0,514	0,494	0,478	0,453	0,434	0,419	0,407	0,396	
3700	0,510	0,524	0,526	0,520	0,512	0,497	0,484	0,473	0,464	0,455	
3900	0,505	0,517	0,524	0,527	0,526	0,520	0,514	0,507	0,501	0,495	
4100	0,503	0,510	0,517	0,523	0,526	0,527	0,526	0,524	0,521	0,518	
4300	0,501	0,506	0,510	0,517	0,521	0,525	0,527	0,528	0,528	0,527	
4500	0,501	0,503	0,506	0,514	0,515	0,520	0,523	0,525	0,527	0,527	

Note: Commas represent decimal points.

TABLE 18. X_O

T, °K	p, atm										
	0,1	0,5	1	2	3	5	7	9	11	13	
1700	0,666 -5	0,228 -5	0,144 -5	0,906 -6	0,691 -6	0,492 -6	0,393 -6	0,332 -6	0,291 -6	0,260 -6	
1800	0,261 -4	0,894 -5	0,563 -5	0,355 -5	0,271 -5	0,193 -5	0,154 -5	0,130 -5	0,114 -5	0,102 -5	
1900	0,882 -4	0,303 -4	0,191 -4	0,120 -4	0,920 -5	0,655 -5	0,523 -5	0,443 -5	0,387 -5	0,346 -5	
2100	0,703 -3	0,244 -3	0,154 -3	0,974 -4	0,744 -4	0,530 -4	0,424 -4	0,359 -4	0,314 -4	0,281 -4	
2300	0,379 -2	0,134 -2	0,853 -3	0,541 -3	0,415 -3	0,296 -3	0,237 -3	0,201 -3	0,176 -3	0,158 -3	
2500	0,149 -1	0,546 -2	0,351 -2	0,225 -2	0,173 -2	0,124 -2	0,995 -3	0,844 -3	0,740 -3	0,663 -3	
2700	0,445 -1	0,173 -1	0,113 -1	0,734 -2	0,568 -2	0,411 -2	0,331 -2	0,282 -2	0,248 -2	0,222 -2	
2900	0,104 0	0,440 -1	0,300 -1	0,200 -1	0,154 -1	0,112 -1	0,911 -2	0,779 -2	0,687 -2	0,618 -2	
3100	0,196 0	0,932 -1	0,648 -1	0,442 -1	0,351 -1	0,261 -1	0,213 -1	0,183 -1	0,162 -1	0,147 -1	
3300	0,302 0	0,166 0	0,121 0	0,855 -1	0,691 -1	0,523 -1	0,434 -1	0,376 -1	0,335 -1	0,304 -1	
3500	0,391 0	0,254 0	0,195 0	0,145 -0	0,120 0	0,929 -1	0,781 -1	0,684 -1	0,614 -1	0,560 -1	
3700	0,446 0	0,339 0	0,278 0	0,217 0	0,184 0	0,148 0	0,126 0	0,112 0	0,101 0	0,931 -1	
3900	0,475 0	0,405 0	0,354 0	0,293 0	0,257 0	0,213 0	0,186 0	0,167 0	0,153 0	0,141 0	
4100	0,488 0	0,448 0	0,411 0	0,360 0	0,326 0	0,281 0	0,250 0	0,229 0	0,212 0	0,198 0	
4300	0,494 0	0,471 0	0,448 0	0,411 0	0,384 0	0,343 0	0,313 0	0,291 0	0,273 0	0,258 0	
4500	0,497 0	0,484 0	0,470 0	0,446 0	0,425 0	0,393 0	0,368 0	0,347 0	0,330 0	0,315 0	

Note: Commas represent decimal points.

TABLE 19. X_C

T, °K	p, atm									
	0,1	0,5	1	2	3	5	7	9	11	13
1700	0,488-22	0,167-22	0,105-22	0,063-23	0,506-23	0,300-23	0,288-23	0,243-23	0,213-23	0,190-23
1800	0,186-20	0,035-21	0,400-21	0,252-21	0,193-21	0,137-21	0,109-21	0,926-22	0,810-22	0,725-22
1900	0,481-19	0,165-19	0,104-19	0,055-20	0,500-20	0,356-20	0,284-20	0,241-20	0,210-20	0,188-20
2100	0,127-16	0,436-17	0,275-17	0,174-17	0,133-17	0,945-18	0,756-18	0,639-18	0,559-18	0,501-18
2300	0,124-14	0,434-15	0,275-15	0,174-15	0,133-15	0,948-16	0,759-16	0,642-16	0,562-16	0,503-16
2500	0,571-13	0,203-13	0,129-13	0,823-14	0,631-14	0,452-14	0,362-14	0,307-14	0,263-14	0,241-14
2700	0,144-11	0,526-12	0,338-12	0,217-12	0,167-12	0,120-12	0,964-13	0,818-13	0,718-13	0,644-13
2900	0,228-10	0,848-11	0,551-11	0,357-11	0,275-11	0,200-11	0,161-11	0,137-11	0,120-11	0,108-11
3100	0,254-9	0,939-10	0,614-10	0,401-10	0,312-10	0,227-10	0,184-10	0,157-10	0,138-10	0,124-10
3300	0,223-8	0,778-9	0,507-9	0,332-9	0,259-9	0,190-9	0,154-9	0,132-9	0,117-9	0,105-9
3500	0,168-7	0,521-8	0,332-8	0,216-8	0,168-8	0,123-8	0,100-8	0,861-9	0,761-9	0,688-9
3700	0,111-6	0,300-7	0,184-7	0,116-7	0,898-8	0,654-8	0,532-8	0,456-8	0,404-8	0,365-8
3900	0,045-6	0,155-6	0,898-7	0,545-7	0,414-7	0,297-7	0,240-7	0,205-7	0,181-7	0,163-7
4100	0,327-5	0,724-6	0,399-6	0,230-6	0,171-6	0,119-6	0,952-7	0,808-7	0,710-7	0,638-7
4300	0,145-4	0,306-5	0,162-5	0,895-6	0,645-6	0,437-6	0,342-6	0,287-6	0,259-6	0,224-6
4500	0,566-4	0,117-4	0,004-5	0,322-5	0,226-5	0,148-5	0,114-5	0,943-6	0,814-6	0,722-6

Note: Commas represent decimal points.

CALCULATING THE STATE OF THE GAS BEHIND AN
ATTACHED WAVE AND THE ANGLE OF INCLINATION
OF A SHOCK ATTACHED TO A WEDGE

The angle of inclination φ_5 of a wave attached to a wedge, of pressure p_5 and temperature T_5 behind the wave (the notation here is that of Fig. 43) were calculated as a function of the wedge angle $\theta_5 = 0 - 45^\circ$. The data thus obtained are presented in Tables 20-23. They correspond to the following velocities of a wave incident upon the wedge: $u_0 = 1.0, 1.3, 1.6, 1.9, 2.2, 2.5$ and 2.8 km/sec; p_0 and T_0 are the temperature and pressure behind the incident shock wave.

The last line of each column contains "limiting" values of variables of states corresponding to such flow conditions when the attached shock becomes detached.

TABLE 20. CARBON DIOXIDE. VERSION I

θ_5	$T_1=1770^\circ \text{ K};$ $p_1=0,995 \text{ atm}$			2000° K; 1,22 atm			2385° K; 1,75 atm			2620° K; 2,21 atm		
	φ_5	$p_5,$ atm	$T_5,$ ° K	φ_5	$p_5,$ atm	$T_5,$ ° K	φ_5	$p_5,$ atm	$T_5,$ ° K	φ_5	$p_5,$ atm	$T_5,$ ° K
0°00'	20°54'	0,995	1770	20°06'	1,22	2000	17°54'	1,76	2385	16°54'	2,22	2320
5 00	24 36	1,31	1830	23 06	1,63	2120	21 24	2,50	2450	20 06	3,12	2680
10 00	28 12	1,72	1890	26 48	2,18	2150	25 00	3,34	2520	23 48	4,22	2750
15 00	32 24	2,26	1970	31 00	2,86	2200	28 48	4,32	2590	27 36	5,72	2830
20 00	37 06	2,86	2050	35 18	3,60	2270	33 24	5,60	2660	32 12	7,40	2910
25 00	42 12	3,60	2120	40 18	4,53	2340	38 00	7,04	2720	37 00	9,40	2990
30 00	47 33	4,38	2210	45 36	5,60	2420	43 00	8,60	2800	41 48	11,65	3070
35 00	54 12	5,26	2285	51 36	6,72	2490	48 48	10,5	2880	47 24	14,2	3150
40 00	58 24	6,40	2370	56 36	7,94	2570	52 24	12,45	2970			
41 30	41 48	7,10	2430									
44 00				70	9,7	2680						

Note: Commas represent decimal points.

TABLE 21. CARBON DIOXIDE. VERSION II

/183

θ_s	$T_1=1390^\circ \text{ K};$ $p_1=0,71 \text{ atm}$			1780° K; 0,98 atm			2220° K; 1,33 atm			2730° K; 1,72 atm		
	φ_s	$p_s,$ atm	$T_s,$ ° K	φ_s	$p_s,$ atm	$T_s,$ ° K	φ_s	$p_s,$ atm	$T_s,$ ° K	φ_s	$p_s,$ atm	$T_s,$ ° K
0°00'	21°24'	0,71	1390		0,98	1780	20°30'	1,33	2220	19°48'	1,72	2730
5 00	25 00	0,98	1420	25°00'	1,30	1850	24 06	1,82	2330	23 06	2,37	2850
10 00	28 36	1,24	1450	29 00	1,72	1930	27 43	2,44	2430	27 00	3,20	2980
15 00	33 00	1,54	1480	33 00	2,24	2025	31 48	3,14	2535	31 12	4,20	3125
20 00	37 48	1,90	1540	37 42	2,86	2120	36 24	4,00	2645	35 48	5,40	3275
25 00	43 12	2,36	1610	42 48	3,55	2210	41 36	5,05	2770	41 00	6,80	3430
30 00	49 06	2,86	1690	48 30	4,36	2320	47 00	6,20	2910	46 18	8,33	3620
35 00	55 30	3,50	1790	55 48	5,35	2470	53 33	7,44	3080	52 48	10,1	3830
40 00							63 12	9,20	3295	61 00	12,3	4080
38 36												
39 24				69 00	6,85	2660						
40 54							67 00	9,9	3380			

TABLE 22. CARBON DIOXIDE. VERSION II

θ_s	$T_1=1900^\circ \text{ K};$ $p_1=0,986 \text{ atm}$			2390° K; 133 atm			2965° K; 1,72 atm		
	φ_s	$p_s,$ atm	$T_s,$ ° K	φ_s	$p_s,$ atm	$T_s,$ ° K	φ_s	$p_s,$ atm	$T_s,$ ° K
0°00'	22°48'	0,99	1900	22°00'	1,34	2390	21°12'	1,74	2970
5 00	26 24	1,34	1990	25 12	1,80	2490	24 36	2,34	3110
10 00	30 12	1,72	2080	29 00	2,36	2610	28 24	3,10	3260
15 00	34 12	2,20	2170	33 15	3,00	2740	32 30	4,02	3420
20 00	38 48	2,76	2260	38 00	3,82	2890	37 00	5,10	3600
25 00	44 12	3,47	2380	43 12	4,84	3040	42 30	6,4	3800
30 00	50 36	4,30	2500	49 24	6,00	3215	48 24	7,88	4040
35 00	58 48	5,26	2680	57 00	7,28	3445	55 42	9,60	4300
37 18	68 00	6,10	2840						
38 06				67 12	8,80	3680			

Note: Commas represent decimal points.

TABLE 23. NITROGEN. VERSION II

/184

θ_s	$T_1=1030^\circ\text{K}; p_1=275\text{ atm}$			$1400^\circ\text{K}; 0,416\text{ atm}$		
	φ_s	$p_s, \text{ atm}$	$T_s, ^\circ\text{K}$	φ_s	$p_s, \text{ atm}$	$T_s, ^\circ\text{K}$
10°00'	49°36'	0,40	1100	43°24'	0,64	1520
15 00	61 36	0,57	1240	51 24	0,84	1640
20 00						
25 00						
19 00				65 00	1,20	1820
22 12						
24 36						
25 36						

TABLE 23 (cont'd)

θ_s	$1800^\circ\text{K}; 0,59\text{ atm}$			$2270^\circ\text{K}; 0,80\text{ atm}$			$2810^\circ\text{K}; 1,025\text{ atm}$		
	φ_s	$p_s, \text{ atm}$	$T_s, ^\circ\text{K}$	φ_s	$p_s, \text{ atm}$	$T_s, ^\circ\text{K}$	φ_s	$p_s, \text{ atm}$	$T_s, ^\circ\text{K}$
10°00'	41°06'	0,96	2010	38°48'	1,29	2550	37°48'	1,76	3140
15 00	47 36	1,23	2140	44 24	1,62	2720	43 36	2,22	3350
20 00	56 30	1,56	2300	51 48	2,1	2900	50 18	2,78	3580
25 00							60 48	3,60	3930
19 00									
22 12	65 30	1,85	2420	65 48	2,93	3180			
24 36							66 00	3,85	4010
25 33									

Note: Commas represent decimal points.

TABLE 26. CARBON DIOXIDE. VERSION II'

ω_1 , deg	ω_2	ω_4	T_2 , °K	u_M , km/sec	θ_3	$p_2=p_3$, atm	T_3 , °K
$u_0=1,9$ km/sec, $T_1=1900^\circ\text{K}$, $p_1=0,986$ atm							
40	-8°34'	92°23'	2220	2,95	21°42'	2,40	3970
45	-10 59	93 17	2125	2,68	28 30	1,97	3340
50	-12 18	94 18	2055	2,47	32 57	1,67	2900
55	-12 15	95 35	2010	2,31	38 23	1,43	2590
60	-10 00	97 09	1975	2,18	43 27	1,33	2360
65	-4 30	99 13	1950	2,07	47 52	1,17	2170
$u_0=2,2$ km/sec, $T_1=2390^\circ\text{K}$, $p_1=1,33$ atm							
50	-13 03	94 12	2590	2,83	33 40	2,25	3760
55	-12 42	95 21	2530	2,67	38 50	1,97	3320
60	-10 42	96 47	2490	2,52	43 40	1,75	3110
65	-5 06	98 55	2450	2,40	48 35	1,57	2770
$u_0=2,5$ km/sec, $T_1=2965^\circ\text{K}$, $p_1=1,72$ atm							
60	-11 10	96 42	3090	2,87	44 23	2,26	3760
65	-6 05	98 43	3030	2,73	49 16	2,05	3440

TABLE 27. NITROGEN. VERSION II

ω_1 , deg	ω_2	ω_4	T_2 , °K	T_3 , °K	$p_2=p_3$, atm	u_M , km/sec
$u_0=1,3$ km/sec, $T_1=1030^\circ\text{K}$, $p_1=0,275$ atm						
30	9°53'	90°34'	1560	3000	1,13	2,60
35	8 28	91 37	1415	2380	0,85	2,26
45	8 14	94 13	1230	1707	0,55	1,83
50	10 12	95 30	1190	1500	0,465	1,69
55	14 12	97 45	1142	1344	0,405	0,57
60	24 12	100 54	1110	1230	0,36	1,48
65	44 56	108 55	1050	1100	0,30	1,36
$u_0=1,6$ km/sec, $T_1=1400^\circ\text{K}$, $p_1=0,416$ atm						
30	7 04	90 55	2110	4240	1,70	3,20
35	5 06	91 53	1910	3360	1,30	2,79
40	4 02	93 02	1745	2790	1,03	2,48
45	3 44	94 23	1630	2360	0,84	2,26
50	4 36	95 51	1560	2080	0,71	2,08
55	7 08	97 56	1495	1850	0,61	1,93
60	13 40	100 26	1460	1680	0,54	1,82

Note: Commas represent decimal points.

TABLE 27 (cont'd)

$u_0=1,9 \text{ km/sec}, T_1=1800^\circ\text{K}, p_1=0,59 \text{ atm}$						
35	2 23	92 02	2390	4500	1,82	3,31
40	1 34	93 03	2240	3680	1,445	2,95
45	1 24	94 15	2135	3140	1,20	2,68
50	2 07	95 53	2035	2740	1,01	2,47
55	4 20	95 43	1965	2440	0,87	2,30
60	7 12	100 10	1900	2220	0,77	2,16
65	17 18	103 33	1835	2020	0,685	2,04
$u_0=2,2 \text{ km/sec}, T_1=2270^\circ\text{K}, p_1=0,80 \text{ atm}$						
40	-0,12	93,07	2830	4720	1,94	3,42
45	-0 36	94 15	2680	4080	1,60	3,10
50	0 00	95 39	2580	3500	2,14	2,86
55	2 12	97 17	2440	3120	1,18	2,66
60	6 46	99 39	2380	2800	1,04	2,50
$u_0=2,5 \cdot 10^5 \text{ m/sec}, T_1=2310^\circ\text{K}, p_1=1,025 \text{ atm}$						
50	-1 34	95 45	3160	4340	1,75	3,25
55	0 42	97 22	3050	3850	1,58	3,03
60	5 29	99 27	2965	3480	1,35	2,85

Note: Commas represent decimal points.

1. Predvoditelev, Ye. V. , Ye. V. Samuylov, I. P. Stakhanov, A. S. Pleshanov and I. B. Rozhdestvenskiy. *Tablitsy termodinamicheskikh funktsiy vozdukha dlya temperatur ot 6000 do 12,000°K i davleniy ot 0.001 do 1000 atmosfer* [Tables of Thermodynamic Functions of Air, for Temperatures from 6000 to 12,000°K and pressures from 0.001 to 1000 atm.] (Published in English translation by ATS, Glen Ridge, N.J.). Moscow, Acad. Sci. USSR Press, 1958.
2. Predvoditelev, A. S. , Ye. V. Stupochenko, A. S. Pleshanov, Ye. V. Samuylov and I. B. Rozhdestvenskiy. *Tablitsy termodinamicheskikh funktsiy vozdukha dlya temperatur ot 200 do 6000°K i davleniy ot 0.00001 do 100 atmosfer* [Tables of Thermodynamic Functions of Air for Temperatures from 200 to 6000°K and Pressures from 0.00001 to 100 Atmospheres]. Moscow, Computer Center Acad. Sci. USSR, 1962.
3. Predvoditelev, A. S. , Ye. V. Stupochenko, I. V. Rozhdestvanskiy, Ye. V. Samuylov and A. S. Pleshanov. *Tablitsy gazodinamicheskikh i termodinamicheskikh velichin potoka vozdukha za pryamym skachkom uplotneniya (dlya skorostey nabegayushchego potoka do 4500 m/sec)* [Tables of Gasdynamic and Thermodynamic Flow Variables for Air Behind a Normal Shock Front (for incoming flow velocities up to 4500 m/sec)]. Moscow, Computer Center Acad. Sci., USSR, 1962.
4. Stupochenko, Ye. V. , I. P. Stakhanov, Ye. V. Samuylov, A. S. Pleshanov and I. B. Rozhdestvenskiy. *Termodinamicheskiye svoystva vozdukha v intervale temperatur ot 1000 do 12,000°K i v intervale davleniy ot 0.001 do 1000 atm* [Thermodynamic Properties of Air in the Temperature Interval from 1000 to 12,000°K and for Pressures from 0.001 to 1000 atm]. In the collection *Fizicheskaya gazodinamika* [Physical Gasdynamics]. Acad. Sci. USSR Press, Moscow, 1959.
5. Stupochenko, Ye. V. , S. A. Losev and A. I. Osipov. *Relaksatsionnyye protsessy v udarnykh volnakh* [Relaxation Processes in Shock Waves]. [Published in English translation by Springer Verlag, as *Relaxation in Shock Waves*, 1967]. Nauka Publishing House, Moscow, 1965.
6. Zel'dovich, Ya. B. , and A. S. Kompaneyets. *Teoriya detonatsii* [Theory of Detonation]. Gostekhizdat, Moscow, 1955.
7. Zel'dovich, Ya. B. and Yu. P. Rayzer. *Fizika udarnykh voln i vysokotemperaturnykh gidrodinamicheskikh yavleniy* [Physics of Shock Waves and High-Temperature Hydrodynamic Phenomena]. [This is the first edition. The second edition was published in English translation under the above title by Academic Press, 1966]. Fizmatgiz, Moscow, 1963.
8. Telenin, G. F. and G. P. Tinyakov. *Doklady AN SSSR*. Vol. 154, No. 5, 1056. 1964.
9. Lick, W. , *J. Fluid. Mech.*, 1960, Vol. 7, p. 1, 128.
10. Duff, R. E. , N. Davidson. *J. Chem. Phys.*, Vol. 31, p. 4, 1018, 1959.
11. Collection *Udarnyye truby* [Shock Tubes]. Kh. A. Rakhmatullin and S. S. Semonov, chief editors [Collection of translated articles]. Foreign Literature Press, Moscow, 1962.
12. Clark, J. *J. Fluid. Mech.*, Vol. 7, p. 4, 577, 1960.

13. Moore, F.K., W.E. Gibson, J. Aero-Space Sce., No. 2, p. 27, 1960.
14. Stupochenko, Ye. V. and I. P. Stakhanov. Dokl. AN SSSR, Vol. 134, No. 5, 1044, 1960.
15. Arkhipov, V.N. and K.S. Khoroshko. PMTF, No. 6, 121. 1962.
16. Wood, W. and R. Parker. Mekhanika, No. 6, 81. 1962 [translated from English].
17. Arkhipov, V.N. PMTF, No. 4, 40. 1962.
18. Spence, D.A. Mekhanika, No. 6, 65. 1962. [translated from English].
19. Eschenroeder, A.Q., W.D. Boyer and J.G. Hall. VRT [Voprosy raketnoy tekhniki]. No. 2, 13. 1963.
20. Wegener, P.P. VRT, No. 4, 3, 1963. (translated from English).
21. Smiley, E. and E. Winkler. J. Chem. Phys., Vol. 22, p. 2018, 1954.
22. Matthews, P. Phys. Fluids, Vol. 2, p. 170, 1954.
23. Blackman, V. J. Fluid. Mech., Vol. 1, p. 61, 1956.
24. Losev, S.A. Dokl. AN SSSR, Vol. 120, 1291, 1958.
25. Losev, S.A. and N.A. Generalov. PMTF, No. 2, 1963; Dokl. AN SSSR, Vol. 133, No. 4, 1960. /190
26. Wegener, P.P., J.D. Cole. VIII Symposium on Combustion. Baltimore, p. 883, 1962.
27. Bray, K.N. J. Fluid. Mech., 6, 1959.
28. Feldman, S. J. Fluid. Mech., 3, 3, 1957.
29. Leskov, L.V. and F.A. Savin. UFN, Vol. 72, Issue 4, 741. 1960.
30. Shchetnikov, Ye. S. Fizika goreniya gazov [Physics of Gas Combustion]. Nauka Publishing House, Moscow, 1965.
31. Gaydon, A.G. and J.R. Hurle. The Shock Tube in High-Temperature Chemical Physics, London, Chapman and Hall Ltd., 1963.
32. Soloukhin, R.I. Udarnyye volny i detonatsiya v gazakh [Shock Waves and Detonation in Gases]. Fizmatgiz, Moscow, 1963.
33. Shchelkin, K.I. and Ya. K. Troshin. Gazodinamika goreniya [Gasdynamics of Combustion]. USSR Acad. Sci. Press, Moscow, 1963.
34. Voytsekhovskiy, B.V., V.V. Mitrofanov and M. Ye. Topchiyan. Struktura fronta detonatsii v gazakh [Structure of the Detonation Front in Gases]. USSR Acad. Sci. Press, Novosibirsk, 1963.
35. Rosa, R.I. Phys. Fluids, Vol. 4, No. 2, p. 182, 1961.
36. Sutton. VRT, No. 8, 3, 1962. [translated from English].
37. Wang, C.J. and J. B. Peterson. Jet Propuls., Vol. 28, No. 5, p. 321, 1958.
38. Bond, J.W. VRT, No. 1, 3, 1959.
39. Adamson, T. VRT, No. 6, 3, 1961.
40. Calcott, G. VRT, No. 3, 22, 1962.
41. Eschenroeder, A.Q. and J.W. Daiber. ARS Journal, Vol. 31, No. 1, p. 28, 1961.
42. White, D. J. Amer. Rocket Sci., No. 9, p. 63, 1959.
43. Gibson, W. E. and P.V. Marrone. Phys. Fluids, Vol. 5, No. 12, p. 1649, 1962.
44. Zel'dovich, Ya. B. Sverkhzvukovoye techeniye i udarnyye volny [Supersonic Flow and Shock Waves]. USSR Acad. Sci. Press, Moscow, 1946.
45. Resler, E.L., S.C. Lin and A.R. Kantrowitz. The Production of High-Temperature Gases in Shock Tubes. J. Appl. Phys., Vol. 23, 12:1390, 1952.

46. Glass, I. I. and G. N. Patterson, J. Aero Sci., Vol. 22, 2:73, 1953.
47. Salamandra, G. D., T. V. Bazhenova, S. G. Zaytsev, R. I. Soloukhin, I. M. Naboko and I. K. Sevast'yanova. Nekotoryye metody issledovaniya bystroprotekayushchikh protsessov i ikh primeneniye k izucheniyu formirovaniya detonatsionnoy volny [Some Methods for the Study of Rapidly Occuring Processes and Their Application of the Study of Detonation-Wave Formation]. USSR Acad. Sci. Press, Moscow, 1960.
48. Salamandra, G. D. Vysokoskorostnaya s'yemka shliren-metodom [High-Speed Photography by the Schlieren Method]. Nauka Publishing House, Moscow, 1965.
49. Bazhenova, T. V., S. G. Zaytsev and I. M. Naboko. Uspekhi nauchnoy fotografii [Progress in Scientific Photography]. IX 215, Nauka Publishing House, Moscow, 1964. T. V. Bazhenova, Z. S. Leont'yeva and V. S. Pushkin. In the collection Gazodinamika i fizika goreniya [Gasdynamics and Physics of Combustion, 95]. USSR Acad. Sci. Press, Moscow, 1959.
50. Salamandra, G. D., I. M. Naboko and I. K. Savost'yanova. PTE, No. 2, 1959.
51. Dubovik, A. S. Fotograficheskaya registratsiya bystroprotekayushchikh protsessov [Photographing of Rapidly Occuring Processes]. Nauka Publishing House, Moscow, 1964.
52. Komel'kov, V. S. and B. P. Surnin. PTE, No. 1, 78, 1956.
53. Gusev, M. V., V. A. Gordyushin and V. D. Lobanov. In the collection Svoystva gazov pri vysokikh temperaturakh [High-Temperature Properties of Gases], 158, Nauka Publishing House, Moscow, 1967.
54. Tarantov, Ye. A. Zhurnal nauchnoy i prikladnoy fotografii i kinematografii. Vol. 4, No. 5, 375, 1959.
55. Dubovik, A. S. and N. M. Sitsinskaya. PTE, No. 5, 166, 1961.
56. Vasil'yev, A. A., S. S. Semenov, Ye. A. Tarantov. Izv. AN SSSR, OTN, No. 11, 186, 1957.
57. Gvozdeva, L. G. In the collection Fizicheskaya gazodinamika i svoystva gazov pri vysokikh temperaturakh [Physical Gasdynamics and High-Temperature Properties of Gases], 157. Nauka Publishing House, Moscow, 1964.
58. Gvozdeva, L. G. Uspekhi nauchnoy fotografii [see [49]]. Vol. IX, p. 213, Nauka Publishing House, Moscow, 1964.
59. Townend, H. C. H. Philos. Mag. and J. Sci., Vol. 14, No. 92, p. 700, 1932.
60. Bomelbourg, H. I., I. Herzog, I. R. Weske and Z. Flugwiss. Vol. 7, No. 11, p. 322, 1959.
61. Rudinger, G. and L. M. Somers. J. Fluid Mech., Vol. 7, No. 2, p. 161, 1960. /191
62. Vasil'yeva, I. A. and P. A. Sofronov. PTE, No. 1, 190, 1964.
63. Kyser, J. B. AIAA Journal, Vol. 2, No. 2, p. 216, 1964.
64. Salamandra, G. D., I. K. Fedoseyeva and N. M. Bykova. Inzhenerno-fizicheskiy zhurnal, Vol. 7, No. 5, 96, 1964.
65. Copper, J. A. AIAA Journal, Vol. 2, No. 10, 190, 1964.
66. Salamandra, G. D. and I. K. Fedoseyeva. Inzhenerno-fizicheskiy zhurnal, Vol. 7, No. 7, 47, 1964.
67. Rudinger, G. AIAA Journal, Vol. 2, No. 8, p. 1517, 1964.
68. Landau, L. D. and Ye. M. Lifshits. Mekhanika sploshnykh sred [Mechanics of Continuous Media]. GITTL, Moscow, 1964.
69. Kyser, J. B. AIAA Journal, Vol. 2, No. 8, p. 1518, 1964.

70. Evans, M.W., F.H. Harlow, and B.D. Mexner. Phys. Fluids, Vol. 5, No. 6, p. 651, 1962.
71. Bazhenova, T.V. In the collection Fizicheskaya gazodinamika i teploobmen [Physical Gasdynamic and Heat Transfer]. USSR Acad. Sci. Press, p. 31, 1961.
72. Zaytsev, S.G. Ob izmerenii bystromenyayushchikhsya davleniy v gazovoy srede [Concerning the Measurement of Rapidly-Varying Pressures in a Gaseous Medium]. PTE, No. 6, 97, 1958.
73. Willmart, W. Miniaturnyye datchiki iz titanata bariya dlya aerodinamicheskikh i akusticheskikh izmereniy davleniya [Miniature Barium-Titanate Pickups for Aerodynamic and Acoustic Pressure Measurements]. In the collection Udarnyye trubyy [Shock Tubes] [collection of translated articles], 344. Foreign Literature Publishing House, Moscow, 1962.
74. Knight, H. P'yezoelektricheskiy datchik dlya udarnykh voln v gazakh nizkoy plotnosti [A Piezoelectric Pickup for Shock Waves in Low-Density Gases]. In the collection Udarnyye trubyy [see [73]], 974. Foreign Literature Publishing House, Moscow, 1962.
75. Edwards, D.H. A piezo-electric pressure bar gauge. J. Scient. Instrum., Vol. 35, No. 9, p. 346, 1958.
76. Soloukhin, R.I. PTE, No. 3, 170, 1961.
77. Gusev, M.V. and O.A. Luneva. P'yezoelektricheskiy datchik davleniya [A Piezoelectric Pressure Pickup]. In the collection Issledovaniya po fizicheskoy gazodinamike [Studies in Physical Gasdynamics], 210. Nauka Publishing House, Moscow, 1966.
78. Polyakov, Yu. A. In the collection Fizicheskaya gazodinamika, teploobmen i termodinamika gazov vysokikh temperatur [Physical Gasdynamics, Heat Transfer and Thermodynamics of High-Temperature Gases], 251. Nauka Publishing House, Moscow, 1962.
79. Mit'kina, Ye. A. and Yu. A. Polyakov. PTE, No. 4, 140, 1961.
80. Golant, V.Ye. ZhTF, Vol. 30, p. 1266, 1960.
81. Lin, S.C., R.A. Neal and W.I. Fyfe. Rate of Ionization Behind Shock Waves in Air. I. Experimental results, Phys. Fluids 5, 1633-1648, 1962.
82. Bazhenova, T.V. and Yu. S. Lobastov. In the collection Fizicheskaya gazodinamika i svoystva gazov pri vysokikh temperaturakh [see [57]], 29, Nauka Publishing House, Moscow, 1964.
83. Drabkin, A.L. and V.L. Zuzenko. Antenno-fidernyye ustroystva [Antenna Feeder Devices]. Sovetskoye radio Publishing House, Moscow, 1961.
84. Lobastov, Yu. V. In the collection Fizicheskaya gazodinamika i svoystva gazov pri vysokikh temperaturakh [see [57]], 22. Nauka Publishing House, Moscow, 1964.
85. Yen, K. J. Appl. Phys., Vol. 35, No. 5, p. 290, 1964.
86. Duff, R.E. Phys. Fluids, Vol. 2, p. 207, 1959.
87. Roshko, A. Phys. Fluids, Vol. 3, p. 835, 1960.
88. Hooker, W.J. Phys. Fluids, Vol. 4, p. 1451, 1961.
89. Mirels, H. Phys. Fluids, Vol. 6, No. 9, p. 1201, 1963; Vol. 9, No. 10, p. 1907, 1966.
90. Anderson, G.F. J. Aero-Space Sci., Vol. 26, p. 184, 1952.
91. Mirels, H. Raketnaya tekhnika i kosmonavtika No. 1, 114, 1964. [translated from English].
92. Mirels, H. In the collection Udarnyye trubyy [see [73]], 286. Foreign Literature Publishing House, Moscow, 1962.

93. Mirels, H. In the collection Udarnyye truby [see [73]], 320. Foreign Literature Publishing House, Moscow, 1962.
94. Spencer, D.A. and B.A. Woods. Hypersonic Flow. (Ed. Collar A. R., Tinkler J.). London, Butterworth, 1960; 332, 1962.
95. Dem'yanov, Yu. A. PMM, Vol. 21, No. 3, 368; No. 4, 473, 1957.
96. Syshchikova, M.P., A. N. Semenov and M.K. Berezkina. In the collection Aerodinamicheskiye issledovaniya sverkhzvukovykh techeniy [Aerodynamic Studies of Supersonic Flows] 21. Nauka Publishing House. Moscow-Leningrad, 1967.
97. Losev, S.A. and A.I. Osipov. UFN, Vol. 74, No. 3, 1961.
98. Trimpi, L.L. and N.B. Cohen. NASA Tech. Rep, R-85, 1961. In the collection Udarnyye truby [see [73]], 299. Foreign Literature Publishing House, Moscow, 1962.
99. Hartunian, R.A., A.M. Russo and P.V. Marrone. JASS, Vol. 27, No. 8, p. 587, 1960. /192
100. Martin, W.A. UTIA, Report, No. 47, 1957.
101. Kireyev, V.T. Izv. AN SSSR, OTN. Mekhanika i mashinostroyeniye, Vol. 144, Issue 6, 1962.
102. Dem'yanov, Yu. A. and V.T. Kireyev. Izv. AN SSSR, Mekhanika zhidkosti i gaza. Issue 3, 31, 1966.
103. Mark, H. J. A. S., Vol. 24, p. 304, 1957.
104. Strehlow, R.A. and A. Cohen. VRT [Voprosy raketnoy tekhniki], No. 9, 50, 1959.
105. Bromberg, R. Jet Propulsion, Vol. 26, 737, 1956. In the collection Udarnyye truby [see [73]], 608. Foreign Literature Publishing House, Moscow, 1962.
106. Bazhenova, T.V. and I.M. Naboko. Dokl. AN SSSR, Vol. 154, No. 2, 401, 1964.
107. Naboko, I.M. Issledovaniya po fizicheskoy gazodinamike [Studies in Physical Gasdynamics], 172. Nauka Publishing House, Moscow, 1966.
108. Bazhenova, T.V. and S.G. Zaytsev. III Vses. soveshch. po teorii goreniya [Third All Union Conference on the Theory of Combustion]. Vol. 1, 208, USSR Acad. Sci. Press, Moscow, 1960.
109. Bazhenova, T.V. and O.A. Predvoditeleva. In the collection Fizicheskaya gazodinamika i teploobmen [see [71]], 15. USSR Acad. Sci. Press, Moscow, 1961.
110. Bazhenova, T.V. and S.G. Zaytsev. In the collection Fizicheskaya gazodinamika, teploobmen i termodinamika gazov pri vysokikh temperaturakh [see [78]], Vol. III. USSR Acad. Sci. Press, Moscow, 1962.
111. Bazhenova, T.V. Dokl. AN SSSR, Vol. 146, No. 3, 554, 1962.
112. Soloukhin, R.I. PMTF, No. 138, 1963.
113. Nikolayev, G.N. and V.P. Ionov. In the collection Svoystva gazov pri vysokikh temperaturakh [see [53]]. Nauka Publishing House, Moscow, 1967.
114. Semenov, S.S. Dokl. AN SSSR, Vol. 114, No. 4, 841, 1957.
115. Broer, L. J. Fluid Mech., Vol. 4, p. 3, 1958.
116. Bergmann, Ludwig. Der Ultraschall, 5th ed. S. Hirzel Verlag, Zurich, Switzerland, 1949. Translated as Ultrasonics by H. Stafford Hatfield and published by John Wiley and Sons, Inc. 1938.
117. Bazhenova, T.V., I.M. Naboko and O.A. Predvoditeleva. In the collection Fizicheskaya gazodinamika i svoystva gazov pri vysokikh temperaturakh [see [57]], 80. Nauka Publishing House, Moscow, 1964.

118. Gurvich, P. V., G. A. Khachkuruzov, et al. Termodinamicheskiye svoystva individual'nykh veschestv [Thermodynamic Properties of Distinct Substances]. USSR Acad. Sci. Press, Moscow, 1962.
119. Bernstein, L. Aeronaut. Council Current Papers, No. 626, 1963.
120. Ferri, A. (ed). Fundamental Data Obtained from Shock Tube Experiments. AGARDograph No. 41. Pergamon Press, New York, 1961. [Published by Atomizdat in Russian translation, Moscow, 1963].
121. Johannesen, N. H. et al. J. Fluid Mech., Vol. 13, pt. 1; p. 213, 1962; pt. 2, p. 213, 1963.
122. Zaytsev, S. G. and Ye. V. Lazareva. In the collection Issledovaniya po fizicheskoy gazodinamike [see [77]], 170. Nauka Publishing House, Moscow, 1966.
123. Samuylov, Ye. V. In the collection Fizicheskaya gazodinamika [Physical Gasdynamics], 59. USSR Acad. Sci. Press, Moscow, 1959.
124. Morse, T. F. Phys. Fluids, Vol. 7, No. 2, p. 159, 1964.
125. Chu, B. T. Proc. Heat Transfer and Fluid Mech. Inst. Berkley, Vol. 80, p. 80, 1958.
126. Nemkov, R. G. In the collection Svoystva Gazov pri vysokikh temperaturakh [see [53]], 59. Nauka Publishing House, Moscow, 1967.
127. Stakhanov, I. P. and Ye. V. Stupochenko. PMTF, No. 2, 3, 1963.
128. Gardiner, W. C. and J. Kistiakowsky. J. Chem. Phys., Vol. 34, No. 8, p. 1080, 1961.
129. Strehlow, R. A. and G. T. Gase. J. Chem. Phys., Vol. 35, No. 4, p. 1506, 1961.
130. Zaytsev, S. G., A. P. Shatilov, Ye. V. Lazareva and A. I. Trukhanova. In the collection Fizicheskaya gazodinamika i svoystva gazov pri vysokikh temperaturakh [see [57]], 115. Nauka Publishing House, Moscow, 1964.
131. Zaytsev, S. G., Ye. V. Lazareva and A. P. Shatilov. PMTF, No. 4, 143, 1964.
132. Skinner, G. B. J. Chem. Phys., Vol. 31, No. 96, p. 218, 1959.
133. Brabbs, T. A., St. A. Zlatarich and F. E. Belles. J. Chem. Phys., Vol. 33, No. 1, 307, 1960.
134. Rudinger, G. Phys. Fluids, Vol. 4, No. 12, p. 1463, 1961.
135. Emrich, R. J. and D. S. Weller. Phys. Fluids, No. 1, p. 14, 1958.
136. Kudryavtsev, Ye. M., N. N. Sobolev, L. N. Tunitskiy and F. S. Fayzullov. Issledovaniye plazmy [Plasma Studies]. FIAN USSR, Vol. 18, 159, 1962. /193
137. Laporte, O. and I. Wilkerson. J. O. S. A., Vol. 50, p. 1293, 1960.
138. Bashenova, T. V. and S. G. Zayzev. VIII Symposium of Combustion. Baltimore, p. 340, 1962.
139. Toennies, J. P. and E. F. Greene. J. Chem. Phys., Vol. 30, p. 257, 1959.
140. Soloukhin, R. I. PTE, No. 1, 1964.
141. Borisov, A. A., S. M. Kogarko and A. V. Lyubimov. PMTF, No. 3, 175, 1960.
142. Gaydon, A. and J. Hurle. Nature, Vol. 184, No. 4702, p. 52, 1959.
143. Toennies, J. P. and E. E. Greene. J. Chem. Phys., Vol. 26, p. 655, 1957.
144. Bazhenova, T. V. and Yu. S. Lobastov. In the collection Issledovaniya po fizicheskoy gazodinamike [see [77]], 131. Nauka Publishing House, Moscow, 1966.
145. Bazhenova, T. V. In the collection Issledovaniya po fizicheskoy gazodinamike [see [77]], 180. Nauka Publishing House, Moscow, 1966.
146. Blackman, V. H. J. Fluid Mech., Vol. 1, No. 6, 1956.

147. Losev, S. A. and N. I. Generalov. Dokl. AN SSSR, Vol. 150, No. 4, 839, 1963.
148. Kantrowitz, A., E. L. Resler and S. C. Lin. VRT, No. 1, 3, 1956. [translated, from English].
149. Petschek, H. I. and S. Byron. Ann. Phys. (N.Y.) Vol. 1, pp. 270-315, 1957. In the collection Udarnyye truby [see [73]], 471. Foreign Literature Publishing House, Moscow, 1962.
150. Bazhenova, T. V., S. G. Zaytsev, A. A. Kon'kov, Yu. S. Lobastov, Yu. V. Makarov, I. M. Naboko, O. A. Predvoditeleva, Ye. V. Samuilov and E. K. Chekalin. Proceedings of the International Symposium on Properties and Utilization of Low-Temperature Plasma at the X Congress of YuPAK. Nauka Publishing House, Moscow, 1967.
151. Sommerfield, A. Z. Math. Phys., Vol. 46, p. 11, 1901.
152. Lighthill, M. I. Proc. Roy. Soc., Vol. 198, No. 1055, p. 454, 1949.
153. Ting, L. and H. F. Ludloff. JAS, Vol. 19, No. 5, p. 317, 1952.
154. Ting, L. and H. F. Ludloff. JAS, Vol. 18, No. 2, p. 143, 1951.
155. Fletcher, G. H., A. H. Taub and W. Blackney. Rev. Mod. Phys., Vol. 23, No. 3, p. 271, 1951.
156. Chester, W. Phil. Mag., Vol. 7, 45, 1293, 1954. [Russian transl. in Mekhanika, No. 3, 17, 1954].
157. White, D. R. JAS, Vol. 18, No. 9, p. 633, 1951.
158. Ryzhov, O. S. and S. A. Khristianovich. PMM, Vol. 22, Issue 5, 1958.
159. Grib, A. A., O. S. Ryzhov and S. A. Khristianovich. PMTF, No. 1, 63, 1960.
160. Smith, G. L. Phys. Rev., Vol. 60, No. 11-12, p. 678, 1946.
161. Taub, A. H. and G. L. Smith. Phys. Rev., Vol. 60, No. 11, p. 671, 1946.
162. Bleakney, W. and A. H. Taub. Rev. Mod. Phys., Vol. 21, No. 4, p. 584. Russian transl. in VRT 1951, No. 1.
163. Bleakney, W., C. M. Fletcher and D. K. Weimer. Phys. Rev., Vol. 76, , p. 323, 1949.
164. Polachek, H. and R. J. Seeger. Proc. Symposia in Appl. Math., Vol. 1, p. 119, 1949.
165. Courant, R. and K. O. Friedrichs. Supersonic Flow and Shock Waves. Wiley (Interscience), 1957.
166. Polacheck, H. and R. J. Seeger. Phys. Rev., Vol. 84, No. 5, p. 922, 1951.
167. Smith, L. G. Bull. Amer. Phys. Soc., Vol. 2, No. 4, p. 216, 1957.
168. Kawamura, R. and H. Satio. J. Phys. Soc. Japan, Vol. 11, 1956.
169. Whitham, G. W. J. Fluid. Mech., Vol. 2, pt. 2 No. 5, p. 548, 1957.
170. Cabannes, H. Lois de la Reflection des Ondes de chock dans les ecoulements plans non-stationnaires. ONERA, No. 8, 1955.
171. Bryson, A. E. and R. W. F. Gross. J. Fluid Mech., Vol. 10, p. 1, 1961.
172. White, D. R. An experimental survey of Mach reflection of shock waves, Proc. 2-nd Mid-West conference of Fluid Mech., p. 253, 1952.
173. Bleakney, W. Proc. Symposia in Appl. Math., Vol. 5, p. 41, 1954.
174. Syshchikova, M. P., A. N. Semenov and M. K. Berezkina. In the collection Aerodinamicheskkiye issledovaniya sverkhzvukovykh techeniy [see [96]]. Nauka Publishing House, Moscow-Leningrad, 1967.
175. Gvozdeva, L. G. and O. A. Predvoditeleva. Dokl. AN SSSR, Vol. 163, No. 5, 1088, 1965.
176. Gvozdeva, L. G. and O. A. Predvoditeleva. In the collection Issledovaniya po fizicheskoy gazodinamike [see [77]], 183. Nauka Publishing House, Moscow, 1966.

177. Fundamentals of Gasdynamics. T. Emmons, editor. Published in Russian translation by Foreign Literature Publishing House, Moscow, 1963.
178. Shchelkin, K.I. UFN, Vol. 87, Issue 2, 273, 1965.
179. Oppenheim, A.K. Proc. Roy. Soc. A, Vol. 268, No. 1333, p. 153, 1962.
180. Salamandra, G.D., T.V. Bazhenova and I.M. Naboko. ZhTF, Vol. 29, Issue 11, 1354, 1959.
181. Salamandra, G.D., T.V. Bazhenova and I.K. Sevost'yanova. Trudy Odesskogo universiteta, Vol. 152, Issue 8, 91, 1962.
182. Salamandra, G.D. In the collection Issledovaniya po fizicheskoy gasodinamike [see [77]], 203. Nauka Publishing House, Moscow, 1966.
183. Urtiew, P.A. and A.K. Oppenheim. Comb. and Flame, Vol. 9, No. 4, p. 405, 1965.
184. Oppenheim, A.K. Proc. Roy. Soc. A, Vol. 295, No. 1440, p. 1, 1966.
185. Pyatnitskiy, L.N. Dokl. AN SSSR, Vol. 144, No. 6, 1262, 1962.
186. Zaytsev, S.G. and R.I. Soloukhin. Dokl. AN SSSR, Vol. 122, No. 6, 1039, 1958.
187. Zaytsev, S.G. III Vses. soveshch po goreniyu [see [108]]. Vol. 1, 214, 1960.
188. Voevodsky, V.V. and R.I. Soloukhin. X Symposium on Combustion. Pittsburgh, p. 279, 1965.
189. Gibert, R.B. and R.A. Strehlow. AIAA Journal, Vol. 4, No. 10, p. 1777, 1966.
190. Soloukhin, R.I. PMTF, No. 4, 42, 1964.
191. Naboko, I.M. In the collection Fizicheskaya gazodinamika i teploobmen [see [71]], 42. USSR Acad. Sci. Press, Moscow, 1961.
192. Holder, D. and A. Chinnek. Mekhanika, No. 2, 78, 1955. [transl. fr. Engl].
193. Aslanov, S.K. PMM, Vol. 18, Issue 5, 561, 1954.
194. Soloukhin, R.I. PMTF, No. 5, 57, 1961.
195. Bashenova, T.V. and R.I. Soloukhin. VII Symposium on Combustion. Baltimore, p. 866, 1959.
196. Oppenheim, A.K. Fourth AGARD Colloquim. Oxford - London - New York, p. 186, 1961.
197. Wood, W.W. and Z.V. Salsburg. Mekhanika, No. 5, 45, 1961. [transl. fr. Engl].
198. Fay, J.A. VIII Symposium on Combustion. Baltimore, p. 30, 1962.
199. Duff, R.E., H.T. Knight and I.P. Rink. Phys. Fluids, Vol. 1, No. 4, p. 393, 1958.
200. White, D.R. Phys. Fluids, Vol. 4, No. 4, p. 465, 1961.
201. Martin, F.I. and D.R. White. VII Symposium on Combustion. London, p. 856, 1959.
202. White, D.R. and K. H. Cary. Phys. Fluids, Vol. 6, No. 5, p. 749, 1963.
203. Borisov, A.A. and S.M. Kogarko. Dokl. AN SSSR, Vol. 149, No. 4, 623, 1963.
204. Schott, G.L. Phys. Fluids, Vol. 8, No. 5, p. 850, 1965.
205. Duff, R.E. Phys. Fluids, Vol. 4, No. 11, p. 1427, 1961.
206. Mitrofanov, V.V. and R.I. Soloukhin. Dokl. AN SSSR, Vol. 159, No. 5, 1003, 1964.
207. Mitrofanov, V.V., V.A. Subbotin and M.Ye. Topchiyan. PMTF, No. 3, 45, 1963.
208. Soloukhin, R.I. Nauchno-tekhnicheskiye problemy goreniya i vzryva [Scientific and Engineering Problems of Combustion and Explosion], No. 2, 35, 1965.

209. Voytsekhovskiy, B. V., V. V. Mitrofanov and M. Ye. Topchiyan. PMTF, No. 3, 28, 1962.
210. Strehlow, R. A., R. Liaugminas, R. H. Watson and I. R. Eyman. XI Symposium on Combustion. Pittsburgh, p. 683, 1966.
211. Gvozdeva, L. G. ZhTF, Vol. 31, Issue 6, 731, 1961.
212. Brochet, C., I. C. Leyer and N. Manson. Comt. Rend. Acad. Sci., Vol. 253, p. 621, 1961.
213. Brochet, C. and N. Manson. C. R. t. No. 254, p. 3992, 1962.
214. Greifer, B., I. C. Cooper, F. C. Gibson and C. M. Manson. J. Appl. Phys., Vol. 28, No. 3, p. 289, 1957.
215. Toennies, J. P. and H. G. Wagner. Z. Electrochem. B, Vol. 59, No. 1, 1957.
216. Denisov, Y. N. and Ya. K. Troshin. X symposium on combustion. Pittsburgh, p. 600, 1965.
217. Trofimov, V. S. and A. N. Dremin. Fizika gorennya i vzryva, No. 3, 19, 1966.
218. Rybanin, S. S. Fizika gorennya i vzryva, No. 1, 29, 1966.
219. Zel'dovich, Ya. B. ZhETF, Vol. 10, 542, 1930. /195
220. Kistiakowsky, G. B., H. T. Knight and M. E. Malin. J. Chem. Phys., Vol. 20, No. 5, p. 876, 1952.
221. Edwards, D. H. and T. G. Jones. Brit. J. Appl. Phys., Vol. 11, No. 5, p. 190, 1960.
222. Edwards, D. H., G. T. Williams and I. G. Breeze. J. Fluid Mech., Vol. 6, p. 4, 497, 1959.
223. Edwards, D. H. and G. T. Williams. B. Price Colloq. intern. Centre. Rech. scient., No. 109, p. 249, 1962.
224. Manson, N. Ch. Brochet, I. Brossard and Y. Pujal. IX symposium on combustion. p. 250, New York, 1953.
225. Brochet, Ch., I. Brossard and N. Manson. Compt. Rend. Acad. Sci., Vol. 250, p. 3949, 1960.
226. Brossard, I., N. Manson, V. Pujal and M. Rouze. Comt. Rend. Acad. Sci., Vol. 255, p. 1190, 1962.
227. Peek, H. M. and R. G. Thrap. J. Chem. Phys., Vol. 26, p. 740, 1957.
228. Eisen, K., R. Gross and T. Rivlin. VRT, No. 1 (73), 20, 1961. [transl. fr. Engl].
229. Glass, I. I. and A. Takano. Progr. Aeron. Sci., Vol. 6, p. 163. Oxford-London, Pergamon Press, 1965.
230. Drewry, J. E. UTIAS Report, No. 124, 1967.
231. Jost, W. Explosion and Combustion in Gases. Published in Russian translation by Foreign Literature Publishing House, Moscow, 1952.
232. Jahn, R. I. J. Fluid. Mech., Vol. 1, No. 5, p. 457, 1961.
233. Zel'dovich, Ya. B., S. M. Kogarko and N. I. Simonov. ZhTF, Vol. 26, Issue 8, p. 7441, 1956.
234. Gvozdeva, L. G. PMTF, No. 5, p. 53, 1961.
235. Gvozdeva, L. G. In the collection Fizicheskaya gazodinamika, teploobmen i termodinamika gazov vysokikh temperatur [see 178], 131, USSR Acad. Sci. Press, Moscow, 1962.
236. Dremin, A. N. Dokl. AN SSSR, Vol. 147, p. 870, 1962.
237. Voyevodskiy, V. V. and R. I. Soloukhin. Dokl. AN SSSR, Vol. 161, No. 5, p. 1118, 1965.
238. Döring, W. and G. Schön. Z. Electrochem. B, Vol. 54, No. 4, p. 231, 1950.

239. Meyer, R. F. J. Fluid. Mech., Vol. 3, pt. 3, p. 309, 1957.
240. Taub, A. H. Phys. Rev., Vol. 72, No. 1, p. 51, 1947.
241. Kittel', H. G. Tsellyuloznyye laki [Celluloid Varnishes]. Goskhimizdat, 1957.
242. Polachek, H. and R. I. Seeger. Phys. Rev., Vol. 34, No. 5, p. 922, 1951.
243. Strehlow, R. A. Phys. Fluids, Vol. 7, No. 6, p. 908, 1964.
244. Strehlow, R. A. and F. D. Fernandes. Comb. and Flame, Vol. 9, No. 2, p. 109 1965.
245. Lin, S. and W. Fife. Phys. Fluids, Vol. 4, p. 238, 1964.
246. Kuznetsov, N. M. IFZh, No. 9, 1960.
247. Bazhenova, T. V. and Yu. S. Lobastov. In the collection Fizicheskaya gazodinamika i teploobmen [see [71]], Vol. 36, USSR Acad. Sci. Press, Moscow, 1959.
248. Lin, S. C. and J. D. Tear. Phys. Fluids, Vol. 6, No. 3, pp. 355-375, 1963.
249. Sayasov, Yu. S. Dokl. AN SSSR, Vol. 146, No. 2, p. 409, 1962.
250. Bazhenova, T. V. and Yu. S. Lobastov. Dokl. AN SSSR, Vol. 151, p. 519, 1963.
251. Bazhenova, T. V. and Yu. S. Lobastov. In the collection Fizicheskaya gazodinamika [see [123]], 17. Nauka Publishing House, Moscow, 1964.
252. Sayasov, Yu. S. PMTF, No. 1, p. 61, 1962.
253. Manchmer, Y., W. Low and J. Fluid. Mech., Vol. 6, p. 449, 1959.
254. Dvir, M. and W. Low. Phys. Fluids, Vol. 7, p. 578, 1964.
255. Niblett, B., V. Blackman. J. Fluid Mech., Vol. 4, p. 191, 1958.
256. Lobastov, Yu. S. In the collection Issledovaniya po fizicheskoy gazodinamike [see [77]], 119. Nauka Publishing House, Moscow, 1966.
257. Lazarev, P. P. Trudy FIAN, Vol. 30, p. 221, Nauka Publishing House, 1964.
258. Hammerling, P., J. Teare and B. Kivel. Proc. 4-th., Int. Conf. Ion. Phen., Uppsala, Vol. 2, 1959.
259. Massey, H. S. W. and E. H. S. Burhop. Electronic and Ionic Impact Phenomena. Fairlawn, N. J., Oxford University Press, 1952.
260. Bradbury, A. and E. Nielsen. Phys. Rev., Vol. 49, p. 388, 1936.
261. Phelps, A., O. Fundingsland and S. Brown. Phys. Rev., Vol. 84, p. 559, 1951.
262. Gould, L. and S. Brown. Phys. Rev., Vol. 95, p. 897, 1954.
263. Goldstein, J. and J. Anderson. Phys. Rev., Vol. 100, p. 1229, 1955.
264. Anderson, J. and L. Goldstein. Phys. Rev., Vol. 102, p. 388, 1956.
265. Biondi, M. Proc. 4-th Int. Conf. Ion. Phen., Uppsala, Vol. 1, p. 72, 1959.
266. Pack, J. and A. Phelps. Phys. Rev., Vol. 121, p. 798, 1961.
267. Bulewicz, E. J. Chem. Phys., Vol. 36, p. 385, 1962.
268. Guenoche, H., M. Billiotte and G. Inglesakis. International Symposium on the Properties and Utilization of Low-Temperature Plasma. Nauka Publishing House, Moscow, 1965.
269. O'Malley, T. Phys. Rev., Vol. 130, p. 1020, 1963.
270. Bekefi, G. and S. Brown. Phys. Rev., Vol. 112, p. 159, 1958.
271. Lin, S. and B. Kivel. Phys. Rev., Vol. 114, p. 1026, 1959.
272. Takeda, S. and A. Dougal. J. Appl. Phys., Vol. 31 p. 412, 1960.
273. Formato, D. and A. Gilardini. Proc. 4-th Int. Conf. Ion. Phen., Uppsala, Vol. 1, p. 99, 1959.
274. Ginzburg, V. L. Rasprostraneniye elektromagnitnykh voln v plazme. Fizmatgiz, Moscow, 1960. Published in English translation as Propagation of Electromagnetic Waves in Plasma (W. L. Sadowski and D. M. Gallik, eds), Gordon and Breach, New York, 1962.

275. Fayzullov, F.S. Trudy FIAN, Vol. 18, p. 105, 1962.
276. Lamb, L. and S.C. Lin. In the collection Udarnyye truby [see [73]]. Foreign Literature Publishing House, Moscow, 1962. [transl. fr. Engl.].
277. Hammerling, P., W. Shine and B. Kivel. J. Appl. Phys., Vol. 28, p. 760 1957.
278. Chinitz, W., K. Eisen and R. Gross. VRT, No. 2, 1960. [transl. fr. Engl.].
279. Kivel, B. Phys. Rev., Vol. 116, p. 926, 1959.
280. Harwell, K. and R. Jahn. Phys. Fluids, Vol. 7, p. 214, 1964.
281. Rozhdestvenskiy, I. B. and Ye. V. Samuylov. In the collection Fizicheskaya gazodinamika, teploobmen i termodinamika gazov vysokikh temperatur [see [78]], 103. Nauka Publishing House, Moscow, 1962.
282. Rozhdestvenskiy, I. B. In the collection Fizicheskaya gazodinamika [see [123]]. USSR Acad. Sci. Press, Moscow, 1959.
283. Pleshanov, A. S. and S. G. Zaytsev. In the collection Fizicheskaya gazodinamika, teploobmen i termodinamika gazov vysokikh temperatur [see [78]], 15. USSR Acad. Sci. Press, Moscow, 1962.

The first part of the paper discusses the importance of understanding the cultural context of the research. It highlights the need for researchers to be sensitive to the values and beliefs of the communities they are studying. This is particularly important in the field of education, where cultural differences can significantly impact learning outcomes. The paper then moves on to discuss the challenges of conducting research in diverse cultural settings. It notes that researchers often face difficulties in establishing rapport with participants and in interpreting their responses. To address these challenges, the paper suggests several strategies, including the use of local researchers and the development of culturally appropriate research instruments. The final part of the paper discusses the importance of ethical considerations in cross-cultural research. It emphasizes the need for researchers to obtain informed consent from participants and to ensure that the research is conducted in a way that respects the dignity and rights of all individuals involved.

1. The first part of the report is a general introduction to the subject of the study. It discusses the importance of the study and the objectives of the research.

2. Methodology

The methodology section describes the research methods used in the study. It includes a discussion of the data sources, the sampling method, and the statistical techniques used to analyze the data. The methodology section also discusses the limitations of the study and the potential for bias.

3. Results and Discussion

The results and discussion section presents the findings of the study. It includes a discussion of the results of the statistical analysis and a discussion of the implications of the findings for the field of study.

4. Conclusion

The conclusion section summarizes the findings of the study and provides a final statement on the importance of the research. It also includes a discussion of the limitations of the study and the potential for future research.

5. References

The references section lists the sources of information used in the study. It includes a list of books, articles, and other sources of information.

6. Appendix

The appendix section contains supplementary material that is related to the study. It includes a list of tables, figures, and other supplementary material. The appendix section also includes a list of abbreviations and a list of symbols.

7. Glossary

The glossary section defines the terms used in the study. It includes a list of terms and their definitions.

8. Index

The index section provides a list of the pages on which the terms are used. It includes a list of terms and the page numbers on which they appear.

9. Bibliography

The bibliography section lists the sources of information used in the study. It includes a list of books, articles, and other sources of information.

01U 001 37 51 3DS 69273 00903
AIR FORCE WEAPONS LABORATORY/WLIL/
KIRTLAND AIR FORCE BASE, NEW MEXICO 87117

ATT E. LOU BOWMAN, CHIEF, TECH. LIBRARY